General Introduction

In all the propulsion concepts that have been presented in the various US, Russian, Japanese or European launch vehicle (SSTO and TSTO) studies, the energy stored in the liquid hydrogen has never been utilized, except in the Liquid Air Cycle Engine (LACE) studied in the 1960's by the Marquardt Company (USA) or, mainly, the Air Collection and Enrichment System (ACES) studied in the 1960's and the early 1990's by the US Air Force at the Wright Laboratory (J. Leingang's USAF team). It is indeed possible to recover a significant portion of the energy required to liquefy the hydrogen if a suitable thermodynamic system is used on board the launch vehicle. A fundamental change in the conception and the performance of (airbreathing) launchers is possible with the incorporation of such a thermodynamic cycle.

In this ACES scheme, the atmospheric air has to be deeply cooled, an O_2-N_2 separation process must then take place and the Liquid Enriched Air (LEA) which is air very enriched in oxygen (or liquid oxygen with impurities) is stored in the tanks for a later use in rocket mode. The separated cryogenic nitrogen can find different uses in function of the propulsion system and the collection Mach number.

The consequence of ACES could be a large reduction of the on board carried oxygen mass and, as a consequence, a much lower Take-Off Gross Weight. But when trying to apply this concept, the blockage appearing very quickly is that a lot of parameters have to reach a high (optimistic) value all together in order to get a real positive effect at the vehicle/launcher level. An ACES SSTO still needs to transition to a pure rocket mode at a high Mach number, what forces to use a scramjet or at least a dual mode ramjet. An ACES TSTO with supersonic staging needs to have a staging (separation between the two stages) Mach number relatively high (at least 4 or even 5), a (very) high purity of the collected oxygen and a low-weight collection plant (thus safe and low-weight heat exchangers). For example, in all Leingang's studies, the maximum airbreathing Mach number remains high, the system is complicated, the masses must be low and the collection plant very efficient.

That is the reason why we are proposing an alternative, or more correctly a first step (but which is already a launcher with good performance) in the ACES approach. That is a system where margins are present and which could prove the ACES concept and permits the testing of the collection plant elements in flight. That is a TSTO with a subsonic staging at 30-40.000 feet altitude and a subsonic collection cruise phase.

The objective of this short study will be to present the different aspects of the ACES Air-Launch TSTO vehicle with the launcher performance (Part 1), the carrier plane propulsion (Part 2) and the carrier plane preliminary design (Part 3).

A low cost but rather extensively validated sizing program applied to the conceptual design of fully reusable or semi-reusable S.S.T.O. and T.S.T.O. space vehicles using airbreathing, pure rocket or Rocket Based Combined Cycles (RBCC) propulsion will be used in Part 1. This code called VPSC has been developed at and by the Royal Military Academy of Belgium.

REPORT DOCUMENTATION PAGE

Form Approved OMB No. 0704-0188

Public reporting burden for this collection of information is estimated to average 1 hour per response, including the time for reviewing instructions, searching existing data sources, gathering and maintaining the data needed, and completing and reviewing the collection of information. Send comments regarding this burden estimate or any other aspect of this collection of information, including suggestions for reducing the burden, to Department of Defense, Washington Headquarters Services, Directorate for Information Operations and Reports (0704-0188), 1215 Jefferson Davis Highway, Suite 1204, Arlington, VA 22202-4302. Respondents should be aware that notwithstanding any other provision of law, no person shall be subject to any penalty for failing to comply with a collection of information if it does not display a currently valid OMB control number.
PLEASE DO NOT RETURN YOUR FORM TO THE ABOVE ADDRESS.

1. REPORT DATE *(DD-MM-YYYY)*	2. REPORT TYPE	3. DATES COVERED *(From – To)*
30-01-2003	Final Report	30 August 2001 - 30-Aug-02

4. TITLE AND SUBTITLE

Air-Launch TSTO With Subsonic In-Flight Collection-System And Technology Study

5a. CONTRACT NUMBER
F61775-01-WE074

5b. GRANT NUMBER

5c. PROGRAM ELEMENT NUMBER

6. AUTHOR(S)

Professor Patrick Hendrick

5d. PROJECT NUMBER

5d. TASK NUMBER

5e. WORK UNIT NUMBER

7. PERFORMING ORGANIZATION NAME(S) AND ADDRESS(ES)
ASBL Renaissance
Renaissance Avenue 30
Brussels 1000
Belgium

8. PERFORMING ORGANIZATION REPORT NUMBER

N/A

9. SPONSORING/MONITORING AGENCY NAME(S) AND ADDRESS(ES)

EOARD
PSC 802 BOX 14
FPO 09499-0014

10. SPONSOR/MONITOR'S ACRONYM(S)

11. SPONSOR/MONITOR'S REPORT NUMBER(S)
SPC 01-4074

12. DISTRIBUTION/AVAILABILITY STATEMENT

Approved for public release; distribution is unlimited.

13. SUPPLEMENTARY NOTES

14. ABSTRACT

This report results from a contract tasking ASBL Renaissance as follows: A conceptual aircraft design tool called RDS will be used in parallel with the (Royal Military Academy) RMA-developed trajectory-sizing tool. The purpose will be to analyze the variants of the Gross Weight evolution in flight using the ACES concept together with the loads existing on the aircraft and the influence on the aircraft structural design and thus its empty weight with a constant feedback into the trajectory code and the mission payload calculation. A specially designed aircraft based on civil airliner components will be used in the study. This conceptual aircraft together with its orbiter or alone has to cruise during rather long periods (2 to 4 hours). The impact of the possible aircraft volume and thus drag increase due to the high hydrogen content must be studied attentively as well as the possibility for the aircraft to reach 10 km altitude at Mach 0.75-0.80 and fly at these conditions. This analysis will be done using well-known and robust commercial software called AAA.

For cruising in these conditions, a hydrogen-fueled turbofan is almost mandatory. The feasibility study and the design of such a high by-pass ratio turbofan would also be part of this study (using the commercial software Gasturb and GSP). The LOX collection plant will also be analyzed. The simulation tool developed for the supersonic collection will be used to calculate the performance of the required collection plant in these collecting conditions. The possible icing problem of the pre-cooler will also be analyzed in these collection conditions. The sizing code developed by ERM for SSTO and TSTO with supersonic staging would be extended to study different cases of this subsonic ACES vehicle, as a three stages concept with a booster for existing aircraft or the one with large extension capabilities specifically designed as multi body (twin fuselage, e.g.) aircraft. The code will mainly test the various concepts with the results of the above-mentioned studies.

15. SUBJECT TERMS
EOARD, Aircraft Design, Aeronautics, Fuels

16. SECURITY CLASSIFICATION OF:			17. LIMITATION OF ABSTRACT	18, NUMBER OF PAGES	19a. NAME OF RESPONSIBLE PERSON
a. REPORT	b. ABSTRACT	c. THIS PAGE			Wayne Donaldson
UNCLAS	UNCLAS	UNCLAS	UL		19b. TELEPHONE NUMBER *(Include area code)* +44 (0)20 7514 4299

Part I

Pre-design of T.S.T.O.'s using subsonic in-flight LOX collection

Nomenclature

Symbols & Acronyms

ACES	Air Collection and Enrichment System
BB	Blended Body aerodynamic configuration
BPR	By-Pass Ratio
Ch_2	hydrogen consumption (kg/s)
Cox	purity of LOX (%)
CR	Collection Ratio (-)
F or FN	thrust (t)
FF	Fuel Flow (kg/s)
fcol	collected fraction (%)
HBPR	High By-Pass Ratio
ISP	engine specific impulse (s)
LBPR	Low By-Pass Ratio (BPR < 1)
LCP	LOX Collection Plant
LEA	Liquid Enriched Air
Lldg	planform loading at landing (t/m²)
LO	Lift-Off
LOGW	Lift-Off Gross Weight (t)
LOX	Liquid Oxygen
LRE	Liquid Rocket Engine
Lto	planform loading at take-off or at lift-off (t/m²)
μstr	average structure index (kg/m²)
M0ce	Mach number at collection end (-)
M0cs	Mach number at collection start (-)
Mcr	cruise Mach number (-)
Msep	separation Mach number (-)
ηsep	LOX collection plant separation efficiency (%)
Oalt	orbit altitude (km)
Oinc	orbit inclination (°)
OWE	Operational Weight Empty (t) (TOGW – Wppl or Wdry + Pay)
PAY	payload mass (t)
RTWt	vehicle thrust-to-take-off weight (-)
Spmx	maximum LOX flow in collection plant or collection plant capacity (kg/s)
SSTO	Single-Stage-To-Orbit
τ (tau)	Küchemann's parameter (-)
T	time
TIT	Turbine Inlet Temperature (K)
TO	Take-Off

TOGW	Take-Off Gross Weight (t)
TSFC	Thrust Specific Fuel Consumption (kg/daNh)
TSTO	Two-Stages-To-Orbit
T/W	engine thrust-to-weight ratio (-)
Vslp	specific volume of the collection plant ($m^3/(kg_{LEA}/s)$)
W+B	Wing plus Body aerodynamic configuration
W2	second stage mass at lift-off (t)
Wdry	dry mass (t) (also called OEW)
Weng	engine mass (t)
W_{LH2}	hydrogen mass in the orbiter (t)
W_{LOX}	quantity of LOX collected or LOX mass in the orbiter at LO for Air-Launch (t)
Wppl	propellant mass on board (or in the orbiter in case of an Air-Launch) (t)
Wslp	specific mass of the collection plant ($kg/(kg_{LEA}/s)$)
WR	Weight Ratio (-) (TOGW/OWE)

Indexes

0	relative to the entire vehicle
1	relative to the first stage
2	relative to the second stage
bcr	before cruise
col	relative to the collection phase or the collection plant
cr	during cruise
H2	hydrogen

Introduction

1. In-Flight LOX Collection TSTO's

The In-Flight LOX Collection concept (or ACES) is not a new idea but apparently a rather disturbing idea. Three main reasons can explain this situation :

- No US- or NASA stamped application has been as loudly advertised as the Space Shuttle in the 1970's or more recently like the Delta Clipper, the NASP X-30/Orient Express and the X33/Venturestar;

- Its system advantages cannot be explained or understood with the simplistic schemes that have become familiar from the literature on scramjet, high pressure staged-combustion rocket propulsion and feather light structures;

- It seems hardly compatible with the SSTO illusion.

Designing an efficient Launch System based on LOX collection demands that many of the common and oldest ways to do this kind of business, which have progressively biased the engineering imaginations, be thoroughly revised.

This ACES concept (or ***In-flight LOX collection*** as it has been called by Dr. Jean Vandenkerckhove in the first steps of the European studies) can be used to improve all possible concepts of launch vehicles : SSTO and TSTO, reusable or semi-reusable, with a large payload or not, with a launch site in CONUS or continental Europe or in Kourou.

In this chapter, the in-flight LOX collection concept will be applied to **TSTO space launchers only**. In the introduction with a supersonic collection phase and a high supersonic staging but mainly in this chapter, on an air-launch vehicle with a subsonic collection and staging. The large advantages of a LOX collection based TSTO vehicle with supersonic staging over a conventional airbreathing TSTO are thus also studied hereafter.

The collection in cruise phase is the most conservative from the point of view of the collection plant. Indeed, in this case, the inlet conditions of the collection plant (mainly at the entrance of the N_2-O_2 separator) are constant, what leads to a collection plant working always at the same conditions.

This chapter is mainly dedicated to a preliminary study of what could be a TSTO with subsonic staging (or Air-Launch option) and subsonic in-flight LOX collection. Three cases will be treated: an existing transport aircraft modified to launch a small ventrally-placed launcher, a large subsonic carrier based on existing elements of civil transport aircraft with a large ventral second stage and, finally, a large single stage orbiter (comparable to the Russian MAKS or to the British Interim HOTOL) in a piggy-back position.
It has to be very clearly notified that this **Subsonic Air-Launch RLV using in-flight LOX collection** has been identified as one of the vehicle concepts and emerging technologies to be deeply analyzed in the frame of the **NASA Space Launch Initiative starting in 2001** with a 3 millions $ contract passed to Andrews Space and Technology in Seattle (ref. 7). Along with this industry contract, the **NASA Marshall Space Flight Center** is also active on its own in

this matter (ref. 8). In this generic paper, NASA identifies also two of the three here studied options as potential candidates to reduce launch costs and limitations. Only the large subsonic carrier based on existing elements of civil transport aircraft, which is a more original concept, is not cited.

2. Comparison with no LOX collection - Problems from the vehicle side

2.1. Sänger-type TSTO with in-flight LOX collection for different staging Mach numbers

First, we want to show the effect of the separation Mach number on a Sänger-type TSTO which uses or not in-flight LOX collection. Sänger-type TSTO means mainly that the aerodynamic configuration of both stages is a blended lifting body (BB), that the first stage has a large aerodynamic reference area which is well suited for a cruise phase and that the first stage uses an airbreathing propulsion consisting of a turbojet followed by a subsonic ramjet. To collect the atmospheric oxygen, the rotary separator characteristics mentioned in the literature are used as a standard (ref. [1]). The collection ratio is about equal to 2.8 and the purity of the collected LOX is about 94%.
We want also to show the advantages of the in-flight LOX collection concept on the vehicle performance. This problem of the in-flight LOX collection for TSTO with a high supersonic separation has already been treated in references [2] & [3].

2.2. *Influence of the separation Mach number for an in-flight LOX collection vehicle*

Figure 1 shows the influence of the separation Mach number (Msep) on the TOGW and on the dry mass of the first stage[1] for a fully reusable vehicle with a blended body aerodynamic configuration (the variation of the second stage dry mass will be treated in paragraph 5). In all cases, the in-flight LOX collection begins at Mach 2 and ends at Mach 5. A cruise phase is performed at Mach 2.5 with the length necessary to insure the collection of the complete amount of oxygen (fcol = 99.5%). A flight back cruise phase is also performed at Mach 3.9 to return to the launch site (Kourou). For this calculation a turboramjet (ref. [4]) is used (turbojet from take-off up to Mach 3.5 and then ramjet up to separation). The mission is the equatorial FESTIP mission (250 km, 5° & PAY = 7 tons).
We can see on the figure 1 the large interest there is to increase the stages separation Mach number. The increase of Msep leads to a much lighter vehicle.

2.3. *Influence of the separation Mach number for a Sänger-type TSTO (without LOX collection)*

Figure 2 shows the influence of the separation Mach number (Msep) on the TOGW and on the dry mass of the first stage for the same technology level (except the collection plant) as in paragraph 3.1.2, but with a shorter cruise[2] phase. Again, we can see that, if we can reach a high separation Mach number, the dry mass of the first stage largely decreases (TOGW too) what could lead to a cheaper first stage (lower dry mass but higher heat loads and more complicated engine and air intake).

For higher staging Mach numbers (from about Mach 7.0 or bit lower), with the same vehicle structure index and the same engine index, it is possible to show with the RMA TSTO trajectory-integrated sizing code that the TSTO TOGW and the first stage dry mass re-

[1] The dry mass of the second stage increase with a decrease of Msep. But, this mass is larger in the case with in-flight LOX collection for a fixed Msep because oxygen is not pure (94%) and thus the specific impulse is lower.
[2] Indeed, a large cruise phase gives more flexibility to the vehicle but is not necessary a requirement (e.g. not in the current FESTIP requirements).

increase with Msep becoming higher. The Mach number at which this "turn" in the curve is taking place will depend on the considered assumptions. Of course, the augmentation of the Wdry1 should be higher and should occur at a lower staging Mach if, as it should be, the structure index of the 1st stage was higher and the engine mass index too with the increase of Msep (thus of the maximum airbreathing Mach number).

2.4. *Comparison of both solutions*

Figure 3 shows the variation of the 1st stage dry mass (with or without in-flight LOX collection) against the separation Mach number. We can see that, for the same 1st stage dry mass (thus a priori about the same cost), the separation Mach number is lower in the case with in-flight LOX collection than in the case without in-flight LOX collection. Therefore, the effort put into the development of an airbreathing engine will be lower in the case of the in-flight LOX collection TSTO vehicle. We can also see that, if we can collect pure oxygen (Cox = 100%), the gain in terms of dry weight is even more important. That means that, maybe, a higher effort must be put on the separator performance than on the airbreathing engine.

This is in good agreement with ideas developed by and values given by C. Johnson (CNES) for a Star-H modified for LOX collection (ref. [5]). A summary of these Star-H results is given in table 1. This table explains how in-flight LOX collection can reduce the separation Mach number for a given launcher. First of all, a calculation with in-flight LOX collection is made with the same Msep (and also the same vehicle !) and leads to a lower TOGW than the reference configuration. After that, Msep is decreased and a cruise phase is performed in order to use all the hydrogen stored in the tanks and therefore to collect the maximum quantity of LOX. We can see, in this table, the large decrease of Msep that we can expect with an in-flight LOX collection vehicle.

System definition	Reference configuration	With LOX Collection		
Msep (-)	6	6	4	3
TOGW (t)	415	350	357	367
Wdry (t)	200	211	211	211
Wppl1 (t)	100	100	100	100
Wdry2 (t)	90	90	120	170
Collection time (min)	/	20	27	38
Air flow rate (kg/s)	/	370	370	370
Collection ratio (-)	/	1.4	1.9	2.7
ηsep (%)	/	75	75	75
Wplant (t)	/	11	11	11

- STAR-H sizing (extracted from reference [5]) -
Table 1

2.5. *Influence of the aerodynamic configuration of the second stage*

In this paragraph, we want to show the influence of the aerodynamics of the 2nd stage. It is clear that if we modify the shape of the 2nd stage the dry mass of this stage will be changed too. Figures 4.a and 4.b show respectively the influence of the separation Mach number on the second stage dry mass and on the TOGW for the three BB cases studied before (respectively without in-flight LOX collection, with in-flight LOX collection when Cox = 94% & with in-flight LOX collection when Cox = 100%). We can see that the Wing+Body configuration

leads always to a larger dry mass and thus also to a larger TOGW (figure 4.b) due the additional mass of the wings. As we can see, this additional mass can be a big problem if Msep becomes too low.
Remark: the 2nd stage dry mass for the case without in-flight LOX collection is not exactly the same as for the case with Cox = 100%. This point could look amazing because both trajectories must be a priori identical. In fact the 2nd stage trajectories are a bit different due to a different mass at separation (because of different TOGW) what leads to a different time for the pull-up maneuver.

2.6. *Airbreathing engine thrust requirements*

The 1st stage engine thrust requirements and the corresponding hydrogen consumption are shown in table 2 for different Mach numbers. The separation Mach number and the TOGW are respectively 6.7 and 285 tons. We can see that we have to perform an engine throttle-down for the two cruise phases (collection cruise & come back cruise).

Mach	TO	2.2	2.5	2.5 (cruise)	3.5	3.9	3.9[3] (cruise)	6.7
F (t)	246.5	201	184	102	175	171	25	134
C_{H2} (kg/s)	30	55	50.6	37	51	49	6	75

- TOGW = 285 tons, PAY = 7 tons, rotary separator with Cox = 94% -
Table 2

2.7. *Influence of the collection method*

It seems clear that the collection plant must be designed for the cruise phase because during this phase 60 to 70% of the LOX quantity is collected. Anyway, if we want to collect also in acceleration & ascent (what is very favorable) in the Mach number range between 2 and 5, we have to know the **off-design performance** of this **collection plant** and this performance can largely influence the results.

Table 3 shows the influence of the collection cruise Mach number for a polar orbit mission (200 km & 98°) with a constant payload mass of about 2 tons from Kourou. We can see in this table that, if the cruise Mach number increases, the TOGW increases too. This is due to the fact that, if the cruise Mach number increases, the length of the cruise phase increases too and thus the return cruise phase will be longer and more hydrogen will be burned (see Wppl1). This effect is reduced by the increase of the hydrogen consumption with the increase of the cruise Mach number which allows to collect a larger mass per time unit.
Another advantage of a not too high cruise Mach number is that the heat and aerodynamic loads will be lower at lower Mach number what will be advantageous for the structure. Thus, a low cruise Mach number is recommended if the off-design working of the collection plant is acceptable.

[3] For this cruise phase, only some of the ramjet engines are used, the others are cut.

Cruise Mach number (-)	2.5	3.0	3.5
TOGW (t)	246	250	251
Collection ratio (-)	2.8	2.8	2.8
Hydrogen consumption during cruise (kg/s)	33.5	42.5	41.8
Wppl1 (t)	65.3	67.3	67.5
Wdry1 (t)	140.0	142.1	142.2

- Come back cruise at M = 3.9 - Polar mission from Kourou -
Table 3

2.8. *Conclusions from the system point of view*

First we have seen the interest of using in-flight LOX collection on the performance of a Sänger-type TSTO. By comparing both solutions, we have noted that LOX collection is a good solution to reduce the separation Mach number and thus to reduce the technology effort on the 1st stage airbreathing engine. A short ramjet phase between Mach 3.8 and 5.0 appears indeed to be feasible.
We have also shown that, due to the not pure collected oxygen, the second stage dry mass is larger in the case of the in-flight LOX collection but this increase is low in comparison with the gain on the first stage dry mass (for a constant payload).
We have also checked the influence of the aerodynamic configuration of the second stage by trying a less advanced configuration (Wing+Body) with in-flight LOX collection. Even if this solution leads to a heavier second stage dry mass, we obtain for a not too low Msep a better result (lower TOGW) than in the case without LOX collection using a Blended Body aerodynamic configuration for both stages.
It is also shown that the influence of the cruise collection Mach number Mcr on the vehicle (system) performance is not large. It is more its impact on the collection plant and, mainly, on the turbofan performance which must be more deeply studied. For the engine and the collection plant, we have proposed to look at two extreme cases : Mcr = 2.5 & Mcr = 3.5.
About the problem of the cruise Mach number choice, we can say that, at a vehicle level, a low supersonic cruise/collection Mach number is favorable[4]. Thus a selection of about Mach 2.5 seems very attractive.

3. Conclusions

It has been shown that the LOX collection concept can be very efficiently used to improve the performance characteristics of high speed staging fully reusable or partly reusable HTOHL TSTO's but the whole system remain complicated even if the ACES concept could be used in a way to decrease the staging Mach number.
In this study, the ACES concept will be applied in a much easier way, with a much lower staging and a much lower cruise collection Mach number as it will be applied at a subsonic speed with a subsonic staging.
The 1st stage airbreathing engine is a hydrogen-fueled HBPR turbofan used from take-off up to Mach 0.75-0.8. The collection plant is not highly integrated with the propulsion plant and collects in cruise at a reasonable Mach 0.75.

---

[4] It must also be added that this cruise Mach number choice can be driven by the off-design working performance of the collection plant that will be studied later.

References

1. J. Leingang, L. Maurice et al. , “In-Flight Oxidizer Collection Systems for Airbreathing Space Boosters”, Developments in High-Speed-Vehicle Propulsion Systems, Vol. 165, Progress in Astronautics and Aeronautics, AIAA, November 1996.
2. P. Hendrick & M. Saint-Mard, "Sänger-type T.S.T.O. using in-flight LOX collection", Joint Propulsion Conference, Seattle, 6-9 July 1997.
3. P. Hendrick & M. Saint-Mard, "ACES Sänger-type T.S.T.O. family with common first stage", Joint Propulsion Conference, Cleveland, 13-15 July 1998.
4. J. Kretschmer, "Konzeptuntersuchung –Antrieb –", MTU report for Sänger study, Munich, December 1992.
5. C. Johnson et al., "Propulsion System Using Deep Cooled Air, Liquefied Air or Oxygen Collection", AAAF, Paris, 22-24 May 1996.
6. OHB System, Report FSS-OHB-SC-2130-001, 28 March 1995.
7. F. Morring, “NASA’s Space Launch Initiative contracts”, AWST, 28 May 2001.
8. K. Sorensen & J. Blevins, “Air Launch and LOX Collection as enabling technologies for Future Launch Systems”, AIAA 2001-3520, JPC, Salt Lake City, 8-11 July 2001.
9. M. Caceres, “Space Mission model 2001-2010”, Aerospace America, June 2001.

Influence of Msep for an in-flight LOX collection vehicle

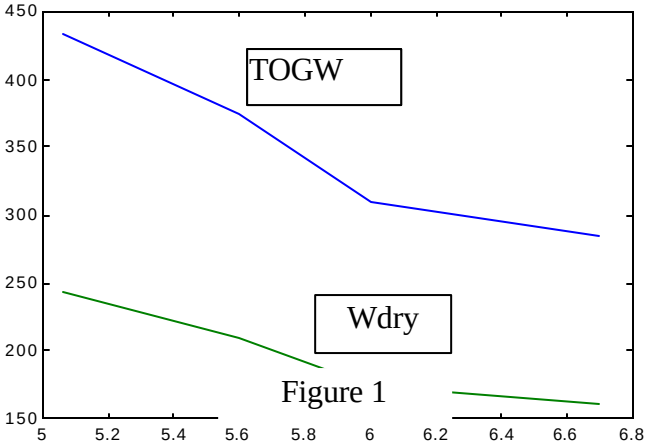

Figure 1

Msep (-)

TOGW & Wdry1 (t)

Influence of Msep for a TSTO without using in-flight LOX collection.

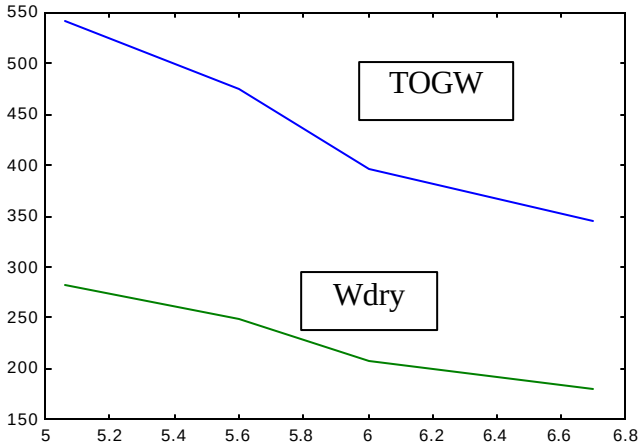

Msep (-)

Figure 2

Msep (-)

Without LOX collection

Cox = 94%

Cox = 100%

With LOX collection

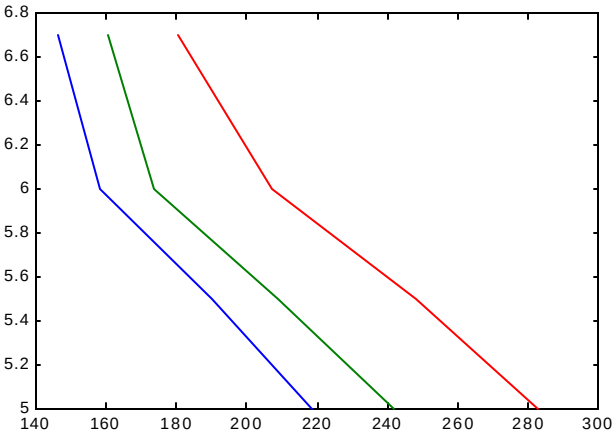

Wdry (t)

Figure 3

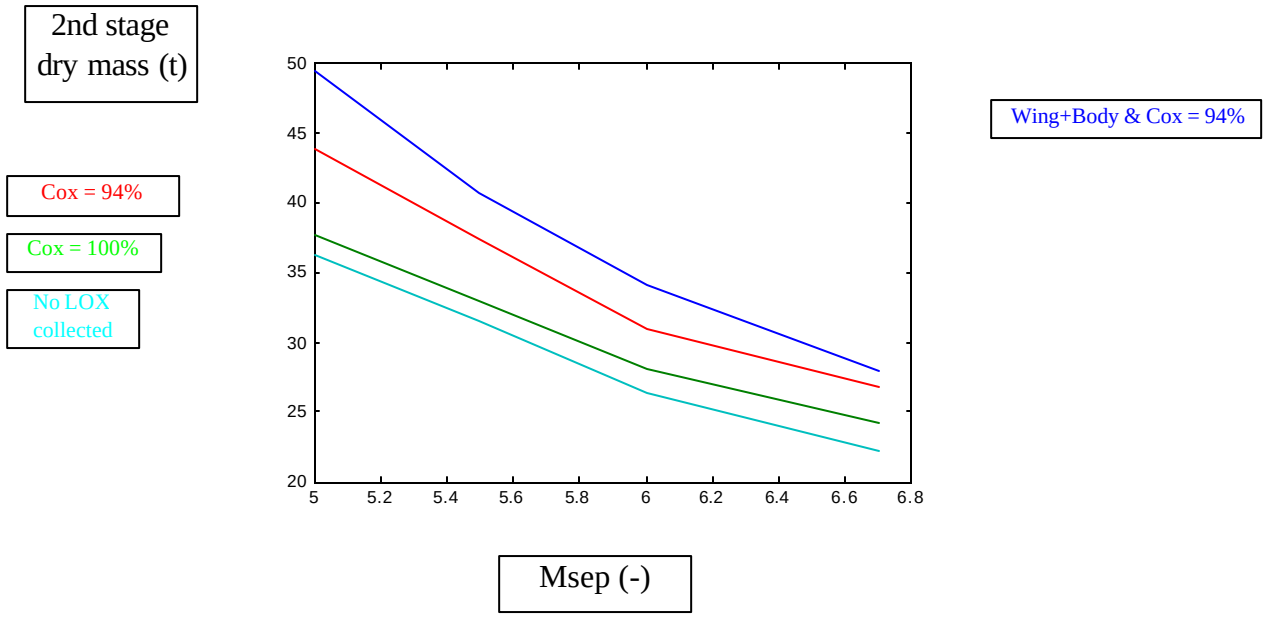

Figure 4.a

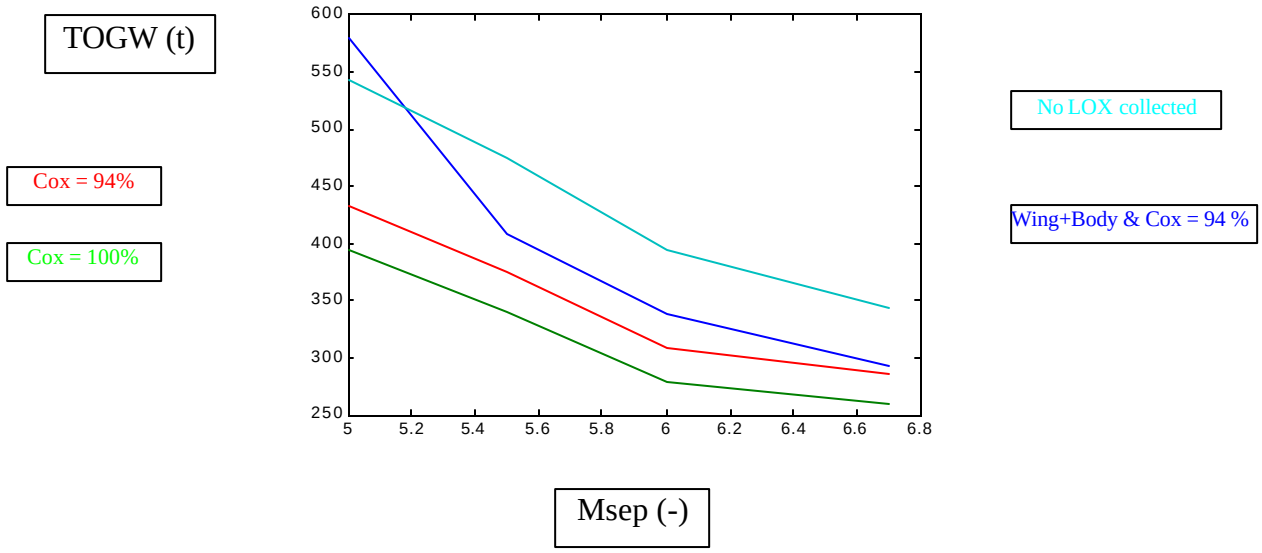

Figure 4.b

In-flight LOX collection for a TSTO with subsonic staging

1. **Introduction**

The subsonic air-launch option is a very attractive solution to improve the performance of an all-rocket space launcher or of a spaceplane (see the current Kelly Space's Astroliner project, ref. 1). The upper part (for a piggy-back configuration) or the lower part (for a ventral configuration) of the launcher is then an orbiter (without or with a booster) which is in fact an all-rocket SSTO vehicle which takes off "horizontally" from an altitude and a Mach number of respectively about 9 km and 0.8. The air-launched case shows significant reductions in ascent ΔV and ΔV losses compared to sea-level launched case : about 1.000 m/s (see also ref. 16). This orbiter can have a Winged Body aerodynamic configuration or a blended body. It can also be fully reusable, semi-reusable (reusable orbiter with an expandable external tank or booster) or fully expandable. This type of concept has already been studied in the United Kingdom with the Interim HOTOL, in Russia with MAKS and in the US with Pegasus (in this case, for a small payload only).

In this chapter, we want to show that using in-flight LOX collection during a subsonic cruise (thus the Lox-Collection-Plant (LCP) is in the subsonic carrier) can be a very interesting solution to make the air-launch option more secure but also to increase the launcher performance.
Most frequently the in-flight LOX collection launch vehicle concept analyses deal with advanced SSTO or fully reusable TSTO and thus the LCP must be extremely light and thermodynamically efficient. Moreover, the purity of collected oxygen, euphemistically called liquid "enriched" air (LEA), must be very high. These requirements oriented researches toward complex thermodynamic cycles, pushing the concept into the field of very long term, advanced, expensive and risky developments. This image should now change: some remarkable and **affordable synergies** can be developed between fully feasible Lox-collection concepts and equally feasible air-breathing propulsion systems, provided **semi-reusable launch vehicles** are considered (ref. 2).
This chapter presents typical applications, ranging from a low-cost operational demonstrator program with a standard subsonic carrier up to a large orbiter launched from a specific subsonic carrier. All of these concepts provide the advantages of an air-breathing first stage cruise together with horizontal take-off and landing that allow to operate from almost anywhere in the world, but without the technical challenges of scramjet, advanced ramjet or sophisticated high Mach turbojets.

These examples illustrate how LOX Collection is a highly synergistic technology as the various components that have to be improved or newly developed will find applications in other fields of daily economic activity. LOX collection increases payload mass in orbit and improves launch flexibility simultaneously. It offers a wide variety of solutions that can bridge the gap between fully expendable vehicles and also future fully reusable
concepts that have yet to be defined, to prove their operational advantages and demonstrate that they can achieve a reasonable Return-on-Investment.

Designing an efficient Launch System based on Lox-collection demands that many of the common and oldest ways to do this kind of business, which have progressively biased the engineering imaginations, be thoroughly revised.

Qualitative arguments are far from being enough to draw long term conclusions on the feasibility and economics of this concept but the full computation of a supersonic carrier TSTO is not an easy task. Sensitivity to parameters like air intake definition, dynamic pressure limits, air-breathing cycle optimization, to quote only a few of them, is critical. The final results may be completely changed by minor modifications that are sometimes nearly unnoticed. Another consequence is that results from independent analyses need to be compared on a whole set of parameters, and with the most extreme precautions, to avoid major errors. The resulting volume of computations is huge and costly, in particular when experimental data cannot help to reduce the scope of parametric investigations.
Conversely, airborne launch vehicles with subsonic carriers can be assessed with relatively "simple" analyses because of much looser interactions between parameters.

One of the objections commonly raised against LOX collection is that not much is known on the feasibility of N2/O2 separation in the operational conditions of a flying plane. This is why the analyses presented in this study are based on assumptions rather less glamorous than usual:

- The reference recovery factor **(**h_{sep}), fraction of atmospheric oxygen actually recovered, is 75%. This goal is felt to be well within the possibilities of the rotary separator, in particular when no stringent weight or volume limitations prevent the design of a two-stage separator and/or the installation of additional heat-exchangers.
- The reference purity (**Cox)** of collected LOX (or LEA) is 90%. The sensitivity of system definition to this parameter is indicated.
- The reference collection ratio (**CR**) , mass of collected LOX per unit mass of hydrogen, is set at CR = 3.0 (see §2 hereafter). Optimization of this parameter is heavily dependent on the type of carrier and on other mission requirements. This problem is addressed for the various examples presented.

Specific weight of the plant (weight of the installation per unit mass of intake air or unit mass of oxygen collected) is not a critical parameter **for multi-stage semi reusable concepts.** This feature is of major importance because more allowable weight means easier improvements of CR, η_{sep} and Cox.

Some nay-sayers often put forward the development cost of a large special carrier plane as a major objection, generally without any serious demonstration. However, the successive developments of the Guppy, Super-Guppy and recently Beluga cargo planes have fairly well demonstrated that this argument has no real weight provided designers abide two basic rules:

- The launch vehicle (LV), be it expendable or partially reusable, must be assembled **below** the carrier plane, allowing simple (ventral) launch and fully natural separation., with adequate aerodynamic margins. Zero-G maneuvers that are sometimes mentioned should rather be qualified "stunt pilot demonstrations" when the L.V area loading is well in excess of 1000 kg /m² while it falls instantly far below 400 kg /m², on a swept wing of excellent lifting qualities, not to mention the fact that the released LV represents 30 to 60 % of the mass of the composite just before separation.
- The few planes that will be required, even if a successful diversification in out-sized cargo transport is achieved, impose to design this plane with as many cannibalized parts as possible, avoiding any specific development of wings, tail-planes, actuators, landing gears, engine nacelles, crew fuselage, etc. that would not be necessary or economically

justified. There are now plenty of hardware available, world around, to make this challenge a realistic one.

The reference 2 underscores the synergies that can be developed around Lox-collection. Everyone of the technologies that contribute to build the proposed systems has its own independent justifications. Hydrogen fuelling of turbojets and turbofans, in particular, is hardly imaginable if generalized to the whole commercial fleet but it will make possible extremely long range or long duration missions. Electric large power plants could also burn hydrogen rich by-products. More powerful and compact heat exchangers will easily find other applications when available to the engineering community. Airborne space launching has evident and practical advantages that are magnified when combined with Lox-collection.

Air Collection and Enrichment System (ACES) for, what they call, the *"Alchemist TSTO"*, i.e. an air-launched all-rocket concept with subsonic staging and collection with Cox = 90%, is also receiving a lot of attention in the NASA SLI program. This *"Alchemist TSTO*" shows a lot of points very comparable with the present RMA concept(s) (ref. 18).

2. **The Lox-Collection Plant (LCP)**

The collection ratio (CR) measures the global thermodynamic efficiency of the LCP. The oxygen purity (Cox) and the recovery factor (ηsep) measure the efficiency of the separation process. All of them essentially depend on the thermodynamic processes which can be implemented, on whether Lox-collection takes place at subsonic or supersonic conditions, on the selected separation process and other contingencies that can derive from vehicle integration.
The physical characteristics, mass and volume or specific mass and volume per unit flow-rate of intake air or collected oxygen, depend of the same parameters but also on the design freedom which is offered by such or such particular application. As already mentioned in the introduction, SSTO or fully reusable TSTO demand the maximization of nearly all of the above defined parameters and make it a real challenge, while partially reusable multistage concepts relax very much these constraints and contributes to its feasibility and affordability.

Figures 4.1 and 4.2 illustrate a typical flow-diagram of a LCP in subsonic collection conditions (at Mach 0.8 and, respectively, 10 and 12 km altitude). The critical components are the heat-exchangers, in particular the most upstream one or pre-cooler, the compressors and the separator(s). A CR of at least 3.0 appears to be feasible (respectively 3.21 and 3.06 in figures 4.1 & 4.2).

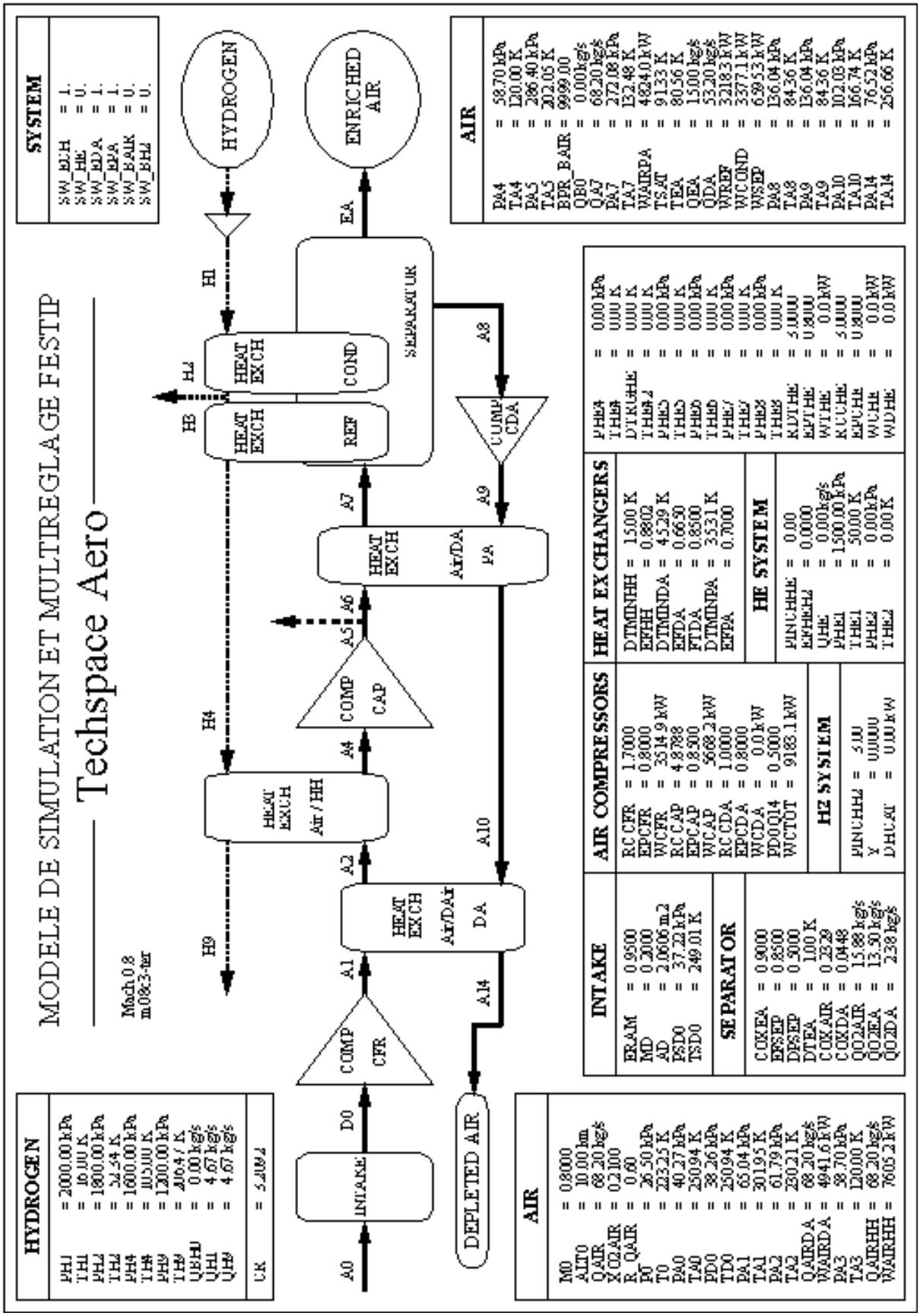
MODELE DE SIMULATION ET MULTIREGLAGE FESTIP
Techspace Aero
Mach 0.8
m08x3-ter
HYDROGEN
ENRICHED AIR
DEPLETED AIR
UNIFARE
COMP CFR
HEAT EXCH Air/DAir DA
HEAT EXCH Air / HH
COMP CAP
HEAT EXCH Air/DA PA
HEAT EXCH REF
HEAT EXCH COND
SEPARATOR
COMP CDA
SYSTEM
AIR
HYDROGEN
INTAKE
AIR COMPRESSORS
HEAT EXCHANGERS
SEPARATOR
HE SYSTEM
H2 SYSTEM

Figure 4.1

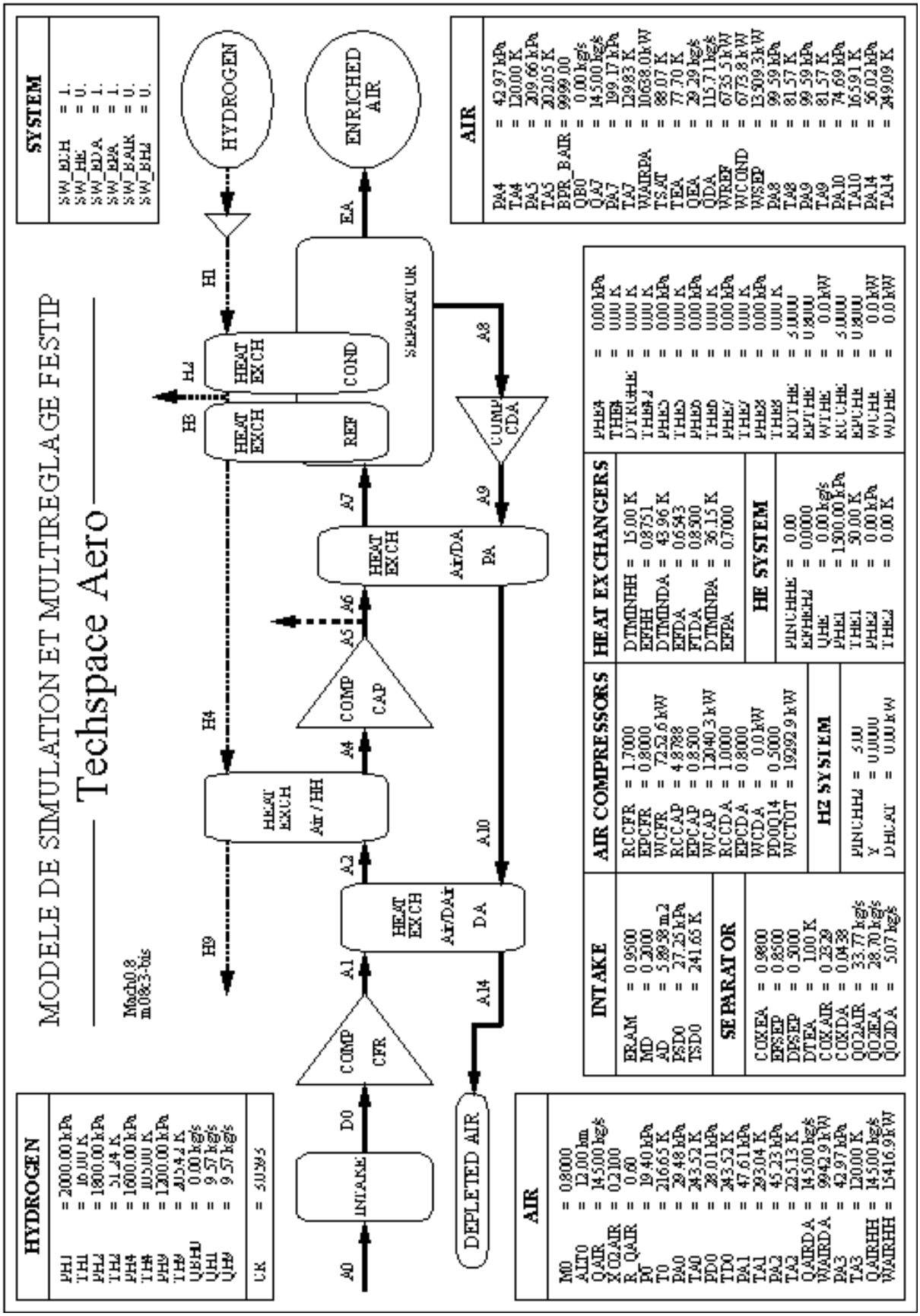
MODELE DE SIMULATION ET MULTIREGLAGE FESTIP
Techspace Aero
Mach0.8
m08x3-bis
SYSTEM
HYDROGEN
ENRICHED AIR
AIR
HEAT EXCH
COND
REF
Air / HH
COMP
CFR
CAP
Air/DAir
DA
Air/DA
PA
CUMP CDA
SEPARATOR
HEAT EXCH
DEPLETED AIR
INTAKE
AIR COMPRESSORS
HEAT EXCHANGERS
SEPARATOR
HE SYSTEM
H2 SYSTEM

Figure 4.2

Many different combinations can be envisaged during the design / optimisation process and the volume of computations swells rapidly. Techspace Aero (Belgium) has developed (in ESA FESTIP program) a very flexible code which solves the full set of equations describing a LCP. Subroutines help in the design of its components and in the estimate of heat-exchangers masses which account for the largest share of the mass breakdown.
The examples of figures 4.1 and 4.2 (CR a bit higher than 3.0 with ηsep = 85% and Cox = 90%) apply to LOX-collection at stationary subsonic conditions (Mach 0.8/cruise). Another example at Mach 2.5 is given in reference 4 where the calculated global efficiency (CR = 3.35) assumes that ηsep = 85% and Cox = 98%, two very high figures expected to be achievable with two-stage vortex-tube arrays. Assuming the much lower ηsep = 65% and Cox = 90% that have been reportedly achieved 30 years ago (Ref. 3 and 5), the same plant would nevertheless achieve CR = 3, however at the cost of a heavier weight deriving from the higher air flow-rate to process for the same LOX flow-rate.
When Lox-collection takes place at subsonic conditions (e.g., M 0.8 and 10 km altitude) a higher compression ratio or an additional compressor has to compensate for the lower intake dynamic pressure. One good solution, among probably some others, is to insert a low pressure fan ($\pi \approx 1.7$) between the intake and the pre-cooler and add an other compressor ($\pi \approx 5$) behind the pre-cooler. This will add a lot of kilograms and specific weight may be increased by a factor 2 to 2.5.

By comparison, collecting at high supersonic / low hypersonic conditions provides plenty of dynamic pressure but higher stagnation temperature requires to build the pre-cooler of heavier materials.

The scheme of Fig. 4.1 does not feature a helium additional loop which could serve two purposes: safety (by preventing any mixing of air and hydrogen) and a better thermodynamic efficiency as proposed in reference 6 for some Rocket Based Combined Cycles (RBCC).

A detailed comparison of these examples is beyond the scope of this short subsonic study which aims at underscoring the “system” benefits of Lox-collection. Published experimental data on O2/N2 separation are too few, many uncertainties or unknowns remain on heat-exchangers efficiencies and even low temperature turbo-machinery to allow for a set of precise figures to be fixed. This is why the reference data used in the hereafter system analyses will appear rather pessimistic, compared to what is usually assumed in most paper dealing with LOX collection or RBCC applied to SSTO or fully reusable TSTO (ref. 4).

Three subsonic cases are presented in the next pages :

a. A converted subsonic carrier (available on the market as a first shot) with an expendable 2^{nd} stage in a ventral configuration;

b. A large special design subsonic carrier (based mainly on cannibalized elements from existing carriers) with an expendable 2^{nd} stage in a ventral configuration;

c. An Interim HOTOL-type ACES TSTO with a reusable or an expendable 2^{nd} stage in a piggy-back configuration.

As already said earlier in this chapter, this ACES TSTO concept with subsonic collection and staging is since mid 2000 studied in details at system level and at the components technology level in the US by Andrews Space and Technology under NASA contracts (SBIR followed by

SLI). They call this concept the “Alchemist TSTO” and claim a reduction of the TOGW by a factor 4 compared with a VTO TSTO for the delivery of 20.000 lbs to ISS (ref.).

3. Converted subsonic carrier

Converting an existing jumbo-jet at reasonable costs implies that a long list of constraints must be respected. Lockheed and MDD tri-engines planes would have advantages (in particular a low acquisition cost) but the middle engine precludes the convenient installation of an external LH2 tank above the fuselage. In addition, their cargo capacity is much lower than what a B.747 allows to carry (~ 60 t versus ~ 90 t). Thus a B.747 offers more payload potential, more flexibility for modifications and finally appears as a better global choice. For simplicity, this will be the only case hereafter considered.

3.1. Initial mass of launch vehicle

It results from the combination of maximum cargo load of the plane, available volume below fuselage, authorised positions of C.G., weight of the Lox-Collection plant (LCP), and mission range.

Landing gear definition severely limits the diameter of tanks as well as overall length and overall width of the L.V thus forbidding LOX/LH2 propulsion. LOX/Kerosene is the best next choice – for performance, safety, environment protection - and oxidiser will contribute to ~ 70 % of propellant load and to more than 60 % of L.V initial mass.

Available volume below a B.747 fuselage allows to design a ≈120 t (total) initial mass L.V., what largely exceeds the maximum capacity of the plane if Lox-collection is not implemented. Actually in this latter case, after accounting for launch crew and on-board launch equipment, mechanical systems to carry and release the L.V., local reinforcement of the plane’s structure, propellant carrier-tanks, C.G. position, etc… the maximum initial mass of L.V is ~ 70 t, achieving 50 % only of what could be put in orbit with a 120 t L.V. Lox-collection saves weight on the 77 t of LOX that would have to be loaded on ground but the exact magnitude of this benefit will depend on the design and optimisation of this system together with how far it can be integrated with the turbofan feed system.

3.2. Mass comparisons

A simple Lox-collection, i.e. without feeding the turbofans with hydrogen, already produces such significant mass savings that it becomes possible to carry the largest L.V. compatible with the plane’s geometry restrictions.

The figures of Table 4.1 have been derived assuming relatively conservative performances of the LCP :
- C.R. = 3 which determines the required mass of LH2, thus the mass of storage tank and associated equipment;
- η_{sep} = 75 % which determines the air flow rate in the LCP;

- Cox = 90% purity of collected "enriched air", which determines the performance of the launch vehicle.

(All masses in Mg)	LOX-Collection	No LOX-Collection	Comments
Loaded LOX	**0**	**77**	
Required LH2 Mass	**26**		
Carrier storage tanks		**0**	
LOX*		**20**	Safety and CG requirements
LH2	**10**	**0**	
LCP Mass	**3,5**	**0**	
LCP operators	**1,5**	**0**	3 people and control equipment
Total for LOX "kit"	**41**	**97**	
Total Propellants in LV	**125**	**110**	14% delta mass for Cox = 90%
LV without oxidiser	**49**	**43**	
Required capacity at TO	**90***	**140****	*L.V + LCP **L.V + LOX tank

*The L.V must be empty during take-off and initial climb, otherwise shocks and vertical or transverse accelerations would exceedingly penalise the L.V structures. Safety would also be compromised with a fuelled L.V in case of aborted take-off or early engine failure.

Table 4.1 – Estimated mass budgets of alternative systems

The maximum standard cargo capacity of a B.747 is ~ 110 Mg (take-off) and adaptations for airborne launching (crew, structural adaptations, release mechanism, etc…) will eat ~ 10 Mg of this capacity. The remaining 100 Mg are quite adequate when Lox-collection is implemented; without this option the initial mass of the L.V must be much lighter and payloads will be much, much lighter.
Total mass of the plane will initially decrease during climb to altitude and then start increasing when Lox-collection starts. Assuming 30 to 40 t (3,5 hours) of kerosene are burnt up to the end of collection the total mass just before L.V. release will be 17 to 27 t heavier than at take-off, exceeding the standard Maximum Zero-Fuel Weight (MZFW) limit; it must be checked that this value is compatible with the actual structural limits and the Certification of the plane as these conditions will be existing for not more than 1 to 2 hours, at the lowest specified turbulence conditions and probably not more than a few dozens times a year.

3.3. LOX collection plant optimization

As already mentioned in the introduction, the subsonic carrier requires a particular optimisation of the LOX collection system.
The Operational Empty Weight (O.E.W.) of a converted B.747 will be ~ 190 t and its kerosene burn-rate 8 to 10 Mg/hour at cruise conditions. If hydrogen is plainly dumped after exiting the LCP it might seem advantageous to design this LCP for a higher flow-rate and shorter collection time. For example, adding a 3.5 t. L.C.P for a one hour shorter collect phase produces about 6 t. net reduction of T.O.G.W. This elementary analysis must be corrected to take into account the highly desired operational flexibility, a major "plus" of airborne launching, that requires a minimum distance can be flown from the take-off airport to the selected launch point. The smaller [flow- rate] LCP can be actually a better choice.

Optimisation is more complex when hydrogen also feeds the turbofans. The equivalent of the 8 to 10 Mg/hour of kerosene is 3 to 4 Mg/hour of hydrogen and thus the LOX flow-rate will be more or less strictly determined by the burn-rate of the turbofans. When CR is as good as 3, LOX flow-rate will vary from 9 to 12 t / per hour, requiring 6,5 to 8,5 hours to collect the full load (77 Mg) of Lox and allowing take-off ≈3000 to 4000 N.M away from the L.V release point. If this range is to be never required, one conclusion could be that not much effort need to be spent to reduce drag (L.V./plane interaction, intake drag of the LCP, etc.) or to integrate the power generation of LCP with turbofans for a better efficiency. Conversely, a higher CR makes it possible to accumulate distance at the most favourable flying conditions, just after take-off when gross weight is lighter, and thus achieve a ≈500 N.M range extension. Improving C.R. has an other advantage: a smaller LH2 storage tank means simpler and normally cheaper transformations of the plane.
A low recovery factor (ex: η_{sep} = 50%) has a relatively low impact as it essentially increases the mass of the LCP (3.5 Mg out of 190 Mg. O. E. W) which has to be designed for a higher air flow rate.
LOX purity (Cox) decaying from 90 % (reference goal) to a low 85 % will induce an additional 7s. loss on the Isp, (less than 3%), and require less than a 5 % increase of propellant mass for the same ΔV, a negligible drawback when compared with the other advantages of Lox-collection.

4. Large special design subsonic carrier

The next to come development of very powerful turbofans (115.000 lbf., maybe even more) and of the large twin engine planes they will power make it possible to consider jumbo carriers that could be derived at moderate development costs and risks for airborne space launch.
The Molnya company (F.D.R) has been proposing such kind of plane (the HERAKLES-1000) for 5 years now, announcing a 450 Mg maximum cargo capacity for this 900 Mg. GTOW special design plane, powered with conventional kerosene fuelled turbofans of P&W-4084 class. Using such kind of plane for airborne launching and the full development of synergies between LOX collection and hydrogen fuelled turbofans would raise to unsuspected summits the advantages already identified at the scale of a B.747 (in §3).
The advertised data for HERAKLES-1000 (Jane's 98-99) are summarised below:

G.T.O.W : ~ 900 t
Engines : 6 × GE90 class
O.E.W : ~ 300 t
Max fuel capacity : 360 t kerosene
Range with Max. PL (450 t): > 1 200 NM
Range with max fuel & 240 t PL : > 4 000 NM

4.1 Hydrogen burning turbofans

Substituting hydrogen to kerosene (see § 6) will drastically reduce the equivalent maximum fuel mass from 360 Mg down to less than 140 Mg but the volume is multiplied by a factor 4.5 and LH2 cannot be stored in conventional wings tanks. A twin fuselage rather than a twin-boom-like (Herakles) fuselage architecture will be needed (see figure 4.3 and ref. 7).

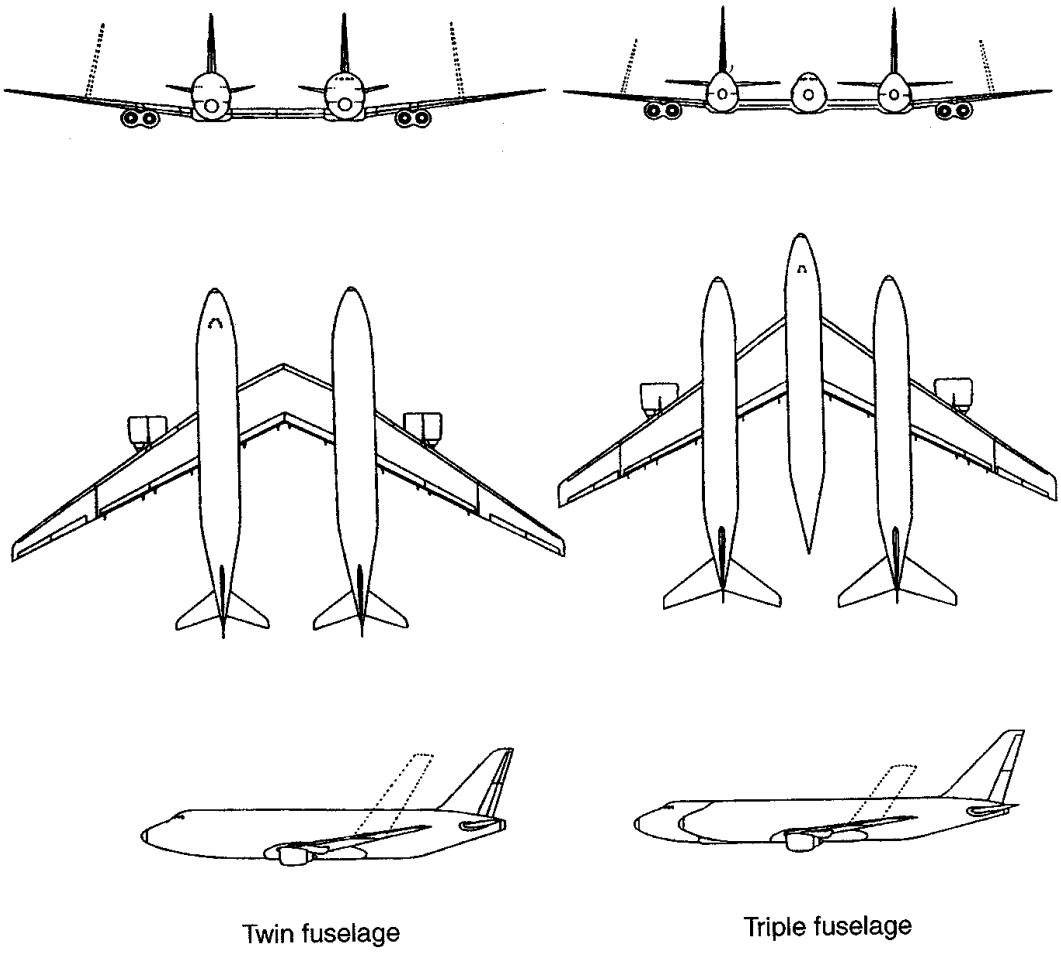

Figure 4.3 Twin or Triple fuselage large airplanes

Fifty percent (70 Mg), at least, of this LH2 load can be used to collect 210 Mg. of LOX with the same CR = 3.0 assumed in §3. That would authorize to design a 300 Mg. initial mass LOX/LH2 LV of more than 360 Mg. with LOX/Kerosene propulsion.(configurations C and D in Table 4.2). An improved LCP achieving CR = 4 would similarly allow to collect 280 Mg. of LOX and launch much heavier vehicles.(configurations E and F). Increasing the percentage of LH2 used for Lox-collection (earlier operation and/or shorter flight after LV release) would also provide a significant increase of the LOX mass available, whatever the CR achieved. Configuration (G) illustrates this point with 58% of the LH2 load instead of 50%.

4.2 LOX-Collection flow rate

Maximising the total mass of collected LOX introduces an important operational constraint : flow-rate is strictly proportional to the burn-rate of the turbofans. As an average hydrogen burn rate of ≈10 Mg/hour can be expected the maximised Lox-collection will extend over ≈7 hours. One of the deriving advantages is the possibility to take-off as far as 3.600 NM away from the selected L.V release point. One drawback could be to have to loiter for a few hours

around the L.V. release point until the required mass of LOX has been collected. In fact, operational flexibility will be provided with additional LCP modules and dumping the hydrogen that is not burnt by the turbofans.

4.3 Mass comparison

Table 4.2 summarises a series of data that have been estimated with 4 different sets of assumptions :

- with kerosene fed turbofans and without LOX collection
- with hydrogen burning turbofans and with the number of LCP-modules required to collect within less than 4 hours
- same as above but with an improved LCP achieving CR = 4.0 (at the cost of a 100 % increase of its mass)
- same as above but with Lox-collection beginning earlier, allowing a larger (58%) share of the LH2 load to be used for Lox-collection.

To simplify the presentation and discussion, the Empty Operational Weight (O.E.W) of the basic plane is kept constant. Consequently the mass of hydrogen (to collect oxygen and feed the turbofans) is also constant. As expected Lox-collection provides spectacular reductions of the GTOW, even after part of the gross reduction has been used for a heavier but more efficient LCP to collect more LOX. It would be possible to push the performance even further up, beyond configuration (G) of Table 4.2, and still remain well below the 900 Mg GTOW limit, but other advantages seem to be preferred:

- more opportunities to reuse structures and parts from ageing aircraft;
- not more than 4 engines;
- shorter take-off distance;
- acquiring experience progressively with increasing LH2 loads, etc.

	Conven tional		**H2 fed eng.// basic LCP**		**H2 feed** and **impr. LCP**		
(All masses in Mg)	**(A)**	**(B)**	**(C)**	**(D)**	**(E)**	**(F)**	**(G) ***
LV propulsion	LOX/LH2	LOX/KER	LOX/LH2	LOX/KER	LOX/LH2	LOX/KER	LOX/LH2
CARRIER PLANE							
OEW (basic)	300	300	300	300	300	300	300
Fuel							
Kerosene	290	230					
LH2			140	140	140	140	140
GTOW	900	900	540	596	575	646	591
Weight at LV release	687	725	652	708	757	828	817
LOX. COLL. PLANT							
System	0	0	10	10	20	20	20
LOX mass collected	0	0	210	210	280	280	324
LAUNCH VEHICLE							
LV at release	300	356	300	356	395	466	455
LV mass at take-off	300	356	90	146	115	186	131
Propellants (total)	245	300	245	300	326	400	378
Mission Range (NM) **	3200	2500	5000	4500	4500	4000	4500

* Common hypothesis is 50% of LH2 used for Lox-collection but 58% for configuration (G).
** Distance from take-off to release point. // 20% of fuel burnt before LOX-collection phase.

Table 4.2 – Mass comparison of various possible design possibilities

A tentative attempt to picture such a large twin fuselage subsonic aircraft (with or without any smaller central fuselage) is done with figures 4.4, 4.5 and 4.6.
The two side fuselages are large liquid hydrogen tanks based on the fuselage of the Boeing 777-300 (length = 73.86 m). The central fuselage (if present) is based on the Airbus A321 (length = 44.51 m). Engines are GE90-type turbofans (GE90-75B or GE90-98B) fueled with hydrogen.

The first configuration is with a central fuselage where the pilot crew, the collection plant and the technical crew for the LCP are located. Two of the four engines are at the same position as on the B777-300 and the two others are placed above the rear part of the central fuselage. That means a reduced Ram Recovery (as high as 5% losses in cruise flight) for these two engines and thus a lower performance (nevertheless, this position is also selected for the Aerospatiale Matra's blended-wing proposal for new airliners of the next century).
In the second configuration, the two "middle" engines are placed on the forward central wing box instead of the rear and their inlets are in front of the wing leading edge, improving much the turbofan Ram Recovery. This location allows also to use the exhaust jet to increase the lift of this wing box and thus reduce the take-off distance as tested on the YC-14 by Boeing (ref. 15). Nevertheless, this construction is certainly more advanced and more difficult to build but it offers a few interesting advantages.
The third configuration has no central fuselage. The crew and the LCP must be located in one of the side B777 fuselage, thus an asymmetric position for the pilots, what could be annoying. The four engines are here placed in pairs under a new pylon (a twice higher thrust is transmitted to the wing) which is placed a bit more near the wing tip. The two engines on each side could also be installed in a common nacelle.
Other configurations are also possible and a more detailed study of each one would be necessary to analyze the pro and cons of the different candidates.

The second stage is an all-rocket vehicle which could be like the one pictured on figure 4.7 or the 2nd stage given on the figure 4.8. The vehicle of figure 4.7 is not a winged-cylindrical body configuration like on figure 4.8. It is a very efficient rocket-derived powered hypersonic glider based on the FDL-7 series of hypersonic gliders developed and tested by A. Draper and M. Buck at the Flight Dynamics Laboratory in the '70's in the USA. This craft shows high aerodynamic performance. The hypersonic lift-to-drag ratio is in excess of 2.7, what means a very large unpowered cross range (a few thousands of km) and a down range of the order of the earth circumference. This craft can thus depart from any low altitude orbit in any location and land in Europe. This vehicle is stable over the entire glide domain.

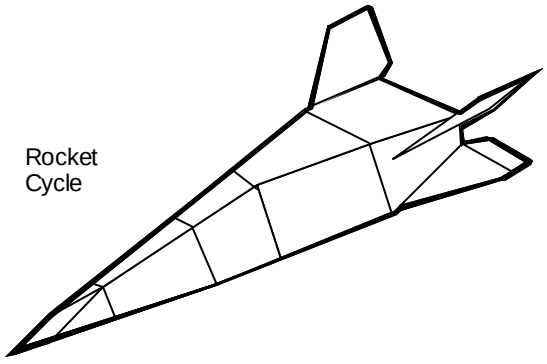

All-rocket 2nd stage launch vehicle
Figure 4.7

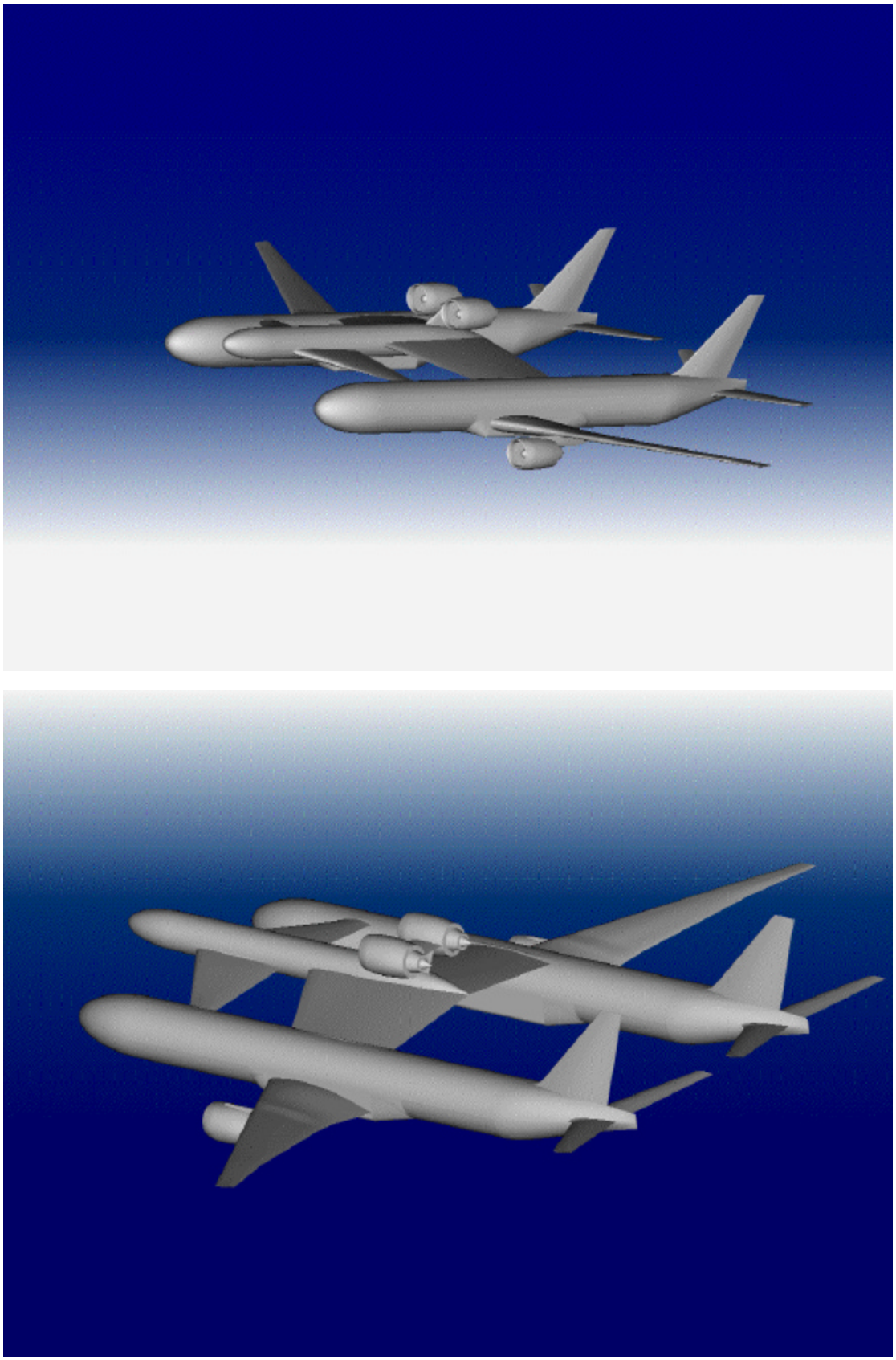

Figure 4.4

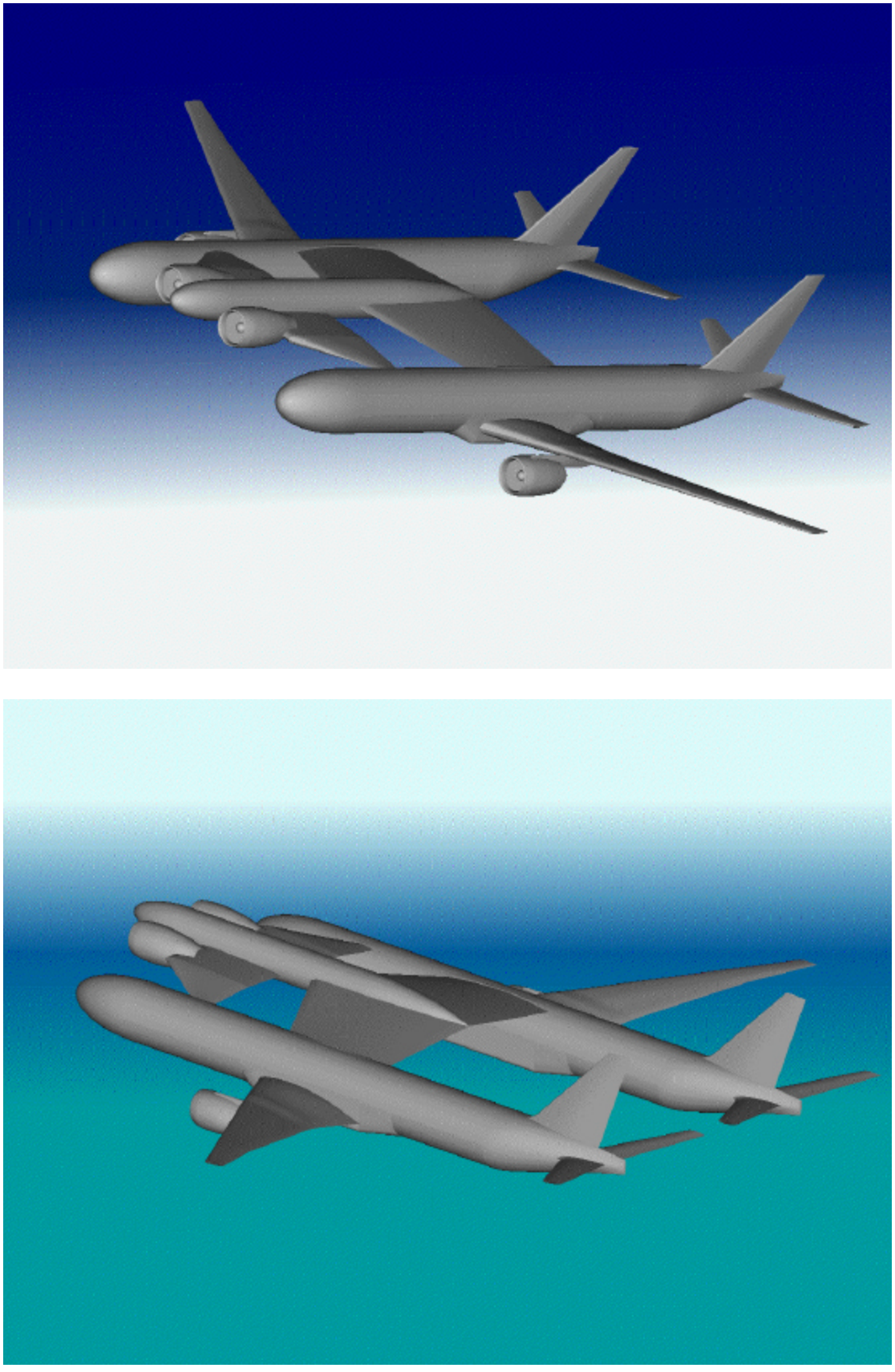

Figure 4.5

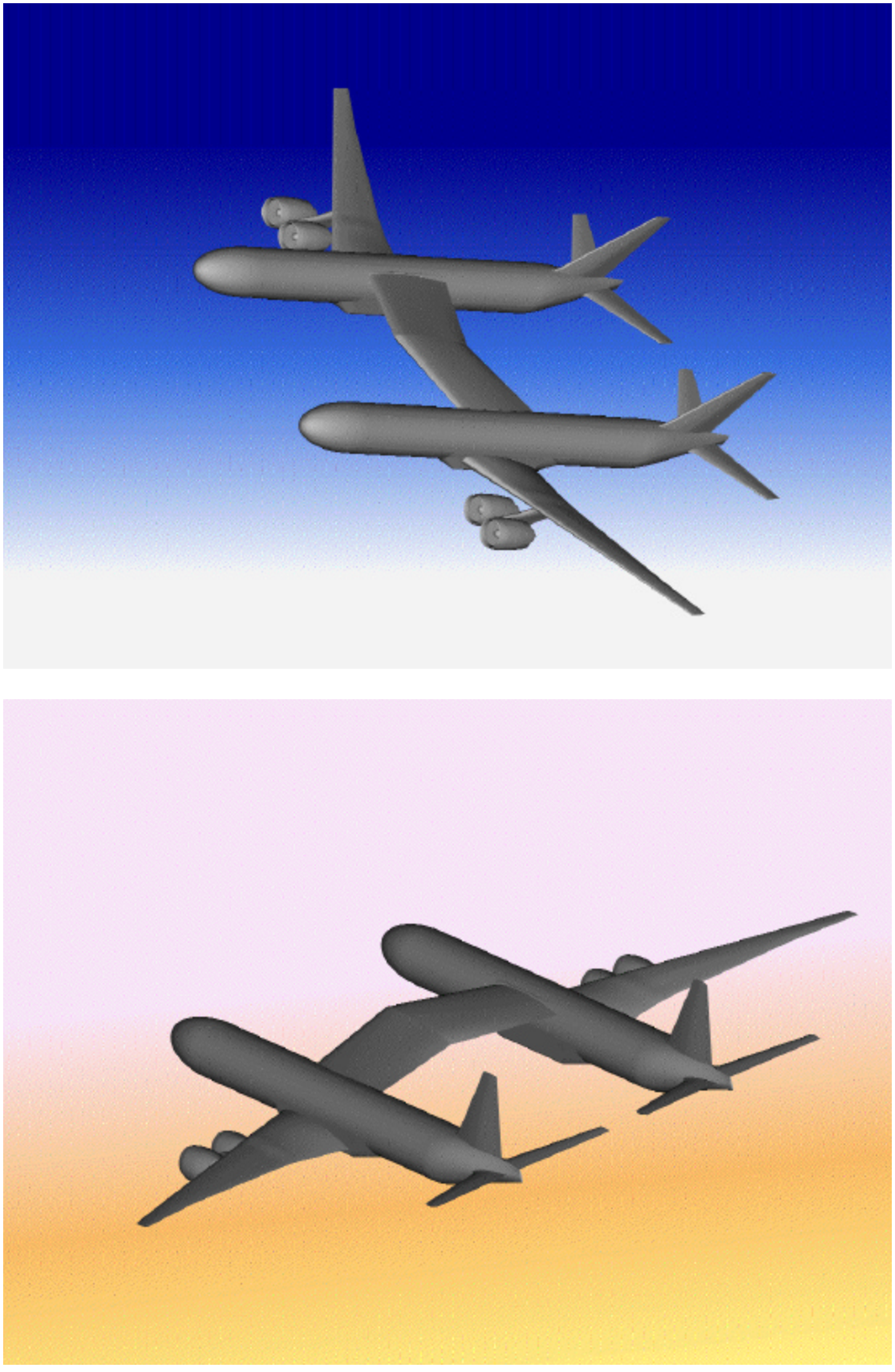

Figure 4.6

5. **Interim HOTOL-type ACES TSTO**

5.1. Introduction

Now one considers a more long term and optimistic perspective of a subsonic air-launch vehicle with use of in-flight LOX collection, the case of a kind of an Interim HOTOL (ref. 8) with implementation of the ACES technology.
In this third case, the ACES option is used to increase the weight of the orbiter what leads to a higher payload (not necessary with a higher payload fraction). Indeed, the in-flight LOX collection, for the same payload injected into orbit, can allow to take-off and climb up to the subsonic cruise phase with a lower mass, what means that, in the case of an emergency, we can land without dumping a large quantity of propellant.

It is also rather important to note that, if the orbiter is lighter, less propellant will be consumed during the trajectory, therefore the subsonic carrier with its orbiter can cruise during a longer time what gives more flexibility to the launcher. In-flight LOX collection can allow to take-off with a larger orbiter, but lighter at take-off (heavier when the orbiter is full of LOX after the collection phase or at separation) because the maximum payload mass (orbiter mass) of the subsonic carrier is fixed by its take-off mass (in fact by the maximum wing loading at take-off).
The subsonic carrier considered here will be mainly the Antonov AN-225 but other subsonic carriers should be considered too (Airbus A330 & A340, Airbus A3XX and others). It is also important to say that, in the case of a subsonic air-launch with in-flight LOX collection, the engines of the subsonic carrier are burning hydrogen what allows to collect LOX and what gives to the subsonic carrier a larger range and/or endurance.

5.2. Sizing exercise and validation

A trajectory-vehicle sizing computer code developed by the ERM is used to evaluate the performance of a subsonic air-launched orbiter (subsonic TSTO). The first step in this paper will be to validate this computer code with results given in the literature for the Interim HOTOL (see figure 4.8).

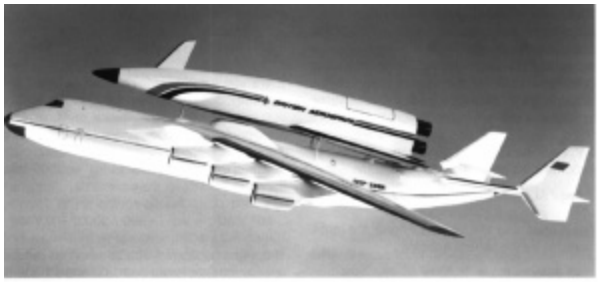

Figure 4.8

Table 4.3 shows the good agreement obtained between our results and results given by reference [8].

Calculation type	Interim HOTOL	ERM Tool
LOGW (t)	249	250
PAY (t)	7.0	7.0
Wdry (t)	32.10	31.14
Weng (t)[5]	4.99	4.96
W_{LH2} (t)	29.9	30.3
W_{LOX} (t)	179.3	181.5
Wppl (t)	209.2	211.8

- Oinc = 7° & Oalt = 275 km - fully reusable - μstr = 22 kg/m² -
Table 4.3

In this paper, we will consider the ERM result of table 4.3 as the reference case. Many different factors of influence will be considered in the next paragraphs, as the influence of using in-flight LOX collection, influence of the LOX purity, influence of the average structure index, influence of the mission, influence of the rocket engines used in the orbiter, influence of the orbiter planform loading at LO (in the reference case: 0.85 t/m²), influence of an expendable second stage and finally influence of the subsonic carrier.

5.3. Influence of using in-flight LOX collection

One of the main critics against the air-launch concept is the lack of flexibility regarding the payload. If the LOGW of the orbiter is fixed, we can say that, for everything staying equal (same technology and mission), the maximum payload capability of the launcher is fixed.
But a good solution to increase this payload capability would be to collect atmospheric oxygen during the (cruise) flight with the first stage and store it into the LOX tank of the orbiter (ref.[2]). Indeed, the maximum payload capability of a subsonic carrier is fixed by take-off and landing (in the case of an abort maneuver) operations[6], **if** an efficient fuel management is done in-flight in such a way that the bending moment of the wing with the maximum orbiter weight is not above the allowed maximum value. Therefore, as we do not take-off with LOX in the orbiter (181 tons less at TO), we can consider an orbiter which will be heavier than 250 tons at lift-off what will lead, of course, to an increase of the payload. We can also note that due to its relatively low payload mass at TO, the subsonic carrier will have a larger cross range capability (then an increased flexibility). This means of launching is also much safer because, in the case of an emergency just after TO, the payload mass at take-off is lower even if the LOGW is larger (Wdry + W_{LH2} ≈ 70 tons mass at TO for a LOGW of 300 tons) than in the case without LOX collection (250 tons).

Figure 4.9 shows the influence of an increase of the LOGW on the payload mass and the orbiter dry mass. We can see the important increase of the payload (7 to 11 tons) for a 30% increase of the LOGW.

[5] Weng is the engine mass including OMS.
[6] Another limitation for the orbiter is its maximum allowable planform area of 450 m² (ref.[3]). For a LOGW of 300 tons, we are still under this limit value (only 353 m²).

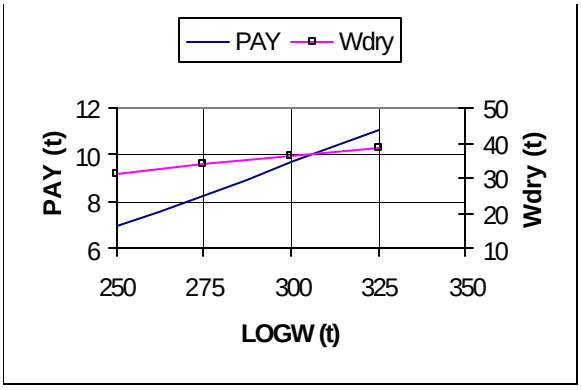

Figure 4.9

In the next paragraphs, an orbiter LOGW of 300 tons will always be considered.

5.4. Influence of the collection plant performance

In paragraph 3, we considered a collection plant which allows to collect pure oxygen (Cox = 100%). It must be clear that, in the case of using in-flight LOX collection, pure oxygen will not be collected. Thus, we have to consider a decrease of the rocket engine specific impulse and analyze its influence. We can estimate that one percent of impurities leads to a lost of 1.5 seconds in specific impulse (with MR = 6).
Figure 4.10 shows the influence of the oxygen purity on the payload mass and on Wppl for a fixed LOGW of 300 tons. On this figure, we can see that, even for a rather low purity (94%), we still have a payload mass much larger than 7 tons.
Anyway, we have to note that the LOX purity must be as high as possible. Therefore, we need a collection plant designed to give a very high purity (thus probably with a small separation efficiency but this is not a problem because the subsonic carrier has a large cross range capability[7]). That means that, in this subsonic case, the accent from the technology point of view has to be placed on the air separator.

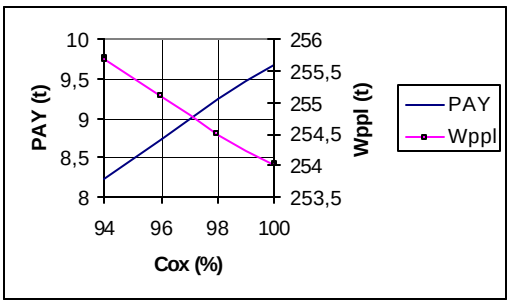

Figure 4.10

For the next paragraphs, we will always consider a LOGW of 300 tons and a LOX purity of 98% (what could be obtained with a 2-stage air separation system in the future, ref.[11]).

[7] That is completely different for a TSTO using supersonic in-flight LOX collection, see ref.[4].

5.5. Influence of the orbiter rocket engines

Table 4.4 shows the vehicle performance obtained with different current (except the RL10C which is an advanced one) cryogenic rocket engine types. We can see that the two main parameters of a LRE are its thrust-to-weight ratio (T/W) and its specific impulse (ISP). A high T/W means that the engine is light and a high ISP means that its propellant consumption is low.
It is very important to note, for European deciders, that, with a VULCAIN rocket engine type, the air-launch solution leads to a payload mass of about 7.0 tons when using in-flight LOX collection.

LRE type	Vulcain II	RD0120	SSME	RL10C
ISP[8] (sec)	432	455	453.5	457.3
T/W (-)	76	58	67	80.4
PAY (t)	7.02	9.26	9.63	11.06
Wppl (t)	258.7	254.5	254.9	254.2

Table 4.4

Thus, even with an existing Vulcain-type LRE, the ACES air launch option would be very interesting.

5.6. Influence of the average orbiter structure index

Figure 4.11 shows the influence of the average orbiter structure index on the payload mass injected into orbit and on the structure mass in the case of a fully reusable orbiter. It is clear that if µstr decreases, the structure mass decreases too and thus the payload mass increases. Therefore, we note that in-flight LOX collection allows to consider a higher µstr for the orbiter (thus a less advanced structure) and still provide a higher payload injected into orbit. Indeed, the reference case with a µstr of 22 kg/m² (without in-flight LOX collection) leads to a payload of 7.0 tons and, on figure 4.11, we see that a very conservative µstr of 24 (then a less advanced structure) leads to a payload of about 7.44 tons when using in-flight LOX collection.

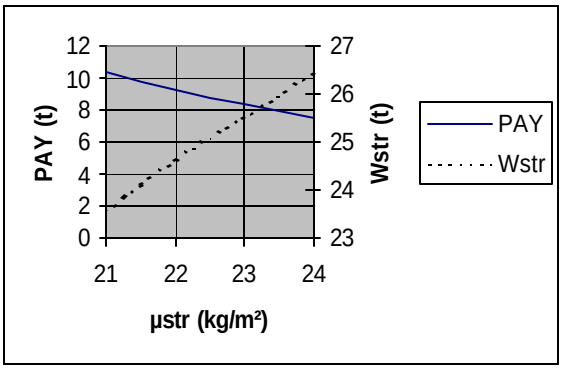

Figure 4.11

[8] The specific impulses given in this table are considered for LRE working with pure LOX. But the results in the table take into account the effect of the unpure oxygen.

5.7. Influence of the orbiter planform loading at lift-off

Figure 4.12 shows the influence of the orbiter planform loading at lift-off on the payload mass, the structure mass and the orbiter Küchemann's parameter.
We can see first that an increase of Lto induces a decrease of the structure mass. Indeed, for the same lift-off mass, if Lto increases the planform area decreases what leads to a vehicle having smaller (and of course lighter) wings thus the structure mass will decrease too. Of course, due to the lighter structure, the payload injected into orbit is larger too.
We have to note that, if Lto increases, the Küchemann's parameter tau increases too (see figure 4.12). If tau becomes larger than 0.18, flight instabilities could be observed at low speed what could be a problem for the landing and separation maneuvers.
As a consequence, for this kind of air-launched vehicle, we have to be rather careful with the aerodynamics of the orbiter and not to increase Lto above about 1 t/m². Another limitation for the Lto is due to the landing speed which depends of the L_{Ldg} (planform loading at landing). This speed must be lower than 180-190 knots (180 knots is the usual landing speed of the F-4). For our orbiter L_{Ldg} = 0.1 t/m², what leads to a (rather low) landing speed of about 130 kts.

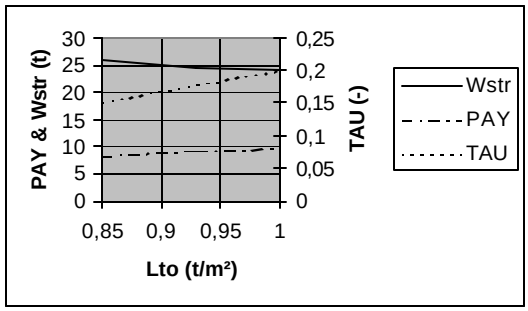

LOGW = 300 t

Figure 4.12

5.8. Influence of using a fully expandable orbiter

The choice of an expandable orbiter[9] allows to lift-off with a lighter structure (lower μstr) for the same LOGW. Indeed, in the case of an expandable second stage, no thermal protections for the reentry are required what leads to a lighter structure.
The choice of an expandable orbiter could also allow to avoid to take on board the landing gear and , of course, the propellant required for the come back maneuvers.
Figure 4.13 shows the influence of the average second stage structure index (lower than in the case of a reusable one) for an expandable orbiter. We can see the very high payload mass (much more than 10 tons) that we can inject into a nearly equatorial LEO with this type of orbiter[10].
This expandable orbiter seems to be a very attractive solution.

[9] This choice is understandable as the orbiter cost is only a small part of the total launcher cost.
[10] For an expandable orbiter having a LOGW of 250 tons with μstr = 22 kg/m² we can inject a payload of 8.5 tons.

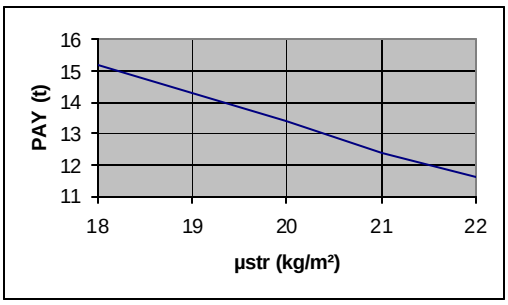

Figure 4.13

For the next paragraph, an average μstr of 20 kg/m² will be considered with an fully expendable orbiter.

5.9. Influence of the mission

In this paragraph, we want to show the influence of the mission for an expandable orbiter with a μstr equal to 20 kg/m². We will first show the influence of the orbit altitude and after the influence of the orbit inclination.

5.9.1. Influence of the orbit altitude

Figure 4.14 shows the influence of the orbit altitude on the payload mass for LEO with an inclination of 7°. If the orbit altitude increases, the orbiter has to reach an orbit with a higher level of energy what means that more propellant will be burned to reach it.

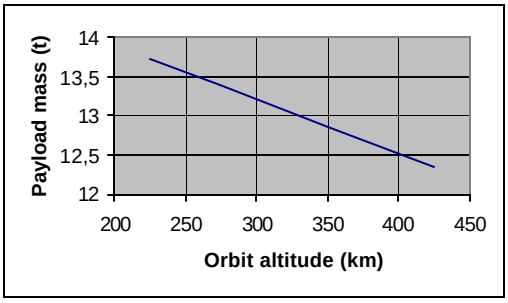

Figure 4.14

For the next calculation, we will consider an altitude of 250 km which is the current ESA FESTIP altitude requirement.

5.9.2. Influence of the orbit inclination

Figure 4.15 shows the large influence of the orbit inclination on the payload mass injected into orbit. The decrease of the payload mass comes from the fact that if the inclination increases the contribution due to the earth rotational forces is lower, what means of course, that more propellant will be burned and thus less payload can be injected into orbit. It is also important to note that, for orbit inclinations larger than 90°, the earth rotation acts negatively on the orbiter at the injection. These orbits are called retrograde orbits and are the most difficult orbits to reach.

The ESA FESTIP inclination requirements are 5° for the equatorial mission (PAY = 13.4 tons) and 98° (PAY = 9.2 tons) for the polar mission.

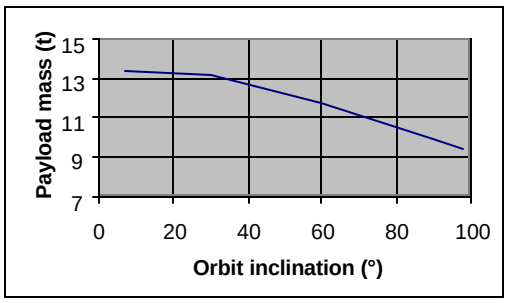

- Oalt = 250 km -
Figure 4.15

5.10. Influence of the subsonic carrier

In this paragraph, we want to show the influence of the LOGW on the payload mass. Or, in other words, the influence of the subsonic carrier choice. Table 4.5 shows the payload capability at take-off for different types of subsonic carriers.

Subsonic Carrier (1st stage)	Maximum weight of the orbiter at take-off
Antonov AN-225	250 tons
Lockheed Tristar L-1011	24 tons
Airbus A330	46 tons
Airbus A340	48 tons
Airbus A3XX	90 tons
Boeing 747	90 tons

Table 4.5

On figure 4.16, we can see the influence of the LOGW (thus of the subsonic carrier) on the payload mass for a fully expandable orbiter having **only** 1 stage. It must be clear that in the case of a decrease of the LOGW (thus when using a small subsonic carrier), it becomes more interesting to choose an orbiter having an underbelly position and consisting of two or three expandable stages as in the Pegasus launch system. Indeed, the LOGW of the Pegasus is only about 24 tons and can already inject about 470 kg (see figure 4.17 from ref.[12]) for an equatorial FESTIP mission.
At this time, the AN-225 is the largest existing subsonic carrier, what "limits" the maximum payload mass. But a large improvement of the payload capability could be obtained with a larger subsonic carrier as the Heracles proposed by NPO MOLNIYA (ref.[13]) which is able to take off with an orbiter of 450 tons (without considering in-flight LOX collection) and with a lower attachment of the orbiter under the fuselage, what leads to a much safer subsonic **ventral separation**.

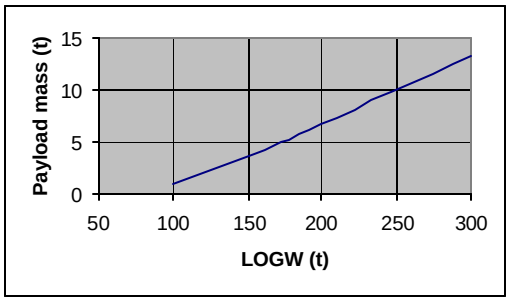

Figure 4.16

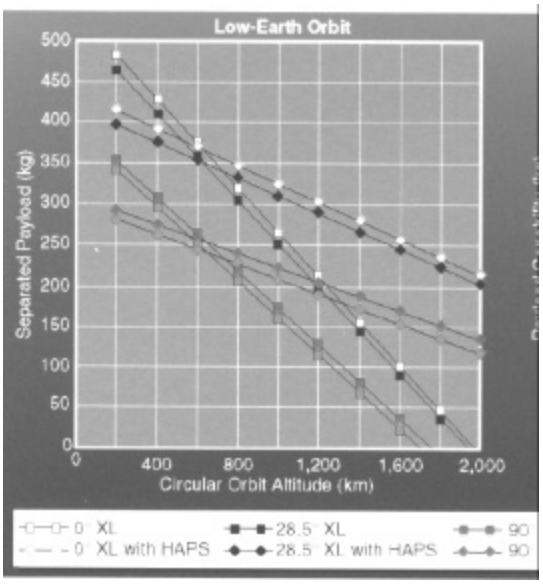

Figure 4.17

6. **High By-Pass Ratio Turbofan burning hydrogen**

The propulsion system for the 1st stage of the subsonic TSTO using in-flight LOX collection has been deeply studied (ref. 14). A lot of cycle calculations for (V)HBPR turbofans (see schematics on figure 4.18) burning hydrogen-fuel have been performed using the gas turbine cycle simulation computer tool Gasturb 8.0 (also used by many different users as VKI, Pratt & Withney, MTU, …).

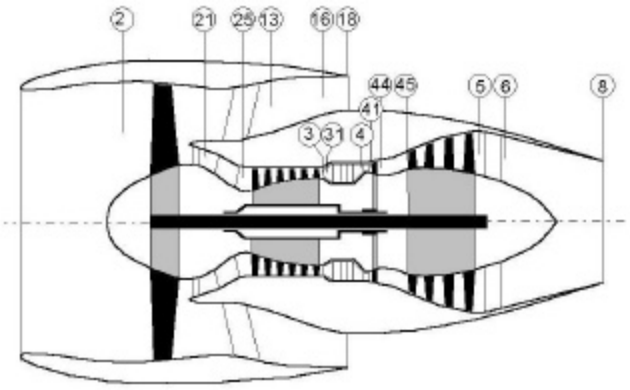

(V)HBPR turbofan and its sections
Figure 4.18

The GE90-75B (figure 4.19) from General Electric and Snecma has been selected as a reference as it is a quite recent turbofan with large upgrades/extension possibilities. This is one of the three proposed motorizations of the Boeing 777-200A+.

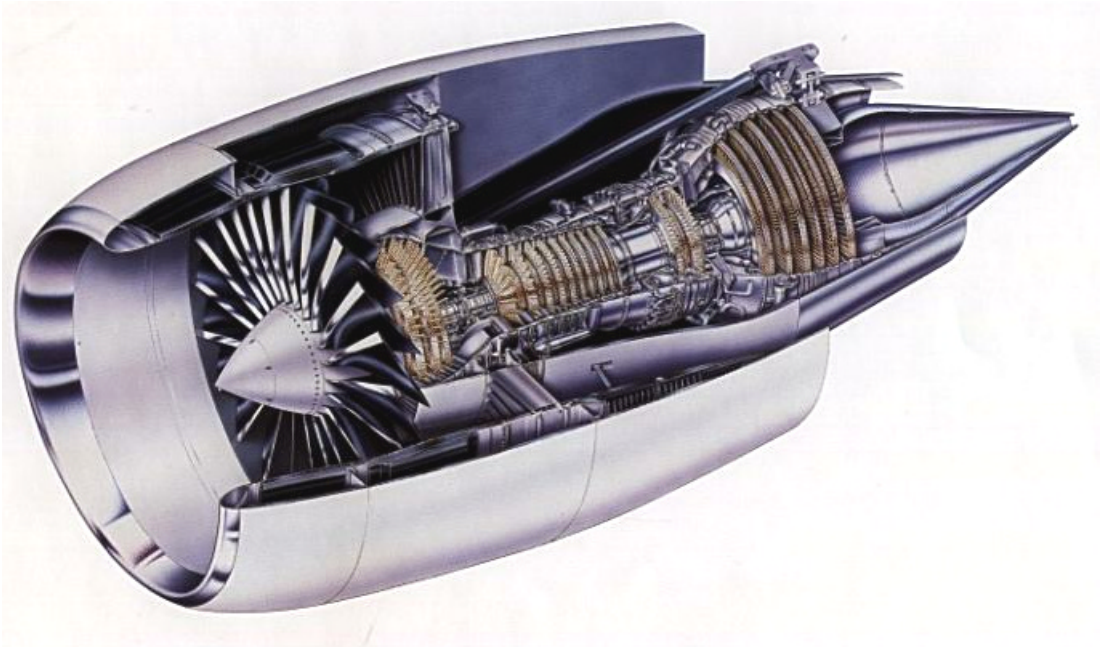

The GE90-75B turbofan
Figure 4.19

The following data for the GE90 were available for the simulation:

- FN = 90.000 lbf = 400,3 kN at Take-Off rating
- BPR = 9,0
- $\pi_g = 40$
- TIT = 1800 K
- Total airflow at TO: W2 = 1542,2 kg/s

The complete simulation results are given in table 4.6 for JP-8 fuel. The most important result is certainly the TSFC of 0,3272 kg/daNh.

If hydrogen fuel is now burned and if one requires that the thrust must remain equal, after iterating on the TIT (which will be much lower, a very good point for the turbine blades and disks), it is found that the TSFC decreases by 64.5 % (table 4.7).

Fuel	Corrected air flow (kg/s)	TIT (K)	FF (kg/s)	TSFC (kg/daNh)	Thrust (kN)
JP-8 kerosene	1542.0	1798.2	3.6378	0.3272	400.3
Hydrogen	1542.0	1747.0	1.2911	0.1161	400.3

Table 4.7: Performance comparison in function of the fuel (TO SLS ISA)

The complete simulation results with hydrogen fuel is given in table 4.8 for SLS ISA conditions at TO rating.

Station	W	T	P	WRstd		
amb		288,15	101,325		FN	= 400,30
2	1526,580	288,15	100,312	1542,000	SFC	= 9,0876
13	1373,922	331,40	155,483		WF	= 3,6378
21	152,658	430,18	351,091	53,831	BPR	= 9,0000
25	152,658	430,18	347,580	54,375	P25/P21	= 0,9900
3	148,078	897,61	3972,842	6,666	Core Eff	= 0,4589
4	133,397	1798,19	3853,657	8,762	Prop Eff	= 0,0000
41	141,030	1753,60		9,148	P3/P2	= 39,605
45	150,189	1306,00	902,066	35,915	P16/P2	= 1,53450
5	154,769	850,66	108,676	247,935	A8	= 2,36864
8	154,769	850,66	106,503	252,994	A18	= 4,17941
18	1373,922	331,40	153,928	969,894	P8/Pamb	= 1,05110
P2/P1 = 0,9900			P4/P3 = 0,9700		P18/Pamb	= 1,51915
Efficiencies:		isentr	polytr	RNI	P/P	P6/P5 = 0,98000
Outer LPC		0,8900	0,8966	0,99	1,550	P16/P13 = 0,99000
Inner LPC		0,8700	0,8905	0,99	3,500	XM8 = 0,27425
HP Compressor		0,8600	0,8969	1,74	11,430	XM18 = 0,79628
HP Turbine		0,8700	0,8462	1,87	4,229	V18/V8,id= 1,76081
LP Turbine		0,8700	0,8302	0,71	8,301	PWX = 100
HP Spool mech		0,9900				WBLD o/b = 1,52658
						WBLD/W21 = 0,00000
						WHc1/W25 = 0,06000
						WLc1/W25 = 0,03000

Simulation of the GE90-75B in TO SLS ISA conditions (JP-8 kerosene)
Table 4.6

Station	W	T	P	WRstd		
amb		288,15	101,325		FN	= 400,30
2	1526,580	288,15	100,312	1542,000	SFC	= 3,2254
13	1373,922	331,25	155,483		WF	= 1,2911
21	152,658	429,83	351,091	53,809	BPR	= 9,0000
25	152,658	429,83	347,580	54,352	P25/P21	= 0,9900
3	148,078	897,14	3972,842	6,664	Core Eff	= 0,4747
4	131,050	1746,99	3853,657	8,484	Prop Eff	= 0,0000
41	138,683	1706,20		8,873	P3/P2	= 39,605
45	147,843	1270,78	906,820	34,691	P16/P2	= 1,53450
5	152,423	822,80	108,781	239,911	A8	= 2,32112
8	152,423	822,80	106,605	244,807	A18	= 4,17914
18	1373,922	331,25	153,928	969,674	P8/Pamb	= 1,05211
P2/P1 = 0,9900			P4/P3 = 0,9700		P18/Pamb	= 1,51915
Efficiencies:		isentr	polytr	RNI	P/P	P6/P5 = 0,98000
Outer LPC		0,8900	0,8966	0,99	1,550	P16/P13 = 0,99000
Inner LPC		0,8700	0,8905	0,99	3,500	XM8 = 0,27580
HP Compressor		0,8600	0,8969	1,74	11,430	XM18 = 0,79666
HP Turbine		0,8700	0,8457	1,97	4,207	V18/V8,id= 1,73554
LP Turbine		0,8700	0,8289	0,75	8,336	PWX = 100
HP Spool mech		0,9900				WBLD o/b = 1,52658
						WBLD/W21 = 0,00000
						WHc1/W25 = 0,06000
						WLc1/W25 = 0,03000
Fuel: Hydrogen with lower FHV = 117,531 MJ/kg						

Simulation of the GE90 with hydrogen fuel, iteration on TIT (TO SLS ISA)
Table 4.8

In cruise conditions at an altitude of 35,000 ft ISA and Mach 0.83, the simulated performance of a hydrogen-fueled GE90 are as follows in table 4.9. The same reduction (about 64 %) of the TSFC is feasible.

Parameter/Fuel	JP-8	H_2	Delta (%)
FN (kN)	53,40	53,40	0,00
TSFC (kg/daNh)	0,6292	0,2250	-64,24
π_{HPC}	18,30	18,61	1,69
$\pi_{fan+booster}$	1,4	1,4	0,00
π_F	1,392	1,394	-0,14
BPR	10,6	10,6	0,00
TIT (K)	1439,48	1414,06	-1,77
W2Rstd (kg/s)	1498,94	1497,91	-0,07

Table 4.9: Results in cruise flight (Alt = 35.000 ft and M = 0,83)

The problem with hydrogen fuel is its very low specific mass. It is thus necessary to think with the fuel volume flow rate instead of the fuel mass flow rate. In TO conditions, the fuel volumetric consumption for the GE90-75B is as follows :

- GE90 with kerosene: $4{,}66.10^{-3}$ m^3/s = 16,8 m^3/h
- GE90 with hydrogen: $1{,}82.10^{-2}$ m^3/s = 65,6 m^3/h

The engine with H2 needs about 4 times (65.6/16,8 = 3,91) more fuel volume for the same flight duration.

In cruise conditions, the B777 with kerosene flies one hour at Ma = 0,83 and 35.000 ft using 3.144,96 kg kerosene per engine. That is **3,93 m³** (with $\rho_{kerosene}$ = 799,76 kg/m^3). The B777 with hydrogen burns only 1.124,64 kg LH_2 per engine but that means **15,88 m³** (with ρ_{LH2} = 70,80 kg/m^3).

The B777-300 fuel tank capacity is about 94 tons of kerosene or only 118 m³ but in our application, the cylindrical part (at least) of the fuselage is also available and that means about 1200 m³ (extra) volume for LH_2 storage (external fuselage diameter of 6.2 m – tank inner diameter of 5.5 m – cylindrical fuselage length of at least 50 m). With two hydrogen feeded turbofans per fuselage burning in total even 45 m³ LH2/h (due to a 40% extra drag due to the launcher), that is still a quite satisfactory autonomy even if the hydrogen used for collection is not reused in the turbofans but expelled through a separate nozzle.
The 2400 m³ available with the two B777 fuselage is certainly enough for the 140 tons (about 1980 m³) of hydrogen needed in the calculation of table 4.2 where 70 were used for collection and 70 for propulsion, i.e. 17 tons of hydrogen fuel per engine or an endurance of more than 10 hours, considering a drag (and thus thrust) increase of 40%.

7. **Conclusions**

In this chapter I, one shows that the RMA computer vehicle sizing code is able to evaluate correctly the performance of an air-launched system.
One explains the large advantages of the in-flight LOX collection concept for an air-launch option. It leads to much more secure take-off, landing and abort maneuvers. It provides

increased operational flexibility with virtually no restriction on launch azimuth and a great operational autonomy (not reliant on launch facilities). The ACES subsonic air-launch concept allows also to proceed with a **stepwise approach**, with, finally, the use of a subsonic carrier based on large existing civil transport aircraft and the use of hydrogen fed propulsion plants.

The in-flight LOX collection could also allow to inject a higher payload mass into orbit for the same orbiter technology.

For this type of launch vehicle, we show the influence of the collection plant performance and demonstrate that even with a relatively poor LOX purity (Cox = 90-94%), the payload mass is higher than in the case without in-flight LOX collection.

Using in-flight LOX collection allows also to use, for the same payload injected into orbit, more conservative technologies (higher average structure index, lower planform loading at lift-off and a Vulcain type rocket engine).

But the biggest advantages (in terms of payload mass and system complexity) come when using an **expendable orbiter**. Indeed, this solution allows to use a lower average structure index (no thermal protection are required for the reentry) what leads, for example, to a payload mass larger than 13 tons on the HOTOL equatorial mission (7° & 275 km) and we show that the payload mass for the FESTIP equatorial mission (5° & 250 km) is larger than 13 tons and larger than 9 tons for the FESTIP polar orbit (98° & 250 km). These are really very high performance.

One shows also the influence of the subsonic carrier choice (thus the influence of the LOGW) which shows that if the payload capability of the subsonic carrier becomes too low, a solution with 2 or 3 expandable stages (as in Pegasus) is well suited.

In all subsonic separation cases, the recommended solution is certainly a **ventral launch** separation.

One must also add that the subsonic air-launched option from a twin fuselage large airplane offers new opportunities in the severe competition of the market for heavy commercial payloads which continues to stagnate. Indeed in this compressed market, this option allows to use the mothership for other missions types, as outsized cargo, and brings a largely increased launch flexibility. That should result in reduced launching costs and a need for less market share to survive, without suffering from a lack of military or scientific missions (e.g. Boeing Sea Launch Zenit survives with only 6 to 7 flights per year in a market of 30 to 35 commercial geosynchronous satellites).

Chapter II will be specifically devoted to the hydrogen-fuelled GE90 turbofan simulation.

References

1. W. B. Scott, “Cash-Starved RLV firms remain grounded”, AWST, 13 December 1999.
2. C. Johnson & P. Hendrick, "LOX collection: a highly synergistic technology", AIAA 99-4830, AIAA Hypersonics Conference, Norfolk, 01-04 November 1999.
3. J. Leingang & L. Maurice, “In-Flight Oxidizer Collection Systems for Airbreathing Space Boosters”, Developments in High-Speed-Vehicle Propulsion Systems, Vol. 165 Progress in Astronautics and Aeronautics, AIAA, Nov 1996.
4. P. Hendrick, M. Saint-Mard & M. Strengnart, “Strutjet-equipped ACES SSTO”, AIAA-98-1502, Norfolk, 27-30 Apr 1998.
5. R. Drnevich & J. Nowobilski, "Airborne Rotary Separator Study", NASA CR-191045, Dec 1992.

6. R. Varvill and A. Bond, “The Skylon Spaceplane”, IAF 95-V3.07, 46th IAF Congress, Oslo, Oct 1995.
7. L. Jenkinson, P. Simpkin and D. Rhodes, “Civil Jet Aircraft Design”, AIAA book, 1999.
8. R. Parkinson et al., "An-225 / HOTOL", AIAA-93-5169, Munich, 1-3 December 1993.
9. P. Czysz, "Rocket-based combined cycle (RBCC) offers developmental and operational advantages", IAF-93-S.4.477, Graz, 16-22 October 1993.
10. P. Hendrick and M. Saint-Mard, "Sänger-type T.S.T.O. using in-flight LOX collection", AIAA 97-2858, Seattle, 6-9 July 1997.
11. P. Ngendakumana, “WP6 - Oxygen separation”, ESA FESTIP Technology phase II, 25 November 1998.
12. Brochure on Pegasus air-launch system from Orbital Sciences Corp., JPC, Cleveland, 12-15, July 1998.
13. G. E. Lozino-Lozinsky et al., "The MAKS project and perspectives of development", AIAA 96-4493, Norfolk, 18-22 November 1996.
14. K. Vanheste & P. Hendrick, “Voorontwerp van een High By-Pass Ratio turbofan op waterstof”, RMA, Brussels, November 1999.
15. J. Wimpress & C. Newberry, “The YC-14 STOL prototype : its design, development and flight test”, AIAA, 1998.
16. K. Sorensen & J. Blevins, “Air Launch and LOX Collection as enabling technologies for Future Launch Systems”, AIAA 2001-3520, JPC 01, Salt Lake City, 8-11 July 2001.
17. J. Andrews & D. Andrews, “Low cost options for the 2nd and 3rd generation reusable launch vehicles”, AIAA 2000-3824, JPC 00, Huntsville, 16-19 July 2000.
18. D. Andrews & J. Andrews, “Air Collection and Enrichment System (ACES) for advanced 2nd generation RLVs”, AIAA 2001-3702, JPC 01, Salt Lake City, 8-11 July 2001.

Part 2

T.S.T.O.'s using subsonic in-flight LOX collection

Carrier Plane hydrogen propulsion pre-study

List of symbols

A	Area
ACES	Air Collection and Enrichment System
AFB	Air Force Base
BET	Burner Exit Temperature
BPR	ByPass Ratio
B777	Boeing 777
c_p	specific heat of air
$C_{F,G}$	Nozzle Thrust Coefficient
CR	Collection Ratio
C_{OX}	Oxygen Purity
D	Drag
DAC	Double Annular Combustor
E^3	Energy Efficiency Engine
ESFC	Energy Specific Fuel Consumption
F_N	Net Thrust
FADEC	Full Authority Digital Engine Control
FHV	Fuel Heating Value
GE	General Electric
HBPR	High ByPass Ratio
HP	High-Pressure
HPC	High-Pressure Compressor
HPT	High-Pressure Turbine
IFPR	Inner Fan Pressure-Ratio
IGW	Increased Gross Weight
IPR	Intake Pressure Ratio
L	Lift
LA	Los Angeles
LCP	Lox Collection Plant
L/D	Lift-to-Drag Ratio
LH_2	Liquid Hydrogen
L-M	Larson-Miller Parameter
LOX	Liquid OXygen
LP	Low-Pressure
LPT	Low Pressure Turbine
LV	Launch Vehicle
M	Mach Number
MTOW	Maximum Take-Off Weight
NGV	Nozzle Guide Vanes
NH,rel	Relative Mechanical High-Pressure Spool Speed
NL,rel	Relative Mechanical Low-Pressure Spool Speed
OEW	Operating Empty Weight
OFPR	Outer Fan Pressure Ratio
P_s	Static Pressure
P_t	Total Pressure
R	Molecular gas constant
R/C	Rate of Climb
R/D	Rate of Descent
RR	Ram Recovery
SLS	Sea Level Static
t	time
T	Thrust
T_t	Total Temperature
TIT	Turbine Inlet Temperature
TO	Take-Off
TOGW	Take-Off Gross Weight
TSFC	Thrust Specific Fuel Consumption
TSTO	Two Stage To Orbit
V	Velocity
$V_{A/C}$	Aircraft Speed
V_{at}	Landing Speed
W	Airflow / Weight
W_{Rstd}	Corrected Airflow
WF	Fuel Flow

a	flight path angle
d	$\frac{P_{t2}}{101.325}$
?	isentropic coefficient
?	Efficiency
?	$\frac{T_{t2}}{288,15}$
p	Pressure Ratio

SUFFIXES

amb	ambient
is	isentropic
sep	separation unit

Introduction

In this work the simulation of a GE90-90B engine has been executed via Gasturb9. This gas turbine engine simulation program allows the user to perform design as well as off-design calculations. The take-off rating of the engine has been determined via the design point option of the program. The cruise rating as well as the engine's performance during climb and descent have been determined via off-design calculations.

First, a short introduction to the GE90 engine is given. The configuration of this VHBPR engine is elucidated. The different components are discussed, a cross-section is given and the available data for the GE90-90B is also stated here. Finally, the first chapter ends with a survey of the nomenclature of Gasturb9.

Now that the engine has been introduced, the actual simulation is started. Since TO is the only rating for which some data is known, this rating is used as the engine's design-point. In Gasturb several parameters need to be determined in order to be able to simulate the engine's design-point. The data from a test on a testbed allows the calculation of the pressure ratios and the efficiencies of the compressor section while standard Gasturb data or other sources are used to determine the other input parameters. Since the data from the test was given for the uninstalled engine, the installation losses are determined next. In Gasturb this is done by an off-design calculation so the choice of the component maps will influence the results. The chosen maps are given and the influence on the results is discussed too. Finally the transition to hydrogen as a fuel is made for both the uninstalled and the installed engine.

After the TO rating has been determined as the design-point of the engine, it is now time to look closer to the cruise rating since most of the time the engine will be running in cruise. First it is explained how the transition from TO to cruise has been executed. This is done for kerosene as well as for hydrogen since both transitions differ. The hydrogen-fuelled engine is namely 'forced' to give the same net thrust as the kerosene-fuelled engine in cruise. Since the real transition cannot be determined exactly this method allows the most comparison between the results for both fuels.

The two major engine ratings have been determined so a mission is calculated next. This option of Gasturb9 allows the calculation of several points of interest in order to simulate a flight. In this work, a flight of a GE90-90B powered Boeing 777-200 is simulated. The plane takes off from and lands on an airport at sea level and cruises at 35.000 ft with ISA conditions during the whole flight. Several points have been determined in five different flight segments: TO, climb, cruise, descent and landing. The range of the kerosene-fuelled aircraft is then calculated. Finally the range of some alternatives for the hydrogen-fuelled aeroplane is calculated and comments are given.

After the simulations of the 777-200, a new mission is tackled next. A large subsonic ACES launcher carrier is simulated. First, the initial sizing of the carrier is executed: both the OEW and the TOGW of the carrier are determined. Then, a reference mission has been calculated. The weights of the carrier at the different mission points are given as well as the distances traveled. Finally, the L/D is altered to check the influence of the chosen values on the results.

Chapter I: The GE90 engine: an introduction

Built by General Electric in conjunction with SNECMA (France), IHI (Japan), and FiatAvio (Italy) the GE90 (see Figure I.1 for a cross-section) was first commissioned by British Airways in 1995 to power their new Boeing 777 fleet. The GE90 is one of today's most powerful commercial aircraft engines and is – according to GE – the most fuel efficient, silent and environment friendly engine of today. The engine should provide an improvement in fuel burn of 5 to 6%, a lower noise pollution and NO_x emissions that are 33% lower than other high bypass ratio engines. As will be shown, except for the fact that it's not a 3-shaft turbofan, most of the technologies used in this engine are innovative, what makes the growth potential of this engine unique and very attractive.

Originally certified for a Take-Off Thrust of 380 kN (85.000 lbf) in November 1994 the engine has a large thrust growth capability. Today versions with a Take-Off Thrust up to 512 kN (115.000 lbf) are being constructed and – again according to GE – a potential grow to 533,4 kN (120.000 lbf) is still possible. The simulated engine is of the 90B type. This GE90-90B is certified for a Take-Off Thrust of 400,3 kN (90.000 lbf).

Below the configuration of the GE90 is shortly treated. The number of stages of the different components is given along with a rough description of the airflow. After this a slightly more profound examination of the different components follows. The fan, compressor, combustor and turbines are dealt with summarily.

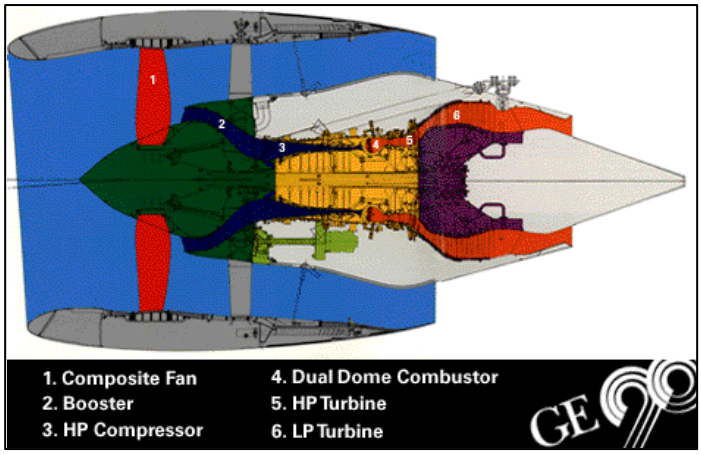

Figure I.1 A cross-sectional view of the GE90

I.1 Engine configuration

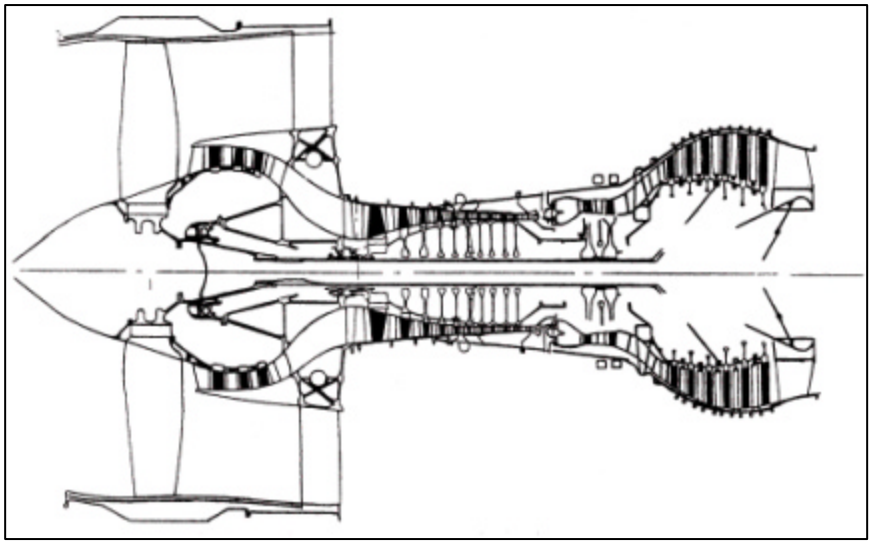

Figure I.2 Cross-section of the GE90

The GE90 is a civil HBPR unmixed flow turbofan. As can be seen from Figure I.2 and the figure in Appendix C the engine has a single stage fan. Once the air has passed the fan the division between core and bypass flow is made. The bypassed air simply flows through the bypass duct and exhaust nozzle and exits the engine. The core flow on the other hand undergoes a pressure rise through the booster and the HP compressor. The booster has 3 stages while the HP compressor exists out of 10 different stages. The total pressure rise through the core is in the vicinity of 42. After this compression the primary air enters the dual dome combustor where the air is burned. The combustion gasses are subsequently expanded through the HP and the LP turbine before leaving the engine through the exhaust nozzle. The HP turbine is a dual staged turbine and the LP turbine has 6 stages. The engine configuration is thus 1-3-10-0[1]-2-6.

I.2 Component description

I.2.1 The fan

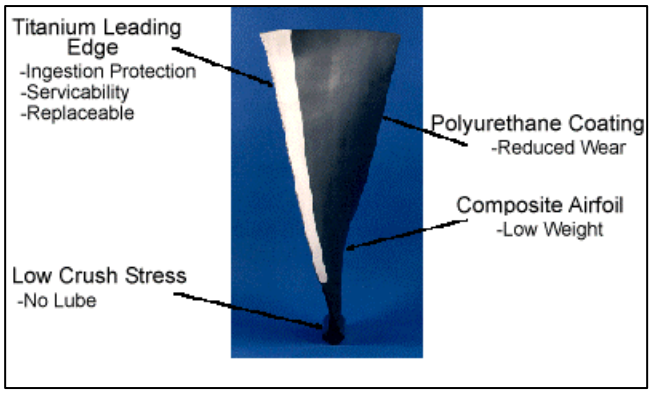

Figure I.3 The composite fan blade

The fan from the GE90 has 22 wide-chord composite blades with a tip diameter of 3,12 m and a hub diameter of 0,91 m. The fan blades have a low tip speed and a low pressure ratio to assure a quiet and efficient operation. The fan's lightweight tri-web disc reduces the engine weight and improves inspectibility while the hybrid spinner guarantees a low core debris ingestion.

The wide chord composite fan blade provides a high performance at a low weight. The polyurethane coating that can be seen on Figure I.3 fully protects the actual blade beneath it. The coating assures that the laminated specimens maintain 95 percent of their base

[1] The combustion chamber has no stages.

properties even when they are fully exposed to aircraft fluids. Finally a layer of titanium protects the leading edge of the blades against impact.

I.2.2 The compressor

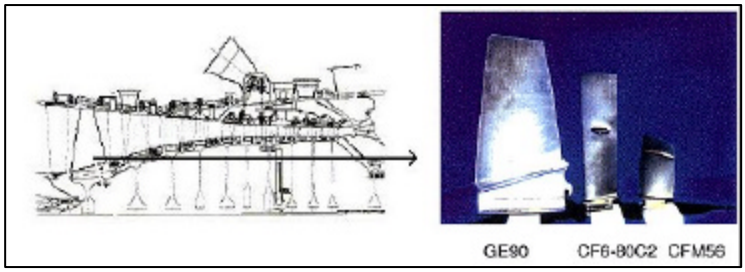

Figure I.4 The HP compressor

The compressor of the GE90 has a compact construction similar to that of the successful CFM56 family. The compressor exists out of rugged, low aspect ratio airfoils and the number of parts is minimized to reduce the operating cost.

The compressor is build up out of a short 3-staged booster (LP compressor) and a HP compressor that has 10 stages (see Figure I.4). This HP compressor section is essentially a scale-up of the GE E^3 (Energy Efficiency Engine) and has a pressure ratio in the vicinity of 23.

I.2.3 The combustor

The dual dome annular combustor or DAC[2] of the GE90 results from successful advanced military programs. It non solely reduces NO_x emission levels to values as low as 10 ppm but it also minimizes smoke levels, unburned hydrocarbons and carbon monoxide emissions. The dome of the combustor is aerodynamically and thermodynamically tuned for the different power settings, which leads to an improved operability and a long-life liner construction. Finally the combustor has an altitude re-light capability up to 30.000 ft (9,144 km).

I.2.4 The turbine

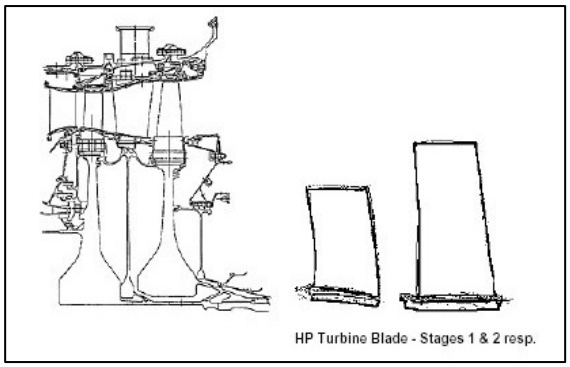

Figure I.5 The HP Turbine

The turbine section is composed out of a 2-stage HP turbine and a 6-stage LP turbine. Both turbines have large aspect ratio blades and low pressure stages. The stiff, simply supported rotor system improves the dynamic stability of the turbines while the multihole turbine cooling technology guarantees a better cooling effectiveness. The cooling hole pattern that must assure this increase in effectiveness is laser drilled into the blades of the two HPT stages. Finally the modular nozzle assemblies are based on the CFM56 and the CF6-80 designs.

[2] DAC or Double Annular Combustor

I.3 Available data for the GE90-90B

As for all recently developed engines, data from the GE90 engine family is hard to find. The only general data available for the 90B version of the GE90 is summarized in Table I.1 (ref. [22]). Table I.2 (ref. [19]) gives some information on the total pressures and total temperatures at the different sections of the engines. This data is available from a ground test on a test bench (SLS ISA). The station designation for this table is based on Gasturb9 and can be found on Figure I.6.

Table I.1 Basic Data for the GE90-90B (SLS ISA)

Net Thrust FN @ TO	90.000 lbf = 400,34 kN
BPR @ TO	8,4
TIT @ TO	Approx. 1800 K
π_g[3] @ TO	Approx. 42
Airflow @ TO	1542,2 kg/s
Corrected Airflow @ cruise[4]	1496,9 kg/s

Table I.2 Total pressures and temperatures at different sections from the

Station	Total temperature [K]	Total Pressure [Pa]
2	288,15	101.352,93
21	306,48	124.105,63
25	349,82	172.368,93
3	888,71	3.930.011,66
4	1.666,48	3.861.064,08

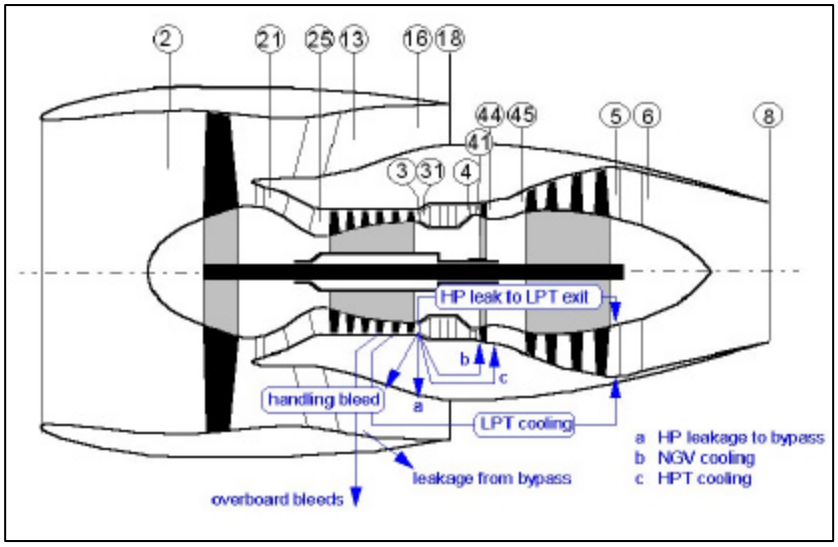

Figure I.6 Station Designation

[3] $\pi_g = \frac{p_{t3}}{p_{t2}}$: global pressure ratio

[4] Mach 0,85 at 35.000 ft

Chapter II Take-off simulation

In order to be able to simulate an engine via Gasturb numerous parameters need to be determined. Below is explained how the variables for the simulation of the Take-Off regime (TO) are determined. Since TO is the only regime for which some data is available this regime is taken as the design point of the engine. In this Chapter the TO rating is simulated for the engine running on kerosene as well as for the engine running on hydrogen.

Since some of the data available for the TO regime is given for an uninstalled engine the distinction between the installed and the uninstalled engine is made in this simulation. Installing an engine in Gasturb is an off-design problem so the data for the simulated installed engine is calculated through the use of component characteristics. The choice of these characteristics will thus influence the performance of the installed engine. Gasturb offers the possibility to choose between standard and special maps for the components. Both options are simulated and the results are compared to each other.

First the engine running on kerosene is dealt with. The determination of values for the compressor pressure ratios and efficiencies is explained as well as the chosen values for the parameters that are altered from the standard Gasturb turbofan input. After a survey of all the Gasturb input parameters the installation losses are evaluated.

Now that the thermodynamic cycle for the TO regime is known for the engine running on kerosene the transition to a hydrogen fuelled engine is carried out. The transition itself is elucidated first. Subsequently the influence of the transition on the performance of the engine and the installation losses of the H_2-fuelled engine are examined.

II.1 The GE90 running on kerosene

Based on the limited available data (see Table I.1 and I.2 in Chapter I) the various input parameters for Gasturb need to be determined. First, the compressor efficiencies and pressure ratios are ascertained. Since the test from which the data is taken was not executed at TO regime the calculated values need to be adapted. After this, a short description of the chosen values for the altered Gasturb parameters is given. As Gasturb offers a reasonable standard value for most of the parameters, only some of those parameters are altered. The mass flow, the isentropic efficiencies and the Burner Exit Temperature (BET) are the main parameters that are modified to fit the simulation to the thermodynamic cycle of the GE90. Finally a summary of all the input parameters for TO is given and the installation losses are calculated.

II.1.1 Compressor Efficiencies and Pressure Ratios

II.1.1.1 Efficiencies and Pressure Ratios from the test

The data from Table I.2 permits to determine the pressure ratios and the efficiencies of the different compressor 'components'. The pressure ratios are obtained by simply dividing the appropriate total pressures. With the data from Table I.2 this leads to the following pressure ratios:

$$\pi_{inner-fan} = 1{,}225$$
$$\pi_{booster} = 1{,}389$$
$$\pi_{fan+booster} = 1{,}701^{5}$$
$$\pi_{HPC} = 22{,}800$$
$$\pi_{g} = 38{,}780$$

The isentropic efficiency of a 'stage', e.g. the fan stage, is calculated in accordance with equations II.1 to II.2.

$$\eta_{is,fan} = \frac{T_{t21_i} - T_{t2}}{T_{t21} - T_{t2}} \qquad \text{(II.1)}$$

Here, T_{t21_i} is the total temperature after an isentropic compression:

$$\frac{T_{t21_i}}{T_{t2}} = \left(\frac{P_{t21}}{P_{t2}}\right)^{\frac{\gamma-1}{\gamma}} \qquad \text{(II.2)}$$

The value for γ is determined at the average temperature of the air flowing through the specific component of the engine. The exact values for γ at those averaged temperatures are obtained via the 7th degree polynomial used in [7]. For the Inner Fan an average temperature of 319 K leads to a value of 1,400[6] for γ. The HP Compressor has an average temperature of 619 K so 1,374 is used for γ. Those values for γ lead to the following efficiencies:

$$\eta_{is,fan+booster} = 0{,}77$$
$$\eta_{HPC} = 0{,}87$$

II.1.1.2 Efficiencies and Pressure Ratios at TO

The test (Table II.2) on which the calculations of the efficiencies is based is unfortunately not at the Take-Off regime. As indicated in Table II.1 the TIT at TO should be approximately 1.800 K. At the test the TIT (T_{t4}) is 'only' 1.666 K so we can definitely speak of two different regimes. The efficiencies of the different components will obviously vary between those two regimes. Since there is no data available for the TO-regime the efficiencies obtained through the test data are normally used as efficiencies at TO. Only the HP Compressor efficiency will be altered (cfr. paragraph II.2.1.2.3). Due to use of efficiencies from a 'lower' regime, the simulation at TO will incorporate an error. The main purpose of this study will however be

[5] In Gasturb one can only enter the pressure ratio of the inner fan and the booster together, as if they form one stage. This pressure ratio is called Inner Fan Pressure Ratio in Gasturb. In order to be complete, the pressure ratios of fan and booster are given separately too.
[6] 1,3998

comparing simulations of the GE90 running on kerosene and running on hydrogen. Since both simulations will incorporate the same error, this 'efficiency substitution' is acceptable.

Besides the efficiency change, an alteration of the regime will also cause a variation of the pressure ratios of the different components. In this simulation the calculated pressure ratios are adapted to obtain a global pressure ratio of 42. This is done in Gasturb by iterating the Inner Fan Pressure Ratio (IFPR). During this iteration the HP Compressor Pressure Ratio is kept at 23, since this is the value given in [20].

The only pressure ratio that hasn't been determined yet is the Outer Fan Pressure Ratio (OFPR). To determine this pressure ratio, both the installed and the uninstalled engine have to be taken into account. In a first step the uninstalled engine performance is calculated. To simulate an uninstalled engine the Intake Pressure Ratio (IPR) is set to unity and the Relative Handling Bleed to Bypass as well as the Power Off-take are fixed to zero. The BET is then iterated to obtain a Net Thrust of 90.000lbf (400,34kN) (see also paragraph II.2.2.5). After this the BET is fixed to the value obtained for the uninstalled engine and the installed engine is simulated. In this simulation the Inlet Corrected Flow is iterated to acquire an engine mass flow of 1542,2 kg/s. At high OFPR this method leads to an error because the calculated Core Velocity of the installed engine is less then 1m/s. The highest OFPR that does not lead to that error is 1,5. Since the value given in [20] for the OFPR is also approximately 1,5 this value is considered for the OFPR of the GE90.

II.1.2 Altered Gasturb input variables

In order to be able to calculate a thermodynamic cycle of a turbofan, numerous input variables need to be specified in Gasturb. Only the parameters for which the value is altered in Gasturb are considered in this paragraph. For all other variables the value 'suggested' by Gasturb is taken. Finally a survey of all parameters is given.

II.1.2.1 Intake Pressure Ratio for the installed engine

Due to the large acceleration of the air in the intake the ram recovery (or IPR, see eq. II.3) of the inlet is relatively low at TO regime compared to cruise. In cruise conditions values up to 0,99 for the intake pressure ratio are normal while at TO conditions ram recovery factors as low as 0,85 are taken for granted for military aircraft.

$$RR = \frac{p_{t2}}{p_{t1}} \qquad \text{(II.3)}$$

For this simulation a value of 0,995 is taken for the Intake Pressure Loss. After all, the engine is designed for subsonic speed so the intake will have fairly rounded lips. It is essentially a smooth short tube with a slight diffusion, which has a length of about half the diameter of the tube.

II.1.2.2 Mass Flow

As stated in Table II.1 the airflow at TO amounts to 1.542,2 kg/s in SLS ISA conditions. In Gasturb however the mass flow input is entered via the corrected flow at the inlet of the compressor (cfr. eq. II.4).

$$W_{2Rstd} = \frac{W_2 * \sqrt{\theta}}{\delta} \qquad \text{(II.4)}$$

with:
W_{2Rstd} the corrected airflow at the compressor inlet [kg/s]
W_2 the airflow at the compressor inlet [kg/s]

$$\theta = \frac{T_{t2}}{288{,}15} = 1$$

$$\delta = \frac{P_{t2}}{101.325} = \frac{IPR * P_{t1}}{101.325} = 0{,}995$$

With the values from this TO simulation this leads to a corrected airflow W_{2Rstd} of 1.549,95 kg/s.

II.1.2.3 Isentropic Efficiencies

Isentropic Outer LPC Efficiency

Since there are no data available for the fan of the GE90 it is impossible to determine the isentropic efficiency. Gasturb gives a standard isentropic efficiency of 90 %. For this simulation the isentropic fan efficiency is though changed to 91 % since the GE90 is a relatively new engine.

Isentropic HPC Efficiency

The efficiency of the HP Compressor has been calculated as 0,87 in paragraph II.2.1.1 and this value is used in this simulation. After all the calculated value is only slightly higher than 0,85, the value obtained via the characteristics of the GE E^3 compressor (see Figure 11.6 in ref. [2]) and the core of the GE90 engine is essentially this E^3 compressor that has undergone a small modification.

Isentropic Turbine Efficiencies

As for the fan, the lack of data for the turbines disallows the calculation of the efficiencies. Since the values proposed by Gasturb are close to the values from [1], the Gasturb standard values are used. This means an isentropic HP Turbine efficiency of 0,880 is used while the LP Turbine operates at an isentropic efficiency of 0,881.

II.1.2.4 Nozzle Thrust Coefficients

The nozzle thrust coefficients play an important role in the determination of the thrust of the simulated engine. In Gasturb they are ‘defined’ by equation (II.5)

$$F_N = W_8 * V_8 * C_{FG,8} + A_8 * (P_{s,8} - P_{amb}) + W_{18} * V_{18} * C_{FG,18} + A_{18} * (P_{s,18} - P_{amb}) - W_2 * V_0 \qquad \text{(II.5)}$$

where:
$C_{FG,8}$ is the core nozzle thrust coefficient
$C_{FG,18}$ is the bypass nozzle thrust coefficient

Gasturb gives a standard value of 1 for both coefficients. In reference [1] the thrust coefficients for a turbofan are given as 0,988 for the core and 0,980 for the bypass duct. Since

those values are relatively low for a new turbofan 0,995 and 0,988 are used in this simulation for the core respectively bypass nozzle thrust coefficient.

II.1.2.5 Burner Pressure Ratio

In Gasturb 9 the BPR is normally set to a value of 0,97. In this simulation it is though assumed that the pressure loss in the combustion chamber amounts up to 5%. This assumption will be more accurate than the standard Gasturb9 value since it lowers the pressure in the main stream enough to allow the cooling air to exit the turbine blades and to mingle into the main stream. A BPR of 0,95 is thus used.

II.1.2.6 Burner Exit Temperature

As stated in Table II.1, the BET (in TO regime) amounts to approximately 1800K at SLS ISA conditions. The exact value of this total temperature is however unknown. In Gasturb this value can be determined through iteration. The BET is iterated to meet an exact thrust of 400,34kN (90.000 lbf.). Since this thrust equals the thrust of an uninstalled engine the simulation must be adapted. To convert the simulation to a simulation of an uninstalled engine at TO the ram recovery must be set equal to 1 and both the power off-take and the bleed air fraction must equal 0. With this set of parameters the iteration converges to a BET of 1.712 K.

II.1.2.7 Cooling Air

In Gasturb 3 different types of cooling air are considered: the NGV cooling air, the HPT cooling air and the LPT cooling air. The difference between the latter two is obvious but the difference between the NGV and the HPT cooling air requires some clarification. In Gasturb9 it is namely assumed that the HPT cooling air is mixed with the main stream after the expansion in the HPT. The HPT cooling air thus puts no power out in the HPT. The NGV cooling air on the other hand is mixed with the main stream inside the HPT and thus exerts power.

Based on the experience of Mr. Jackson the following cooling flows are used in this simulation:

NGV Cooling Air = 10%
HPT Cooling Air = 3%
LPT Cooling Air = 2 %

II.1.3 Summary of the input parameters for the TO rating

Environmental Conditions

✈ Altitude:		0 m
✈ Delta T from ISA:		0 K
✈ Relative Humidity [%]:		0
✈ Mach Number:	0	

Basic Data

✈ Intake Pressure Ratio:	0,995	
✈ Inner Fan Pressure Ratio		1,84
✈ Outer Fan Pressure Ratio		1,50
✈ Compressor Interduct Pressure Ratio:	0,99	

- HP Compressor Pressure Ratio: 23,0
- Bypass Duct Pressure Ratio: 0,98
- Turbine Interduct Reference Pressure Ratio: 0,98
- Design Bypass Ratio 8,4
- Burner Exit Temperature 1.712 K
- Burner Design Efficiency 0,999
- Burner Partload Constant 1,6
- Fuel Heating Value 43,124 MJ/kg
- Overboard Bleed 0 kg/s
- Power Off-take 50 kW
- HP Spool Mechanical Efficiency 0,998
- LP Spool Mechanical Efficiency 0,998
- Burner Pressure Ratio 0,95
- Turbine Exit Duct Pressure Ratio 0,98
- Core Nozzle Thrust Coefficient 0,995
- Bypass Nozzle Thrust Coefficient 0,988
- Design Core Nozzle Angle 10°
- Design Bypass Nozzle Angle 12°

Air System[7]

- Rel. Handling Bleed to Bypass 0
- Rel. HP Leakage to Bypass 0
- Rel. Overboard Bleed 0,0005
- Rel. Enthalpy of Overboard Bleed 1
- NGV Cooling Air 0,1
- LPT Cooling Air 0,02
- Rel. Enthalpy of LPT Cooling Air 0,6
- HPT Cooling Air 0,03
- Rel. HP Leakage to LPT exit 0
- Rel. Fan Overboard Bleed 0

Mass Flow Input

- Inlet Corr. Flow 1.549,95 kg/s

LPC Efficiency

- Isentr. Inner LPC Efficiency 0,77
- Isentr. Outer LPC Efficiency 0,91

HPC Efficiency

- Isentr. HPC Efficiency 0,87

HPT Efficiency

- Isentr. HPT Efficiency 0,88

LPT Efficiency

- Isentr. LPT Efficiency 0,881

[7] The different airflows used for cooling and bleed can be found on Figure I.6 in Chapter I.

II.1.4 Installation losses

Installing the engine in the airplane will cause the performance of the engine to decrease quite heavily. In order to determine these installation losses the performance of the installed engine has to be calculated. This is done in Gasturb by an off-design calculation since installing the engine will cause a change in the airflow through the engine and thus a change in engine parameters. Unfortunately the exact change is hard to simulate since it depends on the characteristics of the FADEC, which are impossible to find. An assumption will thus have to be made in order to calculate the installation losses. In this work the premise of an equal BET for the installed and the uninstalled engine is made as it is assumed that the BET, which is already high for a commercial engine, cannot be increased anymore without any negative influence on the life of the turbine blades.
Finally installing the engine also incorporates changes in IPR and Power Off-take so these parameters will have to be altered. The values used in this simulation are stated in Table II.1. The major contributor to the installation losses is the IPR. The power off-take only has a small contribution to both the rise in TSFC and the drop in FN.

Table II.1 Altered parameters between uninstalled and installed engine at TO SLS

	Uninstalled Engine	**Installed Engine**
Intake Pressure Ratio	1	0,995
Power Off-take [kW]	0	50

Since the installation is an off-design calculation in Gasturb the choice of the component characteristics will influence the result. Gasturb allows the user to choose between standard and special maps. These maps are explained below and the installation losses using both ‘sets of maps’ are given. Only the compressor maps are considered since they are far more important than the turbine maps for the correct engine operation. Surge of the compressors must namely be avoided at all times. Furthermore the operating point will not move very much in the turbine map so the choice of these maps will have a much smaller influence on the results of the simulation.

II.1.4.1 Installation losses using standard maps

When selecting standard maps in Gasturb the program automatically fixes the operating points of the chosen design point in the different maps. In each map the operating point is set to a beta value[8] of 0,5 and a relative spool speed of 1. The used maps are shown in Figure III.1 and Figure III.2. In Gasturb they are denominated LPC01.map and HPC01.map.

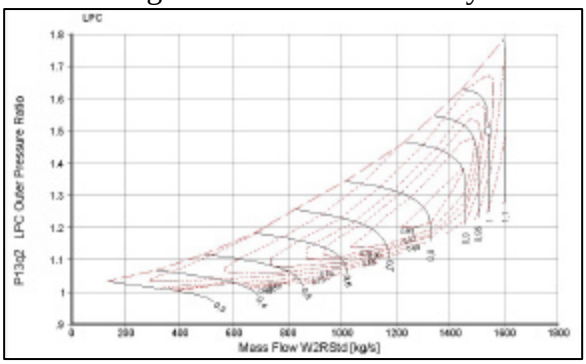

Figure III.1 The standard LPC map

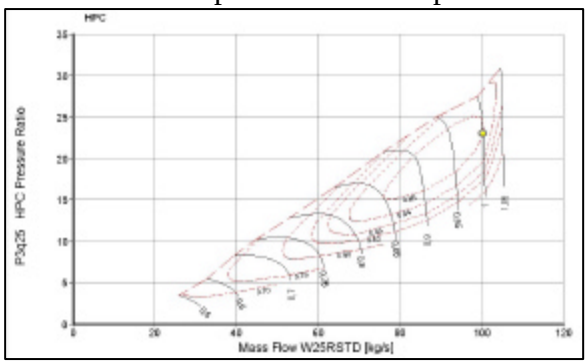

Figure III.2 The standard HPC map

Using these maps in Gasturb to install the engine to an imaginary aircraft leads to the installation losses given in Table II.2. The thermodynamic cycle of both the uninstalled and the installed engine running on kerosene can be found in Appendix A. Appendix A.1 gives the thermodynamic cycle along with the other Gasturb output parameters for the uninstalled engine while the results of Gasturb for the installed engine are given in Appendix A.2.

Table II.2 Installation losses using standard maps at TO SLS

	Uninstalled Engine	**Installed Engine**	**Loss (%)**
FN [kN]	400,3	395,5	(-) 1,2
TSFC [g/kN/s]	8,48	8,54	(+) 0,7

Installing the engine will also change the spool speed of both engine shafts. Since the TO rating for the uninstalled engine is considered as the design point of the engine the relative mechanical spool speed for both shafts equals unity at this point. For the installed engine both spool speeds will decrease. Using the standard maps to install the engine leads to a relative mechanical LP Spool speed (NL,rel) of 0,9973 and to a relative mechanical HP Spool speed (NH,rel) of 0,9990. These values lead to the following relative Corrected Speeds for the different components:

Relative Corrected Fan Speed[9] = 0,997
Relative Corrected HPC Speed = 0,999
Relative Corrected HPT Speed = 0,999
Relative Corrected LPT Speed = 0,997

II.1.4.2 Installation losses using special maps

The special maps option of Gasturb allows the user to choose between a number of compressor and turbine maps furnished with the program. Off course only a limited amount of different component characteristics is provided.

Out of the available maps for the outer fan the map FANBBYP.MAP (see Figure III.3) is chosen because it is the only fan that has a pressure ratio of approximately 1,5 at the design point. The other fans all have pressure ratios in the vicinity of 1,6 or higher at the design point. These are normal values for most modern fans. As stated in Chapter I, General Electric has though chosen for a lower fan pressure ratio for the GE90 to reduce the noise level of the engine.

[8] See [3].

[9] The relative corrected speeds in Gasturb are given by $\frac{\frac{NL}{\sqrt{T_{in}}}}{\left(\frac{NL}{\sqrt{T_{in}}}\right)_D}$, with T_{in} the temperature at the inlet of the specified component.

For the HP Compressor the choice was pretty obvious since the map of the GE E³ compressor is included with Gasturb and since a slightly altered version of this co-developed NASA/GE compressor forms the core of the GE90. The GE10STG.MAP (see Figure III.4) is thus taken as HP Compressor map.

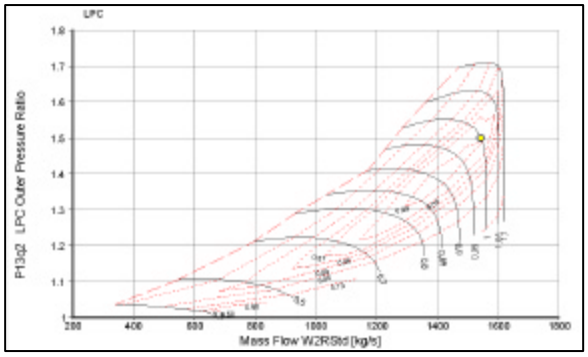

Figure III.3 The chosen LPC map

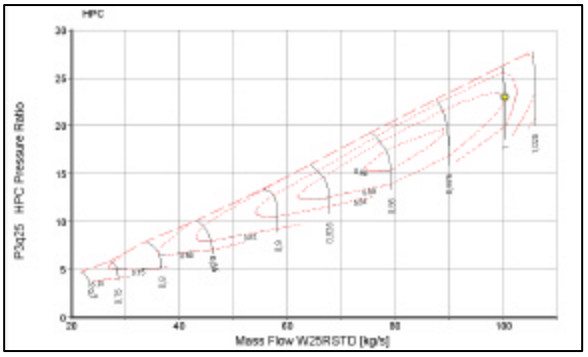

Figure III.4 The chosen HPC map

Using these maps in Gasturb to install the engine to an imaginary aircraft leads to the installation losses given in Table II.3. The Gasturb output for the engine installed via the special maps option is given in Appendix A.3.

Table II.3 Installation losses using special maps at TO SLS

	Uninstalled Engine	**Installed Engine**	**Loss (%)**
FN [kN]	400,3	394,5	(-) 1,4
TSFC [g/kN/s]	8,48	8,55	(+) 0,9

Using special maps to install the engine obviously also leads to a decrease in spool speeds. The relative mechanical LP spool speed decreases to 0,9976 while the HP spool speed reduces to 0,9997. This results in the following corrected speeds for the different components:

Relative Corrected Fan Speed = 0,998
Relative Corrected HPC Speed = 1,00
Relative Corrected HPT Speed = 1,00
Relative Corrected LPT Speed = 0,998

II.4.1.3 Influence of IPR and Power Off-take

Finally the chosen values for the IPR and for the power off-take are altered to verify the influence of the different parameters on the installation losses. This is done using the special maps of the previous paragraph. The results are given in Table II.4.

Table II.4 Installation losses at TO SLS for different sets of IPR and Power Off-take

		Thrust [kN]	TSFC [g/kN/s]
Uninstalled Engine		400,3	8,48
IPR=0,995	Power Off-take = 25 kW	394,8	8,55
	Power Off-take = 50 kW	394,5	8,55
	Power Off-take = 100 kW	394,0	8,56
	Power Off-take = 500 kW	389,9	8,59
IPR = 0,95	Power Off-take = 25 kW	345,9	9,29
	Power Off-take = 50 kW	345,6	9,29
	Power Off-take = 100 kW	345,0	9,30
	Power Off-take = 500 kW	340,8	9,34

As can be seen from Table II.4 the main 'contributor' to the installation losses is the IPR. The Power Off-take only has a minor influence on the installation losses. During the rest of this simulation a Power Off-take of 50 kW is assumed.

II.2 The H2-fuelled GE90

II.2.1 Transition to hydrogen

During the transition from the engine running on kerosene to the engine running on hydrogen the mass flow as well as the efficiencies and pressure ratios of the different components are kept constant. This has as major advantage that the same components (except for the combustion chamber) can be used for both the engines. The compressors, turbines and the inlet operate at the same point for both engines so no redesign has to be taken into account.

The only input parameters that are changed during the transition are the Fuel Heating Value (FHV) and the BET. Selecting hydrogen as fuel changes the FHV and the BET of the uninstalled engines is iterated to obtain the same net thrust for both fuels. The resulting thermodynamic cycle for the uninstalled engine running on hydrogen can be found in Appendix A.4.

Once the thermodynamic cycle of the uninstalled engine is known, the transfer to the installed engine has to be calculated. This is done the same way as for the engines running on kerosene (see paragraph II.2.4). The altered parameters can – again – be found in Table II.1 and the resulting thermodynamic cycle is given in Appendix A.5 and A.6 for the standard respectively special maps.

II.2.2 Influence of the transition to H_2 fuel on performance

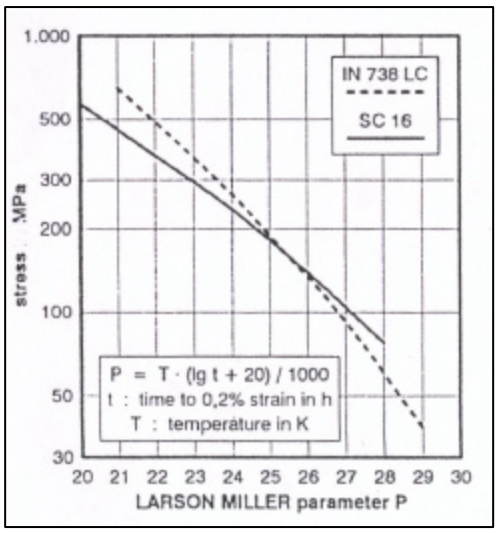

Figure II.5 The Larson-Miller parameter for two materials

The transition to hydrogen as fuel will improve the performance of the engine. Since the BET of the uninstalled engines is iterated to obtain a specified thrust, the 'uninstalled engine thrust' will be equal for both fuels. For the engine running on hydrogen this however means a reduction in BET, which leads to an increase in lifetime for all 'hot' engine parts. This gain in lifetime can easily be shown using the Larson-Miller parameter, which gives a relationship (see equation II.6) between the lifetime of a material and the temperature applied to that material.

$$L - M = T * 10^{-3} * (20 + \log(t)) \qquad \text{(II.6)}$$

For a given material and a given strain the value of this parameter can be found for each applied stress on figures similar to Figure II.5. Let us now assume that the material of the first turbine stage has a Larson-Miller parameter of 34 at the stresses that occur during normal turbine operation and at a strain of 0,02%[10]. At a metal temperature of 1.392 K[11] this leads to a lifetime of approximately 25.600 hours. Lowering the BET with 51 K, as for the engine running on kerosene, increases the lifetime of the turbine considerably to an almost infinite life (257.700 hours).

Besides the BET reduction, the TSFC will also undergo a huge reduction and for the installed engines the thrust will differ. In addition to the reduction in BET and in TSFC there is a very small gain in thrust. The results are stated in Tables II.5 and II.6.

Table II.5 Uninstalled engine performance for kerosene and hydrogen

	TIT [K]	FN [kN]	TSFC [kg/kNs]	WF [kg/s]
Kerosene	1.712	400,3	8,48	3,395
Hydrogen	1.661	400,3	2,98	1,194

Table II.6 Installed engine performance for kerosene and hydrogen (special maps)

	TIT [K]	FN [kN]	TSFC [kg/kNs]	WF [kg/s]
Kerosene	1.712	394,5	8,55	3,374
Hydrogen	1.661	394,3	3,01	1,187

[10] It is assumed that the end of the lifetime of the turbine is encountered when the inelastic strain amounts up to 0,02 %.
[11] It is assumed that the cooling of the first turbine stage leads to a metal temperature that is 320 K lower than the gas temperature.

For the uninstalled engine the transition to hydrogen incorporates a reduction in BET of 51 K and a reduction in TSFC of 64,8 %. The installed engine undergoes the same reduction in BET as the uninstalled engine. The thrust decreases however slightly with 0,2 kN and the TSFC falls with 64,8 %.

Finally the Energy Specific Fuel Consumption (ESFC = SFC * FHV[12]) is also compared for both engines since fuel cost is often related to energy content rather than to weight. Comparing ESFC's shows which engine uses the energy contained in the fuel in the most efficient way to give the required thrust. For the uninstalled engine this leads to:

$$ESFC_{kerosene} = 365,7 \text{ J/(N*s)}$$
$$ESFC_{hydrogen} = 353,2 \text{ J/(N*s)}$$

The uninstalled hydrogen-fuelled engine is thus slightly more energy efficient (3,4 %) than the uninstalled kerosene-fuelled engine. For the installed engines a value of 368,8 J/(N*s) is obtained for kerosene while the hydrogen-fuelled engine is again 3,4 % more energy efficient (ESFC = 356,3 J/(N*s)).

II.2.3 Installation losses for the H_2 fuelled engine

As in paragraph II.2.2 the installation losses are determined. The parameters that are altered between the uninstalled engine simulation and the installed engine simulation are the same as for the engines running on kerosene. They can be found in Table II.1 in paragraph II.2.4. Table II.7 gives the installation losses for the hydrogen fuelled engine using standard maps while Table II.8 gives the installation losses when using special maps.

Table II.7 Installation losses for the H_2 fuelled engine using standard maps (TO SLS)

	Uninstalled Engine	**Installed Engine**	**Loss (%)**
FN [kN]	400,3	395,3	(-) 1,3
TSFC [g/kN/s]	2,98	3,00	(+) 0,7

Table II.8 Installation losses for the H_2 fuelled engine using special maps (TO SLS)

	Uninstalled Engine	**Installed Engine**	**Loss (%)**
FN [kN]	400,3	394,3	(-) 1,5
TSFC [g/kN/s]	2,98	3,01	(+) 0,8

[12] In the calculation of the ESFC the FHV given in Gasturb9 is used:
FHV_{kero} = 43,124 MJ/kg and FHV_{hydro} = 128,392 MJ/kg

III.3 Conclusion

The TO rating is first determined for the uninstalled engine running on kerosene. All input parameters are set to reasonable values, if possible directly based on a source otherwise an estimate or the standard Gasturb value is used. The BET is determined so a net thrust of 90.000 lbf is achieved.

Once the basic (uninstalled) engine performance is calculated the installation losses are determined. Since installing the engine will influence the airflow through the engine this is an off-design calculation in Gasturb. In this work it is assumed that the BET does not change during this 'operation' since the exact FADEC law of the engine is not known. The engine is now installed using both standard and special maps. Even though the installation losses are slightly higher for the special maps (0,2 % more loss in thrust and 0,2 % more rise in TSFC) these maps are chosen especially for this particular engine so the results will be more reliant. In general, the installation losses are in the vicinity of 1 %, which seems a reasonable value.

Finally the transition to hydrogen as a fuel is carried out on the uninstalled engines. During this transition only the FHV and the BET are changed. This has as major advantage that the compressors need no redesign. The combustion chamber will though obviously need to be adapted to hydrogen. The turbines also need a small redesign due to the slightly altered turbine capacities. Finally the core nozzle will also have to undergo a small change.

For both the uninstalled and the installed engine the transition to hydrogen furthermore involves a reduction in BET of approximately 50 K, which improves the lifetime of the 'hot' engine components considerably, a reduction in TSFC of approximately 65% and a reduction in ESFC of 3,5%

Chapter III Cruise simulation

Even though TO is considered as the design point for this simulation the major engine regime of an aircraft is cruise since the plane will spend most of its flying time in these conditions. The TSFC of an engine in cruise at high altitude will thus be a very important factor in the choice of an engine.

Below the transition method used in this simulation is explained first. A distinction is made between the transition for kerosene and the transition for hydrogen. Since this transition is an off-design simulation in Gasturb the distinction between standard and special maps is made again.

After this short explanation the results for the four different cases (hydrogen and kerosene both for standard and special maps) is given in a second paragraph of the text. The results for both fuels using the same sets of maps are compared to each other in a table. A short comment on the results is also given.

III.1 The transition method

III.1.1 The transition for kerosene

For the cruise regime the available data is even scarcer than for TO. Furthermore the available data is for slightly different 'circumstances' than the cruise stated by British Airways. According to British Airways the cruise regime for a Boeing 777 is at 35.000 ft with a Mach number of 0,83 while the corrected airflow of Table I.1 is given for a cruise at the same altitude but with a Mach number of 0,85.

To simulate the engines cruise regime the following steps thus have to be taken. In a first step the single cycle calculation for the uninstalled engine at TO regime (see Chapter II) has to be executed. Now the design point data is loaded into the memory of the computer and the off-design calculation can proceed. During these off-design calculations the changes in engine regime are calculated by means of component characteristics. In Gasturb, standard maps are defined but the user can also choose a special map out of a relatively small amount of maps. Both 'methods' are used below and the results of the methods are compared to one another.

Once the component characteristics are chosen the actual transition to cruise can be simulated. First the regime at Mach 0,85 is simulated. Entering 10.668 m (35.000 ft) as the desired altitude and 0,85 as the desired Mach number does this. The exact point of operation is then established by restricting the inlet corrected airflow to 1496,9 kg/s (see Table I.1). In Gasturb's off-design calculations a limiter does this. Since the transition to cruise departed from the uninstalled engine the final action in this step is to install the engine. As for TO this is done by altering the values for the IPR and the power off-take. The ram recovery for cruise is set to 0,998 while the power off-take is the same as for TO (50kW).

In the third and final step in the transition, the change from cruise at Mach 0,85 to cruise at Mach 0,83 is executed. Since the corrected airflow depends on the Mach number the limiter from the previous step is switched off to allow the (corrected) airflow to change. Finally, entering 0,83 as the desired Mach number finishes off the transition.

III.1.2 The transition for hydrogen

In order to determine the cruise regime for the hydrogen-fuelled engine a different procedure is used. As for the engine running on kerosene the transition starts with the single cycle calculation of the uninstalled (H_2-fuelled) engine at TO. After this single cycle calculation the transition to off-design is made and the engine is installed. This installation is simulated in Gasturb – as for the engine running on kerosene – by setting the IPR and the power off-take to their appropriate values (0,998 and 50 kW respectively). Once this is done the actual transition to cruise is simulated by fixing the altitude to 10.668 m (35.000 ft) and the Mach number to 0,83. Finally the thrust is limited to the value obtained for the cruise regime of the engine running on kerosene. This is done in order to be able to compare the results of both simulations concerning TIT and TSFC. In reality the thrust of the hydrogen-fuelled engine will have to be higher than the thrust of the engine running on kerosene. The drag of the aircraft will namely rise due to the larger volume of fuel[13] as can be seen from the values for the lift-to-drag ratio in cruise used in [1]. Due to this rise in drag the lift-to-drag ratio of the evaluated subsonic passenger aircraft will – according to [1] – decrease from 17,91 for a Jet A-fuelled aeroplane to 16,07 for a LH_2-fuelled plane.

III.2 The transition calculation

As indicated above, the actual transition from TO to cruise is done by an off-design calculation. In these off-design calculations the variations in regime are computed by use of the component characteristics. Gasturb allows the users to choose between standard and special component characteristics (the so-called maps). Of course the choice of these maps will have an influence on the transition and thus also on the cruise regime. Underneath the transition with both the standard and the special maps is executed and both 'methods' are compared to each other.

III.2.1 Transition using standard maps

III.2.1.1 The results for the engine running on kerosene

The Gasturb output for the cruise regime using standard maps for the components can be found in Appendix B. The most important results are also given below.

- FN = 42,3 kN
- TSFC = 18,96 g/kNs
- WF = 0,801 kg/s
- BPR = 10,75
- π_g = 31,3
- π_F (OFPR) = 1,37
- $\pi_{fan + booster}$ (IFPR) = 1,63

[13] Hydrogen takes approximately 4 times the volume of kerosene for the same content of energy.

- π_{HPC} = 19,3
- BET = 1.376 K
- W_{2Rstd} = 1.499 kg/s
- W_2 = 595 kg/s
- T_{t4}/T_{t2} = 5,53

III.2.1.2 The results for the hydrogen-fuelled engine

As for the engine running on kerosene the results for this off-design transition to cruise can be found in Appendix B while the most important results are given below.

- FN = 42,3 kN
- TSFC = 6,70 g/kNs
- WF = 0,283 kg/s
- BPR = 10,76
- π_g = 31,3
- π_F (OFPR) = 1,37
- $\pi_{fan + booster}$ (IFPR) = 1,63
- π_{HPC} = 19,3
- BET = 1.345 K
- W_{2Rstd} = 1498 kg/s
- W_2 = 595 kg/s
- T_{t4}/T_{t2} = 5,40

III.2.1.3 Comparison of the results

- FN = 42,3 kN
- TSFC = 18,96 g/kNs
- WF = 0,801 kg/s
- BPR = 10,75
- π_g = 31,3
- π_F (OFPR) = 1,37
- $\pi_{fan + booster}$ (IFPR) = 1,63
- π_{HPC} = 19,3
- BET = 1.376 K
- W_{2Rstd} = 1.499 kg/s
- W_2 = 595 kg/s
- T_{t4}/T_{t2} = 5,53

Table III.1 Comparison of the results for hydrogen and kerosene at cruise (standard maps)

	W_{2Rstd} [kg/s]	**BET [K]**	**FN [kN]**	**TSFC [g/kNs]**	**ESFC [J/kNs]**	**WF [kg/s]**
Kerosene	1.499	1.376	42,3	18,96	817,5	0,801
Hydrogen	1.498	1.345	**42,3**	6,70	792,9	0,283

As can be seen in Table III.1, the airflow through the engine is approximately equal for both fuels. This has as major advantage that no new intake needs to be designed. Further more the pressure ratios of the different components are only slightly altered with the fuel transition. This means that the different compressors of the engine can be reused without change. The turbines and the core nozzle will though need a small adaptation due to the slightly different airflow at those components. Finally Table III.1 shows a reduction in BET of approximately 31 K. This means a major benefit with respect to lifetime of the engine hot components. Due to the transition to hydrogen as a fuel, the TSFC ultimately undergoes a reduction of approximately 64,7% while the ESFC is reduced with 3%.

III.2.2 Transition using special maps

To investigate the influence of the choice of the maps the transition now is executed by means of the special maps. The special maps used are the same as the ones used for the calculation of the installation losses at the TO rating (Chapter II).

III.2.2.1 The results for the engine running on kerosene

As for the standard maps, the Gasturb output can be found in Appendix B while the most important results are given below.

- FN = 43,9 kN
- TSFC = 19,41 g/kNs
- WF = 0,852 kg/s
- BPR = 10,1
- π_g = 33,6
- π_F (OFPR) = 1,38
- $\pi_{fan + booster}$ (IFPR) = 1,64
- π_{HPC} = 20,7
- BET = 1.399 K
- W_{2Rstd} = 1.505 kg/s
- W_2 = 597 kg/s
- T_{t4}/T_{t2} = 5,62

III.2.2.2 The results for the hydrogen-fuelled engine

The Gasturb output for the hydrogen-fuelled engine using standard maps can also be found in Appendix B.

- FN = 43,9 kN
- TSFC = 6,86 g/kNs
- WF = 0,301 kg/s
- BPR = 10,1
- π_g = 33,6
- π_F (OFPR) = 1,38
- $\pi_{fan + booster}$ (IFPR) = 1,64
- π_{HPC} = 20,7
- BET = 1.368 K
- W_{2Rstd} = 1.504 kg/s

- W_2 = 597 kg/s
- T_{t4}/T_{t2} = 5,49

III.2.2.3 Comparison of the results

Table III.2 Comparison of the results for hydrogen and kerosene at cruise (special maps)

	W_{2Rstd} [kg/s]	BET [K]	FN [kN]	TSFC [g/kNs]	ESFC [J/kNs]	WF [kg/s]
Kerosene	1.505	1.399	43,9	19,41	837,2	0,852
Hydrogen	1.504	1.368	**43,9**	6,86	812,1	0,301

Using special maps instead of standard maps to calculate the transition to cruise leads to the same conclusions as in paragraph III.2.1.3. The airflow through the engine as well as the pressure ratios of the compressor section remain the same for both fuels[14]. This means again that those components (compressor and intake) can be reused. The reduction in BET amounts this time to 31 K, a considerable reduction regarding the lifetime of the hot components. Again the TSFC is reduced with approximately 65 % while the ESFC decreases with 3 % due to the change of fuel.

III.2.3 Comparison between standard and special maps

Comparing Table II.2 and Table III.3 shows us that there is only a small difference for the cruise rating determined through special maps and the cruise rating determined through standard maps. Using the special maps option leads to a slightly higher corrected airflow and a higher BET, which results in a higher thrust.

Since the special maps are chosen for this specific engine it can be assumed that they are the most 'realistic' maps. Nevertheless the standard maps prove to give a good estimate when there is no data available concerning the engine components. They can thus be used without a too big penalty.

III.3 Conclusion

The transition to cruise is first executed – both for the standard and the special maps – for the engine running on kerosene. Iterating the BET to obtain the thrust of the engine running on kerosene then does the transition for the hydrogen-fuelled engine. Even though there are – again – small differences between the two sets of maps the general conclusions are the same. The TSFC and ESFC both decrease with respectively approximately 65 and 3% while the BET is reduced with approximately 31 K

[14] Even though there is obviously a change in results between the standard map and the special map method.

Chapter IV Simulation of a possible mission

Now that the TO and cruise ratings are determined a theoretical flight is simulated in Gasturb via the mission option of the program. This option allows the user to chose several points of interest that the program calculates in one run. First, the chosen mission points are determined. The altitude, the Mach number and the chosen limiter are given per flight segment.

Since the rating of the engine during the climb segment is determined by limiting the required thrust, an expression for the thrust in climb is derived next. The method of operation is explained and the values for the kerosene-fuelled engine are calculated.

Now that the thrust required during climb is known, the whole mission can be calculated. The main results are given in this chapter and are commented if possible. The thermodynamic cycles of the different points are given in Appendix D.

The whole mission for the kerosene-fuelled Boeing 777-200 is now known. Based on the results of the mission the maximum range of the plane is then determined and compared to the values given by Boeing.

Finally, the range of the hydrogen-fuelled aeroplane is calculated. Several options are worked out and compared to the kerosene-fuelled plane. The range for the hydrogen plane with the same mass of fuel, the same volume of fuel and the same energy content in the fuel are calculated. To conclude the mission calculations, the mass of hydrogen needed to give the plane the same range as the kerosene-fuelled plane is determined.

IV.1 The chosen mission points

The mission option of Gasturb allows the user to choose up to 30 different points to define a mission. In this work a standard flight of a Boeing 777-200 is simulated. The aircraft takes off from an airport at sea level and climbs to its cruise altitude (35.000 ft or 10.668 m). Once the 777 arrives at this height it flies in cruise for approximately 9.650 km. After this long cruise flight the plane descents to its destination, an airport at sea level, where it lands. The different speeds during the climb and descent segment of the flight are based on references [2], [15], [17] and [18]. The determination of the different points is explained below for each flight segment. Table IV.1 gives a survey of the chosen mission points. As can be seen from this table the exact points are determined via a limiter. After the table is given, the different mission segments are explained.

Table IV.1 A survey of the chosen mission points

	Rating	Height [ft]	Mach number	Limiter
1	TO SLS ISA	0	0	T_{t4}/T_{t2}
2	TO	50	0,26	T_{t4}/T_{t2}
3	CLIMB	1.000	0,30	F_N
4	CLIMB	10.000	0,41	F_N
5	CLIMB	15.000	0,49	F_N

6	CLIMB	23.000	0,61	F_N
7	CLIMB	30.000	0,75	F_N
8	TOP OF CLIMB	34.500	0,82	F_N
9	CRUISE	35.000	0,83	T_{t4}/T_{t2}
10	TOP OF DESCENT	34.500	0,81	N
11	DESCENT	30.000	0,74	N
12	DESCENT	23.000	0,61	N
13	DESCENT	15.000	0,48	N
14	DESCENT	10.000	0,39	N
15	DESCENT	1.000	0,23	N
16	LAND	50	0,21	T_{t4}/T_{t2}
17	LAND SLS ISA	0	0	T_{t4}/T_{t2}

IV.1.1 The Take Off segment

TO is simulated with two points. The first point represents the moment when the pilot moves his throttle to the TO position and the aircraft begins to accelerate from zero speed. The second point simulates the engine at the moment of take off with the aircraft crossing the threshold height of 50 ft. The plane takes off at a Mach number of 0,26. This value is based on [2] where a take off speed of approximately 90 m/s is given for a large passenger aircraft. [18] gives a range from 270 km/h (70 m/s) to 345 km/h (96 m/s) for a Boeing 777.

In order to fully capture the two points in Gasturb, a limiter must be chosen and switched on. For the Take Off segment, T_{t4}/T_{t2} is chosen and its value is set to the value from Chapter II for both points.

IV.1.2 The climb segment

The different points during the climb segment are determined via references [15], [17] and [18]. Based on reference [15] this flight segment is divided into intervals. In these intervals a constant speed and rate of climb are assumed. Table IV.2 gives a survey of the chosen points and the different speeds in these points.

Table IV.2 The different speeds at the chosen points for the climb segment

	Rating	**Height**	**Mach number**	**Rate of Climb [fpm]**	**Time[s]**
3	CLIMB	1.000 ft	0,30	1.400	386
4	CLIMB	10.000 ft	0,41	1.150	261
5	CLIMB	15.000 ft	0,49	1.000	480
6	CLIMB	23.000 ft	0,61	700	600
7	CLIMB	30.000 ft	0,75	500	540
8	TOP OF CLIMB	34.500 ft	0,82	400	75

During the climb segment the active limiter is the thrust required when climbing at the given rate of climb and speed. How the exact values for the limiter is determined is explained in paragraph IV.2.

IV.1.3 The cruise segment

Maximising the range of an aircraft obliges the plane to follow a flight path called the cruise-climb. In this cruise-climb the aircraft climbs constantly while its weight diminishes in order to fly at a constant lift coefficient. The cruise-climb is normally however not permitted for transport aircraft because of the desire by air-traffic control to keep all aircraft at a constant altitude and airspeed. But on a long flight air-traffic control may nevertheless permit a 'stairstep' flight path in which an aircraft climbs to a more optimal altitude several times during the cruise as fuel is burned off. In this work it is though assumed that the plane flies at 35.000 ft ISA during the whole cruise segment.

The cruise rating is finally completely captured by setting the T_{t4}/T_{t2} ratio to the value obtained in chapter III.

IV.1.4 The descent segment

As for the climb segment the descent is represented by a number of points at a different altitude and speed. For the heights of the different points the values from the climb segment are taken. According to [5] the descent is flown at constant speed with the engine in its idle setting. Below 10.000 ft the speed of a Boeing 777 is however limited – due to airframe structural considerations – to 250 kts or 129 m/s (see reference [15]) while the landing speed (V_{at}) is restricted to 140 kts (72 m/s). This 'descent plan' leads to the Mach numbers given in Table IV.3

Table IV.3 The different speeds at the chosen points for the descent segment

	Rating	Height	Mach number
10	TOP OF DESCENT	34.500	0,81
11	DESCENT	30.000	0,74
12	DESCENT	23.000	0,61
13	DESCENT	15.000	0,48
14	DESCENT	10.000	0,39
15	DESCENT	1.000	0,23

During the descent the engine does not have to deliver thrust to pull the aircraft forward. Therefore a limiter as the thrust or T_{t4}/T_{t2} is not suitable here. In reality, the idle stop is set so that the main generator remains online during the descent. Fixing the actual HP spool speed to approximately 65 to 66% of the spool speed at TO SL does this. Normally, at 10.000 ft, this gives the engine a thrust between –10% to +5% of the TO thrust. At 1.000 ft the actual HP spool speed is again fixed to 100% in order to allow a fly-by.

IV.1.5 The landing segment

During the landing segment the engine is at a high rating since the aircraft must be able to perform a touch and go (overshoot) in case a landing is impossible. In order to simulate that, the engine is set at a rating similar to TO. This is done by setting the ratio T_{t4}/T_{t2} to 5,94 the value obtained in the TO simulation

As for the TO segment the landing is simulated with two points. The first point simulates the engine at the threshold height of 50 ft. A landing speed of approximately 140 kts (M =0,21) is assumed. The second point of the landing segment represents the moment when the aircraft is decelerated to zero speed.

IV.2 Thrust required during climb

During the climb the thrust does non-solely have to compensate the drag, thrust is also needed to counterbalance a part of the weight. Below it is explained how the required thrust is calculated for the different points of the climb segment. At first Newton's law is given for an aircraft in climb and the expression for the thrust is derived. Since the thrust depends on the lift-to-drag ratio this ratio is determined next. Finally the weight of the plane is determined for the chosen climb points and the required thrust is calculated.

IV.2.1 Newton' s second law

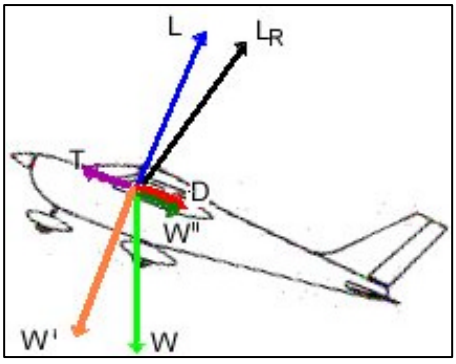

Figure IV.1 The forces acting on a plane in climb

Applying Newton's second law to an aircraft in climb (see Figure IV.1) leads to equation IV.1. Assuming a steady state climb (no acceleration) reduces the right term of equation IV.1 to zero. This obviously incorporates an error. Since the mean acceleration is relatively small (< 0,1m/s²) compared to the acceleration of gravity (9,81m/s²), this error can be neglected regarding the uncertainty of the values of L/D (paragraph IV.2.2). In equation IV.1 it is also assumed that the thrust is coaxial to the plane's axis. Rearranging of equation IV.1 and a projection on the axis of the plane leads to equation IV.2. This equation is used to determine the thrust required in order to achieve a certain rate of climb.

$$\vec{L}+\vec{D}+\vec{T}+\vec{W}=\frac{W}{g}\vec{a} \qquad \text{(IV.1)}$$

$$\frac{T}{W}=\frac{1}{L/D}*\cos\alpha+\sin\alpha \qquad \text{(IV.2)}$$

The angle a in equation II.2 is the angle between the horizontal axis and the axis of the plane (flight path angle). This angle can be determined via equation IV.3. In this equation, R/C stands for the rate of climb (in m/s) and $V_{A/C}$ stands for the horizontal speed of the aircraft.

$$\alpha=\arctan\frac{R/C}{V_{A/C}} \qquad \text{(IV.3)}$$

With the chosen R/C's this leads to the angles a of Table IV.4

Table IV.4 The flight path angle at the chosen points for the climb segment

	Rating	Height	R/C [fpm]	Flight path angle a [°]
3	CLIMB	1.000 ft	1.400	3,99
4	CLIMB	10.000 ft	1.150	2,61
5	CLIMB	15.000 ft	1.000	1,85
6	CLIMB	23.000 ft	700	1,04
7	CLIMB	30.000 ft	500	0,64
8	TOP OF CLIMB	34.500 ft	400	0,48

IV.2.2 The Lift-To-Drag ratio

Equation IV.2 shows that the required thrust during the climb segment depends on the aircraft's weight (W), on the slope of the aircraft (a) and on the lift-to-drag ratio (L/D). Since we do not know the exact lift-to-drag ratio law of a Boeing 777 some assumptions have to be made. Furthermore the values found for L/D are always given for cruise. Since the aircraft flies at a different angle of attack during climb the value of L/D will have to be adjusted. An adjustment is also made for the L/D of a hydrogen-fuelled aircraft.

According to reference [14] the lift-to-drag ratio of a subsonic jet transport aircraft in cruise varies between 16 and 20 while Cumpsty (ref [2]) gives values between 17 and 20 for a new large transport aircraft. In [1] an estimated value for the lift-to-drag ratio of a plane adapted to hydrogen[15] is also given. The values used there are 17,9 for a kerosene-fuelled large transport aircraft and 16,1 for a hydrogen-fuelled large transport aircraft. This work uses 20 as the value for L/D in cruise for the aircraft running on kerosene. For the aircraft running on hydrogen the lift-to-drag ratio is set to 18 in this work.

Once the values for L/D are chosen they still have to be adopted to climb since the angle of attack of the plane in climb will differ compared to the plane in cruise. The larger flight path angle in climb will cause the drag of the plane to rise. The lift will decrease though since the thrust 'helps' the lift to compensate the weight of the aircraft. The combination of these two effects will lead to a smaller lift-to-drag ratio in climb than in cruise. The values used for the different points of the climb segment are stated in Table IV.5.

Table IV.5 The lift-to-drag ratio for the different points of the climb segment

	Height	$L/D_{kerosene}$	$L/D_{hydrogen}$
3	1.000 ft	18	16
4	10.000 ft	18,5	16,5
5	15.000 ft	19	17
6	23.000 ft	19,5	17,5
7	30.000 ft	20	18
8	34.500 ft	20	18

[15] Using hydrogen as a fuel will increase the volume required for fuel. Adding an extra fuel tank on top of the fuselage of the plane creates this extra volume. It unfortunately also increases the drag, so the lift-to-drag ratio will decrease.

As can be seen from Table IV.5 an increase in the lift-to-drag ratio is imposed in order to include the gradual decrease of the flight path angle during the climb segment.

IV.2.3 The gross weigth at a certain altitude

In order to be able to calculate the required thrust through equation IV.2 the gross weight of the aircraft at the different points during the climb segment still has to be determined. This is done based on the weight fractions given in reference [5]. In this work the author gives weight fractions[16] for the different flight segments that are determined through historical data. These fractions can also be found in Table IV.5.

Table IV.6 The weight fractions used in [5]

Flight Segment	**Weight fraction** W_i / W_{i-1}
Warm-up and TO	0,970
Climb	0,985
Landing	0,995

The weight fraction for climb given in Table IV.5 is 0,985. This however is the fraction for the total climb segment from the take-off altitude (zero ft) to the cruise height (35.000 ft). Since the climb segment of this simulation is divided into several height intervals, a fraction must be calculated for each interval. Dividing the climb into intervals of 1.000 ft allows us to calculate these fractions by assuming a constant factor for each of these 1.000 ft intervals. So every time the aircraft climbs a 1.000 ft higher its weight is lowered by a fraction of $\sqrt[35]{0,985}$.

Using this assumption and the Boeing 777-200 Take-off weight of 247.210 kg (545.000 lbs (see reference [16]) leads to the gross weight at an altitude of 1000 ft of Table IV.7. From this point on, the weights of the aeroplane are however determined via the Fuel Flow calculated through Gasturb. These gross weights are also given in Table IV.7. At the beginning of the cruise segment a gross weight of 232.812 kg is thus determined.

Table IV.7 The gross weight of the kerosene-fuelled aircraft for the different points of the climb segment

	Height [ft]	*Weight [kg]*
3	1.000	239.690[17]
4	10.000	238.260
5	15.000	237.414
6	23.000	235.981
7	30.000	234.386
8	34.500	233.007

[16] The weight fraction for a particular flight segment is given as W_i/W_{i-1} with W_i the weight of the aircraft before this flight segment and W_{i-1} the weight of the aircraft after this segment. As can be seen from Table IV.5 the weight fraction for warm-up and take-off is 0,97. This means that at the end of the warm-up and take-off segment there is already 3% of the initial weight used or 97% of the initial weight remains.

[17] $W_{1.000\,ft} = \sqrt[35]{0,985} * W_{0ft} = \sqrt[35]{0,985} * 0,97 * 247.210$

IV.2.4 The required thrust

Since the gross weights (W), the lift-to-drag ratio's (L/D) and the slope of the aircraft (a) is known for each point of the climb segment, equation IV.2 can be solved to obtain the required thrust. Using the values stated in the different tables above leads to the results of Table IV.8.

Table IV.8 The required thrust for the kerosene-fuelled aircraft for the different points of the climb segment

	Height [ft]	*Thrust [kN]*
3	1.000	147,0
4	10.000	116,3
5	15.000	98,9
6	23.000	80,4
7	30.000	70,3
8	34.500	66,7

IV.3 The mission results for the kerosene-fuelled aeroplane

All the selected mission points have been determined unambiguously so Gasturb can now calculate the thermodynamic cycle for every point. The complete Gasturb output of this calculation is given point by point in Appendix D while this paragraph only deals with the most important results. These results are given segment by segment while Figure IV.2 shows the flight profile of the calculated mission.

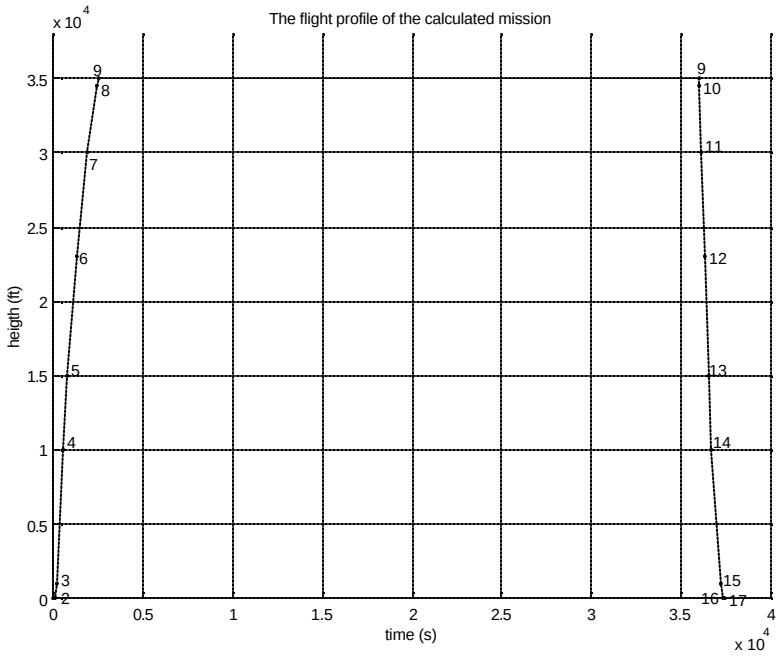

Figure IV.2 The flight plan of the calculated mission

IV.3.1 The take-off segment

In the mission calculation the limiter used in the TO segment is T_{t4}/T_{t2}. The value for the limiter is set to 6,05 as calculated in Chapter II. The IPR is set to 0,995 for both points. Even though there normally is a small improvement in the IPR due to the increasing forward speed of the aircraft (see e.g. reference [4]) both values are equal in this simulation. Between TO (M=0) and cruise (M=0,83) there is namely only a difference of 0,003 for the IPR. The power off-take for both points is set to the value from Chapter II (50 kW). The results for both points of the TO segment can be found in Table IV.9.

Table IV.9 The results for the Take-off segment for the kerosene-fuelled aircraft

	FN [kN]	TSFC [g/kNs]	T_{t4} [K]	T_{t4}/T_{t2}	WF [kg/s]	W_2 [kg/s]	$V_{j,prim}$ [m/s]	$V_{j,sec}$ [m/s]
1	394,5	8,55	1.712	5,94	3,37	1.530	263	260
2	297,2	11,98	1.735	5,94	3,56	1.616	274	275

IV.3.2 The climb segment

As explained in paragraph IV.2 the thrust is limited in the simulation of the climb segment. Again – as for the TO segment – the IPR rises with increasing speed. The exact values for the IPR of each point can be found in Appendix D. During the climb the handling bleed is set to zero while the power off-take remains 50 kW. The main results for the different points are given in Table IV.10

Table IV.10 The results for the climb segment for the kerosene-fuelled aircraft

	FN [kN]	TSFC [g/kNs]	T_{t4} [K]	T_{t4}/T_{t2}	WF [kg/s]	W_2 [kg/s]	$V_{j,prim}$ [m/s]	$V_{j,sec}$ [m/s]
3	147,0	12,60	1.442	4,95	1,85	1.261	177	225
4	116,3	13,93	1.453	5,24	1,62	1.072	204	250
5	98,9	15,09	1.462	5,40	1,49	976	222	266
6	80,4	16,53	1.486	5,70	1,33	829	258	294
7	70,3	18,17	1.537	6,04	1,28	725	313	311
8	66,7	19,53	1.626	6,52	1,30	649	367	311

During the climb segment the aircraft does non-solely have to gain altitude, its speed must rise too. Due to this the Top-of-Climb rating is the most severe rating for the engine even though the temperature will not rise as high as in the TO rating. The parameter used to express the severity of the rating is namely T_{t4}/T_{t2} (see reference [2]). In this reference Cumpsty gives a rise of 4% in T_{t4}/T_{t2} as an example of an existing engine. In this simulation a rise of 10 % is obtained. Even though this value is reasonably higher than the value read in [2], the results are kept as they are. In a real flight the plane will namely climb to a lower cruise altitude and fly a stairstep cruise segment (see also paragraph IV.1.3). An initial cruise altitude of 30.000 ft would namely give a rise in T_{t4}/T_{t2} of only 2% which is in line with the results from Cumpsty. In reference [12] it is also mentioned that the engine for Boeings still-to-be-developed Sonic Cruiser needs a different relationship of climb thrust to take-off thrust

due to its higher cruising altitude. This would – according to the reference – lead to a redesign of the core size, which is normally set by top of climb thrust requirements. Keeping this in mind a rise in T_{t4}/T_{t2} of 10 % is plausible as the aircraft drag of a cryoplane will also be much higher than for a normal aircraft.

IV.3.3 The cruise segment

As in the TO segment the operating point in cruise is fixed by setting the value of T_{t4}/T_{t2} to the value obtained before. Setting T_{t4}/T_{t2} to 5,74 leads to the data from Table IV.11.

Table IV.11 The results for the cruise segment for the kerosene-fuelled aircraft

	FN [kN]	**TSFC [g/kNs]**	**T_{t4} [K]**	**T_{t4}/T_{t2}**	**WF [kg/s]**	**W_2 [kg/s]**	**$V_{j,prim}$ [m/s]**	**$V_{j,sec}$ [m/s]**
9	43,9	19,41	1.399	5,62	0,852	597	277	304

IV.3.4 The descent segment

During the descent the engines operate in their flight idle rating. To simulate this the values of the actual HP spool speed is limited to 67%[18]. The resulting Gasturb output is stated in Table IV.12.

Table IV.12 The results for the descent segment for the kerosene-fuelled aircraft

	FN [kN]	**TSFC [g/kNs]**	**T_{t4} [K]**	**T_{t4}/T_{t2}**	**WF [kg/s]**	**W_2 [kg/s]**	**$V_{j,prim}$ [m/s]**	**$V_{j,sec}$ [m/s]**
10	-4,5	-68,62	768	3,09	0,308	414	57	239
11	-4,9	-53,10	790	3,11	0,258	454	53	222
12	-5,1	-46,46	817	3,13	0,239	487	47	187
13	-5,1	-44,53	801	2,96	0,227	512	40	151
14	-5,9	-30,56	704	2,55	0,181	487	34	222
15	291,9	11,44	1.712	5,92	3,34	1542	268	270

As can be seen from Table IV.12, the value for T_{t4}/T_{t2} at 1.000 ft is in the vicinity of the TO value (5,94). In reality this is also the case since a touch and go should be possible.

IV.3.5 The landing segment

Since T_{t4}/T_{t2} is set to the TO value, the results of the landing segment are very similar to the results of TO. There only is a small difference since the landing speed and the speed at TO are not the same. The results for the landing are given in Table IV.13. During the landing both points have a IPR of 0,995.

[18] In paragraph IV.1.4 65-66% is mentioned, but the iteration performed in Gasturb to determine the exact points of the descent segment does not converge for speeds lower than 67% of the TO speed.

Table IV.13 The results for the landing segment for the kerosene-fuelled aircraft

	FN [kN]	TSFC [g/kNs]	T_{t4} [K]	T_{t4}/T_{t2}	WF [kg/s]	W_2 [kg/s]	$V_{j,prim}$ [m/s]	$V_{j,sec}$ [m/s]
16	311,2	11,23	1.727	5,94	3,49	1.587	270	270
17	394,5	8,56	1.712	5,94	3,37	1.530	263	260

IV.4 The range with The kerosene-fuelled engines

The whole mission is determined in Gasturb. The range of the kerosene-fuelled aircraft can now be calculated since the range is simply the sum of the distances travelled in climb, descent and cruise. In order to be able to sum these three distances the gross weight of the aircraft at the beginning and the end of the cruise segment must be determined first. These gross weights are thus first calculated, keeping a certain amount of backup fuel in mind. After this is done, the cruising distance is determined and finally the range of the kerosene-fuelled aeroplane is calculated.

IV.4.1 The weight at the beginning of the cruise segment

As stated in paragraph IV.2.3, the gross weight of the aeroplane at the beginning of the cruise segment is determined through the calculated fuel flow at each point of the climb segment. This method leads to an aircraft weight of 232.812 kg at the beginning of the cruise phase of the flight.

IV.4.2 The weight at the end of the cruise segment

Even though the weight fraction required during the landing segment of the flight is given in Table IV.6, the calculation of the gross weight at the end of the cruise flight is a bit harder to execute since Raymer gives no weight fraction for the descent segment in reference [5]. Raymer namely assumes that the descent segment is included in the cruise segment. Furthermore a fuel backup is needed to allow the aircraft to loiter around its destination or to fly to an alternative airport in case of bad weather conditions at the airport of destination.

Below these gross weights are calculated. At first, the weight of the backup fuel is determined. Using this mass allows us then to calculate the landing weight of the aeroplane. Finally the fuel burned off during the descent segment is calculated and the weight of the aeroplane at the end of the cruise segment is given.

IV.4.2.1 The weight of the fuel used as a backup

For a normal long-range flight a backup fuel is needed for a loiter time of approximately 20 to 30 minutes and a touch and go in case of an overshoot. Loiter is normally is flown at a flight level of approximately 20.000 ft and a Mach number in the vicinity of 0,5. The amount of fuel needed for backup is then given by equation IV.5.

$$W_{backup} = 2 * t * (WF)_{loiter} \qquad \text{(IV.5)}$$

A loiter time of 30 minutes (3.600 s) at 20.000 ft (WF=1,175 kg/s) leads to an amount of backup fuel of approximately 4.230 kg.

IV.4.2.2 The landing weight of the aircraft

Now that the amount of backup fuel is known, it is easy to calculate the gross weight of the aircraft after the landing using equation IV.6

$$W_{land} = W_{empty\ +\ payload} + W_{backup} \qquad \text{(IV.6)}$$

First the weight of the empty aircraft and the payload ($W_{empty\ +\ payload}$) has to be determined. This is done by simply subtracting the maximum fuel capacity (117.335 l or 93.868 kg) from the maximum Take-off gross weight (MTOW=247.210 kg). This results in a $W_{empty\ +\ payload}$ of 153.342 kg. Using the calculated value of 4.230 kg for W_{backup} finally leads to a landing weight of 157.572 kg.

The weight of the plane before it begins its landing segment is now calculated through the weight coefficient for landing (0,995) of Table IV.6. This leads to a weight before landing of approximately 158.365 kg.

IV.4.2.3 The weight of the fuel used during the descent segment

The fuel used during the descent segment is determined via the calculated descent points of the mission. In the calculation of the used weight the following assumptions are made:

- Between two calculated points the rate of descent is a constant
- Between two calculated points the fuel flow (WF) is a constant
- During the whole descent segment the plane flies at a slope of 3°

These assumptions and equation IV.3 allow us to determine the rate of descent (R/D) in every interval. The R/D then allows the calculation of the time needed for each interval[19]. The calculated R/D's and times are given in Table IV.14. The R/D and the time at a certain height (i) in this table is the R/D respective the time used in the interval between height (i) and height (i+1).

Table IV.14 The R/D, the time and the fuel flow for each interval of the descent segment

	Height [ft]	**Mach number**	**R/D [fpm]**	**Time [s]**	**WF [kg/s]**
9	35.000	0,83	2.540	12	0,852
10	34.500	0,83	2.540	106	0,308
11	30.000	0,81	2.540	165	0,258
12	23.000	0,79	2.540	215	0,239
13	15.000	0,58	1.933	184	0,227
14	10.000	0,39	1.327	508	0,181
15	1.000	0,23	797	75	3,34

[19] For altitudes lower than 23.000 ft the time needed is calculated based upon the average R/D of that interval since the airspeed (and thus also the R/D) is decreasing from there on.

Using these values for the fuel flow leads to an amount of approximately 2.740[20] kg of fuel burned off during the descent.

IV.4.2.4 The weight of the aircraft at the end of the cruise segment

The gross weight of the aircraft at the beginning of the descent segment is now easily determined as the sum of the weight before landing and the weight of the fuel used during the descent. This leads to an aircraft weight at the end of the cruise segment of 161.105 kg.

IV.4.3 The cruise distance

In order to be able to determine the cruise distance as accurate as possible, this flight segment is divided into 30 minutes intervals. For each point the required thrust is then determined through equation IV.2. In cruise a flight path angle (a) of zero degrees is assumed and a value of 20 is taken for the lift-to-drag ratio of the kerosene-fuelled plane. For the hydrogen-fuelled Boeing a lift-to-drag ratio of 18 is assumed. The weights of the plane at the different points are calculated through the fuel flow obtained by Gasturb. A constant fuel flow for each 30 minutes interval is assumed.

Since the duration of the cruise segment for the kerosene-fuelled plane exceeds 10 hours not all the calculated points are given below. Only four points are given to elucidate the evolutions of the different parameters. The first point is the beginning of the cruise segment and a point is given for every three hours 30 minutes of cruise[21]. Table IV.15 gives the results for these points.

Table IV.15 The results for the cruise segment (kerosene-fuelled aircraft)

	W [kg]	FN [kN]	TSFC [g/kNs]	T_{t4} [K]	T_{t4}/T_{t2}	WF [kg/s]	W_2 [kg/s]	$V_{j,prim}$ [m/s]	$V_{j,sec}$ [m/s]
1	232.812	57,1	18,83	1.508	6,06	1,075	629	327	308
2	207.054	50,8	18,82	1.449	5,82	0,956	615	301	306
3	183.934	45,1	19,28	1.408	5,65	0,870	601	281	305
4	162.851	39,9	19,88	1.369	5,50	0,793	587	263	304

Since the gross weight at the end of the cruise segment only amounts to 161.105 kg, 1.746 kg of fuel still needs to be burned after 10 hours and 30 minutes of cruise. With the fuel flow of point 4 of Table IV.15 and two engines this leads to an extra cruise time of 1.101 s. The total cruise time then equals 38.901 s or 10 hours, 48 minutes and 21 seconds.

Since a cruise at constant speed and constant altitude is assumed, the distance travelled in cruise can now easily be determined by simply multiplying the cruise speed and the total cruise time. With a cruise speed of 246,1 m/s (M=0,83 @35.000 ft) and the time calculated above, this leads to a cruising distance of approximately 9.574 km.

[20] For the calculation of the fuel used during the descent between 10.000 ft and 1.000 ft the averaged value is used for the fuel flow ($FF_{used} = \frac{FF_{10kft} + FF_{1kft}}{2}$). This is done since the rating of the engines is changed somewhere in between of the two points.

[21] So the second point is after exactly 3 hours 30 minutes of cruise, the third point after 7 hours of cruise and so on.

IV.4.4 The range

In order to calculate the range of the aircraft the distances flown during climb and descent must still be calculated. These distances are calculated via the assumption that the forward speed of the aeroplane and the rate of climb respectively descent is constant for each considered altitude interval. The rate of climb / descent then enables the calculation of the time spent in each interval and a simple multiplication of this time and the forward speed of the aeroplane finally gives the distance travelled for each interval. Summing these distances then gives the total distance travelled during climb respectively descent. This method of operation leads to a climb distance of 406 km and a descent distance of 203 km.

The total range of the aircraft is now given by the sum of the distances travelled in climb, cruise and descent. The calculated values lead to a range of 10.183 kilometres. Since the official range (see reference [16]) of a Boeing 777-200 is 9.649 km the error made is only 5,5%, which seems a reasonable result, seen the many assumptions made during the calculation.

IV.5 The range with the hydrogen-fuelled engines

Now that the cruise distance for the kerosene-fuelled aircraft is known the mission for the hydrogen-fuelled aeroplane is launched. Several options now are open. In this work four of the possible options are calculated and compared to the original kerosene-fuelled aircraft.

At first, a hydrogen-fuelled plane with the same take-off weight as the kerosene-fuelled aircraft is chosen. This means that the mass of fuel for both planes will be equal (constant payload is assumed). Next, the original plane filled with hydrogen is simulated. The volume of the fuel tanks now determines the amount of hydrogen available. In a third mission for the hydrogen-fuelled aircraft the energy content of the fuel is kept equal for both the planes. The energy content is the product of the mass of fuel and its lower heating value. Finally, in a fourth mission, the amount of hydrogen needed to give the plane the same range as the kerosene-fuelled plane is determined.

IV.5.1 The same mass of fuel

Even though the TO gross weight will be the same[22] the different flight segments all have to be recalculated since the TSFC, and thus the fuel spending, will be different. Since the fuel fractions of Raymer are derived based on older aircraft, these values will definitely no longer be applicable. Therefore, the weights at the different points of the climb segment are again calculated based upon the TSFC given by Gasturb. Below the climb and the descent segment are first determined. The range is then calculated and compared to the range of the kerosene-fuelled aircraft.

[22] Since there is no data available to calculate the changes to the weight of the structure due to the transition to hydrogen, it is assumed here that the structure weight of the hydrogen-fuelled aeroplane equals that of the kerosene-fuelled plane.

IV.5.1.1 The climb segment

Since the TSFC of the engine running on hydrogen is much lower than the TSFC of the kerosene-fuelled engine the weight ratios of Table IV.6 will no longer be applicable. To overcome this, the weights at the different altitudes are determined based on the calculated fuel flow of the previous point. In this calculation it is assumed that the engine is running at the same rating (same fuel flow) during the whole altitude interval. Since there is no data available to calculate the total amount of fuel burned during the TO segment the ratio of Table IV.6 is used here. Based on these calculated weights the required thrust is determined in the same way as for the kerosene-fuelled engine. The values for L/D used are stated in Table IV.5. These calculations lead to the weights and required thrusts in the climb segment given in Table IV.16.

Table IV.16 The gross weights and the required thrusts for the different points of the climb segment of an hydrogen-fuelled Boeing 777-200

	Weight [kg]	*Thrust [kN]*	T_{t4}/T_{t2}
3	239.690	155,1	4,90
4	239.161	124,4	5,21
5	238.844	106,7	5,38
6	238.303	88,0	5,70
7	237.693	77,8	6,20
8	237.138	74,4	6,75

These values lead to a gross weight of the aircraft at the beginning of the cruise segment of 237.058 kg. Again, as for the kerosene-fuelled engine, the ratio T_{t4}/T_{t2} is higher in the top of climb rating than in the TO rating. At TO the ratio amounts to 5,76, so at the top of climb a rise of 17% is achieved. A top of climb at 30.000 ft would give a rise in T_{t4}/T_{t2} of 8% a good result compared to reference [2].

IV.5.1.2 The descent segment

As for the hydrogen-fuelled engine the descent segment is calculated by limiting the actual HP spool speed to 67%. Using the same Mach numbers as for the kerosene-fuelled engine this leads to an amount of fuel burned off during the descent segment of 960 kg.

IV.5.1.3 The cruise distance

In order to be able to determine the cruise distance, the weight at the end of the cruise segment must first be known. This weight is calculated with the same assumptions as for the kerosene-fuelled engine. These assumptions lead to an amount of fuel used for backup of 1.483 kg and thus a landing weight of 154.825 kg. The weight before the landing segment now becomes 154.603 kg. Finally the weight at the end of the cruise segment is 156.563 kg.

As in paragraph IV.4.3 the cruise segment of the flight is again divided into 30 minutes intervals. During such an interval the rating of the engine is assumed to be constant (constant thrust and fuel flow) and the thrust required is calculated as in paragraph IV.4.4.

Using this method leads to a cruise segment of more then 31 hours. The results for only a few of these calculated points are given in Table IV.17. Point 1 of this table corresponds to the

beginning of the cruise phase. The other points are taken every 10 hours[23] so point 2 is taken after a cruise flight of 10 hrs and point 3 after 20 hours cruise. Finally, point 4 is taken after a cruise flight of 31 hours.

Table IV.17 The results for the cruise segment (hydrogen-fuelled aircraft)

	W [kg]	FN [kN]	TSFC [g/kNs]	T_{t4} [K]	T_{t4}/T_{t2}	WF [kg/s]	W_2 [kg/s]	$V_{j,prim}$ [m/s]	$V_{j,sec}$ [m/s]
1	237.058	64,6	6,89	1.567	6,29	0,445	640	369	310
2	207.598	56,6	6,64	1.466	5,89	0,376	628	329	307
3	182.138	49,6	6,68	1.406	5,65	0,331	612	301	306
4	157.282	42,9	6,90	1.361	5,46	0,296	595	277	304

Since the weight of the plane at the end of the cruise segment is only 156.563 kg, 719 kg of hydrogen still needs to be burned after 31 hours of cruise flight (point 4 in Table IV.17). With a fuel flow of 0,296 kg/s per engine this gives the plane an extra cruise time of 1.215 seconds. The total cruise time then amounts to 112.815 s. At a speed of 246,1 m/s this leads to a cruise distance of approximately 27.765 km or a range of 28.373 km. Using the same mass of fuel for a hydrogen-fuelled aeroplane would thus increase the range by a factor 2,79.

IV.5.1.4 The extra volume needed to store the fuel

Since the same mass of fuel is assumed for both kerosene and hydrogen and since the density of liquid hydrogen is much smaller than the density of kerosene an extra volume will be needed for the storage of the hydrogen fuel.

For both fuels an amount of 93.868 kg is used. For kerosene this mass equals 117.335 l (density of 0,8 kg/m³) or 117 m³. 93.868 kg of hydrogen though equals 1.327.246 l (density of 70,8 kg/m³) or 1.327 m³ so an extra fuel tank of 1210 m³ is needed. Suppose now that this extra tank would be placed in the cabin of the Boeing 777. With an interior cabin width of 5,86 m, this would lead to a cylindrical tank of nearly 45 meters long or, with a total length of the aeroplane of 63,7 m, 70% of the interior volume would be taken by fuel.

IV.5.2 The same volume of fuel

Using the Boeing 777-200 as it is without any changes limits the volume of fuel to the standard capacity of 117.355 l. With the volumetric mass of liquid hydrogen (70,8 kg/m³) this leads to a fuel weight of 8.307 kg.

Recalculating the TO weight and the weights during the climb segment as in paragraph IV.4.1[24] leads to a weight at the beginning of the cruise segment of 158.126 kg. This means that 3.523 kg of fuel is used for the climb segment. Since the descent segment in the simulation is independent of the aircraft weight the amount of fuel burned off during descent equals 960 kg so during the climb and descent segment 5.966 kg of fuel is used (including the

[23] Almost one third of the total cruise time
[24] Since the MTOW is much smaller and since the fuel flow of the hydrogen-fuelled engines is only one third of the fuel flow of the kerosene-fuelled engine, a factor of 0,99 is used here for the TO segment instead of the value proposed by Raymer (0,97).

backup fuel of 1483 kg). Since there was only 8.307 kg available the range of this mission will be very small. Using the 30 minutes intervals leads to a cruising time and distance of respectively 43 min 57 s (2637 s) and 649 km. The range is thus only 1.258 km. Even though the calculated range is very small, this 'option' might come in useful for domestic flights in China or Europe e.g. During these flights the cruise segment is namely executed at much lower altitudes which could give the plane a (small but sufficient) range.

IV.5.3 The same amount of energy

In a third mission for the hydrogen-fuelled aircraft the amount of energy contained in the fuel is held constant. The amount of energy of the fuel is the product of the mass of the fuel and the lower heating value of the fuel. Since the mass of the kerosene as well as the lower heating values[25] for both kerosene and hydrogen are known the amount of hydrogen needed to fulfil the requirement of constant energy content is found by equation IV.8

$$WF_{hydro} = \frac{WF_{kero} * LHV_{kero}}{LHV_{hydro}} \qquad \text{(IV.8)}$$

With an amount of kerosene of 93.868 kg (117.335 l @ 0,8 kg/l) this leads to a total energy content of 4.047.964 MJ and to a mass of 34.191 kg hydrogen. Using this amount of fuel allows us to calculate the whole mission using the same procedure as in paragraph IV.1. Below, some of the results of this calculation are given.

The plane takes off with a mass of 187.533 kg and climbs to its cruising altitude. It reaches this altitude with a mass of 181.646 kg. At the end of the cruise segment the aircraft still weighs 156.563 kg. It then uses 960 kg of fuel to descent. Finally after the landing the aeroplane has a mass of 154.825 kg (1.483 kg backup fuel).

Again, as in previous paragraphs the cruise segment is divided into 30 minutes intervals. Using the weights above, the fuel flow as calculated by Gasturb and the cruising speed of 246,1 m/s (M=0,83 @35.000 ft) gives a cruising distance of 9.864 km or a range of 10.473 km or 2,8 % more than the range obtained for the kerosene-fuelled engine. So, in spite of the decrease in ESFC of 3%, the range of the hydrogen-fuelled aircraft is only 2,8 % smaller than the range of the kerosene-fuelled airplane. Due to the lower lift-to-drag ratio the hydrogen-fuelled engines will namely have to provide a higher thrust.

IV.5.4 The same range

In the final mission for the hydrogen-fuelled Boeing 777-200, it is determined how much hydrogen is needed to give the plane the exact same range of the kerosene-fuelled aircraft. Since the same rate of climb and rate of descent is assumed for both airplanes during the whole mission it is only necessary to assure that the same cruising distance is attained. The distance traveled during climb and descent will match too.

[25] The values used for the lower heating value (LHV) of the fuels are the values given by Gasturb:
LHV_{kero}=43,124 MJ/kg
LHV_{hydro}=118,392 MJ/kg

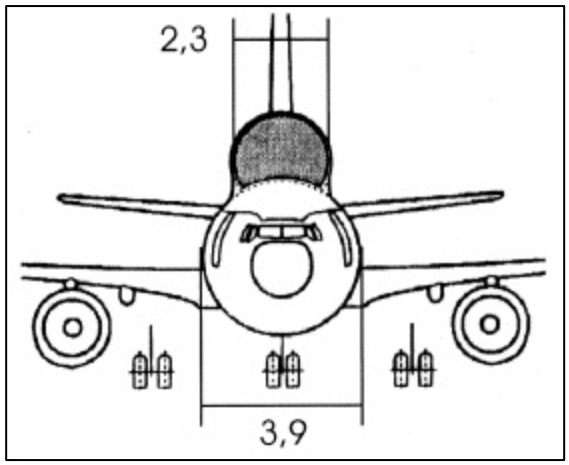

Figure IV.3 The A310 Cryoplane

Since the airspeed in cruise is the same for the hydrogen and the kerosene-fuelled airplane, the time flown in cruise is known (38.901s). In order to be able to determine the TO weight (and thus the fuel weight) required to be able to fly in cruise for that time a method is used that is similar to the method used in previous paragraphs. The cruise segment is also divided into intervals of 30 minutes with a constant engine rating. The only difference here is that the first calculated point is the last point of the cruise phase and that the fuel used in the interval must be added to the weight instead of subtracted. Basically the methods are thus the same but the 'time handling' is inverted. Using this method, a weight of 180.742 kg is calculated for the plane at the beginning of the cruise flight.

Iterating on the thrust required for climb and the weights at the different heights then enables us to calculate the weight of the plane at 1.000 ft. Finally, using the weight fraction for the TO segment of Table IV.6 a value of 186.603 kg is obtained for the TO weight. This means that a reduction of 24,5% of the take-off weight is achieved.

In order to fly a mission with the hydrogen-fuelled plane that has the exact same range as the original mission of the kerosene-fuelled plane an amount of 33.261 kg or 469,79 m³ hydrogen is needed. This means that an extra fuel tank of 352,46 m³ must be provided. Suppose now that this tank is placed above the cabin as in Figure IV.3. Keeping the same ratio between the diameter of the upper tank and the diameter of the cabin leads to a fuel tank diameter of 3,45 m (59% of the interior cabin diameter). Finally, assuming that the area of the tank is 80% of the area of a circle leads to a tank length of 47,13 m or 74% of the total length of the airplane.

IV.6 Conclusion

In this chapter a standard flight of a Boeing 777-200 has been calculated through the mission option of Gasturb. Therefore the flight has been divided into several flight segments. Each of these segments is at its turn represented by one or more points and the determination of each point has been elucidated. The results are given too.

Based on these results, the range of a classic Boeing 777-200 has been determined. Powered by kerosene-fuelled GE90-90B engines the 777 has – according to the outcome of the calculations – a range of 10.183 km. Official data state a range of 9.649 km so an error of only 5,5 % is made. Seen the many assumptions made during the calculations this seems a reasonable result.

Now that the range of the kerosene-fuelled aeroplane is determined, several options for the hydrogen-fuelled Boeing remain open. In this work the range of 4 different hydrogen-fuelled 777's is determined even though not all the theoretical missions offer the same practical possibilities.

First, the range of a hydrogen-fuelled Boeing 777 with the same TO weight as the kerosene-fuelled Boeing has been calculated. Taking off with the same mass of fuel would almost triple the range of the aeroplane according to the calculations. However an extra volume of 1210 m^3 would be required to store the liquid hydrogen. This means that 70% of the total cabin volume would be needed to store the fuel so this is not really a practical alternative.

After this the range of an existing Boeing 777-200 filled with hydrogen has been determined. Using only the existing volume to store the fuel however leaded to a very small range of 1.258 kilometres. It might however be possible to use this alternative for relatively short domestic flights with a much lower cruising altitude.

Finally the TO weight of a hydrogen-fuelled 777 with a range of 10.183 km has been determined since this is the range that has been calculated for the kerosene-fuelled aircraft. A take-off gross weight of 186.603 kg has been determined. This would mean a reduction of 24,5% of the take-off gross weight but would also require an extra fuel tank of 470 m^3. This means an extra fuel tank over almost the whole length of the plane, so the reduction in TO weight will be reasonably smaller than the calculated reduction.

Chapter V
Simulation of a mission for a large subsonic ACES launcher carrier

After calculating and comparing several missions for a Boeing 777-200, a mission for a large subsonic ACES launcher carrier based on 777 structural elements and running on hydrogen as a fuel is now determined.

After a short introduction on the carrier, both the operational empty weight and the take-off gross weight of the carrier are determined.

After this initial sizing of the carrier, the calculated mission is presented. Since the mission shows several similarities with the missions of the previous chapter, only the altered flight segments are dealt with. Therefore, attention mainly goes out to the cruise segment.

Next, the carrier sizing results for the reference lift-to-drag curve are given. Not only the weights at the different mission points are indicated, but the distances travelled are also given and a consideration is made concerning the fuel storage.

Thereafter, the influence of the estimated lift-to-drag curve is given. The leap in-lift-to-drag due to the second stage launch, the average L/D level and the slope of the collection L/D curve are altered and the results are compared.

V.1 The weight of the carrier

Below, the carrier is first introduced briefly. Some of the reasons, which led to the choice of this type of aircraft, are indicated. More information on this and some other carriers can however be found in reference [8]. After this short introduction, the operational empty weight (OEW) and the take-off gross weight (TOGW) of the carrier are calculated. The OEW of a plane is the sum of the weights of the structure (including the engines), the crew, and the extra fuel needed to compensate boiled-off or trapped fuel. The TOGW on the other hand is the sum of the OEW of a plane, the weight of the payload and the weight of the fuel. The assumptions made and the values used from literature are indicated.

V.1.1 The large subsonic carrier plane

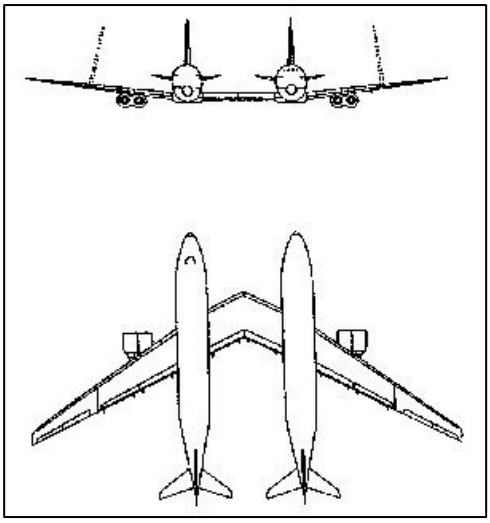

Figure V.1 The twin fuselage subsonic carrier plane

The choice for the carrier plane stems from several limitations, which have to be fulfilled simultaneously. Two of these 'conditions' mainly lead to the chosen configuration. First of all, the maximum cargo capacity of the plane must be high enough to be able to carry the launch vehicle and lift it of the ground. Besides that, a large volume must be available to store the amount of hydrogen needed to fly the launch mission. To meet both limitations, a twin fuselage architecture with four engines has been chosen for the carrier plane (see Figure V.1). This large subsonic carrier plane will launch an expendable second stage in ventral position.

In order to avoid the huge development costs of such a large plane, it has been chosen to use as many cannibalized parts from existing airliners as possible. The few planes that will be required, even if a successful diversification in out-sized cargo transport is achieved, would namely not economically justify any specific development of wings, tails, actuators,… There is now plenty of hardware available, to make this challenge realistic.

V.1.2 The operational empty weight of the carrier

For this mission simulation, a Boeing 777-200-IGW has been selected as the basis for the carrier plane. The two fuselages of the carrier are adapted 777-200 fuselages and the wings are also derived from the same 'motherplane'. In order to be able to simulate the mission though, several assumptions have to be made beforehand to calculate the gross take-off weight of the plane. The following paragraph will present the used assumptions and the results concerning the different calculated weights.

First, the O.E.W of a Boeing 777-200 is given. Then, the weight of a wing of a 777 is calculated as well as the weight of the interfuselage wing. Subsequently, an estimation is made for the weight of the additional equipment, such as the LOX collection plant, launching devices,…. Finally, based on these assumptions, the O.E.W. of the carrier is determined.

V.1.2.1 The empty weight of a Boeing 777-200

The aircraft's operational empty weight (O.E.W.) can be found in reference [13]. For the 777-200-IGW, which is powered by 90.000 lbf-class engines as the GE90-90B, the reference gives an O.E.W. of 315.168 lb or approximately 143.000 kg ($W_{777\text{-}200}$). This value is used in the simulation. It includes the mass of two engines (e.g. the basic engine weight of a GE90-90B is approximately 7.550 kg).

$$O.E.W._{777\text{-}200} = 143.000 \text{ kg}^{26}$$

V.1.2.2 The weight of a wing

Since the chosen carrier plane can be considered as two 777-200 ‘s with one wing, assembled together through the interfuselage wing, the weight of a wing has to be determined in order to be able to calculate the empty weight of the carrier. No data concerning the weight of a B777 wing was available, but Raymer mentions in [5] that the weight of the wings is approximately 15% of the total empty weight of the plane. One wing contributes thus to approximately 7,5% of the total empty weight. With the total empty weight value given above, this leads to:

$$W_{wing} = 10.725 \text{ kg}$$

V.1.2.3 Additional Weights

The weight of the interfuselage wing ***($W_{INT.\ WING}$)***
The weight of the interfuselage wing has to be estimated, since this is one of the few to-be-developed parts. Even though this connection will be much shorter than an actual wing, the weight is taken to be equal to the weight of the wing ($W_{INT.\ WING}$ = 10.725 kg). The connection will namely have to carry the load of the launch vehicle during the whole mission, so a very strong and stiff structure will be needed.

$$W_{INT.\,WING} = 10.725 \text{ kg}$$

The weight of the liquid hydrogen fuel tanks and systems ***(W_{SYS})***
Due to its cryogenic properties hydrogen preferably needs to be stored in cylindrical tanks because the boiled-off fraction would be too big otherwise. Furthermore, a substantial amount of isolation is needed too along with several pumps. In reference [1], Brewer compares several possible configurations for the fuel containment and supply system. Not only weight is considered, safety, reliability and economic factors also play an important role. After weighing the pros and the cons, Brewer finally chooses the two best alternatives and gives weight estimations for both systems. These weight estimations include not only the fuel containment system and its insulation, but also the fuel system (engine supply, fuelling / defuelling, pressurisation / vent).

In this simulation an averaged value of the adapted weights of both alternatives is used. The weights are adapted because Brewer considers two separate tanks[27] in his design and thus two dome ends, while our design contains only one (huge) tank that fills in the whole fuselage. With this adaptation, the values given by Brewer lead to:

$$\frac{W_{SYS}}{W_{FUEL}} = 0{,}365$$

The weight of the LOX Collection Plant ***(W_{LCP})***
The weight of the liquid oxygen collection plant mainly depends on the operational conditions of the plant. Since, in this case, the collection only takes place in cruise, the inlet conditions of the plant will be practically constant and a relatively light-weight plant can be used. Several

[26] The TOGW of a 777-200-IGW is 648.158 lb or 294.000 kg
[27] One in front and one at the back of the fuselage, with the passenger cabin in between.

references, including reference [9], give an estimate of 10.000 kg for the weight of a LCP (including a compression unit for the entering air) operating under these conditions. This value is also used here.

$$W_{LCP} = 10.000 \text{ kg}$$

The weight of the required additional equipment *($W_{ADD.}$)*
The use of the plane as a subsonic carrier for a launch vehicle causes the need for additional equipment. Not only the launch crew and the on-board launch equipment have to be accounted for. Several mechanical systems to carry and release the L.V. as well as the necessary local reinforcements of the plane's structure,… are also required. As in reference [9], an estimated weight of 10 tons is used for this additional equipment.

$$W_{ADD} = 10.000 \text{ kg}$$

V.1.2.4 The operational empty weight of the carrier

All assumptions necessary to calculate the O.E.W. are now made. Since the weight of the fuel systems depends on the amount of fuel needed, this amount still needs to be determined first though. This is done below.

The amount of fuel required for the mission
The total amount of block fuel required for the calculated mission is estimated in reference [9] as 140 tons. Since some of the fuel will be trapped or boiled-off an additional amount of fuel will be needed though. Raymer (ref. [5]) indicates that the fuel weight for kerosene should be multiplied with a factor 1,06 to account for the trapped and boiled-off fuel and for the small dispersion in S.F.C. of an engine type. Hydrogen fuel will however require another factor for several reasons. First of all, the boiled-off fraction will be much higher using hydrogen. In reference [1], the author mentions a boiled-off fraction of 4.1 %[28] for hydrogen versus 0,89 % for kerosene (Jet A). On the other hand, due to its lower density, the weight of the trapped hydrogen will be smaller (for a constant volume of trapped fuel) so less (weight of) fuel will be trapped. Based on mainly these two considerations a factor of 1,10 is chosen to account for trapped and boiled-off fuel leading to a total amount of fuel of 154.000 kg.

REMARK:

An additional amount of 14 tons of LH_2 ($W_{EXTRA\ FUEL}$) is thus necessary to compensate the boiled-off and the trapped fuel. In reality, some of this fuel (the boiled-off fraction) will be lost during the flight. It is however not possible to make a reasonable estimation of when how much fuel will be lost. To compensate that, the whole 14 tons are considered as trapped fuel and remain in the fuselage during the whole, simulated flight. This will add 14 tons to the carriers O.E.W., but it also adds some safety margin to the calculations since this leads to an overestimation of the real O.E.W.

$$W_{EXTRA\ FUEL} = 14.000 \text{ kg}$$
$$W_{TOT\ FUEL} = W_{OPS\ FUEL} + W_{EXTRA\ FUEL} = 154.000 \text{ kg}$$

[28] Percent of the usable fuel weight

The weight of the fuel system
In a previous paragraph the weight of the fuel system was given as a fraction (0,365) of the total fuel weight. Since this weight is now known (154.000 kg), it is easy to calculate the weight of the fuel system as:

$$W_{FUEL\ SYS} = 56.200 \text{ kg}$$

The operational empty weight of the carrier
All the weights, necessary to calculate the operational empty weight of the carrier are now determined[29]. The O.E.W. of the carrier is then determined by:

$$OEW_{CARRIER} = 2*W_{777\text{-}200} - 2*W_{wing} + W_{INT.\ WING} + W_{FUEL\ SYS} + W_{LCP} + W_{ADD} + W_{EXTRA\ FUEL}$$

Using the values given above then leads to an O.E.W. of approximately 365.500 kg.

$$OEW_{CARRIER} = 365.500 \text{ kg}$$

V.1.3 The Take-off gross weight of the carrier

Now that the OEW of the carrier is known, it is easy to determine its TOGW. Simply adding the operational fuel and the payload weight will do so. Since the operational fuel weight is already known (140.000 kg), it is now sufficient to obtain the mass of the launch vehicle, which is the only useful payload.

The weight of the L.V. *($W_{L.V.}$)*
As in reference [9], the weight of the L.V. at take-off is taken as 90.000 kg (LH_2 fuel included). During the cruise phase 210 tons of LOX are collected, so at the release, the L.V. has a weight of 300 tons.

$$W_{LV} = 90.000 \text{ kg}$$

The TOGW of the carrier
Since all the 'component weights' are known, simply summing these weights gives us the TOGW of the fully operational carrier with its second stage:

$$TOGW_{CARRIER} = OEW_{CARRIER} + W_{OPS\ FUEL} + W_{LV}$$

$$TOGW_{CARRIER} = 595.000 \text{ kg}$$

For comparison, the values given by Lozino-Lozinski in reference [11] are 900 tons for the TOGW and 300 tons for the OEW of his proposed dual-boom subsonic TSTO launcher without ACES.

[29] In reality, the weight of the landing gear will also change. The landing gear weight is namely roughly 3% of the take-off gross weight. Since the weight of the carrier is not equal to twice the weight of a 777-200, the landing gear weight will alter. This weight change has though been omitted here.

V.2 The calculated mission

Basically, only the cruise segment of the mission will be altered compared to the mission of the previous chapter. Since the climb segment will be slightly different too (due to the change in L/D), this segment is given here too. Descent, landing and TO, which remain unaltered, are not mentioned here.

V.2.1 The climb segment

As mentioned, this flight segment essentially does not undergo any change. Only the lift-to-drag ratio of the plane is altered. Due to the double fuselage and the presence of the launch vehicle, the drag will namely rise. Table V.1 summarises the data used for the climb segment.

Table V.1 The chosen points for the climb segment

	Height	Mach number	Rate of Climb [fpm]	Flight path angle a [°]	L/D
3	1.000 ft	0,30	1.400	3,99	14
4	10.000 ft	0,41	1.150	2,61	14,5
5	15.000 ft	0,49	1.000	1,85	15
6	23.000 ft	0,61	700	1,04	15,5
7	30.000 ft	0,75	500	0,64	16
8	34.500 ft	0,82	400	0,48	16

V.2.2 The cruise segment

The cruise segment is the only segment of the flight, which is actually changed compared to the missions of the previous chapter. Not only will the L.V. be released during this flight segment, the required LOX will be collected too. Due to this LOX collection, the weight of the plane actually increases during the collection phase of the cruise flight.

V.2.2.1 The LOX Collection Plant

During the cruise flight, the LCP will collect and enrich a part of the atmospheric air by condensing it and separating the oxygen from the nitrogen. This ‘enriched’ air will then be stored in the L.V. as the oxidiser for the propellant. Since this LCP and its operation are not crucial for this simulation, they are not dealt with here. Only a short survey of the parameters of the LCP, which are necessary for the simulation will be given. Additional information concerning the plant and the used values can be found in reference [8].

Essentially there are only three parameters necessary to define the LOX Collection plant. The collection ratio (CR) measures the global thermodynamic efficiency of the LCP, while the oxygen purity (Cox) and the recovery factor ($?_{sep}$) measure the efficiency of the separation process.

$$CR = \frac{W_{LOX}\,(kg/s)}{W_{H_2}\,(kg/s)} = 3{,}0$$

$$C_{ox} = \frac{W_{O_2\,LOX}\,(kg/s)}{W_{H_2}\,(kg/s)} = 90\%$$

$$\eta_{sep} = \frac{W_{O_2\,LOX}\,(kg/s)}{W_{O_2\,AIR}\,(kg/s)} = 0{,}75$$

The values used here for these parameters stem from reference [9], where the author indicates that these assumptions are rather less glamorous than usual because not much is known on the feasibility of N_2/O_2 separation in the operational conditions of a flying plane.

With a CR of 3 and 210 tons of hydrogen needed (reference [9] or USAF contract Part 1), 50 % of the total fuel weight will be used to collect LOX.

V.2.2.2 The lift-to-drag ratio's used

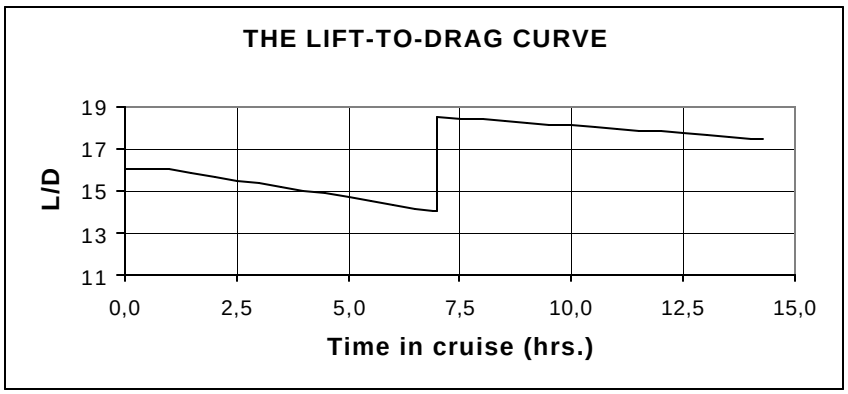

Figure V.2 The lift-to-drag curve of the reference mission

Due to the presence of the launch vehicle at TO and at the beginning of the cruise flight, an additional drag will have to be accounted for in these flight phases. Due to this additional drag, the lift-to-drag ratio will be lower than the lift-to-drag ratio of the plane after the release of the L.V. Furthermore, the slope of the lift-to-drag curve will also change due to the weight increase from the LOX collection. It is however not possible to determine the exact influence of both the presence of the LV and the LOX collection. To overcome that problem, a reference lift-to-drag curve is proposed first and the whole mission is calculated. Afterwards, the influence of the slope and of the absolute values[30] of the lift-to-drag curve is checked by changing the respective parameters (cfr. paragraph V.4). The reference lift-to-drag curve can be found in Figure V.2.

The lift-to-drag curve of Fig.V.2 can be divided into several cruise phases. During the first hour of cruise the lift-to-drag ratio is held constant at 16. LOX collection has not yet started. This hour of cruise are added to assure that the release of the LV happens approximately in the middle of the cruising distance. Assuring this allows the plane to take off from and land on the same airport if necessary. After this initial hour of cruise, the LOX collection starts. Due to this LOX collection the lift-to-drag ratio will decrease rather heavily. For this reference curve a decrease in L/D from 16 to 14 is chosen for approximately 5,5 hours of cruise with LOX collection. Once LOX collection has been completed (after 7 hours of cruise) the launch vehicle will be released, which causes a sudden change in L/D. It is assumed here, for the reference curve, that the L/D will rise to 18.5[31] due to the release. In the

[30] The term absolute values is used here to indicate the average level of the lift-to-drag curve of a specific phase of the cruise segment.
[31] In [1], a value of approximately 18 is used for the L/D ratio of a hydrogen-fuelled plane.

last phase of the cruise segment, the lift-to-drag ratio will finally decrease again. The weight of the carrier namely constantly decreases due to the spent fuel, which causes a need for less lift or thus a smaller angle of attack of the plane. Due to this change in angle of attack the drag will also decrease. The net result is then a decrease in L/D. This decrease will however be rather moderate compared to the decrease in the LOX collection phase. Here, a decrease to 17.5 is assumed in 10,5 hours of cruise.

V.3 The carrier sizing results

V.3.1 The weights at the different mission points

The gross weight of the carrier plane during the whole mission is determined analogously to the missions of Chapter IV. Exactly the same procedures, speeds and heights are used. The calculation of the weight of the fuel needed for backup, descent, … is therefore not repeated here. Only the results are given:

$$W_{backup} = 3.144 \text{ kg}$$
$$W_{descent} = 2.035 \text{ kg}$$

Based on these values, the weight of the carrier during the whole mission simulation can now be determined. Since the method used is, again, analogously to the mission calculations of Chapter IV, only the outcome of the simulation has been given below. Table V.2 shows the weight of the carrier plane at the different mission points of the climb segment while Fig. V.3 indicates the evolution of the weight during the cruise segment.

Table V.2 The weights at the different points of the climb segment

	Height [ft]	Weight [kg]
3	1.000	589.290
4	10.000	587.929
5	15.000	587.099
6	23.000	585.649
7	30.000	583.796
8	34.500	582.099
9	35.000	581.858

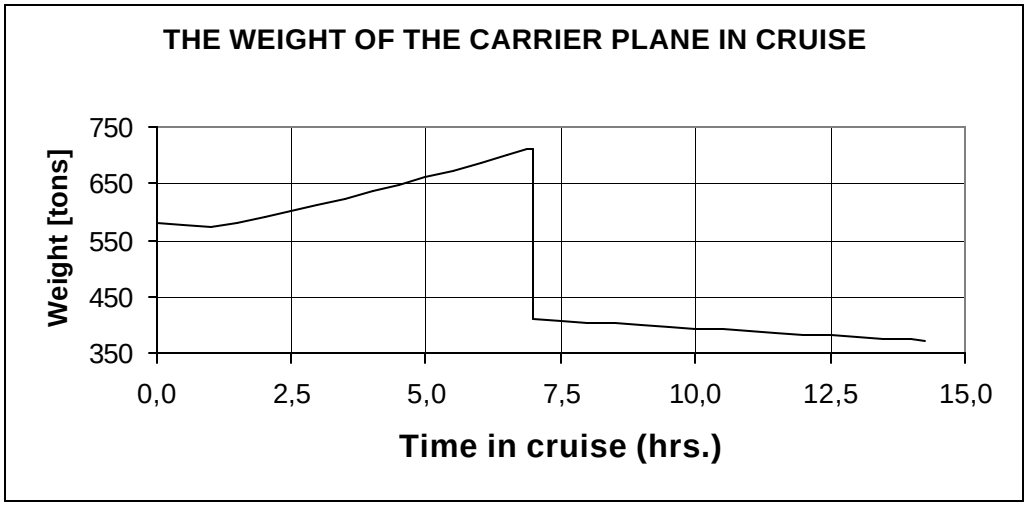

Figure V.3 The gross weight of the carrier plane in cruise

As can be seen from mission point 9 of Table V.2 (the top of climb or the beginning of the cruise), the weight of the carrier at the beginning of the cruise segment is 581.858 kg or 97,8 % of the TOGW. During cruise, the weight of the carrier initially decreases (cfr. Figure V.3). Once the LOX collection begins though, the weight rises, again continuously, till a maximum value of 712.026 kg (119,6 % of the TOGW) is obtained at the end of the collection phase (after 10 hrs 11 min 23 s of cruise). At the moment of the launch of the orbiter (10 hrs 30 min), the plane weighs approximately 710.008 kg (119,2 % of the TOGW) and, finally, at the end of the cruise segment, the weight of the plane is only 372.984 kg or 62,6 % of the TOGW).

V.3.2 Distances traveled - range

The purpose of a flight of the carrier plane mainly is the launch of the orbiter. It is therefore logical to use the distance traveled in cruise before the launch of the orbiter as a ground for comparison. The total range will be given too, in order to be as complete as possible. Roughly spoken, the range will however be twice the distance traveled before the launch, since the objective was a launch practically in the middle of the cruise segment.

In the reference mission, a cruise flight of approximately 7 hours precedes the launch (cfr. Fig. V.2 and V.3). At that time a distance of approximately 6.202 km is traveled. The total range of the mission is then approximately 13.228 km (12.619 km of cruise).

Figure V.4 The area available for launch

With a distance in cruise before the launch of 6.200 km, the distance traveled between the airport of departure and the launching site is approximately 6.600 km. A departure from Vandenberg AFB, in the vicinity of LA, would then allow a launch from every point lying in the circle on Figure V.4[32]. As can be seen from the dot on the figure, the carrier plane can also use the launch site used for the Boeing Sea Launch (154°-longitude west; 0° latitude, reference [21]).

A final parameter that can be useful for comparison is the time needed to collect the 210 tons of LOX. For the reference mission 5 h 51 min 47 s of cruise flight is needed to collect all the LOX. This equals an average collection rate of 9,949 kg LOX per second.

[32] Exept for the deformation of the circle due to the projection used (Mollweideprojection) to draw the map, which has not been considered here.

V.3.3 Fuel storage

Even though the required volume of fuel does not depend on the results for the mission (it was namely assumed that 154.000 kg of LH_2 was needed), it seemed interesting to insert here a comparison of the available volume in the carrier and the required volume of fuel.

First of all, a Boeing 777-200-IGW has a cabin length of 49,1 m and a cabin width of 5,87 m (ref. [13]). Assuming that only 5,5 m of this width[33] and only 46 m of this length are available for fuel storage leads to an available volume of 2186 m³. An amount of 154 tons of LH_2 on the other hand requires approximately 2175 m³ [34] of storage room. The fuel would thus just fit the carrier.

V.4 Influence of the estimated l/D curve

As can be seen from Figure V.2 several assumptions concerning the lift-to-drag ratio had to be made. Not only the average level was assumed, the slopes of the different parts of the curve are also estimated. In the following paragraph, the influence of these estimations is checked.

V.4.1 Influence of Delta LV

The first parameter from which the influence on the results is verified is the leap (large increase) in lift-to-drag due to the launch of the orbiter. As can be seen from figure V.2 this leap, called delta LV from hereon, is taken as 4.5 for the reference cycle[35]. Changing Delta LV and recalculating the mission then leads to Figure V.6 while Figure V.5 shows the lift-to-drag curve of one altered cycle (Delta LV = 5,5). This figure also shows that the first half of the cruise segment is not altered. Nor the lift-to-drag ratios used, nor the time of the launch is altered. The extra cruise distance is thus simply added (or subtracted) to the end of the cruise segment. As can be seen from Figure V.6 the range is extended by choosing a higher value for L/D. This is only logical since a higher lift-to-drag ratio means a lower drag for the same weight.

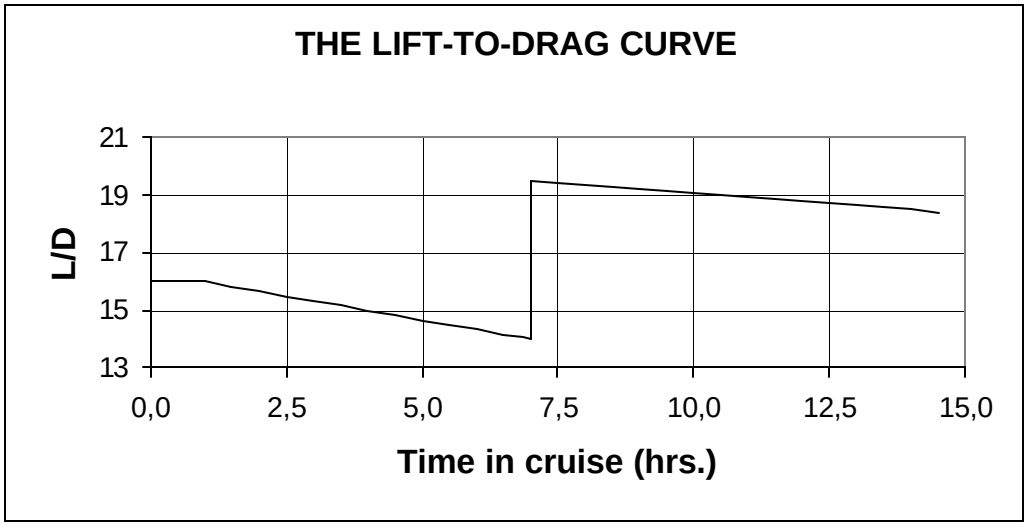

Figure V.5 The lift-to-drag curve of an altered mission (Delta LV = 5,5)

[33] The rest is filled with insulation, equipment, pumps,…
[34] LH_2 has a density of 70,80 kg/m³ (cfr. reference [6])

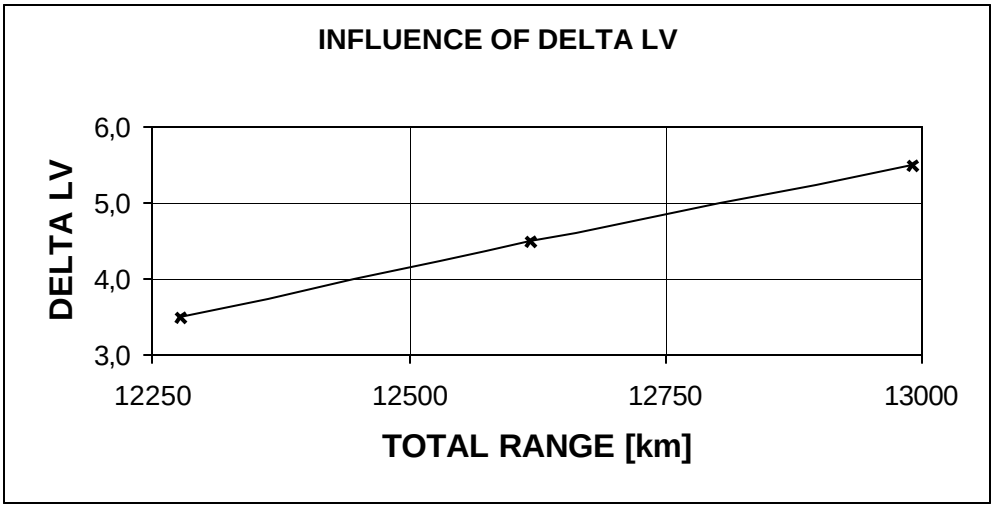

Figure V.6 The influence of Delta LV on the total range of the mission

V.4.3 The influence of the average L/D level

The exact values of the lift-to-drag curve are not known. The influence of the chosen lift-to-drag levels on the range and the distance traveled before the launch must therefore be checked. Shifting the whole lift-to-drag curve up and down does this. In the curve on Figure V.7, e.g., the reference curve has been shifted down with one unit. Unfortunately, the first half of the curve can not be held constant during the shifting operation. Changing the lift-to-drag ratio will namely change the fuel flow of the engine, and therefore the collected amount of LOX at a certain time. Because a fixed total amount of collected LOX is chosen, this will alter the time needed to collect LOX and thus also the distance traveled from TO till the end of the collection phase. Figure V.8 gives the distance traveled from the beginning of the cruise to the end of the LOX collection. This distance is called here distance to the launch since, in reality, the launch can take place immediately after the completion of the LOX collection. In the simulation it is (for reasons of convenience) however only possible to launch the vehicle at the end of the 30 minutes interval in which the LOX collection is completed. As can be seen from Figure V.8, shifting the average level of L/D with one unit changes the distance to the launch with approximately 395 km. Furthermore, Figure V.9 indicates the total distance traveled in cruise. The figure shows us that a shift in L/D of one unit changes the distance traveled in cruise with approximately 870 km. Finally, Figure V.10 shows the influence of the average level on the weight of the carrier at the end of the LOX collection phase. A shift in lift-to-drag of one unit leads to a weight change of approximately 1,2 to 1,3 tons.

[35] Delta LV = $(L/D)_{\text{without LV}}$ - $(L/D)_{\text{with LV}}$ = 18.5-14

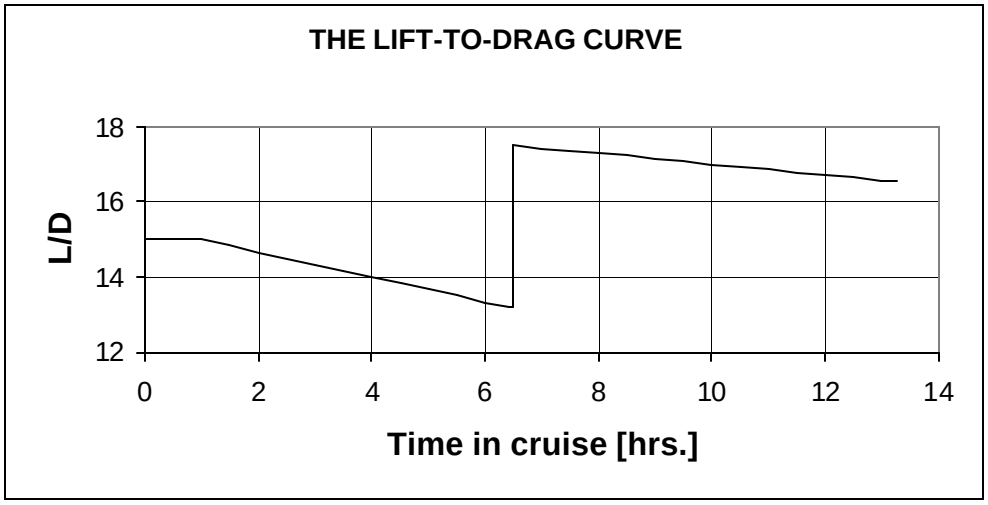

Figure V.7 The lift-to-drag curve of an altered mission

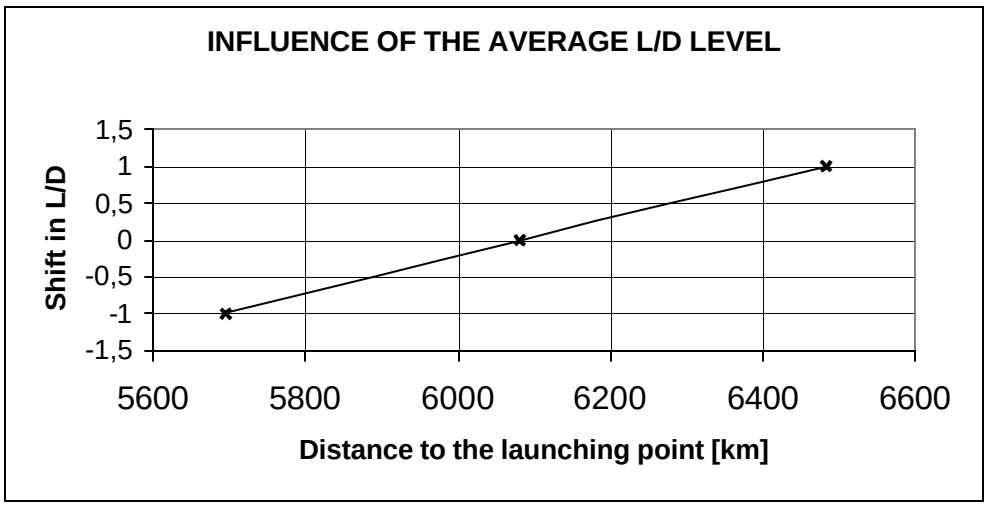

Figure V.8 The influence of the average L/D level on the distance

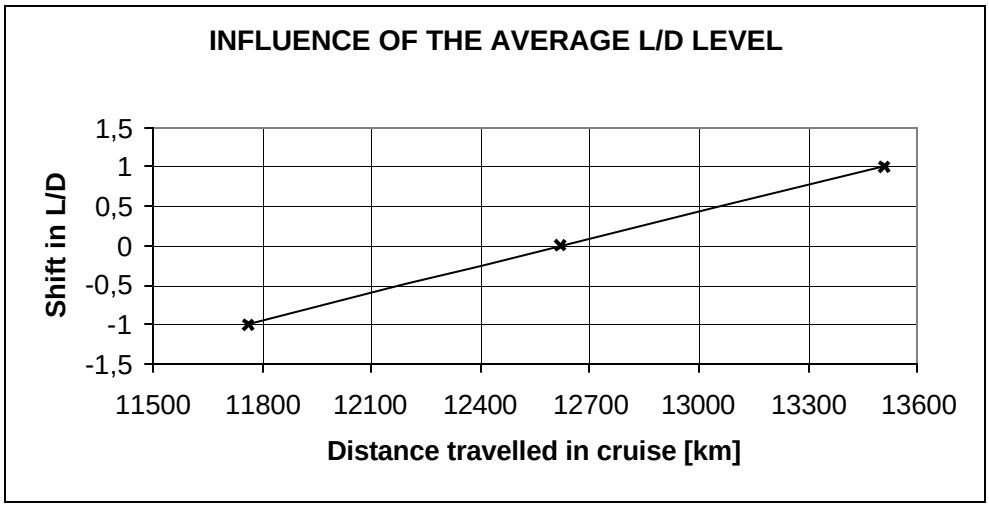

Figure V.9 The influence of the average L/D level on the distance

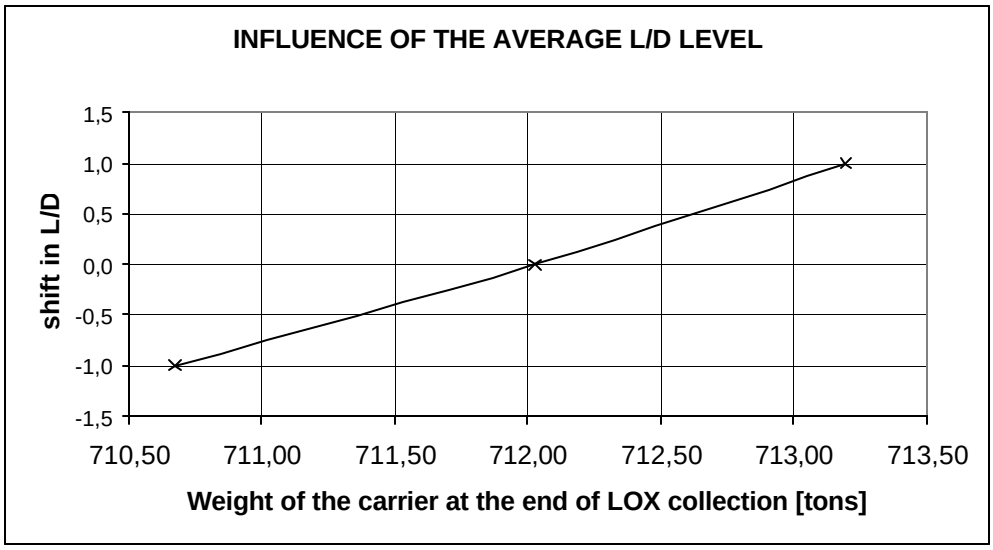

Figure V.10 The influence of the average L/D level on the weight

V.4.4 Influence of the slope of the collection L/D curve

As a final exercise, the influence of the slope of the lift-to-drag curve during the LOX collection has been verified. Figure V.11 shows one of the cycles used to check this. As can be seen from that figure, the only phase of the curve, which has been altered, is the collection phase. The lift-to-drag curve remains equal to the reference curve for the rest of the mission.

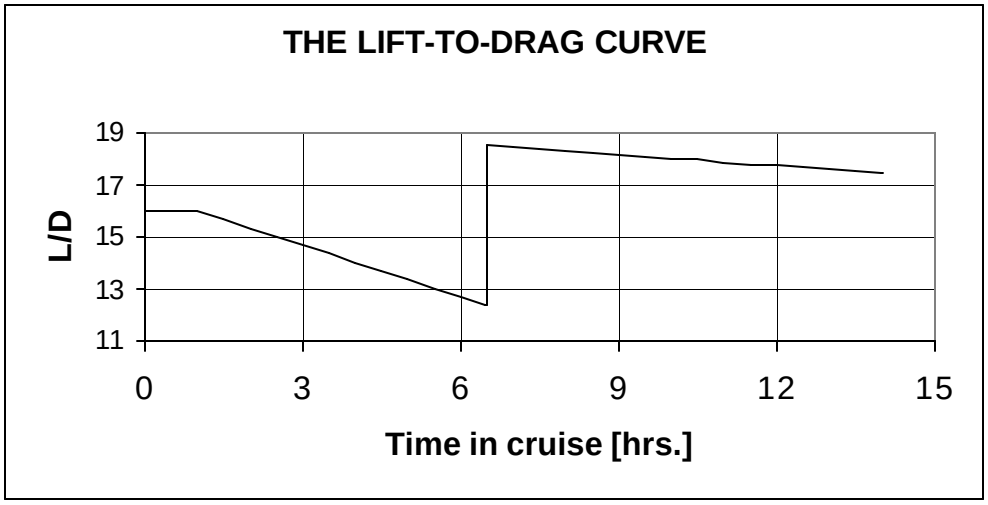

Figure V.11 The lift-to-drag curve of an altered mission

Figure V.12 finally gives the influence of the slope of the lift-to-drag curve to the distance traveled in cruise till the end of the collection phase. The reference curve has a slope of –0.33 while the curve of Figure V.11 has a slope of –0.73. It can be seen from Figure V.12 that a decrease of the absolute value of the slope of the curve during the collection phase largely increases the distance traveled. A decrease from –0.33 to 0 entails an increase of approximately 415 km.

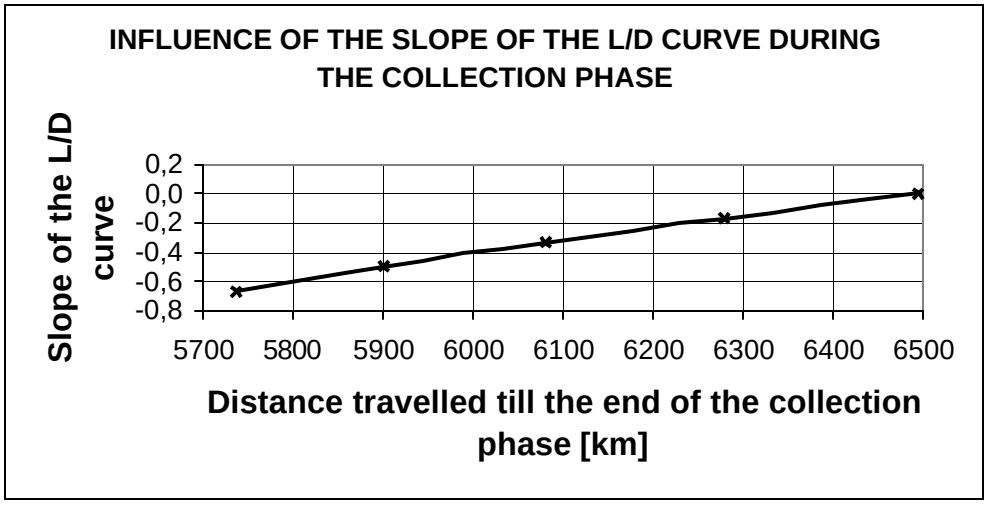

Figure V.12 The influence of the slope of the collection L/D curve

V.5 Conclusion

The results of this simulation for a large subsonic ACES launcher carrier prove that a similar mission would quite well be possible. With the reference lift-to-drag curve, a distance of approximately 6.200 km namely can be bridged before the launch of the orbiter. This would give the plane a total range of more then 13.000 km and thus a large freedom to choose a safe launching point in function of the satellite orbit parameters.

However, these results must be carefully interpreted since they largely depend on the values used for the lift-to-drag ratio. It is shown that the range can vary with several percents due to a change in the assumed L/D ratio. Particular interest should go out to the collection phase of the cruise segment since a small change in the slope of the lift-to-drag curve of that phase can reduce the range with several percents.

In Part 3, the realism of the assumed lift-to-drag ratios and various weights will be examined more in detail. That will then allow refining the results of this Part 2. The influence of the assumed collection ratio and the amount of fuel used to collect LOX will also be addressed.

Conclusion

In this work, the GE90-90B engine has been simulated through Gasturb 9. In this simulation kerosene as well as hydrogen is used as a fuel. The TO and cruise ratings have first been determined for both fuels. Afterwards a mission for a Boeing 777-200 powered by two GE 90 engines is calculated.

The TO rating has been determined via the data available from a test at SLS ISA conditions. Based on this data, a reasonable value for the different Gasturb parameters is determined. Finally the BET is iterated to achieve a net thrust of 90.000 lbf for the uninstalled engine. A TSFC of 8,48 g/kNs or 0,306 kg/daNh is calculated. Subsequently the installation losses of the kerosene-fuelled engine have been determined for both the standard and the special component maps of Gasturb. With a ram recovery (or IPR) of 0,995 the installation losses are in the vicinity of 1 % (for both TSFC and net thrust). Eventually the transition to hydrogen as a fuel has been carried out. In Gasturb, altering only the FHV and the BET does this since the values for the specific heats of the combustion gasses are changed automatically. This has as major advantage that the compressor section can be reused. The turbines and the core nozzle will need a small adaptation due to the small change in airflow. The transition to hydrogen involves a reduction of 51K in BET, which improves the lifetime of the 'hot' engine components considerably. A reduction of approximately 65% in TSFC and 3% in ESFC is calculated too.

After the determination of the TO rating as the design-point of the engine, the cruise rating deserves some special attention since the engine will spend most of its lifetime at this rating. The transition is first carried out for kerosene. For the hydrogen-fuelled engines the BET is then iterated to achieve the same net thrust as the kerosene-fuelled engines. The transition to cruise (with the special maps) leads to a thrust of approximately 44 kN and a TSFC of 19,41 g/kNs for kerosene and 6,86 g/kNs for hydrogen.

Next, a mission of a Boeing 777-200 powered by two GE90-90B engines has been simulated. In this mission, the plane takes off from and lands on an airport at sea level. The cruise is flown at 35.000 ft ISA and a Mach number of 0,83. Using these and other assumptions the range of the Boeing has been determined as 10.183 km or an error of 5,5% has been made regarding Boeing's data. After this, four alternative missions have been calculated for the hydrogen-fuelled Boeing and their practical relevancy has been checked. First, the range of the hydrogen-fuelled plane with the same take-off gross weight has been determined as 28.373 km or roughly 3 times the original range. This mission was however not a very useful alternative since 70 % of the total volume of the plane would consist out of fuel tanks. On the other hand, using only the existing volume for storage of hydrogen would lead to a range of almost zero kilometres, which has no real practical significance too. Finally, the hydrogen-fuelled plane would only need 470 m^3 of extra fuel storage (and thus an extra tank on top of the fuselage) to achieve the same range as the kerosene-fuelled plane. The take-off gross weight would however undergo a reduction of approximately 25%.

Finally, a mission for a large subsonic ACES carrier has been simulated. In order to do this, the weights of the different subsections of the carrier had to be determined first. The calculations / estimations of the subsection weights lead to a carrier that has an OEW and a

TOGW of 365,5 respectively 595 tons. Using these weights, along with a Collection Ratio CR of 3.0, an amount of 210 tons of LOX to be collected and the reference L/D curve, the simulation indicates that a distance of approximately 6.200 km can be bridged before the launch of the orbiter (2^{nd} stage). A similar mission would thus quite well be possible since a large freedom to choose a safe launching point is available. However, prudence is in order when interpreting these results. It is namely shown that the range can vary with several percents due to a change in the assumed lift-to-drag ratio.
The assumptions regarding the aircraft structure, loads and aerodynamic data will now be checked with more details in the frame of the part 3 of this study.

References

Books

[1] Brewer G.D., "*Hydrogen Aircraft technology*", CRC Press, 1991

[2] Cumpsty N., "*Jet Propulsion – A simple guide to the aerodynamic and thermodynamic design and performance of jet engines*", Cambridge, 1999

[3] Kurzke J., "*Gasturb 9 User's manual – A program to calculate design and off-design performance of gas turbines*", Germany, 2001

[4] Mattingly J.D., Heiser W.H. & Daley D.H., "*Aircraft Engine Design*", AIAA Education Series, 1987

[5] Raymer D.P., "*Aircraft Design: a Conceptual Appoach*", AIAA Education Series, 1992

[6] Vanheste K., "*Voorontwerp van een high by-pass ratio turbofan op waterstof*", Koninklijke Militaire School, Final Project 1999

[7] Walsh P.P. & Fletcher P.,"*Gas Turbine Performance*", Blackwell Series Ltd., 1998

Articles

[8] Hendrick P., Bizzarri D., Breugelmans F., Ngendakumana P., Promper C., Saint-Mard M.,"*Fully and Partially Reusable TSTO launchers using in-flight LOX collection*", ISTS 2000-8-09, ISTS, Morioka, May 28-June 4, 2000

[9] Hendrick P., Saint-Mard, "*Subsonic in-flight LOX collection for an all-rocket air-launched orbiter*", AIAA 99-2351, JPC, Los Angeles, 20-24 June 1999

[10] Johnson C., Hendrick P., "*LOX Collection: a highly synergistic technology*", AIAA 99-4830, AIAA Hypersonics Conference, Norfolk, 01-04 Nov 1999

[11] G. E. Lozino-Lozinsky et al., "*The MAKS project and perspectives of development*", AIAA 96-4493, Norfolk, 18-22 November 1996

[12] Norris G., "*Boeing rethinks Cruiser engine*", Flight International, 20-26 nov. 2001

[13] "*No Nonsense Facts & Figures: Boeing 777*", Aircraft Technology Engineering & Maintenance, Issue 32, February/March 1998

World Wide Web

[14] http://aerodyn.org/Highlift/ld-tables.com

[15] http://webpages.charter.net/rtpete/html/777.html

[16] http://www.boeing.com/commercial/777family/pf/pf_200product.html

[17] http://www.ivao.org/db/aircraft/Aircraft.asp?Id=B772

[18] http://www.laudaair.com/e/ueberuns/flotte/777200_daten.asp

[19] http://www-psao.grc.nasa.gov/Portfolio/commercial/ge90.html[36]

[20] http://www.sae.org/aeromag/aircraftengines/02.htm

[21] http://www.sea-launch.com

[22] http://www.stanford.edu/class/me131b/handouts/ho6.html en ho4.html

[36] Unfortunately, at the moment of publishing this text references [17] and [19] are no longer available. The data from these sources can however be found in reference [6].

APPENDIX A: The Gasturb output for TO

A.1 Uninstalled engine – kerosene

Station	W	T	P	WRstd
amb		288,15	101,325	
2	1542,200	288,15	101,325	1542,201
13	1378,136	326,97	151,988	
21	164,064	359,49	186,897	99,348
25	164,064	359,49	185,028	100,352
3	160,782	918,32	4255,650	6,834
31	139,372	918,32	4255,650	
4	142,767	1712,26	4042,868	8,722
41	159,173	1636,37	4042,868	9,507
43	159,173	1147,61	671,515	
44	164,095	1141,10	671,515	
45	164,095	1141,10	658,085	50,278
49	164,095	799,00	120,739	
5	167,376	797,17	120,739	233,630
8	167,376	797,17	118,324	238,398
18	1378,136	326,97	148,948	998,660

P2/P1= 1,0000

Efficiencies:	isentr	polytr	RNI	P/P
Outer LPC	0,9100	0,9150	1,000	1,500
Inner LPC	0,7700	0,7888	1,000	1,845
HP Compressor	0,8700	0,9115	1,257	23,000
Burner	0,9990			0,950
HP Turbine	0,8800	0,8554	2,204	6,021
LP Turbine	0,8810	0,8564	0,650	5,450
HP Spool mech	0,9980	Nominal Spd		1
LP Spool mech	0,9980	Nominal Spd		1

Fuel	FHV	humidity	war2
Generic	43,124	0,0	0,0000

FN	=	400,34
TSFC	=	8,4794
WF	=	3,39463
BPR	=	8,4000
s NOx	=	2,0894
Core Eff	=	0,4637
Prop Eff	=	0,0000
P3/P2	=	42,0000
P16/P13	=	0,98000
P16/P6	=	1,25881
P16/P2	=	1,47000
P6/P5	=	0,98000
A8	=	1,45625
A18	=	4,55588
P8/Pamb	=	1,16777
P18/Pamb	=	1,47000
CD8	=	0,94537
CD18	=	0,95915
XM8	=	0,48525
XM18	=	0,76285
V18/V8,id=		0,99205
Loading %=		100,00
PWX	=	0
ZWBLD	=	0,00000
WBLD/W21	=	0,00000
WHcl/W25	=	0,03000
WLcl/W25	=	0,02000

A.2 Installed engine – kerosene – standard maps

Station	W	T	P	WRstd
amb		288,15	101,325	
2	1531,615	288,15	100,818	1539,312
13	1368,459	326,93	151,305	
21	163,156	359,42	186,094	99,216
25	163,155	359,42	184,238	100,214
3	159,892	917,75	4231,775	6,832
31	138,600	917,75	4231,775	
4	141,978	1712,26	4020,287	8,723
41	158,294	1636,33	4020,287	9,507
43	158,294	1147,81	667,966	
44	163,189	1141,27	667,966	
45	163,189	1141,27	654,611	50,270
49	163,189	799,95	120,546	
5	166,452	798,09	120,546	232,844
8	166,452	798,09	118,132	237,569
18	1368,459	326,93	148,295	995,962

P2/P1= 0,9950

Efficiencies:	isentr	polytr	RNI	P/P
Outer LPC	0,9120	0,9169	0,995	1,501
Inner LPC	0,7717	0,7904	0,995	1,846
HP Compressor	0,8701	0,9116	1,252	22,969
Burner	0,9990			0,950
HP Turbine	0,8797	0,8551	2,192	6,019
LP Turbine	0,8805	0,8560	0,646	5,430
HP Spool mech	0,9980	Nominal Spd		1
LP Spool mech	0,9980	Nominal Spd		1

Fuel	FHV	humidity	war2
Generic	43,124	0,0	0,0000

FN	=	395,49
TSFC	=	8,5416
WF	=	3,37809
BPR	=	8,3874
s NOx	=	2,0776
Core Eff	=	0,4623
Prop Eff	=	0,0000
P3/P2	=	41,9742
P16/P13	=	0,98010
P16/P6	=	1,25512
P16/P2	=	1,47091
P6/P5	=	0,98013
A8	=	1,45623
A18	=	4,55589
P8/Pamb	=	1,16607
P18/Pamb	=	1,46056
CD8	=	0,94525
CD18	=	0,95874
XM8	=	0,48295
XM18	=	0,75825
V18/V8,id=		0,99063
Loading %=		100,65
PWX	=	50
ZWBLD	=	0,00000
WBLD/W21	=	0,00000
WHcl/W25	=	0,03000
WLcl/W25	=	0,02000

A.3 Installed engine – kerosene – special maps

Station	W	T	P	WRstd
amb		288,15	101,325	
2	1529,536	288,15	100,818	1537,223
13	1366,537	326,93	151,171	
21	162,999	359,43	185,868	99,242
25	162,999	359,43	184,013	100,242
3	159,739	917,86	4227,865	6,833
31	138,467	917,86	4227,865	
4	141,842	1712,26	4016,560	8,722
41	158,192	1636,34	4016,560	9,507
43	158,192	1147,71	667,361	
44	163,032	1141,18	667,361	
45	163,032	1141,19	654,021	50,265
49	163,032	799,98	120,515	
5	166,292	798,13	120,515	232,696
8	166,292	798,13	118,124	237,396
18	1366,537	326,93	148,167	995,421

P2/P1= 0,9950

Efficiencies:	isentr	polytr	RNI	P/P
Outer LPC	0,9099	0,9149	0,995	1,499
Inner LPC	0,7699	0,7887	0,995	1,844
HP Compressor	0,8701	0,9116	1,250	22,976
Burner	0,9990			0,950
HP Turbine	0,8799	0,8553	2,190	6,019
LP Turbine	0,8806	0,8560	0,646	5,427
HP Spool mech	0,9980	Nominal Spd		1
LP Spool mech	0,9980	Nominal Spd		1

Fuel	FHV	humidity	war2
Generic	43,124	0,0	0,0000

FN	=	394,54
TSFC	=	8,5527
WF	=	3,37440
BPR	=	8,3837
s NOx	=	2,0781
Core Eff	=	0,9621
Prop Eff	=	0,0000
P3/P2	=	41,9355
P16/P13	=	0,98012
P16/P6	=	1,25433
P16/P2	=	1,46964
P6/P5	=	0,99016
A8	=	1,45625
A18	=	4,55589
P8/Pamb	=	1,16580
P18/Pamb	=	1,46229
CD8	=	0,99521
CD18	=	0,95965
XM8	=	0,48258
XM18	=	0,75734
V18/V8,id=		0,99028
Loading %=		100,68
PWX	=	50
ZWBLD	=	0,00000
WBLD/W21	=	0,00000
WHcl/W25	=	0,03000
WLcl/W25	=	0,02000

A.4 Uninstalled engine – hydrogen

Station	W	T	P	WRstd
amb		288,15	101,325	
2	1542,200	288,15	101,325	1542,201
13	1378,136	326,97	151,988	
21	164,064	359,49	186,897	99,348
25	164,064	359,49	185,028	100,352
3	160,783	918,36	4255,650	6,834
31	139,372	918,36	4255,650	
4	140,566	1660,90	4042,868	8,661
41	156,973	1591,82	4042,868	9,445
43	156,973	1112,54	676,171	
44	161,895	1107,15	676,171	
45	161,895	1107,15	662,648	49,530
49	161,895	769,35	121,116	
5	165,176	768,11	121,116	230,190
8	165,176	768,11	118,694	234,888
18	1378,136	326,97	148,948	998,660

P2/P1= 1,0000

Efficiencies:	isentr	polytr	RNI	P/P
Outer LPC	0,9100	0,9150	1,000	1,500
Inner LPC	0,7700	0,7888	1,000	1,845
HP Compressor	0,8700	0,9115	1,257	23,000
Burner	0,9990			0,950
HP Turbine	0,8800	0,8551	2,315	5,979
LP Turbine	0,8810	0,8558	0,687	5,471
HP Spool mech	0,9980	Nominal Spd		1
LP Spool mech	0,9980	Nominal Spd		1

Fuel	FHV	humidity	war2
Hydrogen	119,992	0,0	0,0000

FN	=	400,34
TSFC	=	2,9830
WF	=	1,19420
BPR	=	8,4000
s NOx	=	2,0889
Core Eff	=	0,4806
Prop Eff	=	0,0000
P3/P2	=	42,0000
P16/P13	=	0,98000
P16/P6	=	1,25489
P16/P2	=	1,47000
P6/P5	=	0,98000
A8	=	1,42020
A18	=	4,55589
P8/Pamb	=	1,17141
P18/Pamb	=	1,47000
CD8	=	0,94567
CD18	=	0,95915
XM8	=	0,48979
XM18	=	0,76285
V18/V8,id=		0,97899
Loading %=		100,00
PWX	=	0
ZWBLD	=	0,00000
WBLD/W21	=	0,00000
WHcl/W25	=	0,03000
WLcl/W25	=	0,02000

A.5 Installed engine – hydrogen – standard maps

Station	W	T	P	WRstd
amb		288,15	101,325	
2	1531,199	288,15	100,818	1538,894
13	1368,196	326,91	151,283	
21	163,004	359,38	186,057	99,136
25	163,004	359,38	184,204	100,134
3	159,743	917,45	4227,730	6,831
31	138,472	917,45	4227,730	
4	139,659	1660,91	4016,511	8,662
41	155,960	1591,74	4016,511	9,445
43	155,960	1113,01	672,647	
44	160,850	1107,58	672,647	
45	160,850	1107,58	650,660	49,519
49	160,850	770,60	120,900	
5	164,110	769,32	120,900	229,299
8	164,110	769,32	118,501	233,942
18	1368,196	326,91	148,274	995,874

P2/P1= 0,9950

Efficiencies:	isentr	polytr	RNI	P/P
Outer LPC	0,9122	0,9171	0,995	1,501
Inner LPC	0,7719	0,7906	0,995	1,845
HP Compressor	0,8702	0,9117	1,252	22,951
Burner	0,9990			0,950
HP Turbine	0,8796	0,8546	2,300	5,971
LP Turbine	0,8805	0,8552	0,682	5,448
HP Spool mech	0,9980	Nominal Spd		1
LP Spool mech	0,9980	Nominal Spd		1

Fuel	FHV	humidity	war2
Hydrogen	118,392	0,0	0,0000

FN	=	395,29
TSFC	=	3,0050
WF	=	1,18787
BPR	=	8,3937
s NOx	=	2,0737
Core Eff	=	0,4789
Prop Eff	=	0,0000
P3/P2	=	41,9341
P16/P13	=	0,98011
P16/P6	=	1,25124
P16/P2	=	1,47070
P6/P5	=	0,98015
A8	=	1,42020
A18	=	4,55589
P8/Pamb	=	1,16951
P18/Pamb	=	1,46335
CD8	=	0,94551
CD18	=	0,95872
XM8	=	0,48725
XM18	=	0,75810
V18/V8,id=		0,97757
Loading %=		100,84
PWX	=	50
ZWBLD	=	0,00000
WBLD/W21	=	0,00000
WHcl/W25	=	0,03000
WLcl/W25	=	0,02000

A.6 Installed engine – hydrogen – special maps

Station	W	T	P	WRstd
amb		288,15	101,325	
2	1529,056	288,15	100,818	1536,740
13	1366,183	326,91	151,149	
21	162,873	359,40	185,822	99,185
25	162,868	359,40	183,969	100,181
3	159,611	917,66	4224,397	6,832
31	138,356	917,66	4224,397	
4	139,543	1660,91	4013,315	8,662
41	155,830	1591,76	4013,315	9,445
43	155,830	1112,84	672,080	
44	160,716	1107,42	672,080	
45	160,716	1107,42	650,107	49,515
49	160,716	770,55	120,858	
5	163,973	769,28	120,858	229,180
8	163,973	769,28	118,462	233,815
18	1366,183	326,91	148,141	995,312

P2/P1= 0,9950

Efficiencies:	isentr	polytr	RNI	P/P
Outer LPC	0,9099	0,9149	0,995	1,499
Inner LPC	0,7699	0,7887	0,995	1,843
HP Compressor	0,8701	0,9116	1,250	22,963
Burner	0,9990			0,950
HP Turbine	0,8799	0,8550	2,298	5,971
LP Turbine	0,8805	0,8553	0,682	5,445
HP Spool mech	0,9980	Nominal Spd		1
LP Spool mech	0,9980	Nominal Spd		1

Fuel	FHV	humidity	war2
Hydrogen	118,392	0,0	0,0000

FN	=	394,30
TSFC	=	3,0093
WF	=	1,18657
BPR	=	8,3880
s NOx	=	2,0752
Core Eff	=	0,4788
Prop Eff	=	0,0000
P3/P2	=	41,9011
P16/P13	=	0,98013
P16/P6	=	1,25053
P16/P2	=	1,46938
P6/P5	=	0,98018
A8	=	1,42020
A18	=	4,55589
P8/Pamb	=	1,16913
P18/Pamb	=	1,46203
CD8	=	0,94551
CD18	=	0,95864
XM8	=	0,48672
XM18	=	0,75715
V18/V8,id=		0,97753
Loading %=		100,83
PWX	=	50
ZWBLD	=	0,00000
WBLD/W21	=	0,00000
WHcl/W25	=	0,03000
WLcl/W25	=	0,02000

APPENDIX B: The Gasturb output for cruise

B.1 Standard Maps - Kerosene

Station	W	T	P	WRstd
amb		218,81	23,842	
2	595,019	249,02	37,395	1498,800
13	544,361	274,64	51,371	
21	50,657	296,87	61,001	85,407
25	50,656	296,87	60,551	86,041
3	49,643	736,44	1170,510	6,870
31	43,033	736,44	1170,510	
4	43,834	1376,37	1111,366	8,734
41	48,899	1314,53	1111,366	9,522
43	48,899	919,72	185,361	
44	50,419	914,46	185,361	
45	50,419	914,46	181,680	50,093
49	50,419	621,87	29,838	
5	51,432	620,79	29,838	256,352
8	51,432	620,79	29,120	262,677
10	544,361	274,64	50,192	1072,853

PZ/P1= 0,9980

Efficiencies:	isentr	polytr	RNI	P/P
Outer LPC	0,9294	0,9277	0,472	1,379
Inner LPC	0,7822	0,7966	0,472	1,631
HP Compressor	0,8655	0,9075	0,568	19,331
Burner	0,9834			0,949
HP Turbine	0,8563	0,8263	0,870	5,996
LP Turbine	0,8596	0,8277	0,258	6,089
HP Spool mech	0,9980	Nominal Spd		1
LP Spool mech	0,9980	Nominal Spd		1

Fuel	PHV	humidity	war2
Generic	43,124	0,0	0,0000

FN	=	42,26
TSFC	=	18,9559
WF	=	0,80099
BPR	=	10,7459
s NOx	=	0,4889
Core Eff	=	0,4847
Prop Eff	=	0,8746
P3/P2	=	31,3013
P16/P13	=	0,97706
P16/P6	=	1,72364
P16/P2	=	1,34222
P6/P5	=	0,97592
A8	=	1,45625
A18	=	4,55588
P8/Pamb	=	1,22136
P18/Pamb	=	2,10518
CD8	=	0,99969
CD18	=	0,97600
XM8	=	0,59821
XM18	=	1,00000
V18/V8,id=		1,23392
Loading %=		578,07
PWX	=	50
ZWBLD	=	0,00000
WBLD/W21	=	0,00000
WHcl/W25	=	0,03000
WLcl/W25	=	0,02000

B.2 Special Maps - Kerosene

Station	W	T	P	WRstd
amb		218,81	23,842	
2	597,418	249,02	37,395	1504,845
13	543,672	276,66	51,494	
21	53,746	300,62	61,210	90,874
25	53,746	300,62	60,698	91,641
3	52,671	759,12	1256,182	6,896
31	45,657	759,12	1256,182	
4	46,510	1399,42	1192,234	8,711
41	51,884	1337,35	1192,234	9,500
43	51,884	925,47	197,045	
44	53,496	920,68	197,045	
45	53,496	920,68	193,120	50,172
49	53,496	621,05	30,557	
5	54,571	620,28	30,557	265,491
8	54,571	620,28	29,768	272,530
10	543,672	276,66	50,313	1072,856

PZ/P1= 0,9980

Efficiencies:	isentr	polytr	RNI	P/P
Outer LPC	0,8635	0,8696	0,472	1,377
Inner LPC	0,7307	0,7487	0,472	1,637
HP Compressor	0,8663	0,9087	0,558	20,696
Burner	0,9869			0,949
HP Turbine	0,8759	0,8492	0,907	6,051
LP Turbine	0,8609	0,8286	0,272	6,320
HP Spool mech	0,9980	Nominal Spd		1
LP Spool mech	0,9980	Nominal Spd		1

Fuel	PHV	humidity	war2
Generic	43,124	0,0	0,0000

FN	=	43,91
TSFC	=	19,4131
WF	=	0,85241
BPR	=	10,1156
s NOx	=	0,5652
Core Eff	=	0,4954
Prop Eff	=	0,8708
P3/P2	=	33,5924
P16/P13	=	0,97706
P16/P6	=	1,69016
P16/P2	=	1,34545
P6/P5	=	0,97417
A8	=	1,45625
A18	=	4,55588
P8/Pamb	=	1,24854
P18/Pamb	=	2,11024
CD8	=	0,95176
CD18	=	0,97600
XM8	=	0,57840
XM18	=	1,00000
V18/V8,id=		1,17934
Loading %=		500,77
PWX	=	50
ZWBLD	=	0,00000
WBLD/W21	=	0,00000
WHcl/W25	=	0,03000
WLcl/W25	=	0,02000

B.3 Standard Maps - Hydrogen

Station	W	T	P	WRstd
amb		218,81	23,842	
2	594,856	249,02	37,395	1498,385
13	544,264	274,62	51,360	
21	50,592	296,83	60,982	85,317
25	50,592	296,83	60,533	85,951
3	49,580	736,42	1170,532	6,861
31	42,978	736,42	1170,532	
4	43,261	1345,42	1111,543	8,677
41	48,320	1287,66	1111,543	9,463
43	48,320	898,15	186,943	
44	49,838	893,50	186,943	
45	49,838	893,50	183,083	49,338
49	49,838	604,20	29,971	
5	50,850	603,47	29,971	252,636
8	50,850	603,47	29,249	258,872
18	544,264	274,62	50,181	1072,849

P2/P1= 0,9980

Efficiencies:	isentr	polytr	RNI	P/P
Outer LPC	0,9246	0,9279	0,472	1,373
Inner LPC	0,7823	0,7968	0,472	1,631
HP Compressor	0,8655	0,9075	0,568	19,337
Burner	0,9835			0,950
HP Turbine	0,8572	0,8272	0,900	5,946
LP Turbine	0,8595	0,8271	0,270	6,109
HP Spool mech	0,9980	Nominal Spd		1
LP Spool mech	0,9980	Nominal Spd		1

Fuel	PHV	humidity	war2
Hydrogen	118,392	0,0	0,0000

FN	=	42,26
TSFC	=	6,6973
WF	=	0,28302
BPR	=	10,7578
s NOx	=	0,4889
Core Eff	=	0,5003
Prop Eff	=	0,8741
P3/P2	=	31,3018
P16/P13	=	0,97706
P16/P6	=	1,71565
P16/P2	=	1,34193
P6/P5	=	0,97591
A8	=	1,42020
A18	=	4,55589
P8/Pamb	=	1,22678
P18/Pamb	=	2,10472
CD8	=	0,95011
CD18	=	0,97600
XM8	=	0,55442
XM18	=	1,00000
V18/V8,id=		1,21725
Loading %=		577,44
PWX	=	50
ZWBLD	=	0,00000
WBLD/WZ1	=	0,00000
WHcl/WZ5	=	0,03000
WLcl/WZ5	=	0,02000

B.4 Special Maps – Hydrogen

Station	W	T	P	WRstd
amb		218,81	23,842	
2	597,252	249,02	37,395	1504,419
13	543,552	276,64	51,481	
21	53,699	300,58	61,188	90,822
25	53,700	300,58	60,676	91,588
3	52,626	759,20	1256,761	6,887
31	45,618	759,20	1256,761	
4	45,919	1367,78	1192,948	8,653
41	51,289	1310,03	1192,948	9,441
43	51,289	903,58	198,798	
44	52,900	899,50	198,798	
45	52,900	899,50	194,680	49,416
49	52,900	603,23	30,709	
5	53,974	602,81	30,709	261,578
8	53,974	602,81	29,916	268,512
18	543,552	276,64	50,300	1072,847

P2/P1= 0,9980

Efficiencies:	isentr	polytr	RNI	P/P
Outer LPC	0,8635	0,8696	0,472	1,377
Inner LPC	0,7307	0,7486	0,472	1,636
HP Compressor	0,8663	0,9087	0,558	20,713
Burner	0,9869			0,949
HP Turbine	0,8769	0,8502	0,939	6,001
LP Turbine	0,8609	0,8280	0,284	6,339
HP Spool mech	0,9980	Nominal Spd		1
LP Spool mech	0,9980	Nominal Spd		1

Fuel	PHV	humidity	war2
Hydrogen	118,392	0,0	0,0000

FN	=	43,91
TSFC	=	6,8592
WF	=	0,30119
BPR	=	10,1221
s NOx	=	0,5655
Core Eff	=	0,5114
Prop Eff	=	0,8703
P3/P2	=	33,6077
P16/P13	=	0,97706
P16/P6	=	1,68137
P16/P2	=	1,34510
P6/P5	=	0,97417
A8	=	1,42020
A18	=	4,55589
P8/Pamb	=	1,25475
P18/Pamb	=	2,10971
CD8	=	0,95222
CD18	=	0,97600
XM8	=	0,58502
XM18	=	1,00000
V18/V8,id=		1,16348
Loading %=		499,86
PWX	=	50
ZWBLD	=	0,00000
WBLD/WZ1	=	0,00000
WHcl/WZ5	=	0,03000
WLcl/WZ5	=	0,02000

APPENDIX C: A cross-section of the GE90 engine

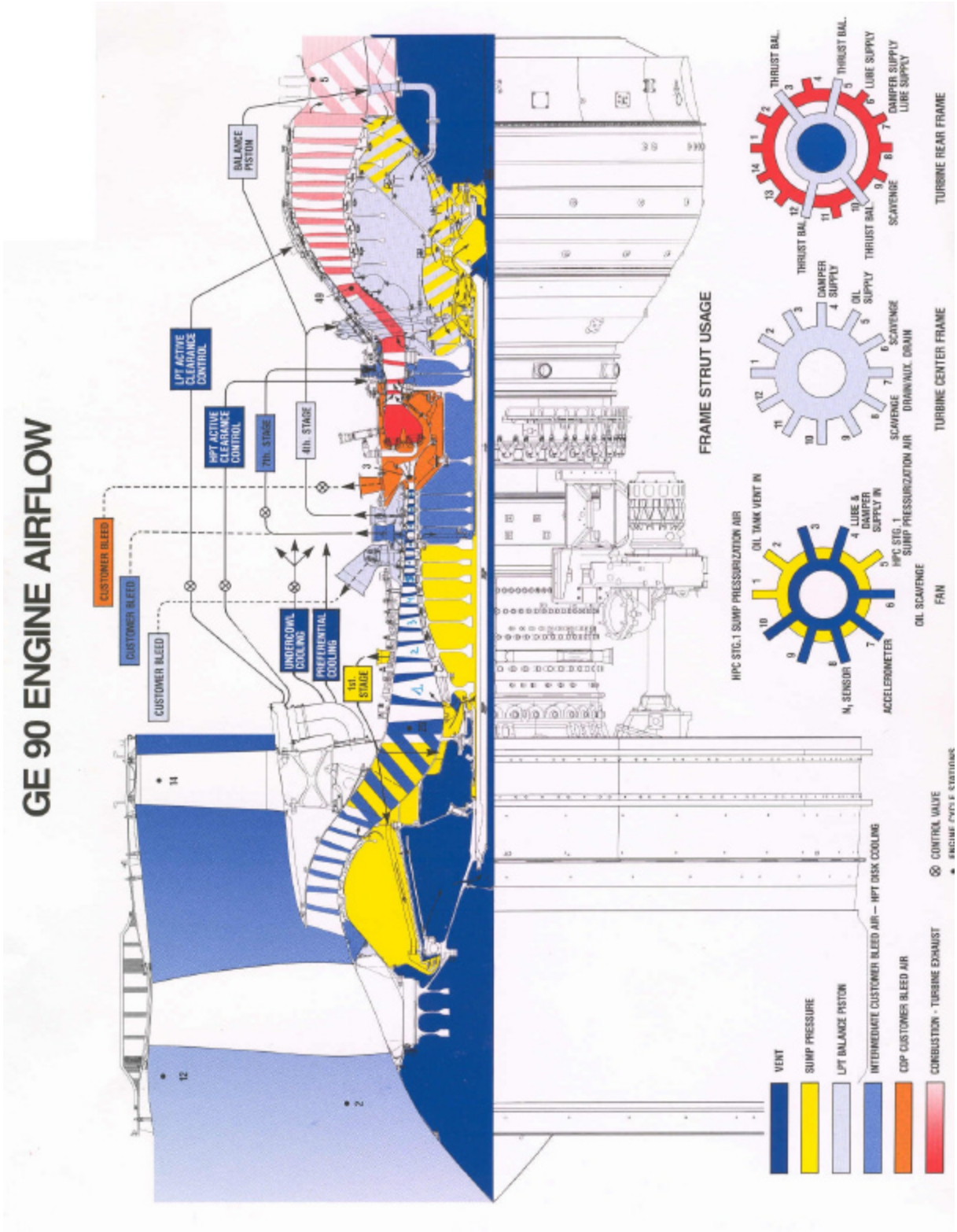

APPENDIX D: The Gasturb output for the mission simulation

D.1 The take-off phase

D.1.1 Point 1

Station	W	T	P	WRstd
amb		288,15	101,325	
2	1529,550	288,15	100,818	1537,237
13	1366,550	326,93	151,172	
21	163,000	359,43	185,870	99,242
25	163,001	359,43	184,015	100,242
3	159,741	917,87	4227,932	6,833
31	138,469	917,87	4227,932	
4	141,844	1712,27	4016,625	8,722
41	158,144	1636,34	4016,625	9,507
43	158,144	1147,71	667,368	
44	163,034	1141,18	667,368	
45	163,034	1141,18	654,020	50,265
49	163,034	799,98	120,513	
5	166,294	798,13	120,513	232,692
8	166,294	798,13	118,122	237,402
18	1366,550	326,93	148,168	995,425

P2/P1= 0,9950

Efficiencies:	isentr	polytr	RNI	P/P
Outer LPC	0,9099	0,9149	0,995	1,499
Inner LPC	0,7699	0,7887	0,995	1,844
HP Compressor	0,8701	0,9116	1,250	22,976
Burner	0,9990			0,950
HP Turbine	0,8799	0,8553	2,190	6,019
LP Turbine	0,8806	0,8560	0,646	5,427
HP Spool mech	0,9980	Nominal Spd		1
LP Spool mech	0,9980	Nominal Spd		1

Fuel	FHV	humidity	war2
Generic	43,124	0,0	0,0000

FN	=	394,54
TSFC	=	0,5520
WF	=	3,37445
BPR	=	0,3037
s NOx	=	2,0782
Core Eff	=	0,4621
Prop Eff	=	0,0000
P3/P2	=	41,9361
P16/P13	=	0,98012
P16/P6	=	1,25436
P16/P2	=	1,46965
P6/P5	=	0,98016
A8	=	1,45625
A18	=	4,55588
P8/Pamb	=	1,16578
P18/Pamb	=	1,46230
CD8	=	0,94522
CD18	=	0,95865
XM8	=	0,48255
XM18	=	0,75735
V18/V8,id	=	0,99034
Loading %=		100,68
PWX	=	50
ZWBLD	=	0,00000
WBLD/W21	=	0,00000
WHcl/W25	=	0,03000
WLcl/W25	=	0,02000

D.1.2 Point 2

Station	W	T	P	WRstd
amb		288,05	101,142	
2	1615,874	291,95	105,480	1562,428
13	1446,947	331,14	157,514	
21	168,927	364,05	193,370	99,494
25	168,927	364,05	191,430	100,502
3	165,548	929,69	4412,114	6,829
31	143,503	929,69	4412,114	
4	147,062	1734,86	4191,836	8,722
41	163,955	1658,02	4191,836	9,506
43	163,955	1163,73	695,787	
44	169,023	1157,07	695,787	
45	169,023	1157,07	681,842	50,332
49	169,023	806,91	121,942	
5	172,401	805,13	121,942	239,457
8	172,401	805,13	119,380	244,595
18	1446,947	331,14	154,240	1018,992

P2/P1= 0,9950

Efficiencies:	isentr	polytr	RNI	P/P
Outer LPC	0,9021	0,9073	1,018	1,493
Inner LPC	0,7633	0,7825	1,018	1,833
HP Compressor	0,8693	0,9110	1,273	23,048
Burner	0,9991			0,950
HP Turbine	0,8800	0,8554	2,236	6,025
LP Turbine	0,8805	0,8555	0,658	5,592
HP Spool mech	0,9980	Nominal Spd		1
LP Spool mech	0,9980	Nominal Spd		1

Fuel	FHV	humidity	war2
Generic	43,124	0,0	0,0000

FN	=	297,16
TSFC	=	11,9775
WF	=	3,55922
BPR	=	8,5655
s NOx	=	2,2465
Core Eff	=	0,4668
Prop Eff	=	0,4911
P3/P2	=	41,8289
P16/P13	=	0,97921
P16/P6	=	1,29201
P16/P2	=	1,46227
P6/P5	=	0,97899
A8	=	1,45625
A18	=	4,55588
P8/Pamb	=	1,18032
P18/Pamb	=	1,52490
CD8	=	0,94641
CD18	=	0,96246
XM8	=	0,50217
XM18	=	0,80051
V18/V8,id	=	1,00370
Loading %=		92,89
PWX	=	50
ZWBLD	=	0,00000
WBLD/W21	=	0,00000
WHcl/W25	=	0,03000
WLcl/W25	=	0,02000

D.2 The climb phase

D.2.1 Point 3

Station	W	T	P	WRstd
amb		286,17	97,717	
2	1260,767	291,33	103,493	1241,142
13	1143,109	315,29	133,124	
21	117,658	336,60	153,541	83,918
25	117,658	336,60	152,446	84,521
3	115,304	807,14	2796,891	6,991
31	99,950	807,14	2796,891	
4	101,802	1441,47	2650,539	8,704
41	113,568	1379,96	2650,539	9,501
43	113,568	956,66	444,662	
44	117,097	952,32	444,662	
45	117,097	952,32	436,043	49,467
49	117,097	703,16	106,887	
5	119,451	701,67	106,887	176,700
8	119,451	701,67	105,664	178,745
18	1143,109	315,29	130,921	926,134

P2/P1= 0,9950

Efficiencies:	isentr	polytr	RNI	P/P
Outer LPC	0,9051	0,9084	1,003	1,286
Inner LPC	0,7658	0,7784	1,003	1,484
HP Compressor	0,8815	0,9177	1,157	18,347
Burner	0,9969			0,948
HP Turbine	0,8816	0,8564	1,915	5,961
LP Turbine	0,8713	0,8491	0,580	4,079
HP Spool mech	0,9980	Nominal Spd		1
LP Spool mech	0,9980	Nominal Spd		1

Fuel	FHV	humidity	war2
Generic	43,124	0,0	0,0000

FN	=	147,00
TSFC	=	12,5979
WF	=	1,85184
BPR	=	9,7155
s NOx	=	0,9966
Core Eff	=	0,4174
Prop Eff	=	0,6363
P3/P2	=	27,0249
P16/P13	=	0,98270
P16/P6	=	1,23809
P16/P2	=	1,26406
P6/P5	=	0,98856
A8	=	1,45625
A18	=	4,55588
P8/Pamb	=	1,08133
P18/Pamb	=	1,33878
CD8	=	0,93781
CD18	=	0,94977
XM8	=	0,34141
XM18	=	0,65937
V18/V8,id=		1,27490
Loading %=		221,14
PWX	=	50
ZWBLD	=	0,00000
WBLD/W21	=	0,00000
WHcl/W25	=	0,03000
WLcl/W25	=	0,02000

D.2.2 Point 4

Station	W	T	P	WRstd
amb		268,34	69,682	
2	1072,398	277,37	77,921	1368,177
13	972,272	303,56	103,755	
21	100,127	326,46	121,556	88,838
25	100,126	326,46	120,584	89,554
3	98,124	802,64	2387,937	6,949
31	85,057	802,64	2387,937	
4	86,677	1453,34	2264,491	8,710
41	96,690	1390,92	2264,491	9,504
43	96,690	963,57	377,129	
44	99,694	958,90	377,129	
45	99,694	958,90	369,712	49,842
49	99,694	687,67	78,740	
5	101,696	686,32	78,740	201,966
8	101,696	686,32	77,563	205,030
18	972,272	303,56	101,697	998,284

P2/P1= 0,9960

Efficiencies:	isentr	polytr	RNI	P/P
Outer LPC	0,9036	0,9075	0,820	1,332
Inner LPC	0,7646	0,7789	0,820	1,560
HP Compressor	0,8794	0,9170	0,964	19,803
Burner	0,9956			0,949
HP Turbine	0,8807	0,8553	1,616	6,005
LP Turbine	0,8700	0,8452	0,486	4,695
HP Spool mech	0,9980	Nominal Spd		1
LP Spool mech	0,9980	Nominal Spd		1

Fuel	FHV	humidity	war2
Generic	43,124	0,0	0,0000

FN	=	116,30
TSFC	=	13,9288
WF	=	1,61999
BPR	=	9,7104
s NOx	=	0,9141
Core Eff	=	0,4438
Prop Eff	=	0,7136
P3/P2	=	30,6456
P16/P13	=	0,98017
P16/P6	=	1,31115
P16/P2	=	1,30513
P6/P5	=	0,98505
A8	=	1,45625
A18	=	4,55588
P8/Pamb	=	1,11311
P18/Pamb	=	1,43946
CD8	=	0,94065
CD18	=	0,95847
XM8	=	0,40014
XM18	=	0,75516
V18/V8,id=		1,22461
Loading %=		253,92
PWX	=	50
ZWBLD	=	0,00000
WBLD/W21	=	0,00000
WHcl/W25	=	0,03000
WLcl/W25	=	0,02000

D.2.3 Point 5

Station	W	T	P	WRstd
amb		258,43	57,182	
2	976,272	270,86	67,116	1428,948
13	885,539	298,14	90,720	
21	90,733	321,84	106,984	90,819
25	90,733	321,84	106,090	91,584
3	88,919	801,29	2169,273	6,926
31	77,078	801,29	2169,273	
4	78,371	1461,83	2057,871	8,714
41	87,649	1398,06	2057,871	9,505
43	87,649	969,15	341,975	
44	90,366	964,28	341,975	
45	90,366	964,28	335,216	49,967
49	90,366	681,00	66,120	
5	92,181	679,73	66,120	216,962
8	92,181	679,73	64,979	220,770
18	885,539	298,14	88,803	1027,773

P2/P1= 0,9960

Efficiencies:	isentr	polytr	RNI	P/P
Outer LPC	0,8942	0,8986	0,735	1,352
Inner LPC	0,7566	0,7721	0,735	1,599
HP Compressor	0,8754	0,9146	0,869	20,448
Burner	0,9950			0,949
HP Turbine	0,8803	0,8548	1,455	6,018
LP Turbine	0,8696	0,8422	0,437	5,070
HP Spool mech	0,9980	Nominal Spd		1
LP Spool mech	0,9980	Nominal Spd		1

Fuel	FHV	humidity	war2
Generic	43,124	0,0	0,0000

FN	=	98,90
TSFC	=	15,0916
WF	=	1,49260
BPR	=	9,7598
s NOx	=	0,8736
Core Eff	=	0,4571
Prop Eff	=	0,7579
P3/P2	=	32,3204
P16/P13	=	0,97987
P16/P6	=	1,36663
P16/P2	=	1,32309
P6/P5	=	0,98275
A8	=	1,45625
A18	=	4,55588
P8/Pamb	=	1,13636
P18/Pamb	=	1,55299
CD8	=	0,94271
CD18	=	0,96401
XM8	=	0,43746
XM18	=	0,81847
V18/V8,id=		1,20112
Loading %=		274,75
PWX	=	50
ZWBLD	=	0,00000
WBLD/WZ1	=	0,00000
WHcl/WZ5	=	0,03000
WLcl/WZ5	=	0,02000

D.2.4 Point 6

Station	W	T	P	WRstd
amb		242,58	41,001	
2	828,717	260,67	52,559	1519,536
13	750,863	290,58	73,440	
21	77,854	316,28	87,020	94,101
25	77,854	316,28	87,040	94,953
3	76,297	803,50	1875,284	6,884
31	66,137	803,50	1875,284	
4	67,466	1485,90	1780,143	8,720
41	75,251	1420,06	1780,143	9,509
43	75,251	986,24	295,112	
44	77,587	980,99	295,112	
45	77,587	980,99	289,239	50,148
49	77,587	674,27	50,005	
5	79,144	673,11	50,005	245,106
8	79,144	673,11	48,904	250,623
18	750,863	290,58	71,780	1064,389

P2/P1= 0,9970

Efficiencies:	isentr	polytr	RNI	P/P
Outer LPC	0,8752	0,8810	0,614	1,397
Inner LPC	0,7406	0,7587	0,614	1,671
HP Compressor	0,8688	0,9106	0,734	21,545
Burner	0,9941			0,949
HP Turbine	0,8785	0,8528	1,227	6,032
LP Turbine	0,8692	0,8405	0,366	5,784
HP Spool mech	0,9980	Nominal Spd		1
LP Spool mech	0,9980	Nominal Spd		1

Fuel	FHV	humidity	war2
Generic	43,124	0,0	0,0000

FN	=	80,40
TSFC	=	16,5255
WF	=	1,32865
BPR	=	9,6445
s NOx	=	0,9336
Core Eff	=	0,4801
Prop Eff	=	0,7978
P3/P2	=	35,6795
P16/P13	=	0,97740
P16/P6	=	1,46777
P16/P2	=	1,36570
P6/P5	=	0,97799
A8	=	1,45625
A18	=	4,55588
P8/Pamb	=	1,19276
P18/Pamb	=	1,75071
CD8	=	0,94742
CD18	=	0,97227
XM8	=	0,51511
XM18	=	0,93126
V18/V8,id=		1,13866
Loading %=		304,15
PWX	=	50
ZWBLD	=	0,00000
WBLD/WZ1	=	0,00000
WHcl/WZ5	=	0,03000
WLcl/WZ5	=	0,02000

D.2.5 Point 7

Station	W	T	P	WRstd
amb		228,71	30,090	
2	725,398	254,50	43,577	1585,145
13	654,920	288,43	63,337	
21	70,478	317,16	76,953	97,359
25	70,478	317,16	76,214	98,303
3	69,069	819,92	1726,244	6,839
31	59,871	819,92	1726,244	
4	61,148	1536,96	1639,814	8,726
41	68,196	1468,05	1639,814	9,511
43	68,196	1023,20	271,855	
44	70,310	1017,40	271,855	
45	70,310	1017,40	266,425	50,245
49	70,310	683,00	40,134	
5	71,720	681,88	40,134	278,537
8	71,720	681,88	38,993	286,687
18	654,920	288,43	61,894	1072,855

P2/P1= 0,9970

Efficiencies:	isentr	polytr	RNI	P/P
Outer LPC	0,8468	0,8547	0,530	1,453
Inner LPC	0,7165	0,7303	0,530	1,766
HP Compressor	0,8629	0,9070	0,640	22,650
Burner	0,9941			0,950
HP Turbine	0,8766	0,8508	1,070	6,032
LP Turbine	0,8653	0,8335	0,318	6,638
HP Spool mech	0,9980	Nominal Spd		1
LP Spool mech	0,9980	Nominal Spd		1

Fuel	PHV	humidity	war2
Generic	43,124	0,0	0,0000

FN	=	70,30
TSFC	=	18,1666
WF	=	1,27713
BPR	=	9,2925
s NOx	=	0,8775
Core Eff	=	0,5048
Prop Eff	=	0,8252
P3/P2	=	39,6137
P16/P13	=	0,97706
P16/P6	=	1,58703
P16/P2	=	1,42011
P6/P5	=	0,97157
A8	=	1,45625
A18	=	4,55588
P8/Pamb	=	1,29591
P18/Pamb	=	2,05666
CD8	=	0,95321
CD18	=	0,97600
XM8	=	0,62810
XM18	=	1,00000
V18/V8,id=		1,04862
Loading %=		302,58
PWZ	=	50
ZWBLD	=	0,00000
WBLD/W21	=	0,00000
WHcl/W25	=	0,03000
WLcl/W25	=	0,02000

D.2.6 Point 8

Station	W	T	P	WRstd
amb		219,80	24,415	
2	649,470	249,42	37,906	1615,212
13	584,190	288,01	56,456	
21	65,280	320,39	69,238	100,734
25	65,280	320,39	68,526	101,781
3	63,974	848,99	1645,593	6,761
31	55,455	848,99	1645,593	
4	56,757	1625,88	1565,051	0,729
41	63,285	1551,65	1565,051	9,508
43	63,285	1088,96	260,370	
44	65,244	1082,10	260,370	
45	65,244	1082,10	255,178	50,204
49	65,244	719,18	35,495	
5	66,549	717,78	35,495	299,831
8	66,549	717,78	34,326	310,044
18	584,190	288,01	55,160	1072,856

P2/P1= 0,9980

Efficiencies:	isentr	polytr	RNI	P/P
Outer LPC	0,7802	0,7922	0,477	1,489
Inner LPC	0,6602	0,6876	0,477	1,827
HP Compressor	0,8491	0,8981	0,565	24,014
Burner	0,9949			0,951
HP Turbine	0,8728	0,8467	0,932	6,011
LP Turbine	0,8637	0,8306	0,275	7,189
HP Spool mech	0,9980	Nominal Spd		1
LP Spool mech	0,9980	Nominal Spd		1

Fuel	PHV	humidity	war2
Generic	43,124	0,0	0,0000

FN	=	66,70
TSFC	=	19,5259
WF	=	1,30241
BPR	=	8,9490
s NOx	=	0,9997
Core Eff	=	0,5166
Prop Eff	=	0,8270
P3/P2	=	43,4129
P16/P13	=	0,97706
P16/P6	=	1,60697
P16/P2	=	1,45520
P6/P5	=	0,96706
A8	=	1,45625
A18	=	4,55588
P8/Pamb	=	1,40593
P18/Pamb	=	2,25928
CD8	=	0,96235
CD18	=	0,97600
XM8	=	0,72486
XM18	=	1,00000
V18/V8,id=		0,94570
Loading %=		277,26
PWZ	=	50
ZWBLD	=	0,00000
WBLD/W21	=	0,00000
WHcl/W25	=	0,03000
WLcl/W25	=	0,02000

D.3 The cruise phase – point 9

Station	W	T	P	WRstd
amb		218,81	23,842	
2	597,418	249,02	37,395	1504,845
13	543,672	276,66	51,494	
21	53,746	300,62	61,210	90,874
25	53,746	300,62	60,698	91,641
3	52,671	759,12	1256,182	6,896
31	45,657	759,12	1256,182	
4	46,510	1399,42	1192,234	8,711
41	51,884	1337,35	1192,234	9,500
43	51,884	925,47	197,045	
44	53,496	920,68	197,045	
45	53,496	920,68	193,120	50,172
49	53,496	621,05	30,557	
5	54,571	620,28	30,557	265,491
8	54,571	620,28	29,768	272,530
18	543,672	276,66	50,313	1072,956

P2/P1= 0,9980

Efficiencies:	isentr	polytr	RNI	P/P
Outer LPC	0,8635	0,8696	0,472	1,377
Inner LPC	0,7307	0,7497	0,472	1,637
HP Compressor	0,8663	0,9087	0,558	20,696
Burner	0,9869			0,949
HP Turbine	0,8759	0,8492	0,907	6,051
LP Turbine	0,8609	0,8286	0,272	6,320
HP Spool mech	0,9980	Nominal Spd		1
LP Spool mech	0,9980	Nominal Spd		1

Fuel	FHV	humidity	war2
Generic	43,124	0,0	0,0000

FN	=	43,91
TSFC	=	19,4131
WF	=	0,85241
BPR	=	10,1156
s NOx	=	0,5652
Core Eff	=	0,4954
Prop Eff	=	0,8708
P3/P2	=	33,5924
P16/P13	=	0,97706
P16/P6	=	1,69016
P16/P2	=	1,34545
P6/P5	=	0,97417
A8	=	1,45625
A18	=	4,55588
P8/Pamb	=	1,24854
P18/Pamb	=	2,11024
CD8	=	0,95176
CD18	=	0,97600
XM8	=	0,57840
XM18	=	1,00000
V18/V8,id=		1,17934
Loading %=		500,77
PWX	=	50
ZWBLD	=	0,00000
WBLD/W21	=	0,00000
WHcl/W25	=	0,03000
WLcl/W25	=	0,02000

D.4 The descent phase

D.4.1 Point 10

Station	W	T	P	WRstd
amb		219,80	24,415	
2	414,447	248,70	37,526	1039,650
13	400,193	251,19	37,966	
21	14,254	253,65	38,269	35,411
25	14,254	253,65	38,220	35,455
3	13,969	477,97	253,051	7,204
31	12,109	477,97	253,051	
4	12,417	768,11	238,992	8,595
41	13,842	739,97	238,992	9,404
43	13,842	523,70	50,048	
44	14,270	522,38	50,048	
45	14,270	522,38	49,425	39,388
49	14,270	451,10	24,771	
5	14,555	449,91	24,771	74,392
8	14,555	449,91	24,721	74,544
18	400,193	251,19	37,177	1018,360

P2/P1= 0,9980

Efficiencies:	isentr	polytr	RNI	P/P
Outer LPC	0,3341	0,3352	0,474	1,012
Inner LPC	0,2827	0,2847	0,474	1,020
HP Compressor	0,8040	0,8476	0,467	6,621
Burner	0,2881			0,944
HP Turbine	0,8655	0,8387	0,485	4,775
LP Turbine	0,7948	0,7787	0,181	1,995
HP Spool mech	0,9980	Nominal Spd		1
LP Spool mech	0,9980	Nominal Spd		1

Fuel	FHV	humidity	war2
Generic	43,124	0,0	0,0000

FN	=	-9,49
TSFC	=	-68,6239
WF	=	0,30762
BPR	=	28,0751
s NOx	=	0,0701
Core Eff	=	0,0659
Prop Eff	=	1,0233
P3/P2	=	6,7434
P16/P13	=	0,97924
P16/P6	=	1,50389
P16/P2	=	0,99072
P6/P5	=	0,99797
A8	=	1,45625
A18	=	4,55588
P8/Pamb	=	1,01252
P18/Pamb	=	1,52271
CD8	=	0,93109
CD18	=	0,96233
XM8	=	0,13447
XM18	=	0,79866
V18/V8,id=		4,21904
Loading %=		6063,96
PWX	=	50
ZWBLD	=	0,00000
WBLD/W21	=	0,00000
WHcl/W25	=	0,03000
WLcl/W25	=	0,02000

D.4.2 Point 11

Station	W	T	P	WRstd
amb		228,71	30,090	
2	453,574	253,81	43,213	998,163
13	437,878	256,18	43,650	
21	15,696	258,52	43,952	34,274
25	15,696	258,52	43,899	34,315
3	15,382	483,12	280,918	7,184
31	13,334	483,12	280,918	
4	13,592	790,49	265,396	8,595
41	15,162	760,22	265,396	9,402
43	15,162	542,17	57,519	
44	15,633	540,43	57,519	
45	15,633	540,43	56,845	38,161
49	15,633	472,77	30,453	
5	15,947	471,25	30,453	67,854
8	15,947	471,25	30,401	67,968
18	437,878	256,18	42,813	977,134

P2/P1= 0,9980

Efficiencies:	isentr	polytr	RNI	P/P
Outer LPC	0,3101	0,3111	0,528	1,010
Inner LPC	0,2624	0,2642	0,528	1,017
HP Compressor	0,7990	0,8430	0,520	6,399
Burner	0,4019			0,945
HP Turbine	0,8629	0,8963	0,514	4,614
LP Turbine	0,7998	0,7856	0,195	1,867
HP Spool mech	0,9980	Nominal Spd		1
LP Spool mech	0,9980	Nominal Spd		1

Fuel	FHV	humidity	war2
Generic	43,124	0,0	0,0000

FN	=	-4,06
TSFC	=	-53,1181
WF	=	0,25831
BPR	=	27,8972
s NOx	=	0,0751
Core Eff	=	0,0838
Prop Eff	=	1,0247
P3/P2	=	6,5008
P16/P13	=	0,98082
P16/P6	=	1,40826
P16/P2	=	0,99075
P6/P5	=	0,99831
A8	=	1,45625
A18	=	4,55588
P8/Pamb	=	1,01037
P18/Pamb	=	1,42285
CD8	=	0,93088
CD18	=	0,95602
XM8	=	0,12237
XM18	=	0,72784
V18/V8,id=		4,20722
Loading %=		5438,58
PWX	=	50
ZWBLD	=	0,00000
WBLD/W21	=	0,00000
WHcl/W25	=	0,03000
WLcl/W25	=	0,02000

D.4.3 Point 12

Station	W	T	P	WRstd
amb		242,58	41,001	
2	486,722	260,67	52,612	891,559
13	468,786	262,91	52,956	
21	17,935	265,13	53,193	32,772
25	17,935	265,13	53,135	32,807
3	17,577	489,98	325,058	7,145
31	15,236	489,98	325,058	
4	15,475	817,20	307,295	8,593
41	17,268	784,95	307,295	9,398
43	17,268	566,42	69,881	
44	17,807	564,15	69,881	
45	17,807	564,15	69,130	36,519
49	17,807	503,82	41,369	
5	18,165	501,86	41,369	58,716
8	18,165	501,86	41,317	58,791
18	468,786	262,91	52,144	870,124

P2/P1= 0,9980

Efficiencies:	isentr	polytr	RNI	P/P
Outer LPC	0,2171	0,2179	0,615	1,007
Inner LPC	0,1837	0,1850	0,615	1,011
HP Compressor	0,7927	0,8371	0,603	6,118
Burner	0,5312			0,945
HP Turbine	0,8604	0,8343	0,563	4,397
LP Turbine	0,9217	0,9111	0,221	1,671
HP Spool mech	0,9980	Nominal Spd		1
LP Spool mech	0,9980	Nominal Spd		1

Fuel	FHV	humidity	war2
Generic	43,124	0,0	0,0000

FN	=	-5,14
TSFC	=	-46,4459
WF	=	0,23881
BPR	=	26,1376
s NOx	=	0,0824
Core Eff	=	0,0958
Prop Eff	=	1,0288
P3/P2	=	6,1784
P16/P13	=	0,98467
P16/P6	=	1,26205
P16/P2	=	0,99111
P6/P5	=	0,99874
A8	=	1,45625
A18	=	4,55588
P8/Pamb	=	1,00772
P18/Pamb	=	1,27179
CD8	=	0,93064
CD18	=	0,94418
XM8	=	0,10566
XM18	=	0,59612
V18/V8,id=		3,98089
Loading %=		4670,70
PWX	=	50
ZWBLD	=	0,00000
WBLD/W21	=	0,00000
WHcl/W25	=	0,03000
WLcl/W25	=	0,02000

D.4.4 Point 13

Station	W	T	P	WRstd
amb		258,43	57,182	
2	512,418	270,36	66,751	753,440
13	491,266	272,03	67,120	
21	21,152	273,69	67,375	31,003
25	21,151	273,69	67,309	31,031
3	20,728	494,82	379,024	7,262
31	17,968	494,82	379,024	
4	18,195	801,41	357,627	8,597
41	20,310	770,72	357,627	9,411
43	20,310	554,07	81,591	
44	20,944	552,31	81,591	
45	20,944	552,31	80,669	36,421
49	20,944	511,74	57,555	
5	21,367	509,73	57,555	50,031
8	21,367	509,73	57,502	50,077
18	491,266	272,03	66,393	728,475

P2/P1= 0,9970

Efficiencies:	isentr	polytr	RNI	P/P
Outer LPC	0,2559	0,2565	0,733	1,006
Inner LPC	0,2165	0,2176	0,733	1,009
HP Compressor	0,7833	0,8279	0,724	5,631
Burner	0,6178			0,944
HP Turbine	0,8654	0,8399	0,675	4,386
LP Turbine	0,8358	0,8293	0,267	1,402
HP Spool mech	0,9980	Nominal Spd		1
LP Spool mech	0,9980	Nominal Spd		1

Fuel	FHV	humidity	war2
Generic	43,124	0,0	0,0000

FN	=	-5,08
TSFC	=	-44,6081
WF	=	0,22656
BPR	=	23,2252
s NOx	=	0,0899
Core Eff	=	0,0775
Prop Eff	=	1,0333
P3/P2	=	5,6782
P16/P13	=	0,98916
P16/P6	=	1,15460
P16/P2	=	0,99463
P6/P5	=	0,99908
A8	=	1,45625
A18	=	4,55588
P8/Pamb	=	1,00561
P18/Pamb	=	1,16108
CD8	=	0,93007
CD18	=	0,93377
XM8	=	0,09012
XM18	=	0,46679
V18/V8,id=		3,73488
Loading %=		4110,86
PWX	=	50
ZWBLD	=	0,00000
WBLD/W21	=	0,00000
WHcl/W25	=	0,03000
WLcl/W25	=	0,02000

D.4.5 Point 14

Station	W	T	P	WRstd
amb		268,34	69,682	
2	486,690	276,51	77,080	626,728
13	462,990	276,72	77,148	
21	23,700	276,92	77,195	30,496
25	23,698	276,92	77,122	30,522
3	23,224	490,03	399,164	7,688
31	20,132	490,03	399,164	
4	20,312	709,34	373,907	8,606
41	22,682	682,54	373,907	9,460
43	22,682	468,20	73,987	
44	23,393	468,86	73,987	
45	23,393	468,86	72,969	41,436
49	23,393	464,58	70,028	
5	23,867	463,42	70,028	43,795
8	23,867	463,42	69,979	43,825
18	462,990	276,72	76,576	600,349

P2/P1= 0,9960

Efficiencies:	isentr	polytr	RNI	P/P
Outer LPC	0,3484	0,3485	0,815	1,001
Inner LPC	0,2948	0,2949	0,815	1,001
HP Compressor	0,7722	0,8171	0,814	5,176
Burner	0,5948			0,937
HP Turbine	0,8809	0,8547	0,864	5,054
LP Turbine	0,8005	0,7996	0,317	1,042
HP Spool mech	0,9980	Nominal Spd		1
LP Spool mech	0,9980	Nominal Spd		1

Fuel	FHV	humidity	war2
Generic	43,124	0,0	0,0000

FN	=	-5,91
TSFC	=	-30,5293
WF	=	0,18057
BPR	=	19,5356
s NOx	=	0,0895
Core Eff	=	-0,0076
Prop Eff	=	1,0500
P3/P2	=	5,1786
P16/P13	=	0,99259
P16/P6	=	1,09427
P16/P2	=	0,99346
P6/P5	=	0,99930
A8	=	1,45625
A18	=	4,55588
P8/Pamb	=	1,00426
P18/Pamb	=	1,09894
CD8	=	0,93024
CD18	=	0,92729
XM8	=	0,07841
XM18	=	0,36956
V18/V8,id=		3,61462
Loading %=		4263,66
PWX	=	50
ZWBLD	=	0,00000
WBLD/W21	=	0,00000
WHcl/W25	=	0,03000
WLcl/W25	=	0,02000

D.4.6 Point 15

Station	W	T	P	WRstd
amb		286,17	97,717	
2	1542,481	289,20	100,077	1552,161
13	1381,016	327,63	150,386	
21	161,465	359,91	184,501	99,103
25	161,465	359,91	182,665	100,099
3	158,236	918,34	4187,656	6,835
31	137,165	918,34	4187,656	
4	140,503	1711,73	3978,209	8,722
41	156,650	1635,89	3978,209	9,507
43	156,650	1147,16	660,517	
44	161,494	1140,65	660,517	
45	161,494	1140,65	697,297	50,296
49	161,494	796,63	117,140	
5	164,723	794,85	117,140	236,645
8	164,723	794,85	114,736	241,603
18	1381,016	327,64	147,294	1013,014

P2/P1= 0,9930

Efficiencies:	isentr	polytr	RNI	P/P
Outer LPC	0,9075	0,9125	0,989	1,491
Inner LPC	0,7679	0,7866	0,989	1,829
HP Compressor	0,8702	0,9116	1,238	22,925
Burner	0,9990			0,950
HP Turbine	0,8800	0,8554	2,170	6,023
LP Turbine	0,8803	0,8534	0,639	5,526
HP Spool mech	0,9980	Nominal Spd		1
LP Spool mech	0,9980	Nominal Spd		1

Fuel	FHV	humidity	war2
Generic	43,124	0,0	0,0000

FN	=	291,93
TSFC	=	11,4356
WF	=	3,33837
BPR	=	8,5530
s NOx	=	2,0752
Core Eff	=	0,4657
Prop Eff	=	0,4526
P3/P2	=	41,5126
P16/P13	=	0,97944
P16/P6	=	1,28377
P16/P2	=	1,46018
P6/P5	=	0,97948
A8	=	1,45625
A18	=	4,55588
P8/Pamb	=	1,17417
P18/Pamb	=	1,50736
CD8	=	0,94589
CD18	=	0,96144
XM8	=	0,49389
XM18	=	0,78874
V18/V8,id=		1,00734
Loading %=		101,30
FWX	=	50
ZWBLD	=	0,00000
WBLD/W21	=	0,00000
WHcl/W25	=	0,03000
WLcl/W25	=	0,02000

D.5 The landing phase

D.5.1 Point 16

Station	W	T	P	WRstd
amb		288,05	101,142	
2	1586,701	290,60	103,778	1555,760
13	1419,787	329,64	155,274	
21	166,913	362,40	190,758	99,428
25	166,910	362,40	188,848	100,431
3	163,571	925,50	4348,697	6,830
31	141,790	925,50	4348,697	
4	145,284	1726,80	4131,496	8,722
41	161,975	1650,28	4131,496	9,507
43	161,975	1157,99	685,983	
44	166,983	1151,38	685,983	
45	166,983	1151,38	672,247	50,310
49	166,983	804,21	121,383	
5	170,321	802,43	121,383	237,256
8	170,321	802,43	118,980	242,253
18	1419,787	329,64	152,090	1011,699

P2/P1= 0,9950

Efficiencies:	isentr	polytr	RNI	P/P
Outer LPC	0,9060	0,9112	1,010	1,496
Inner LPC	0,7666	0,7856	1,010	1,838
HP Compressor	0,8696	0,9112	1,265	23,028
Burner	0,9991			0,950
HP Turbine	0,8800	0,8554	2,221	6,023
LP Turbine	0,8806	0,8557	0,654	5,538
HP Spool mech	0,9980	Nominal Spd		1
LP Spool mech	0,9980	Nominal Spd		1

Fuel	FHV	humidity	war2
Generic	43,124	0,0	0,0000

FN	=	311,17
TSFC	=	11,2308
WF	=	3,49470
BPR	=	8,5061
s NOx	=	2,1858
Core Eff	=	0,4654
Prop Eff	=	0,4222
P3/P2	=	41,9040
P16/P13	=	0,97950
P16/P6	=	1,27936
P16/P2	=	1,46554
P6/P5	=	0,97937
A8	=	1,45625
A18	=	4,55588
P8/Pamb	=	1,17537
P18/Pamb	=	1,50373
CD8	=	0,94602
CD18	=	0,96122
XM8	=	0,49560
XM18	=	0,78628
V18/V8,id=		0,99974
Loading %=		95,54
FWX	=	50
ZWBLD	=	0,00000
WBLD/WZ1	=	0,00000
WHcl/W25	=	0,03000
WLcl/WZ5	=	0,02000

D.5.2 Point 17

Station	W	T	P	WRstd
amb		288,15	101,325	
2	1529,541	288,15	100,818	1537,228
13	1366,541	326,93	151,172	
21	163,000	359,43	185,868	99,242
25	163,000	359,43	184,014	100,242
3	159,740	917,87	4227,911	6,833
31	138,468	917,87	4227,911	
4	141,843	1712,27	4016,604	8,722
41	158,143	1636,34	4016,604	9,507
43	158,143	1147,71	667,366	
44	163,033	1141,18	667,366	
45	163,033	1141,18	654,026	50,265
49	163,033	799,99	120,516	
5	166,293	798,13	120,516	232,696
8	166,293	798,13	118,126	237,395
18	1366,541	326,93	148,167	995,422

P2/P1= 0,9950

Efficiencies:	isentr	polytr	RNI	P/P
Outer LPC	0,9099	0,9149	0,995	1,499
Inner LPC	0,7699	0,7887	0,995	1,844
HP Compressor	0,8701	0,9116	1,250	22,976
Burner	0,9990			0,950
HP Turbine	0,8799	0,8953	2,190	6,019
LP Turbine	0,8806	0,8560	0,686	5,427
HP Spool mech	0,9980	Nominal Spd		1
LP Spool mech	0,9980	Nominal Spd		1

Fuel	FHV	humidity	war2
Generic	43,124	0,0	0,0000

FN	=	394,54
TSFC	=	8,5528
WF	=	3,37444
BPR	=	8,3837
s NOx	=	2,0782
Core Eff	=	0,4621
Prop Eff	=	0,0000
P3/P2	=	41,9359
P16/P13	=	0,98012
P16/P6	=	1,25432
P16/P2	=	1,46960
P6/P5	=	0,98016
A8	=	1,45623
A18	=	4,55588
P8/Pamb	=	1,16581
P18/Pamb	=	1,46230
CD8	=	0,94521
CD18	=	0,95865
XM8	=	0,48259
XM18	=	0,75734
V18/V8,id	=	0,99024
Loading %=		100,68
FWX	=	50
ZWBLD	=	0,00000
WBLD/W21	=	0,00000
WHcl/W25	=	0,03000
WLcl/W25	=	0,02000

PART 3: PRELIMINARY SIZING OF THE MOTHERSHIP

INTRODUCTION

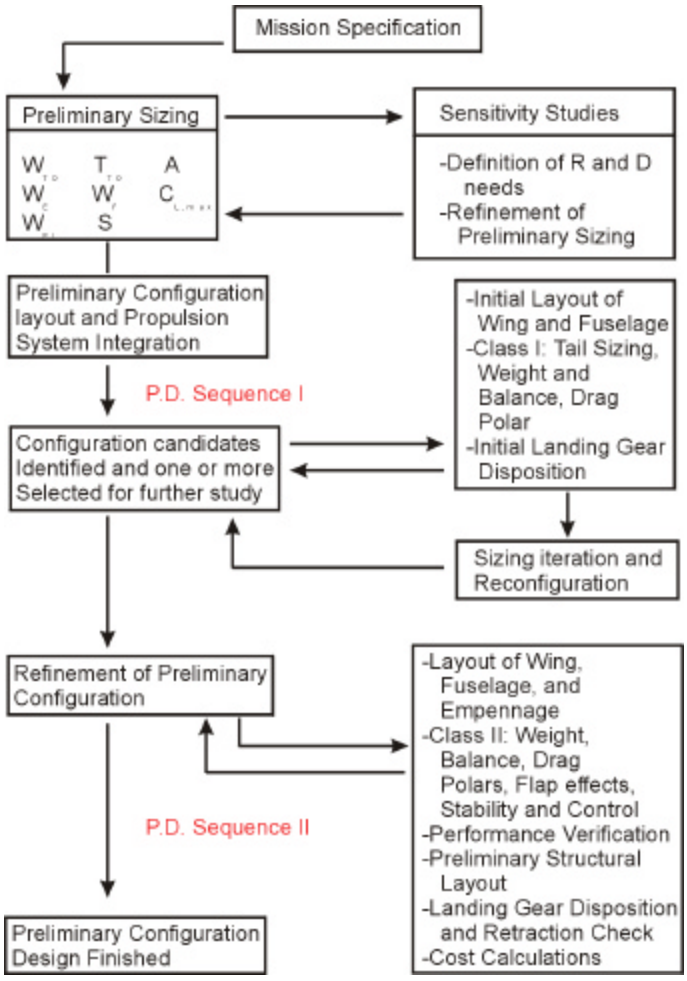

From ref.[6] Chapter I

In this part 3 of our study, the preliminary sizing of the mothership is tackled with the aid of the Advanced Aircraft Analysis (AAA) software from Darcorp and several books including Roskam 's Airplane Design books. Since both AAA and the books of Roskam follow the same structure for the preliminary design of an aircraft, this contribution also uses this structure which can be found in the adjacent figure. As can be seen on that figure the preliminary design process is divided into 3 phases: Preliminary Sizing, Preliminary Design Sequence I and Preliminary Design sequence II. As already mentioned, this part of the text focuses on the Preliminary sizing phase. In this phase, several weights of the airplane are determined (take-off, payload, empty and fuel weight) as well as the required take-off thrust, the wing area and the aspect ratio of the wing.

Here, the preliminary sizing is done for three different airplanes: the Boeing 777-200 (Chapter I), a hydrogen-fuelled version of the Boeing 777 (Chapter II) and the mothership (Chapter III). For each subsection of the preliminary sizing, the method used is briefly explained in Chapter I. Since exactly the same methods are used in both other chapters, the "theory" is not repeated there. Only the appropriate input and output data are given there.

CHAPTER I

PRELIMINARY SIZING OF THE KEROSENE-FUELLED BOEING 777

In this first chapter, the preliminary sizing of the Boeing 777 is tackled. This is done as a validation for the method used and to test the accuracy of AAA. Besides this, this case is also used to explain the equations used in the different sizing modules of the program.

First of all, a definition of preliminary sizing must be given. According to Roskam (see ref. [6] page 2), preliminary sizing is defined as the process, which results in the numerical definition of the following airplane design parameters:

- Gross take-off weight, W_{TO}
- Empty weight, W_E
- Mission fuel weight, W_F
- Maximum required take-off thrust, T_{TO}
- Wing area, S and wing aspect ratio, A
- Maximum required lift coefficient (clean), $C_{L_{max}}$
- Maximum required lift coefficient for take-off, $C_{L_{max,\,TO}}$
- Maximum required lift coefficient for landing, $C_{L_{max,\,L}}$

The method Roskam uses for this preliminary sizing calculations is based on a mission specification. The specification used in this design is thus given first. After this, the different weights are estimated. The take-off gross weight, the empty weight and the mission fuel weight are determined in a second paragraph. After this the wing area, take-off thrust and maximum lift coefficients for the different configurations (clean, take-off and landing) are determined. This is done via several sizing requirements, which can be found in paragraph I.2. Some of these requirements depend though on the drag of the airplane so drag polars need to be determined. This is done in the third paragraph of this chapter.

I.1 THE MISSION SPECIFICATION OF THE BOEING 777-200

As mentioned in the introduction, the method implemented in AAA uses a mission specification as a base to start the sizing of the plane under consideration. The mission specification given here is determined through the data given in the example 777 file included with the program. This results in:

Role: large long-range civil transport airplane

Payload: 79,500 lbs (36,061 kg)

Crew: the weight of the crew is included in the payload weight

Performance:

- **Range:** Still air range in cruise of 4,240 nm (7,852 km) with reserves equal to 10% of the mission fuel
- **Speed:** Mach 0.83 at 35,000 ft (10,668 m)
- **Field length:** takeoff and landing field length determined based on real values for B777-200
- **Climb:** direct climb to 35,000 ft in 19.5 minutes

Powerplants: 2 GE90-85B

Certification: FAR25

Mission Profile:

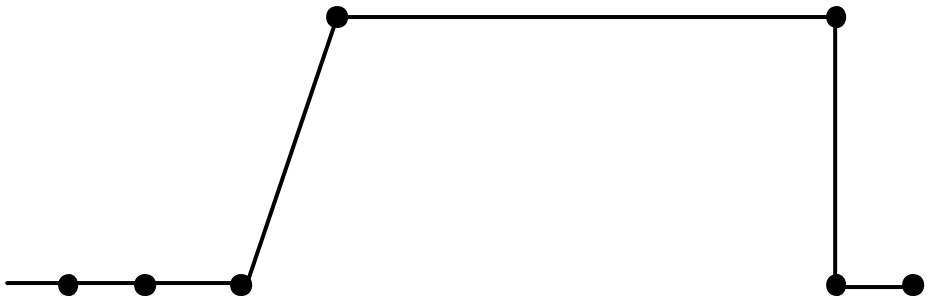

1. Engine start and Warm-up
2. Taxi
3. Takeoff
4. Climb to 35,000 ft
5. Cruise at constant altitude
6. Descent
7. Landing, taxi & shutdown

I.2 ESTIMATION OF TAKE-OFF GROSS WEIGHT, EMPTY WEIGHT AND MISSION FUEL WEIGHT

I.2.1 GENERAL OUTLINE OF THE METHOD

Below, a concise outline of the iterative method used is given. A more elaborate survey of the method can be found in ref. [6] and ref. [1].

To start the iterative process of determining the take-off gross weight, this weight is first broken down as follows:

$$W_{TO} = W_{OE} + W_F + W_{PL} \qquad (1.1)$$

where:

W_{TO} is the take-off gross weight,
W_{OE} is the airplane operating weight empty,
W_F is the mission fuel weight,
W_{PL} is the payload weight.

The operating weight empty, W_{OE} is also frequently written as follows:

$$W_{OE} = W_E + W_{tfo} + W_{crew} \qquad (1.2)$$

where:

W_E is the empty weight,
W_{tfo} is the weight of all trapped (=unusable) fuel and oil,
W_{crew} is the weight of the crew required to operate the airplane

Once this breakdown has been established the following seven steps must be executed in an iterative process to estimate values for W_{TO}, W_E and W_F:

1. Determine the mission payload weight, W_{PL} and the crew weight, W_{crew}.
2. Guess a likely value of the take-off weight, $W_{TO,\,guess}$.
3. Determine the mission fuel weight, W_F.
4. Calculate a tentative value for W_{OE} from:
$$W_{OE,\,tent} = W_{TO,\,guess} - W_F - W_{PL} .$$
5. Calculate a tentative value for W_E from:
$$W_{E,\,tent} = W_{OE,\,tent} - W_{tfo} - W_{crew} .$$
6. Find the allowable value of W_E.
7. Compare the values for $W_{E,\,tent}$ and for W_E as obtained from steps 5 and 6. Next, adjust the value of $W_{TO,\,guess}$ and repeat steps 3 through 6. Continue this process until the values of $W_{E,tent}$ and W_E agree with each other to within some pre-selected tolerance. A tolerance of 0.5% is, according to ref. [6] sufficient at this design level.

Next, each step will be considered shortly and the values resulting from the iteration will be given.

I.2.2 DETERMINATION THE MISSION PAYLOAD AND CREW WEIGHT

For this simulation, the mission payload weight is taken as 79,500 lbs (36,061 kg). This was the value already entered in the example file included with AAA for the 777-200. This weight also includes the weight of the crew. A typical arrangement for this mission would thus be 360 passengers and 10 crew. This would lead to a payload weight of 79,450 lbs[1] with the following assumptions (as suggested by AAA for long distance commercial flights):

Passenger	Weight per passenger	175 lbs
	Weight per baggage	40 lbs
Crewmember	Weight per crewmember	175 lbs
	Weight per baggage	30 lbs

[1] 360*(175+40)+10*(175+30)

Since the maximum capacity of the two-class seating arrangement is 375 passengers (30 first class and 345 economy class), this value seems reasonable as an estimate of the payload of a typical 777-200 mission.

I.2.3 GUESSING A LIKELY VALUE OF TAKE-OFF WEIGHT, $W_{TO, GUESS}$

An initial 'guess' of the value of the take-off weight, $W_{TO, guess}$, is, according to Roskam, usually obtained by comparing the mission specification of the airplane with the mission capabilities of similar airplanes. Since this guess only serves as a starting value for the iteration, which is done in AAA, it is unimportant which value has been chosen. Nevertheless a reasonable estimate should be used to minimise the number of iterations. Since the actual take-off weight of the 777 is known, this value is taken as the initial guess:

$$W_{TO, guess} = 535{,}000 \text{ lbs } (242{,}630 \text{ kg})$$

I.2.4 DETERMINATION OF MISSION FUEL WEIGHT, W_F

Before starting the actual calculations the mission fuel weight is broken down into:

$$W_F = W_{F, used} + W_{F, res} \qquad (1.3)$$

where:

$W_{F, used}$ is the fuel actually used during the mission,
$W_{F, res}$ are the fuel reserves required for the mission.

To determine the fuel weight actually used during the mission $W_{F,used}$, the so-called fuel-fraction method is used in AAA and in Dr. Roskam's books. In this method the airplane mission is broken down into a number of mission phases. The fuel used during each phase is then found from a simple calculation (for the fuel intensive phases[2]) or estimated on the basis of experience (for the fuel un-intensive phases[3]). The weight of the fuel reserves required for the mission are given in AAA as a fraction of $W_{F,used}$. In the mission specification a fraction of 10% is wanted as reserves.

The fuel fraction for phase i of the mission is defined as the ratio of the end weight W_i to the begin weight of the phase, W_{i-1}. The mission fuel fraction, M_{ff}, can then be calculated from:

$$M_{ff} = \frac{W_1}{W_{TO}} \prod_{i=2}^{n} \frac{W_i}{W_{i-1}} \qquad (1.4)$$

where n is the number of mission phases.

The fuel used during the mission, $W_{F,used}$, can then be found from:

$$W_{F,used} = (1 - M_{ff}) * W_{TO} . \qquad (1.5)$$

Now, the value for the mission fuel weight, W_F can finally be determined from:

$$W_F = (1 - M_{ff}) * W_{TO} + W_{F, res} \qquad (1.6)$$

Below, the mission specification in subsection I.1 is used to explain the method more into detail and to give the values determined for each phase. The distinct phases used here (and their numeration) can also be found on this mission specification.

[2] These are flight phases during which a relatively large amount of fuel is used; e.g. prolonged climbs and descents, cruise,…
[3] The fuel un-intensive phases are flight phases during which a relatively small amount of fuel is used. Examples are: warm-up, taxi, take-off,…

I.2.4.1 PHASE 1: ENGINE START AND WARM-UP

The begin weight of this phase is the gross take-off weight W_{TO}. The end weight is W_1. The fuel fraction for this phase is by previous definition given by: W_1/W_{TO} .

For the jet transport category of aircraft, Roskam (see ref. [6]) gives a value of 0.990 for the fuel fraction of the engine start and warm-up segment[4]. Raymer (ref. [5]) only gives values for the warm-up, taxi and take-off segments together. He suggests values between 0.97 and 0.99 for the fraction of all 3 phases together. Multiplying the values given by Roskam (see also I.2.4.2 and I.4.2.3) would lead to a total fraction of 0.975 for those 3 phases. Both values are comparable, thus Roskam's values are taken:

$$\frac{W_1}{W_{TO}} = 0.9900 \ .$$

I.2.4.2 PHASE 2: TAXI

The begin weight of this phase is the end weight of the previous phase, W_1. The end weight is W_2. The fuel fraction for this phase is by previous definition given by: W_2/W_1 .

Again, the value that Roskam proposes (0.99) for the considered aircraft category is in agreement with Raymer's values. The value taken for this simulation is thus:

$$\frac{W_2}{W_1} = 0.9900 \ .$$

I.2.4.3 PHASE 3: TAKE-OFF

The begin weight of this phase is the end weight of the previous phase, W_2. The end weight is W_3. The fuel fraction for this phase is thus given by: W_3/W_2 .

Again, the value that Roskam proposes (0.995) for the considered aircraft category is in agreement with Raymer's values. The value taken for this simulation is thus:

$$\frac{W_3}{W_2} = 0.9950 \ .$$

I.2.4.4 PHASE 4: CLIMB

The begin weight of this phase is the end weight of the previous phase, W_3. The end weight is W_4. The fuel fraction for this phase is thus given by: W_4/W_3 .

The climb phase is considered as a fuel-intensive phase. Therefore, the Breguet equation for endurance is used to determine the fuel fraction for this flight phase. For jet airplanes this Breguet equation is given by:

$$E_{cl} = \left(\frac{1}{c_j}\right)_{cl} * \left(\frac{L}{D}\right)_{cl} * \ln\left(\frac{W_3}{W_4}\right) \qquad (1.7)$$

where:

E_{cl} is the endurance of the climb phase,
c_j is the thrust specific fuel consumption (lbs/hr/lb or kg/hr/N),
(L/D) is the lift-to-drag ratio,
the index cl indicates that the values are for the climb phase.

[4] These values are estimated from statistical data.

To determine the fuel fraction used during climb, it is thus necessary to estimate or calculate average values for c_j and for (L/D) during climb. The values used for c_j and (L/D) for this simulation are those given in the example file of AAA. Since AAA calculates the endurance based on the average rate of climb and the altitude to climb to, these values must also be given. In the original 777 simulation included with AAA, a cruise altitude (h) of 39,000 ft and a rate of climb (RC) of 2,000 ft/min were used. These values are adapted here to a cruise altitude of 35,000 ft since this was the altitude used in our previous calculations. The rate of climb has also been adopted to obtain the endurance (and thus the fuel fraction) from in the original simulation (E=19.5 min). This leads to the following values:

$$c_j = 0.700 \frac{lb/hr}{lb} = 0.0714 \frac{kg/hr}{N}$$

$$\left(\frac{L}{D}\right)_{cl} = 10$$

$$RC = 1{,}794.87 \ \frac{ft}{min} = 9.1179 \frac{m}{s}$$

h = 35,000 ft = 10,668 m

Based on the values of the altitude and the average rate of climb, the endurance can be calculated (E=h / RC). Using (1.7), this leads to:

$$\frac{W_4}{W_3} = 0.9775 \ .$$

I.2.4.5 PHASE 5: CRUISE

The begin weight of this phase is the end weight of the previous phase, W_4. The end weight is W_5. The fuel fraction for this phase is thus given by: W_5 / W_4 .

Again, as for the climb phase, this flight phase is considered as a fuel-intensive phase. The Breguet equation for range is used to determine the fuel fraction for this flight phase. For jet airplanes this Breguet equation is given by:

$$R_{cr} = \left(\frac{V}{c_j}\right)_{cr} * \left(\frac{L}{D}\right)_{cr} * \ln\left(\frac{W_4}{W_5}\right) \qquad (1.8)$$

where:

R_{cr} is the range in cruise (nm or km)
V is the airplane cruise speed (kts or km/hr)
c_j is the thrust specific fuel consumption (lbs/hr/lb or kg/hr/N),
(L/D) is the lift-to-drag ratio,
the index cr indicates that the values are for the cruise phase.

Again, as for the climb phase, average values for these parameters have to be estimated. The values used are, again, the values from the example included with AAA except for the cruise speed. This speed was namely given as Mach 0.83 at 39,000 ft (V= 476 kts). In this simulation though, the cruise height is 35,000 ft. The cruise speed was thus recalculated to give a Mach number of 0.83 at 35,000 ft. This leads to the following values:

$$V = 478.56 \text{ kts} = 886.29 \frac{km}{hr}$$

$$c_j = 0.500 \frac{lb/hr}{lb} = 0.0510 \frac{kg/hr}{N}$$

$$\left(\frac{L}{D}\right)_{cl} = 15$$

R = 4,240 nm = 7,852.48 km

The value for the cruise fuel fraction is now determined with (1.8) as:

$$\frac{W_5}{W_4} = 0.7443 .$$

I.2.4.6 PHASE 6: DESCENT

The begin weight of this phase is the end weight of the previous phase, W_5. The end weight is W_6. The fuel fraction for this phase is thus given by: W_6/W_5 .

The descent phase will be considered as a fuel un-intensive flight phase (the engine is running at idle rating) in this simulation so the historically estimated fractions suggested by Roskam and Raymer will be used again. For jet transports Roskam gives a value of 0.99 in ref. [6] for the descent phase. Raymer estimates this fraction as 0.990 to 0.995. Since these values are in accordance with each other, the value of Roskam is taken. It was namely this value that was used in the example file too. Thus:

$$\frac{W_6}{W_5} = 0.9900 .$$

I.2.4.7 PHASE 7: LANDING, TAXI & SHUTDOWN

The begin weight of this phase is the end weight of the previous phase, W_6. The end weight is W_7. The fuel fraction for this phase is thus given by: W_7/W_6 .

Since landing, taxi and shutdown is a flight phase in which a relatively small amount of fuel is used, the statistical estimations are used again. For this phase Roskam suggests a value of 0.992 for jet transports while Raymer indicates a range between 0.992 and 0.997. Again, both numbers are well in accordance, so the value from the example file is kept:

$$\frac{W_7}{W_6} = 0.9920 .$$

I.2.5 FINDING THE ALLOWABLE VALUE FOR W_E

In AAA, a linear relationship between $\log_{10} W_E$ and $\log_{10} W_{TO}$ is used:

$$\log_{10} W_{TO} = A + B * \log_{10} W_E \qquad (1.9)$$

where A and B are the so-called regression coefficients. This relationship is determined for each airplane category though the use of data from existing airplanes and is shown graphically in ref. [6]. Based on these figures, the coefficients A and B are determined for each category. The allowable value for W_E can then be found from equation (1.10).

$$W_E = \text{inv.log}_{10}\left(\frac{\log_{10} W_{TO} - A}{B}\right) \qquad (1.10)$$

The values given for the jet transport category are:

A = 0.0833
B = 1.0383

This linear relationship is used during the iteration to determine the empty weight for a given take-off weight. Since the latter is not known yet, the value of W_E cannot be given now. The iteration has to be done first. Therefore, the value of W_E is given in paragraph I.2.6.

I.2.6 THE RESULTS FOR W_{TO}, W_F AND W_F

In this simulation, the iteration is done in AAA with the take-off weight option from the weight sizing module. In order to perform the calculation, the following input variables are requested:

the regression coefficient A,
the regression coefficient B,
the estimated airplane take-off weight $W_{TO,est}$,
the payload weight (including crew weight), W_{PL}
the trapped fuel and oil weight as a fraction of the take-off weight M_{tfo},
the reserve fuel weight as a fraction of the fuel weight used in the mission $M_{F,res}$,

The following values are entered as inputs for the iteration:

A = 0.0833	$W_{TO, est}$ = 535,000 lbs	M_{tfo} = 0.5%
B = 1.0383	W_{PL} = 79,500 lbs	$M_{F, res}$ = 10%

With these values, the program gives as output:

M_{ff} = 0.6968	W_F = 176,534.7 lb	$W_{F, res}$ = 16,048.6 lb	W_E = 270,600.6 lb
$W_{F, used}$ = 160,486.1 lb	$W_{F, max}$ = 176,534.7 lb	W_{tfo} = 2,646.4 lb	W_{TO} = 529,281.8 lb

Furthermore, a mission profile table is also given. In this simulation the table is as follows:

	Mission Profile	W_{begin} (lb)	?$W_{F, used}$ (lb)	$W_{F, begin}$ (lb)
1	Warm-up	529,281.8	5,292.8	176,534.7
2	Taxi	523,988.9	5,239.9	171,241.9
3	Take-off	518,749.0	2,593.7	166,002.0
4	Climb	516,155.3	11,610.0	163,408.3
5	Cruise	504,545.3	129,020.3	151,798.3
6	Descent	375,525.0	3,755.3	22,778.0
7	Land/Taxi	371,769.8	2,974.2	19,022.8

I.2.7 COMPARISON WITH THE REAL 777 VALUES

Since this simulation of the 777 mainly serves as a validation base for the method used for the subsonic mothership and for AAA, a comparison with the real values for the 777 is now in order. Some remarks have to be made beforehand though. First of all, the calculated empty weight must, according to Roskam (ref. [6] page 17), be seen as a “minimum allowable” value at the current “state-of-the-art” of airplane design. Even though every airplane manufacturer will try to keep the empty weight as low as possible for a given take-off weight, the real value of the empty weight is likely to be slightly higher than the calculated weight. Second, the method used in the preliminary sizing has, again according to Roskam (ref. [7] page 128), only an accuracy of ± 10% and last but not least, the mission profile used is only a rough approximation of reality. Splitting up the cruise phase into segments of a half-hour and adapting the values for the lift-to-drag ratio and for the specific fuel consumption would for instance normally increase the accuracy of the calculation. This is however not done here since this would cause a major increase in engineering man-hours for this validation.

I.2.7.1 THE TAKE-OFF GROSS WEIGHT

Since several versions of the baseline 777-200 exist (see ref. [11]), one version has to be selected to form a basis. For this work, the baseline airplane with a maximum design take-off weight of 535,000 lbs (242,630 kg) is taken as the basis for comparison. This was namely also the weight used as a start value for the weight iteration.

As can be seen from subsection I.2.6, the calculated take-off weight is 529,282 lb. This means that there is only a difference of 1.1 % between the calculated and the real take-off weight, which is remarkably accurate.

I.2.7.2 THE EMPTY WEIGHT

The only empty weight data given in de documents from ref. [11] is the specific operating empty weight. As can be seen in subsection I.2.1 the operating empty weight is the sum of the airplane empty weight, the crew weight and the weight of the trapped fuel and oil:

$$W_{OE} = W_E + W_{tfo} + W_{crew}.$$

With the data used in the previous paragraphs for the crew and the trapped fuel and oil weight and the calculated empty weight from subsection I.2.6, this leads to an operating empty weight of approximately 275.300 lbs (124.874 kg).

To be able to compare this calculated value with the real data for the 777-200, some averaging has to be done first. The given operating empty weight namely depends on the engines used. The following operating empty weights are given in ref. [11]:

Engine manufacturer	Operating empty weight (lbs)
General Electric	299,550
Pratt & Whitney	297,250
Rolls-Royce	294,050

Finally, these specific operating empty weights apply to a baseline configuration of 375 passengers. In our case, only 360 passangers are embarked on the plane so the specific operating empty weight will be slightly different[5]. Since this is the only data available, the average of these weights ($W_{OE,\ av}$) will nevertheless be used to compare the values:

$$W_{OE,\ av} = 296{,}950 \text{ lbs}$$

Comparing the calculated operating empty weight and the data from Boeing shows that there is a difference of 7.3% in operating empty weight. Keeping in mind that the mission was extremely simplified and that there's a margin of 10% on the weight data[6], this seems a very reasonable result for the rather low amount of work that was required.

I.2.7.3 THE MISSION FUEL WEIGHT

The weight of fuel required to perform the mission from paragraph I.1 is calculated as:

$$W_F = 176{,}535 \text{ lbs } (80{,}075 \text{ kg})$$

From that fuel, 160,486 lbs is used during the mission and the rest is reserve fuel.

There's little sense in comparing the mission fuel weight with the usable fuel data from ref. [11] since they only give the maximum amount of usable fuel. Therefore, we can only check whether our mission could be flown with a 777-200. This is the case when the required amount of mission fuel is smaller than the maximum amount of usable fuel. For a Boeing 777-200 in the selected baseline configuration this maximum amount of usable fuel equals 207,700 lbs. Since only 85 % of the maximum amount of fuel are needed for our mission, the mission can be flown.

I.2.7.4 THE PAYLOAD-RANGE DIAGRAM

Finally, a check is made whether the selected range can be flown with the specified payload according to the payload-range diagrams given by Boeing. This check though has to be executed with great caution since all the assumptions should be equal in order to be able to compare the data. Here, this is not the case. The payload-range diagram given by Boeing (see Figure 1.1) namely is for a Mach 0.84 step cruise[7]. The cruise phase of our mission on the other hand is flown at a constant altitude of 35,000 ft and at a Mach number of 0.83[8].

[5] e.g. due to the different number of seats,…
[6] due to the use of statistical data and due to the dispersion in the data
[7] Cruise Step means that the cruise height is changed as the weight of the plane changes to optimise the fuel consumption.
[8] This choice has been made because the preceding engine and rough sizing calculations of Part 2 have been executed under the same assumptions.

Nevertheless, our selected payload and range (the red dot on Figure 1.1) lies in the area of possible payload-range combinations, which gives an additional indication that the simulation is reasonable.

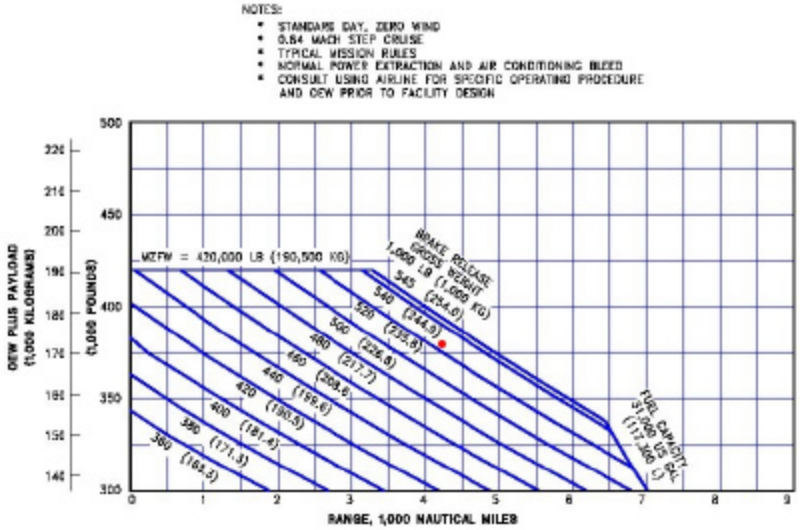

Figure 1.1 The payload range diagram of a typical baseline Boeing 777-200 (ref. [11])

I.2.8 SENSITIVITY CALCULATIONS

It is evident from the way that the results for this simulation are obtained, that their outcome depends on the values selected for the various parameters in the range and endurance equations. The calculated take-off weight will strongly depend on the values chosen for:

payload weight W_{PL},
empty weight W_E,
range R,
endurance E,
lift-to-drag ratio L/D and
thrust specific fuel consumption, c_j.

It is therefore mandatory to conduct sensitivity studies after preliminary design of an airplane. These sensitivity studies will allow finding out which parameters drive the design. They also provide quick estimates of the impact on the design of selecting an optimistic (pessimistic) value for the parameters mentioned above. Below only a very brief general introduction to the method will be given. More information and a complete derivation of all the necessary formulae can be found in ref. [6].

In this reference, it is shown that equations (1.1),(1.2) and (1.6) can be written as:

$$\log_{10} W_{TO} = A + B * \log_{10}(C * W_{TO} - D) \qquad (1.11)$$

with:

$$C = \left\{1 - \left(1 + M_{F,res}\right) * \left(1 - M_{ff}\right) - M_{tfo}\right\} \qquad (1.12)$$

$$D = W_{PL} + W_{crew} + W_{p,exp}{}^{9} \qquad (1.13) \text{ and}$$

A and B the regression coefficients from paragraph I.2.6

If the sensitivity of W_{TO} to some parameter y is desired, it is now possible to obtain that sensitivity by partial differentiation of W_{TO} in equation (1.11). As shown in ref. [6] this results in:

$$\frac{\partial W_{TO}}{\partial y} = \frac{B * W_{TO}^2 * \frac{\partial C}{\partial y} - B * W_{TO} * \frac{\partial D}{\partial y}}{C * (1 - B) * W_{TO} - D} \qquad (1.14).$$

The parameter y can be any one of those listed above. The sensitivity of the take-off weight to several parameters will now be calculated.

[9] $W_{p,exp}$ is the weight of the expended payload. For this mission this weight equals zero.

I.2.8.1 SENSITIVITY OF TAKE-OFF WEIGHT TO PAYLOAD WEIGHT

If the payload weight is taken as parameter y, it follows from (1.12) and (1.13) that:

$$\partial D / \partial W_{PL} = 1 \text{ and } \partial C / \partial W_{PL} = 0 .$$

Therefore, it follows from equation (1.13) that:

$$\frac{\partial W_{TO}}{\partial W_{PL}} = \frac{B * W_{TO}}{D - C * (1 - B) * W_{TO}} . \qquad (1.15).$$

The derivative $\partial W_{TO} / \partial W_{PL}$ is called the airplane growth factor due to payload. For our simulation this factor amounts to:

$$\frac{\partial W_{TO}}{\partial W_{PL}} = 5.91 .$$

This means that for each pound of payload added, the aircraft take-off weight will have to be increased by 5.91 lbs for the same mission performance.

I.2.8.2 SENSITIVITY OF TAKE-OFF WEIGHT TO EMPTY WEIGHT

The take-off weight to empty weight sensitivity follows from a partial derivation of W_{TO} to W_E of equation (1.9):

$$\frac{\partial W_{TO}}{\partial W_E} = \frac{B * W_{TO}}{\text{inv}\log_{10}\left(\frac{\log_{10} W_{TO} - A}{B}\right)} \qquad (1.16)$$

The growth factor due to empty weight can now be determined. For our mission it is:

$$\frac{\partial W_{TO}}{\partial W_E} = 2.03$$

For each pound of increase in empty weight, the take-off weight must thus be increased by 2.03 lbs, to keep the mission performance the same.

I.2.8.3 SENSITIVITY OF TAKE-OFF WEIGHT TO RANGE, ENDURANCE, SPEED, THRUST SPECIFIC FUEL CONSUMPTION AND LIFT-TO-DRAG RATIO

The sensitivity of the take-off weight to any parameter y, which is not payload[10], is found from eqn. (1.14) as:

$$\frac{\partial W_{TO}}{\partial y} = \frac{B * W_{TO}^2 * \frac{\partial C}{\partial y}}{C * (1 - B) * W_{TO} - D} \qquad (1.17)$$

where C is defined by (1.12), which can also be written as:

$$C = M_{ff} * (1 + M_{F,res}) - M_{tfo} - M_{F,res} \qquad (1.18)$$

Partial derivation of (1.18) with respect to y gives:

$$\frac{\partial C}{\partial y} = (1 + M_{F,res}) * \frac{\partial M_{ff}}{\partial y} .$$

The differential $\partial M_{ff} / \partial y$ can be found from equation (1.4) as:

$$\frac{\partial M_{ff}}{\partial y} = M_{ff} * \frac{W_i}{W_{i+1}} * \frac{\partial\left(W_{i+1} / W_i\right)}{\partial y} ,$$

where the ratio W_i / W_{i+1} can be determined from Breguet equations. These Breguet equations take on two different forms, depending on whether range or endurance is sought. They can be generalised

[10] With payload all three terms of the right term of equation (1.13) are considered here.

as $\overline{R} = \ln\left(\frac{W_i}{W_{i+1}}\right)$ or as $\overline{E} = \ln\left(\frac{W_i}{W_{i+1}}\right)$. The quantities $\overline{R}$ and $\overline{E}$ for jet airplanes[11] are in turn found from (1.8) and (1.7) respectively as:

$$\overline{R} = \frac{R * c_j}{V * L/D} \qquad (1.19)$$

$$\overline{E} = \frac{E * c_j}{L/D} \qquad (1.20)$$

In ref. [6], it is shown that the sensitivity of W_{TO} with respect to y now can be derived as:

$$\frac{\partial W_{TO}}{\partial y} = F * \frac{\partial \overline{R}}{\partial y}$$

for the case involving a ratio W_{i+1}/W_i dependent on range, and as:

$$\frac{\partial W_{TO}}{\partial y} = F * \frac{\partial \overline{E}}{\partial y}$$

for the case involving a ratio W_{i+1}/W_i dependent on endurance. The factor F in these equations is defined as:

$$F = \frac{-B * W_{TO}^2 * (1 + M_{F,res}) * M_{ff}}{C * W_{TO} * (1 - B) - D}$$

The so-called Breguet partials $\partial\overline{R}/\partial y$ and $\partial\overline{E}/\partial y$ can now easily be derived by partially differentiating equations (1.19) and (1.20) with respect to R, E, V, c_j or L/D. They are given in Table 1.1[12].

Tabel 1.1 The Breguet partials for a jet airplane

y	**$\partial\overline{R}/\partial y$**	**$\partial\overline{E}/\partial y$**
R	$\frac{c_j}{V * L/D}$	Not applicable
E	Not applicable	$\frac{c_j}{L/D}$
c_j	$\frac{R}{V * L/D}$	$\frac{E}{L/D}$
V	$\frac{-R * c_j}{V^2 * L/D}$	Not applicable
L/D	$\frac{-R * c_j}{V * (L/D)^2}$	$\frac{-E * c_j}{(L/D)^2}$

In this mission, only the climb and the cruise phases were considered as fuel intensive phases. Only for those two flight phases, the Breguet equations were used so the Breguet partials can only be determined for those two phases. The results of the calculations can be found in Table 1.2.

Tabel I.2 The results for the sensitivities

	$\partial W_{TO}/\partial c_j$ (lb-hr)	**$\partial W_{TO}/\partial R$** (lb/nm)	**$\partial W_{TO}/\partial (L/D)$** (lb)	**$\partial W_{TO}/\partial E$** (lb/hr)
Climb	77,986	- - -	-5,459	167,969
Cruise	1,417,335	167	-47,245	- - -

[11] For propeller driven airplanes the formulae can be derived analogously. This derivation and the resulting formulae can be found in ref. [6]
[12] with R in Nm and V in kts

The significance of these sensitivities is as follows. If the range in the mission specification of subsection I.1 is decreased from 4,240 nm to 4,140 nm, the take-off gross weight can be decreased by 100*167 = 16,700 lbs. With the cruise data given in subsection I.2.4.5, this decrease in range only leads to a decrease in fuel weight of approximately 3,000 lbs (1,392 kg). An additional 13,700 lbs can thus be saved in empty weight. Similarly, if for instance the lift-to-drag ratio of the airplane in cruise is increased by 1, the take-off weight will go down by 47,245 lbs.

From these sensitivity data, it is obvious that the take-off gross weight of a range-dominated airplane like the one under consideration is very sensitive to changes in lift-to-drag ratio and in thrust specific fuel consumption. Therefore, these parameters will have to be accurately estimated or determined in order to have a good approximation of the real take-off gross weight.

I.3 ESTIMATION OF WING AREA, TAKE-OFF THRUST AND MAXIMUM LIFT COEFFICIENT

In addition to meeting range, endurance and cruise speed objectives, airplanes are usually designed to meet performance objectives in the following categories:

- Stall speed
- Take-off field length
- Landing field length
- Cruise speed (sometimes maximum speed)
- Climb rate (AEO[13] and OEI[14])
- Time to climb to some altitude

These performance objectives are mainly impacted by the following airplane design parameters:

- Wing Area S,
- Take-off thrust T_{TO},
- Maximum required take-off lift coefficient with flaps up $C_{L,\,max}$ (clean),
- Maximum required lift coefficient for take-off $C_{L,\,max\,TO}$
- Maximum required lift coefficient for landing $C_{L,\,max\,L}$.

In this subsection, methods will be presented for a rapid estimation of these parameters. These methods will result in a determination of a range of values of wing loading, thrust loading and maximum lift coefficient, within which certain performance requirements are met. According to Roskam (ref. [6]), the combination of the highest possible wing loading and the lowest possible thrust loading which still meets all performance requirements results in an airplane with the lowest weight and the lowest cost. Since the take-off weight was already determined, it is clear that the wing area and the take-off thrust will now be determined.

The actual calculation of each requirement is done with AAA. Below, for each requirement, the method used by AAA and described in Roskam 's books is briefly described first. The input data for the appropriate AAA performance sizing module is given and the calculated requirement is shown graphically. After this, all sizing requirements are matched and the matching plot is given.

I.3.1 SIZING TO STALL SPEED REQUIREMENTS

For some airplanes the mission task demands a stall speed not higher than some minimum value. In such a case, the mission specification will include a requirement for a minimum stall speed. FAR 23 certified single engine airplanes for instance may not have a stall speed greater than 61 kts at W_{TO}. For FAR 25 certified airplanes on the other hand, there is no stall speed requirement. Nevertheless, this sizing method will here be applied to the Boeing 777 to illustrate the method used.

The power-off stall speed of an airplane may be determined from:

$$V_S = \sqrt{\frac{2 * W/S}{\rho * C_{L,max}}} \qquad (1.21)$$

By specifying a maximum allowable stall speed at some altitude, equation (1.21) defines the maximum allowable wing loading W/S at a certain flight condition for a given value of $C_{L,\,max}$[15]. The corresponding maximum allowable wing loading at take-off to meet the stall speed requirement can then be computed from equation (1.22).

$$\left(\frac{W}{S}\right)_{TO} = \frac{W_{TO}}{W_S}\left(\frac{W}{S}\right)_S \qquad (1.22)$$

[13] All Engines Operative
[14] One Engine Inoperative
[15] the $C_{L,\,max}$ of equation (1.21) is the trimmed $C_{L,max}$ of the airplane. Trimmed means here that every moment around the centre of gravity of the airplane is zero.

In AAA, the following values are entered for the stall speed sizing in the Class I performance sizing module:

h_S = 39,000 ft	W_S = 475,000 lb	$C_{L,\,max,\,S}$ = 1.2
V_S = 311.34 kts	W_{TO} = 529,282 lb	

Where h_S, V_S, W_S and $C_{L,\,max,\,S}$ are the altitude, the speed, the weight and the lift coefficient at which the stall speed are evaluated. W_{TO} is the take-off gross weight.

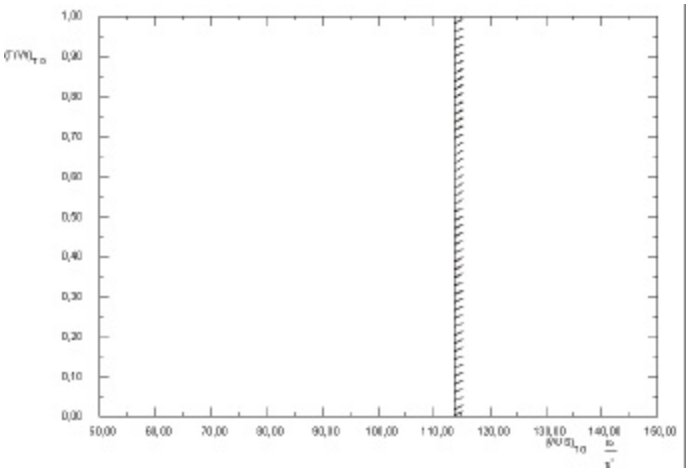

Figure 1.2 The results of the stall speed sizing submodule of AAA

The values given above are the values as entered in the original AAA example file. Even though our simulation has been changed here and there, the values here are kept. The sizing module for this airplane is namely only calculated as an example since there are no requirements for maximum stall speed in the case of FAR 25 certified aircraft.

The result of the stall speed sizing from AAA is the vertical line on Figure 1.2. This line limits the maximum wing loading that is possible for the aircraft. The stall speed requirement is namely only met for a wing loading, which is less than or equal to the value represented by the vertical line. For our Boeing 777, the maximum wing loading that is in agreement with the stall speed requirement is 114 lb/ft² (approximately 5,460 N/m²).

Comparing this number with the actual wing loading of the Boeing 777 (110 lb/ft² or approximately 5,270 N/m²) shows that this could be a reasonable stall speed sizing of the Boeing 777 (keeping in mind that FAR 25 certified airplanes are not required to have stall speed limits).

I.3.2 SIZING TO TAKE-OFF DISTANCE REQUIREMENTS

Take-off distances of airplanes are determined by the following factors:

- Take-off weight W_{TO},
- Take-off speed V_{TO} (also called lift-off speed or rotating speed),
- Thrust-to-weight ratio at take-off $(T/W)_{TO}$,
- Aerodynamic drag coefficient on the ground C_{D_G} and ground friction coefficient μ_G,
- Pilot technique

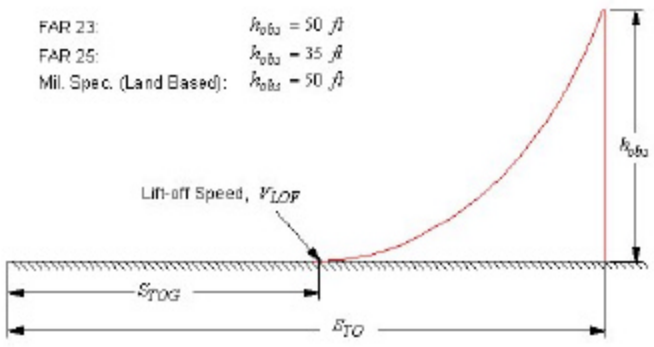

Figure 1.3 Definition of FAR 25 take-off distances (ref. [2])

Take-off distance requirements are normally given by in terms of take-off field length requirements. These requirements differ widely and depend on the type of airplane under consideration. Since the Boeing 777 is a FAR 25 certified airplane, those requirements must be adhered to. Only those take-off distance requirements will be discussed here. FAR 23 and military take-off distance requirements can be found in reference [6]. Figure 1.3 defines those quantities important to FAR 25 take-off field length requirements.

In reference [6], it is shown that the take-off field length S_{TO} can be written as equation (1.23)

$$S_{TO} = \frac{37.5 * \left(W/S\right)_{TO}}{\sigma * C_{L,max\,TO} * \left(T/W\right)_{TO}} \qquad (1.23)$$

where:

$\left(W/S\right)_{TO}$ is the airplane wing-loading at take-off,
σ is the density ratio of the air at take-off conditions to air at sea-level and ISA conditions,
$C_{L,max\,TO}$ is the airplane maximum lift coefficient at take-off,
$\left(T/W\right)_{TO}$ is the airplane thrust-to-weight ratio at take-off.

In AAA, this correlation is slightly altered to correct the thrust of the engines for humidity, temperature and altitude. This correlation is given in (1.24):

$$\left(T/W\right)_{TO} = \frac{\left(W/S\right)_{TO}}{0.0267 * \sigma * C_{L,max\,TO} * S_{TO} * F_{TO}} \qquad (1.24)$$

where F_{TO} is the ratio of take-off thrust at take-off conditions to that at take-off sea level ISA to correct for humidity, temperature and altitude.

The values entered for the Boeing 777 are as follows:

h_{TO} = 0 ft	?T = 0.0°R	$C_{L,\,max,\,TO}$ = 2.0
F_{TO} = 1.000	S_{TO} = 7,600 ft	Plot ?$C_{L\,max}$ = 0.4

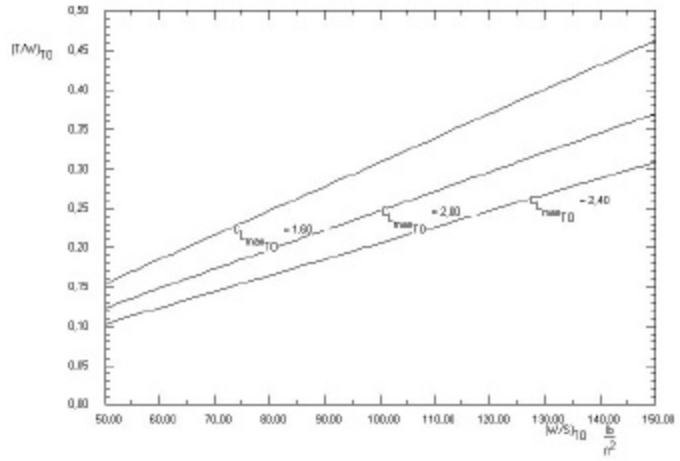

Figure 1.4 The results for the take-off distance sizing submodule

Where Plot ?$C_{L\,max}$ indicates the variation in the maximum lift coefficient which has to be used to construct the matching plot (see subsection I.3.7). Calculations are made for $C_{L,\,max}$ - Plot ?$C_{L\,max}$, for $C_{L,max}$ and for $C_{L\,max}$ + Plot ?$C_{L\,max}$.

Figure 1.4 shows the results calculated by AAA for the take-off distance sizing of the Boeing 777-200 under consideration. To meet the performance requirements represented by the line, the thrust-to-weight ratio must be greater than or equal to (above or on) the value represented by the matching plot line for a given wing loading.

I.3.3 SIZING TO LANDING DISTANCE REQUIREMENTS

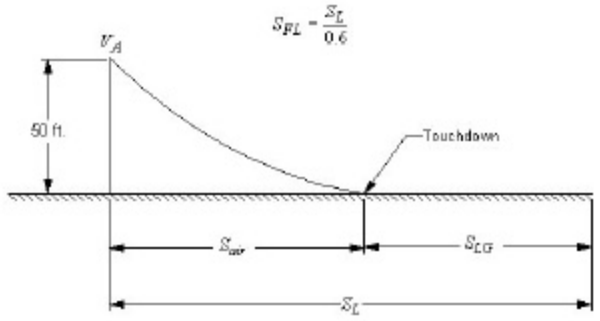

Figure 1.5 Definition of the FAR 25 landing distances

Landing distances of airplanes are determined by five factors:

- landing weight W_L,
- approach speed V_A,
- deceleration method used,
- flying qualities of the airplane
- pilot technique.

Figure 1.5 defines the quantities, which are important in the FAR 25 field length requirements. The figure defines the total landing distance, S_L, as the sum of the

landing distance on the ground, S_{LG}, and S_{air}, the ground distance needed to descent the airplane from a screen height of 50 ft to the actual touchdown on the runway. The according FAR landing field length, S_{FL} is defined as the total landing distance divided by 0.6.

$$S_{FL} = S_L / 0.6 \qquad (1.25)$$

This factor of safety is included to account for variations in pilot technique and other factors beyond the control of FAA.

In reference [6], Roskam relates the field length for FAR 25 landing distance requirements to V_A^2 as in equation (1.26).

$$s_{FL} = 0.3 * V_A^2 \qquad (1.26)$$

where s_{FL} is in ft and V_A is in kts ($V_A = 1.3*V_{S,L}$).
With the help of equation (1.21) and a requirement for a maximum acceptable landing field length it is again possible to relate $(W/S)_L$ (and thus $(W/S)_{TO}$) to C_{L,max_L}.

In AAA, the following equation is used to determine the wing loading to meet landing distance requirements:

$$\left(\frac{W}{S}\right)_L = \frac{\rho_{(at\ h_L,\ ISA)}}{2} * C_{L,max_L} * S_L * F_1 * \frac{W_{TO}}{W_L} \qquad (1.27)$$

where:

$\rho_{(at\ h_L,\ ISA)}$ is the density of the air at the landing altitude, ISA conditions,
C_{L,max_L} is the design airplane maximum lift coefficient in the landing condition,
S_L is the landing distance,
F_1 is the factor correction for type of certification,
W_{TO} is the take-off weight,
W_L is the landing weight.

For a FAR 25 certified airplane, F_1 equals 5.63.

The values for these parameters, which are used for the landing distance calculations for the simulation of the Boeing 777 can be found in Table 1.3

Table 1.3 The values entered for the landing distance calculations in the performance-sizing module

h_L = 0 ft	W_L = 372,000 lbs	$C_{L,\ max,\ L}$ = 2.4	S_L = 3,710 ft
?T = 0.0°R	W_{TO} = 529,281.8 lbs	Plot ?$C_{L\ max}$ = 0.4	

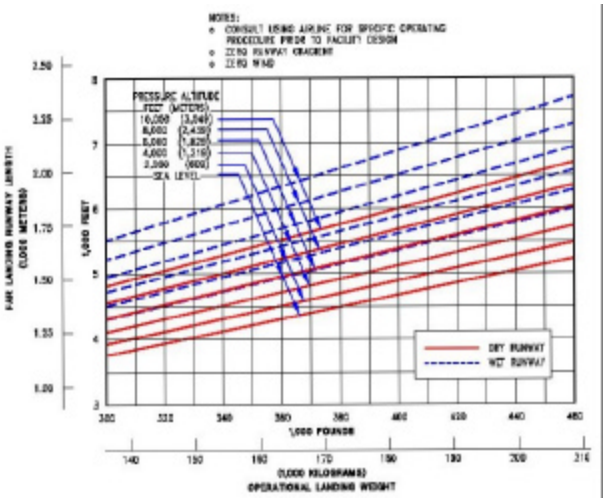

Figure 1.6 FAR landing runway lengths for a Boeing 777 (ref.[11])

All the values from the table are taken from the example file included with AAA, except the value for the landing distance since this field was left blank in the example file. This value has been determined as follows. First of all, the distance on the ground S_{LG} (see Figure 1.5) is determined through Figure 1.6. With the landing weight and height from Table 1.3, this figure gives a FAR landing runway length of approximately 4,350 ft. This equals a distance S_{LG} of 2,610 ft[16]. Now, the distance S_{air} (see Figure 1.5) still has to be determined. With a flight path angle of 3° and an approach speed of 140 kts (ref. [12]) this distance is now determined according to the method given in reference [3] as approximately 1,100 ft. This results in a landing distance of 3,710 ft and thus according to equation 1.25 a landing field length of 6,183 ft.

[16] The FAR landing runway length (S_{FLG}) in the ordinate of Figure 1.6 is related here to the landing distance on the ground (S_{LG} of Figure 1.5) as $S_{FLG}/0.6$.

With the values from Table 1.3, equation (1.26) is solved in AAA. This leads to Figure 1.7.

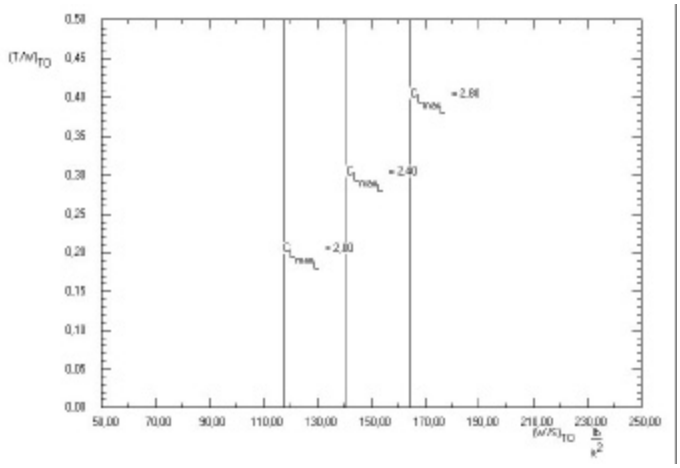

Figure 1.7 The results for the landing distance sizing submodule

I.3.4 SIZING TO CLIMB REQUIREMENTS

All airplanes must meet certain climb rate or climb gradient requirements. To size an airplane for climb requirements, it is though necessary to have an estimate for the airplane drag polar. These drag polars are determined in paragraph I.4. This is however an iterative process. The drag polar of the airplane namely also depends on the wing area, which depends on its turn on the wing loading and the take-off gross weight. Since the wing loading and thus the wing area are determined here (paragraph I.3), the drag polar cannot be calculated yet. Some arbitrary area thus has to be chosen to initiate the iteration. Since the real wing area of the Boeing 777 is known, this iteration can however be avoided here.

Since the Boeing 777 is a FAR 25 certified airplane, the climb requirements of these regulations must also be satisfied. The FAR 25 stipulates both take-off climb requirements (FAR 25.111 and FAR 25.121) as well as landing climb requirements (FAR 25.119 and FAR 25.121). All these requirements are for the airplane with OEI[17]. AEO[18] requirements are omitted. The reason is that the OEI requirements are so severe, that climb with AEO is not a problem in FAR 25 airplanes. The FAR 25 climb requirements will not be repeated here. They can be found in reference [13]. A summary is also given in reference [6].

Input Parameters

$F_{fltexcont}$	0,800	W_{TO}	529281,8 lb	$C_{D_{D_{TO\_up}}}$	0,0283	$CGR_{25.121_T}$	0,000
F_{Bzec}	0,900	W_L	372000,0 lb	$C_{D_{D_{TO\_down}}}$	0,0483	$CGR_{25.121_{SS}}$	0,024
$C_{L_{max_{clean}}}$	1,200	AR_w	8,27	e_L	0,7500	$CGR_{25.121_{BR}}$	0,012
$C_{L_{max_{TO}}}$	2,000	e_{clean}	0,8500	$C_{D_{D_{L\_down}}}$	0,0883	$CGR_{25.121_L}$	0,021
$C_{L_{max_A}}$	2,200	$C_{D_{D_{clean,M}}}$	0,0138	$\Delta C_{D_{o_A}}$	0,0000	$CGR_{25.119}$	0,032
$C_{L_{max_L}}$	2,400	e_{TO}	0,8000	$CGR_{25.111}$	0,012		

Output Parameters

$B_{DP_{clean}}$	0,0453	$B_{DP_{TO\_up}}$	0,0481	$B_{DP_{TO\_down}}$	0,0481	$B_{DP_{L\_down}}$	0,0513

Figure 1.8 The input for the calculation of the climb requirements

[17] One Engine Inoperative
[18] All Engines Operative

Even though the FAR 25 climb requirements are pre-programmed in AAA, several variables still have to be determined before the program can calculate the results. These input variables and the values used for this simulation as well as the output from the calculations are given in Figure 1.8. The choice of the values for the parameters is only illuminated if necessary. Several values namely stem from previous calculations or from the drag polars of subsection I.4. The abbreviations in this figure have the following meaning:

- $F_{MaxCont}$ is the ratio of the Maximum Continuous Thrust to that at take-off at sea-level ISA conditions. A value of 0.8 was used in the AAA example file and is retained here.
- $F_{8,sec}$ is the ratio of the thrust after 8 seconds to that at take-off at sea-level ISA conditions. With the thrust after 8 seconds, the thrust level corresponding to that obtained 8 seconds after moving the throttles from minimum flight idle to take-off position is meant. Again, the value of 0.9 is taken from the example file.
- $C_{L,\,max\,clean}$ is the airplane maximum lift coefficient without flap effects.
- $C_{L,\,max\,TO}$ is the airplane maximum lift coefficient at take-off.
- $C_{L,\,max\,A}$ is the airplane maximum lift coefficient at approach. This is usually assumed halfway between take-off and landing flaps.
- $C_{L,\,max\,L}$ is the airplane maximum lift coefficient at landing.
- W_{TO} is the airplane take-off weight.
- W_L is the airplane landing weight.
- AR_W is the aspect ratio of the wing. The value from the example file is kept.
- e_{clean} is the Oswald efficiency factor in the clean configuration.
- $C_{D0,\,clean,M}$ is the airplane zero lift drag coefficient corrected for Mach effects with gears and flaps retracted.
- e_{TO} is the Oswald efficiency factor in the take-off configuration.
- $C_{D0,\,TO\text{-}up}$ is the airplane zero lift drag coefficient at take-off with the landing gear up.
- $C_{D0,\,TO\text{-}down}$ is the airplane zero lift drag coefficient at take-off with the landing gear down.
- e_L is the Oswald efficiency factor in the landing configuration.
- $C_{D0,\,L\text{-}down}$ is the airplane zero lift drag coefficient at landing with the landing gear down.
- ?$C_{D0,\,A}$ is the change in airplane zero lift drag coefficient due to flaps in the approach position
- $CGR_{25.111}$ is the FAR 25.111 climb gradient. The value taken here is the value suggested in the help file for a twin engine airplane.
- $CGR_{25.121\,T}$ is the FAR 25.121 transition segment climb gradient.
- $CGR_{25.121\,S}$ is the FAR 25.121 second segment climb gradient.
- $CGR_{25.121\,ER}$ is the FAR 25.121 en-route segment climb gradient.
- $CGR_{25.121\,L}$ is the FAR 25.121 climb gradient at landing conditions.
- $CGR_{25.119}$ is the FAR 25.119 climb gradient at landing conditions.
- $B_{DP\,clean}$ is the B of the drag polar in the clean configuration. The drag polar is written as: $C_D = C_{D_0} + B_{DP} * C_L^2$
- $B_{DP\,TO\text{-}up}$ is the B of the drag polar in the take-off configuration with gear up.
- $B_{DP\,TO\text{-}down}$ is the B of the drag polar in the take-off configuration with gear down.
- $B_{DP\,L\text{-}down}$ is the B of the drag polar in the landing configuration with gear down.

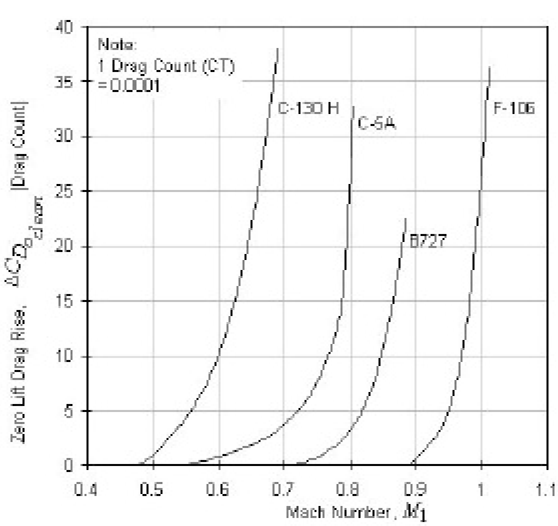

Figure 1.9 Drag rise estimate for typical aircraft (ref. [2])

A small remark concerning the parameter $C_{D0\,clean,M}$ is now in order. This is the airplane zero lift drag coefficient corrected for Mach effects. Due to compressibility effects (in theory above the drift-divergence Mach number), a modification of C_{D_0} is namely necessary. This ΔC_{D_0} can easily be found from Figure 1.9 (ref. [6] or [2]) for some typical aircraft. In paragraph I.4 this is shown.

The output for the climb requirements submodule is again, as in the previous paragraphs, given in a graphical way. Figure 1.10 shows the results when the values of Figure 1.8 are used.

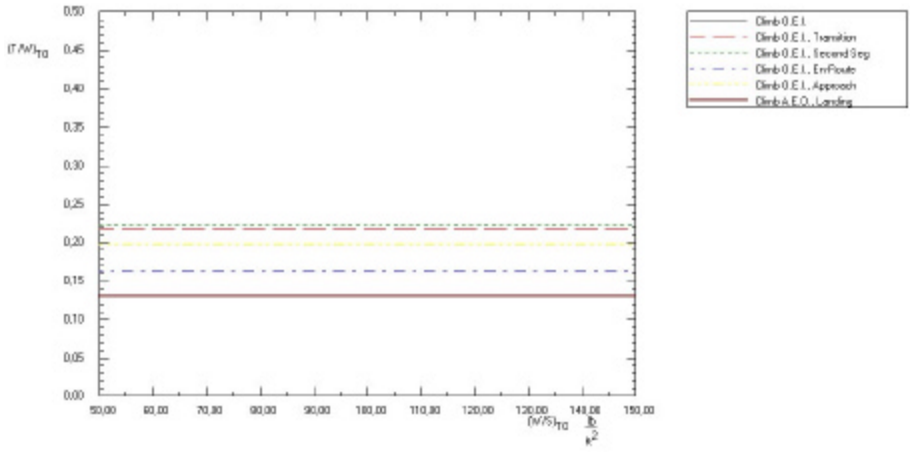

Figure 1.10 The results for the climb requirements submodule

I.3.5 SIZING TO MANOEUVRING REQUIREMENTS

Specific requirements for sustained manoeuvring capability (including specific turn rate) are often contained in the mission specification for utility, agricultural, aerobatic or for military airplanes. Sustained manoeuvring requirements are usually formulated in terms of a combination of sustained load factor (g's) to be pulled at some combination of speed and altitude. Even though FAR 25 certified airplanes normally do not have this type of requirement, the method used in AAA will be explained with the Boeing 777 as an example because this requirement can be of some importance for the design of the mothership.

The sustained manoeuvring capability of an airplane depends strongly on its maximum lift coefficient and on its installed thrust. For equilibrium perpendicular to the flight path, it is namely necessary that:

$$n * W = C_L * \bar{q} * S .$$

The maximum load factor capability of an airplane, n_{max} can then be found from equation (1.28).

$$n_{max} = \frac{\bar{q} * C_{L_{max}}}{W/S} \qquad (1.28)$$

This load factor can be sustained as long as there is sufficient thrust:

$$T = C_{D_0} * \bar{q} * S + \frac{C_L^2}{\pi * A * e} * \bar{q} * S \qquad (1.29)$$

Dividing equation (1.28) by the manoeuvring weight W_M and rearranging then gives the manoeuvring requirement (1.29):

$$\frac{T}{W_M} = \frac{C_{D_0} * \bar{q}}{W_M/S} + \frac{W_M/S * n_{max}^2}{\pi * A * e * \bar{q}} \qquad (1.30)$$

If some maximum load factor is desired on a sustained basis at a given combination of Mach number and altitude, then equation (1.30) can be used to find the relation between T/W and W/S, for a given value of $C_{D,0}$.

In AAA, equation (1.30) is slightly rearranged to give the thrust-to-weight ratio at take-off as a function of the wing loading at take-off. An additional factor F_M is also included to be able to calculate the available thrust at the manoeuvring point[19]. The equation then becomes:

$$\left(\frac{T}{W}\right)_{TO} = \frac{C_{D0\,clean,M} * \bar{q}}{F_M * \left(W/S\right)_{TO}} + \left(\frac{W}{S}\right)_{TO} * \left(\frac{n * W_M}{W_{TO}}\right)^2 * \frac{B_{DP_{clean}}}{F_M * \bar{q}} \qquad (1.31)$$

[19] Since only the take-off thrust needs to be entered, the factor F_M, which is the ratio of the manoeuvre thrust to take-off thrust, is necessary to be able to calculate the manoeuvre thrust.

To size the Boeing 777 for manoeuvring requirements, the values from the original example are kept, except for the manoeuvring height (h_M) and the manoeuvring speed (V_M). These are, again, set to the previously used values. The input then becomes:

h_M = 35,000 ft	W_{TO} = 529,281.8 lbs	AR_W = 8.27
V_M = 478.56 kts	W_M = 475,000 lbs	$C_{D0,\ clean,\ M}$ = 0.0139
n = 0.93 g	F_M = 0.18	e_{clean} = 0.85

With these input values, the sizing plot can be made from equation (1.31). The result is given in Figure 1.11.

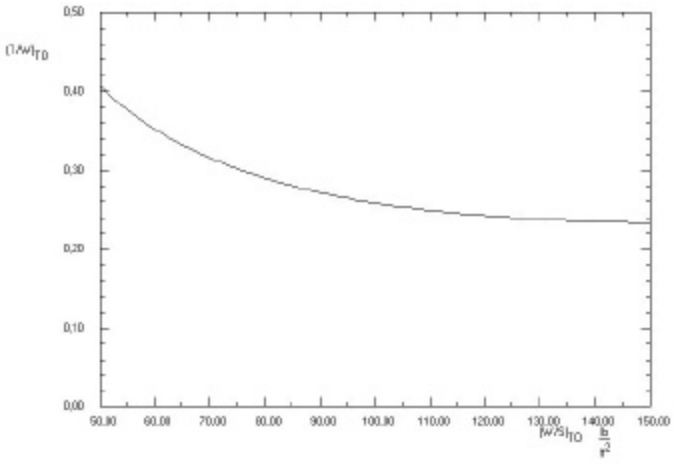

Figure 1.11 The results for the manoeuvring sizing

I.3.6 SIZING TO CRUISE SPEED REQUIREMENTS

At maximum level speed the following equations are simultaneously satisfied:

$$T_{reqd} = C_D * \bar{q} * S \qquad (1.32)$$

$$W = C_L * \bar{q} * S \qquad (1.33)$$

If a parabolic drag polar is assumed (cfr. paragraph I.4), equation (1.32) can be written as:

$$T_{reqd} = C_{D_0} * \bar{q} * S + \frac{C_L^2 * \bar{q} * S}{\pi * A * e}$$

Dividing this equation by the weight gives us equation (1.34):

$$\left(\frac{T}{W}\right)_{reqd} = \frac{C_{D_0} * \bar{q}}{W/S} + \frac{W/S}{\bar{q} * \pi * A * e} \qquad (1.34)$$

If the maximum speed is specified at some combination of Mach number and altitude, then the dynamic pressure $\bar{q}$ is known. For a given value of zero lift drag coefficient $C_{D,0}$, it is possible to use equation (1.34) to construct relations between T/W and W/S which satisfy the maximum speed requirements.

The maximum speed tends to be specified at a value of weight below the take-off weight. That is at:

$$W = k * W_{TO} \text{ with } 0 < k < 1$$

The required wing loading must therefore be obtained from equation (1.35):

$$\left(\frac{W}{S}\right)_{TO} = \frac{\left(W/S\right)_{eqn(1.33)}}{k} \qquad (1.35)$$

Similarly, the required thrust-to-weight ratio at take-off must also be reconstructed from the thrust-to-weight ratio found from equation (1.33). To do this requires knowledge of how the installed thrust of the airplane varies with Mach number and with altitude. Both these adaptations are done in AAA. The resulting formula then is:

$$\left(\frac{T}{W}\right)_{TO} = \frac{C_{D0\,clean,M} * \bar{q}}{F_{Cr} * \left(W/S\right)_{TO}} + \left(\frac{W_{Cr}}{W_{TO}}\right)^2 * \frac{B_{DP\,clean}}{\bar{q} * F_{Cr}} \left(\frac{W}{S}\right)_{TO}$$

with:

F_{Cr} the ratio of cruise thrust to take-off thrust
W_{Cr} is the cruise weight

To allow AAA to calculate the max cruise speed requirement, the following parameters have to be specified. The values given here are the values used in the Boeing 777 simulation:

h = 35,000 ft	W_{TO} = 529,281.8 lbs	$V_{Cr,\,max}$ = 501.62 kts	$C_{D0,\,clean,M}$ = 0.0139
F_{Cr} = 0.18	W_{Cr} = 475,000 lbs	AR_W = 8.27	e_{clean} = 0.85

The values chosen for W_{Cr} and F_{Cr} are the ones given in the example file. The max cruise speed has been taken as Mach 0.87 at 35,000 ft. The results for this sizing are given in Figure 1.12.

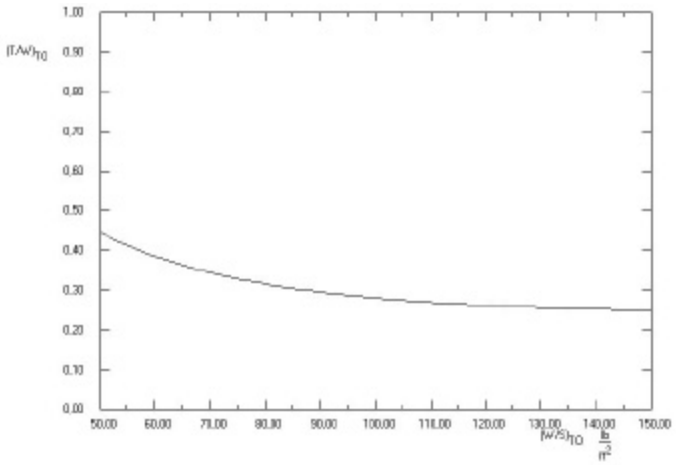

Figure 1.12 The results for the maximum cruise speed sizing

I.3.7 MATCHING OF ALL SIZING REQUIREMENTS

Having established a series of relationships between:
Take-off thrust-to-weight ratio,
Take-off wing loading,
Maximum required lift coefficients and
Aspect Ratio
It is now possible to determine the 'best' combination of these quantities for the design at hand. What is usually done at this point is to overlay all requirements and select the lowest possible thrust-to-weight ratio and the highest possible wing loading which are consistent with all requirements. This process is known as the matching process.

In AAA, this matching process is easily done by selecting the matching plot button in the performance sizing module. For the Boeing 777-200 as simulated here, the matching plot is given in Figure 1.13.
As can be seen from that figure, the wing loading has to be smaller than 114 lb/ft² due to the stall speed sizing requirement. For the remaining possible wing loadings, the thrust-to-weight ratio is determined almost entirely through the maximum cruise speed sizing requirement. The real values for the Boeing 777-200 are given in AAA (ref. [2]) as:

$$\frac{W}{S} = 110\,\frac{lb}{ft^2}$$

$$\frac{T}{W} = 0.281$$

This point is marked with a red dot on Figure 1.13. As can be seen, the wing loading is almost as high as possible (110 lb/ft² while the maximum is 114 lb/ft²) and the thrust-to-weight ratio is practically as low as possible (0.281 while the minimum is 0.272).

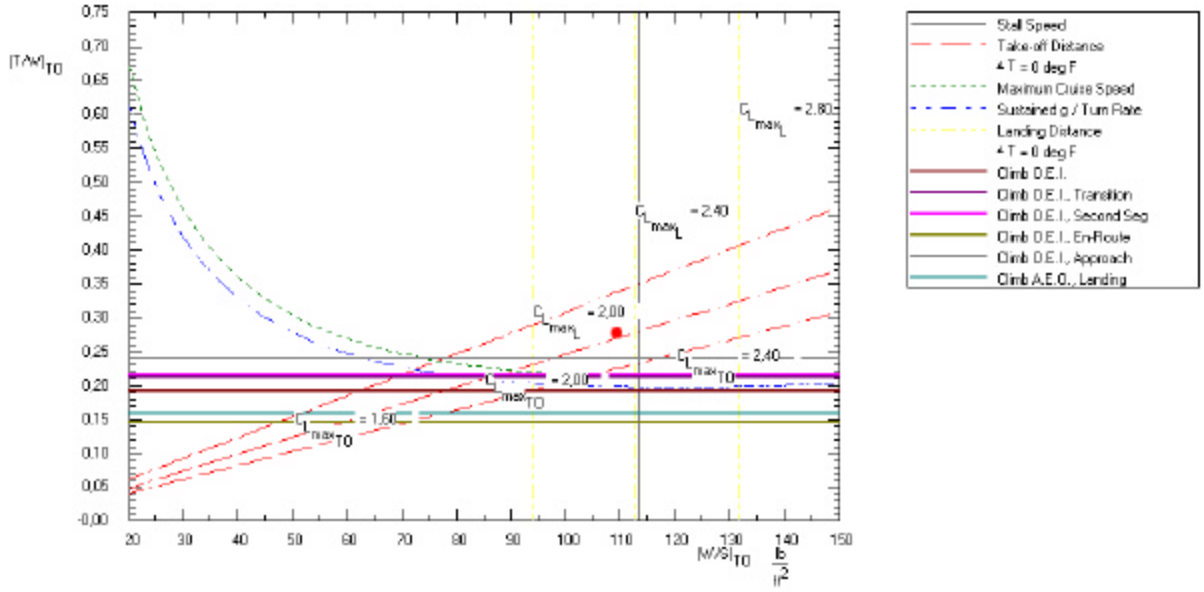

Figure 1.13 The matching plot for the Boeing 777-200 simulation

I.4 ESTIMATION OF THE DRAG POLARS

I.4.1 INTRODUCTION

For many conventional aircraft it has been found possible to represent the relationship between drag and lift coefficients for low subsonic flight conditions by the following parabolic relation:

$$C_D = C_{D_O} + \frac{C_L^2}{\pi * A * e} \qquad (1.36)$$

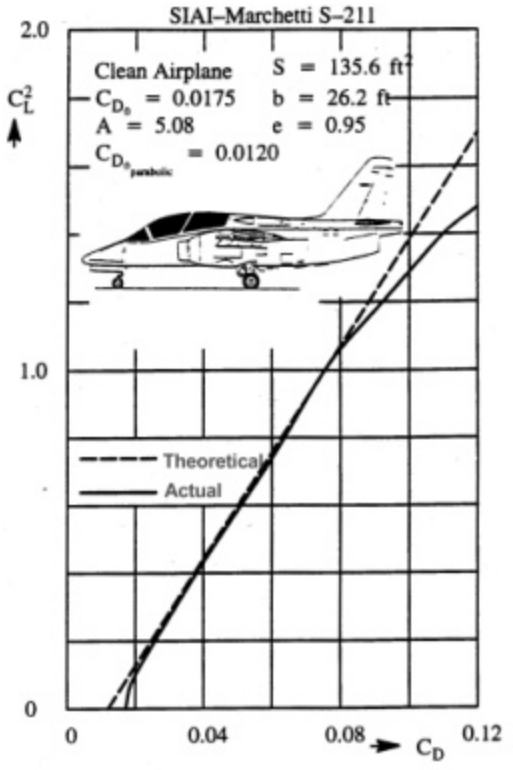

Figure 1.14 Comparison of the actual drag polar with the parabolic approximation for the S-211 (ref. [4])

If the drag coefficient, C_D, is plotted versus the square of the lift coefficient, C_L^2, a straight line should be the result. However, in reality a difference occurs. Figure 1.14 presents a comparison of actual and theoretical values of C_D plotted against C_L^2 for the SIAI-Marchetti S-211. From that figure, it is clear that the parabolic form of the drag polar is reasonable only for a limited range of lift coefficients. One reason for this is that at higher values of the lift coefficient the flow will usually begin to separate from an airplane.

For highly cambered airfoils, a better representation for the drag polar is, according to reference [4], given by equation (1.37):

$$C_D = C_{D_{min}} + \frac{\left(C_L - C_{L_{min\ drag}}\right)^2}{\pi * A * e} \qquad (1.37)$$

where:

$C_{D,\,min}$ is the minimum drag coefficient

$C_{L,\,min\ drag}$ is the lift coefficient corresponding with the minimum drag coefficient.

Finally, at high subsonic speeds, whenever shock waves occur and/or whenever shock induced boundary layer separation occurs, the drag rises much more rapidly with lift coefficient than indicated by either of the parabolic approximations given by equations (1.36) and (1.37).

Despite of all these approximations, Roskam indicates in reference [6] that the drag polars obtained by the method explained below, will give a good first estimate for preliminary sizing purposes. AAA also uses this method for the determination of the drag polars. Since the program only uses these drag polars to calculate the climb requirements, the low subsonic conditions will be fulfilled even for an airplane with a high cruise Mach number. The results for the clean airplane drag polar however have to be taken with a grain of salt for airplanes with a high cruise Mach number as can be seen from the deviations between the theoretical and actual drag polars of Figure 1.14.

As a final remark, it should be noted here that all drag polars given below use the clean airplane wing area as the reference area. This is done in order to be able to compare the drag polars for the different flap settings with each other.

I.4.2 GENERAL OUTLINE OF THE METHOD

Assuming a parabolic drag polar, the drag coefficient of an airplane is written in AAA as:

$$C_D = C_{D_{O_{clean}}} + \Delta C_{D_0} + \frac{C_L^2}{\pi * A * e}.$$

The zero-lift drag coefficient of this parabolic drag polar, C_{D_O} can be expressed as:

$$C_{D_O} = \frac{f}{S}$$

where f is the so-called equivalent parasite area and S is the wing area. According to Roskam (ref. [6]), it is possible to relate equivalent parasite area, f to wetted area S_{wet} for clean airplanes. This is shown in Figure 1.15.

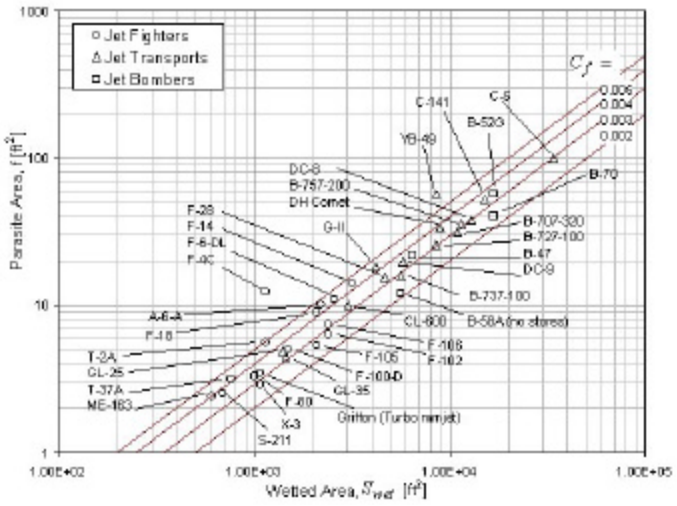

Figure 1.15 Parasite area vs. wetted area for jet fighters, jet bombers and jet transports (ref. [6])

It is now possible to represent Figure 1.15 with the following empirically obtained equation:

$$\log_{10} f = a + b * \log_{10} S_{wet} \qquad (1.38)$$

As can be seen from Figure 1.15, the correlation coefficients a and b are themselves a function of the equivalent skin friction coefficient of the airplane, C_f. The latter is determined by the smoothness and streamlining designed into the airplane. The manufacturing techniques and the paint used also are of major importance for the skin friction coefficient. Figure 1.15 allows us to quickly estimate a realistic value for C_f.

It is evident, that this method for estimating drag now boils down to the ability to predict a realistic value for S_{wet}. In reference [6], Roskam graphically shows that the wetted area correlates well to the take-off weight. Based on these figures the following relationship is derived:

$$\log_{10} S_{wet} = c + d * \log_{10} W_{TO} \qquad (1.39)$$

The constants c and d in equation (1.39) are the regression line coefficients, which are derived from the figures of reference [6]. Values for c and d are obtained by correlating wetted area and take-off weight data for more than 200 airplanes, divided into 12 categories. Due to the difference in wing loading, cabin size and nacelle design there however is some scatter on this data. According to Roskam, most airplanes however fall into the 10 percent band. This seems a reasonable accuracy due to the simplicity and the low amount of man-hours required.

Since an estimate for W_{TO} was already obtained in paragraph I.1, the drag polar for the clean airplane can now be determined. For take-off and landing, the effect of the flaps and of the landing gear need to be accounted for. The additional zero-lift drag coefficients due to flaps and due to landing gear are strongly dependent on the size and type of these items.

I.4.3 THE DRAG POLAR FOR THE CLEAN AIRPLANE

Now that the method used is explained, the drag polar for the clean airplane can be determined. In AAA this is simply done by entering values for the following parameters:

W_{TO} = 529,281.8 lbs	d = 0.7531	S_W = 4,833.31 ft²	$C_{Lplot,\,min}$ = 0
AR_W = 8.27	a = -2.5229	E_{clean} = 0.8500	$C_{Lplot,\,max}$ = 2
c = 0.0199	b = 1.000	$?C_{D0,\,clean}$ = 0.0005	

Where:

c is the regression coefficient to estimate wetted area from take-off weight (equation (1.39))
d is the regression coefficient to estimate wetted area from take-off weight (equation (1.39))
a is the regression coefficient to estimate parasite area from wetted area (equation (1.38))
b is the regression coefficient to estimate parasite area from wetted area (equation (1.38))
S_w is the wing area
$?C_{D0,\,clean}$ is the increment of zero-lift drag coefficient due to compressibility (cf. Figure 1.9)
$C_{Lplot,\,min}$ is the minimum lift coefficient for plotting the drag polar
$C_{Lplot,\,max}$ is the maximum lift coefficient for plotting the drag polar

The values given here for this parameter are the values used for the simulation of the Boeing 777-200. To determine the regression coefficients a and b, Figure 1.15 is used. As can be seen from that figure, a value of the skin friction coefficient has to be determined first. Here, a value of 0.003 is assumed for C_f. Figure 1.15 shows that that is a reasonable value for the chosen airplane. Once this value is chosen, a and b can be read from the help file of AAA (ref. [2]). The value for $?C_{D0,\,clean}$ can be determined through Figure 1.9. As can be seen from that figure, the zero lift drag rise due to compressibility effects for a Boeing 727 flying at Mach 0.83 is approximately 6 drag counts. Since the 777 is built using far more advanced technologies this drag rise is lowered to 5 counts for this simulation.

With these values entered as input, AAA can now determine the parabolic drag polar of the clean airplane. The program gives a mathematical expression and a plot of the drag polar as well as values for the following parameters. The values mentioned below are the values given as output by AAA with the input given just above:

S_{wet} =21,399.75 ft²	$C_{D0,\,clean}$ = 0.0133	$B_{DP,\,clean}$ = 0.0453
f = 64.20 ft²	$C_{D0,\,clean,\,M}$ = 0.0138	

The drag polar is: $C_D = 0.0138 + 0.0453 * C_L^2$. The plot of the drag polar of the clean Boeing 777 at Mach 0.83 can be found in Figure 1.16.

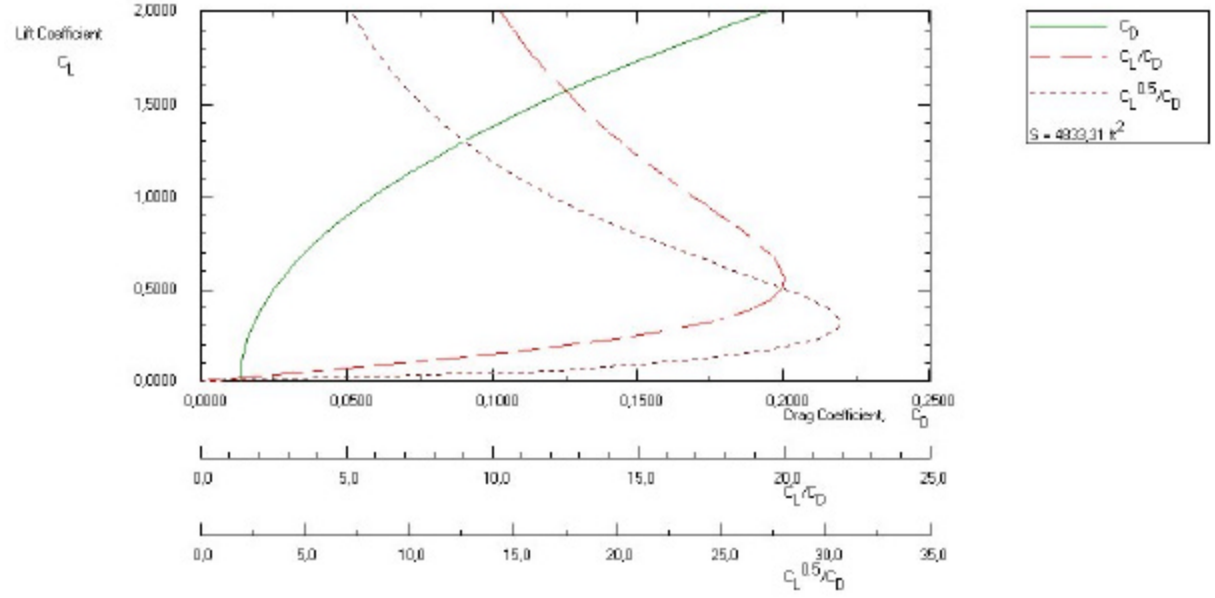

Figure 1.16 The drag polar of the clean airplane

I.4.4 THE DRAG POLAR FOR THE AIRPLANE IN THE TAKE-OFF CONFIGURATION WITH THE GEARS UP

As mentioned before, the effect of flaps and of landing gear on the drag polar for take-off and landing needs to be accounted for. This is done by changing the Oswald efficiency factor e and by adding an additional zero-lift drag coefficient, ΔC_{D_0}. Roskam gives the "ranges" of Table I.4 as a first estimate for these changes in reference [6]):

Table I.4 First estimates for ΔC_{D_0} and 'e' with flaps and gears down

Configuration	ΔC_{D_0}	e
Clean	0	0.80-0.85
Take-off flaps	0.010-0.020	0.75-0.80
Landing flaps	0.055-0.075	0.70-0.75
Landing gears	0.015-0.025	No effect

Which values are selected depends on flap and gear type. Split flaps are for instance more 'draggy' than Fowler flaps. Full span flaps are also more 'draggy' than partial span flaps. Wing mounted landing gears on high wing airplanes are more 'draggy' than those on low wing airplanes.

For the simulation of the Boeing 777-200 in the take-off configuration with the gear up, the following input is given:

W_{TO} = 529,281.8 lbs	d = 0.7531	S_W = 4,833.31 ft²	$C_{Lplot,\,min}$ = 0
AR_W = 8.27	a = -2.5229	e_{TO} = 0.8000	$C_{Lplot,\,max}$ = 2
c = 0.0199	b = 1.000	$\Delta C_{D0,\,TO}$ = 0.015	

Comparing these values with the values from paragraph I.4.2 shows us that only the values for e and ΔC_{D_0} have changed. The Oswald efficiency factor e has changed from 0.85 to 0.8 due to the deploying of the flaps. Table I.4 indicates that this change should be reasonably correct. For both configurations, the maximum possible value for e is namely used. The increment in zero-lift drag coefficient due to the flaps is taken as 0.0145 (0.0150 – 0.005). Since Fowler flaps are used, a ΔC_{D_0} of 0.0145 is reasonable.

With this input, AAA calculates the drag polar as $C_D = 0.0283 + 0.0481 * C_L^2$. Figure 1.17 shows this drag polar.

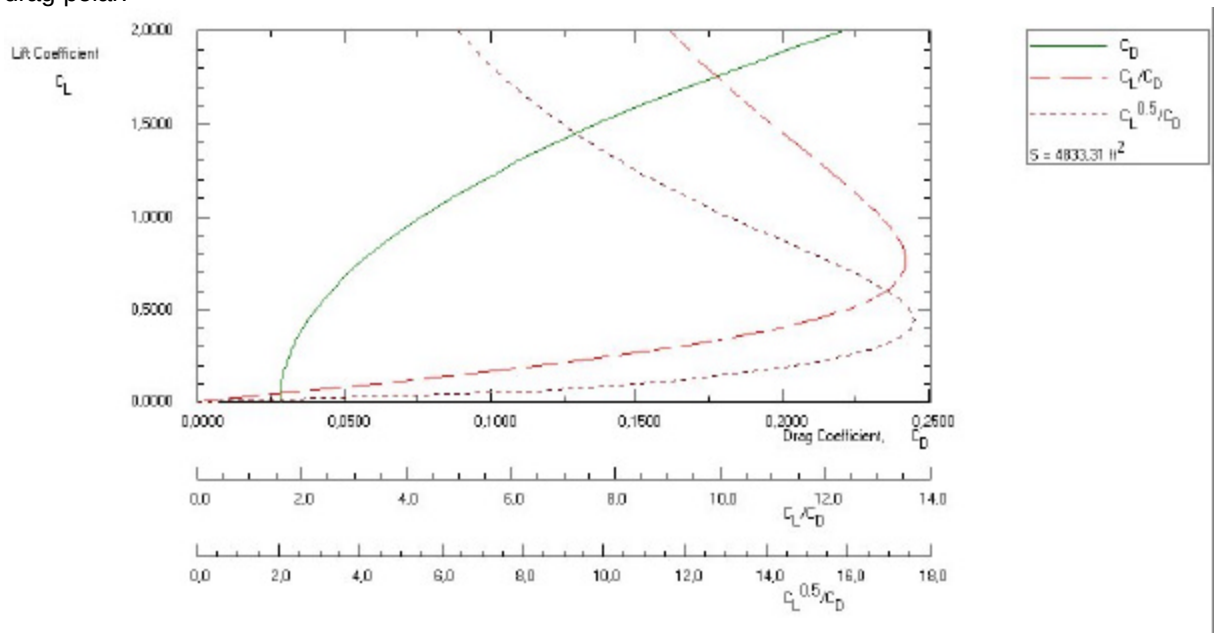

Figure 1.17 The drag polar of the airplane in the take-off configuration with the gear up

I.4.5 THE DRAG POLAR FOR THE AIRPLANE IN THE TAKE-OFF CONFIGURATION WITH THE GEARS DOWN

At the beginning of the climb, the aircraft flies with the gears down and the flaps in the take-off position. This situation is evaluated now. Since the only difference with the previous paragraph is the landing gear position, only ΔC_{D_0} has to change. The increment in zero-lift drag coefficient due to the folding out of the landing gears is taken as 0.020 (0.035 – 0.015). Again, the assumed value seems reasonable seen the values given in Table I.4. For the simulation of the Boeing 777-200 in the take-off configuration with the gears down, the following input is thus given:

W_{TO} = 529,281.8 lbs	d = 0.7531	S_W = 4,833.31 ft²	$C_{Lplot,\,min}$ = 0
AR_W = 8.27	a = -2.5229	e_{TO} = 0.8000	$C_{Lplot,\,max}$ = 2
c = 0.0199	b = 1.000	$?C_{D0,\,TO}$ = 0.035	

With these values as input, AAA gives $C_D = 0.0483 + 0.0481 * C_L^2$ for the drag polar. The corresponding drag polar is plotted in Figure 1.18.

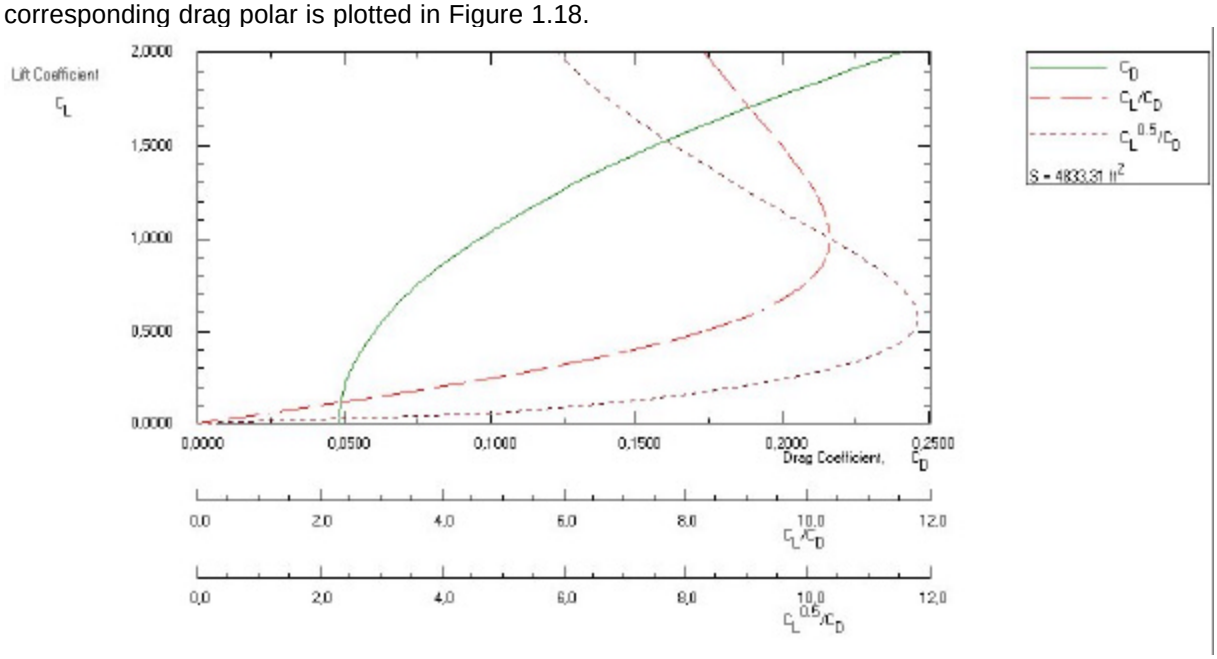

Figure 1.18 The drag polar of the airplane in the take-off configuration with the gear down

I.4.6 THE DRAG POLAR FOR THE AIRPLANE IN THE LANDING CONFIGURATION WITH THE GEARS UP

Again, the only parameters that will change compared to the clean airplane configuration are the Oswald efficiency factor and the zero-lift drag coefficient. The following input is given for the airplane in the landing configuration with the gears down:

W_{TO} = 529,281.8 lbs	d = 0.7531	S_W = 4,833.31 ft²	$C_{Lplot,\,min}$ = 0
AR_W = 8.27	a = -2.5229	e_L = 0.7500	$C_{Lplot,\,max}$ = 2
c = 0.0199	b = 1.000	$?C_{D0,\,L}$ = 0.055	

As in the previous paragraphs, the maximum value of the range proposed in Table I.4 is taken for the Oswald efficiency factor. In the landing configuration, this equals e_L = 0.7500. The zero-lift drag coefficient increment due to the landing flaps is taken as 0.055. Since Fowler flaps are used, this value is reasonable.

With this input, AAA calculates the drag polar as $C_D = 0.0683 + 0.0513 * C_L^2$. Figure 1.19 shows this drag polar.

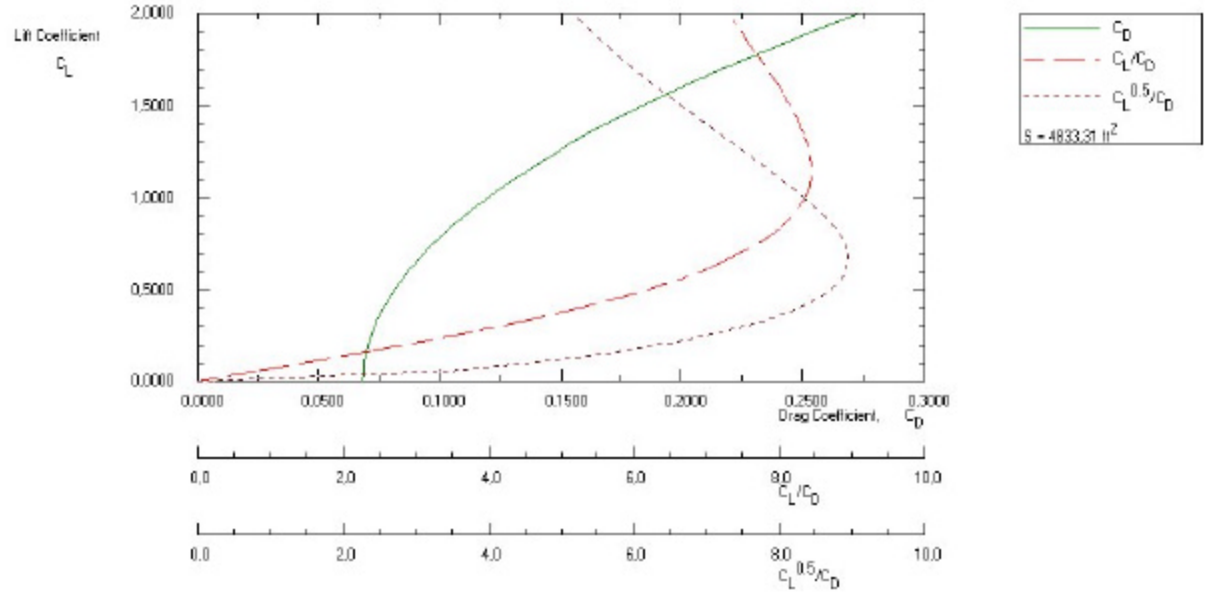

Figure 1.19 The drag polar of the airplane in the landing configuration with the gear up

I.4.7 THE DRAG POLAR FOR THE AIRPLANE IN THE LANDING CONFIGURATION WITH THE GEAR DOWN

Now, only the effect of the folding out of the landing gear must be addressed. The effect of the flaps in the landing configuration was namely already investigated in the previous paragraph. Therefore, only an additional ΔC_{D_0} is needed. As in paragraph I.4.5, the increment in zero-lift drag coefficient due to the folding out of the landing gear is taken as 0.020. With this increment and with the data from the previous paragraph, the input for the calculation of the drag polar for the airplane in the landing configuration with the gear down becomes:

W_{TO} = 529,281.8 lbs	d = 0.7531	S_W = 4,833.31 ft²	$C_{Lplot,\,min}$ = 0
AR_W = 8.27	a = -2.5229	e_L = 0.7500	$C_{Lplot,\,max}$ = 2
c = 0.0199	b = 1.000	?$C_{D0,\,L}$ = 0.075	

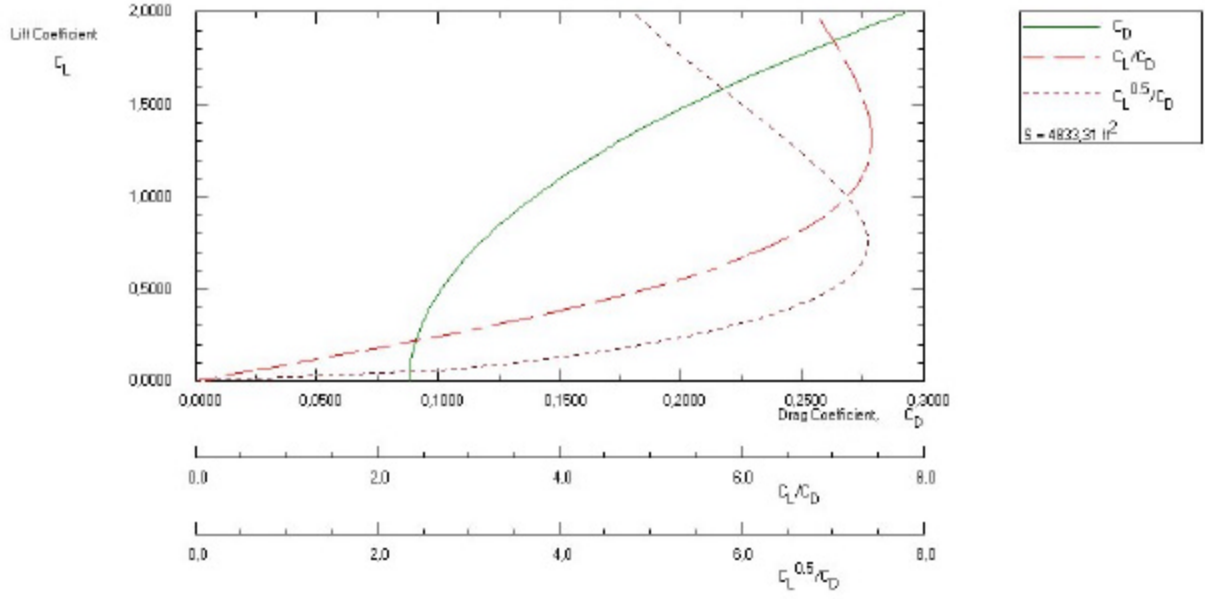

Figure 1.20 The drag polar of the airplane in the landing configuration with the gear down

With this input, the drag polar is given as $C_D = 0.0883 + 0.0513 * C_L^2$. Figure 1.20 shows this drag polar.

I.4.8 THE DRAG POLAR FOR THE AIRPLANE WITH ONE ENGINE INOPERATIVE

Finally, the drag polar for the airplane with one engine inoperative (OEI) has to be determined. In AAA, no specification is given concerning the flight condition in which the OEI case has to be evaluated. Here, the landing condition with the gear down is taken, since this was already the worst condition with regard to the aircraft drag. Therefore, this is also the most 'demanding' condition when one engine fails and thus the 'best' choice to evaluate the flight with OEI.

Due to the windmilling engine, an additional drag will occur. According to Roskam (ref. [8]), an engine failure leads to a ΔC_{D_0} of 0,0050, which equals 6,67% of the drag in the landing configuration with the gears down. With the values from paragraph I.4.7 and an increment in zero-lift drag coefficient of 50 counts, the input for AAA then becomes:

W_{TO} = 529,281.8 lbs	d = 0.7531	S_W = 4,833.31 ft²	$C_{Lplot,\,min}$ = 0
AR_W = 8.27	a = -2.5229	E_{OEI} = 0.7500	$C_{Lplot,\,max}$ = 2
c = 0.0199	b = 1.000	? $C_{D0,\,OEI}$ = 0.080	

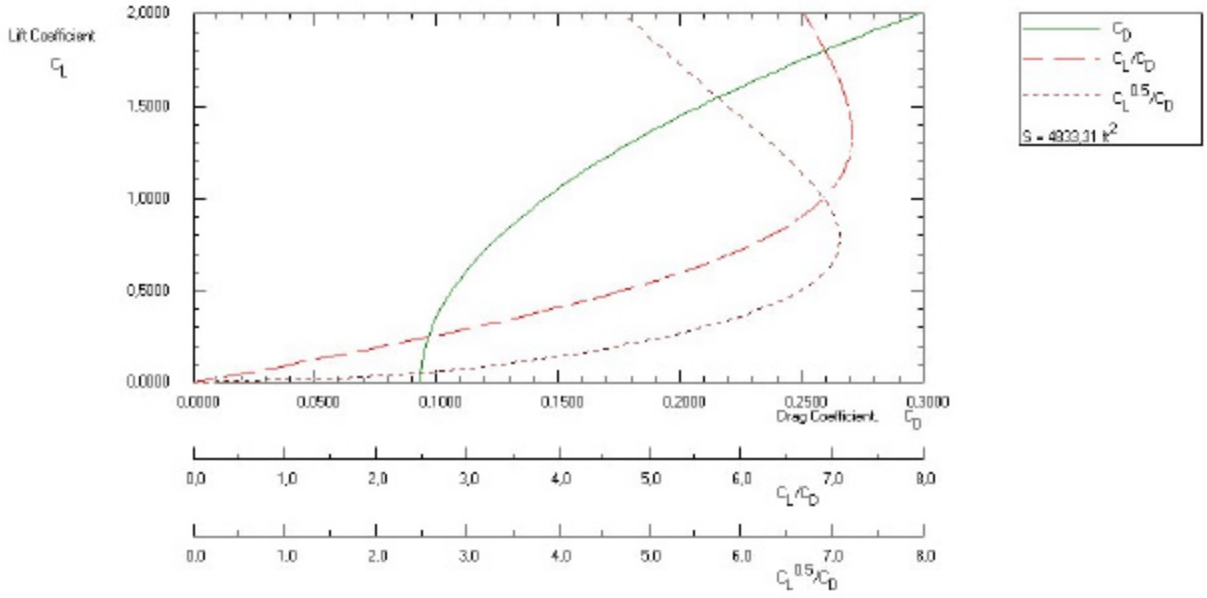

Figure 1.21 The drag polar of the airplane with one engine inoperative

With this input, the drag polar is calculated as $C_D = 0.0933 + 0.0513 * C_L^2$. This polar is shown in Figure 1.21.

I.5 CONCLUSION

In this chapter, the preliminary sizing of the kerosene-fuelled Boeing 777 is calculated using AAA to validate both the program and the method used. Since the results from the calculations correspond well with the actual data from the 777, despite of the many simplifications and assumptions, it can be concluded that the selected method and the program are reasonably accurate. The calculated take-off gross weight e.g. is only 1% different from the actual weight and the empty weight also lies well within the accuracy of 10% given by Roskam. Furthermore, the design point falls inside the payload-range diagram given by Boeing.

Not only the weight data is relatively accurately estimated with AAA, the performance requirements results also show a good accuracy. The actual wing loading and thrust-to-weight ratio namely are really close to the optimum design point given by AAA calculations.

I.6 REFERENCES

BOOKS

[1] Darcorporation, "*Advanced Aircraft Analysis User's Manual Version 2.3*", Darcorporation, 2001

[2] Darcorporation, "*Advanced Aircraft Analysis Version 2.3 help files*", Darcorporation, 2001

[3] Jenkinson L., Simpkin P. & Rhodes D., "*Civil Jet Aircraft Design*", AIAA Education Series, 1999

[4] Lan C.E. & Roskam J., "*Airplane Aerodynamics and Performance*", DAR Corporation, 1997

[5] Raymer D.P., "*Aircraft Design: a Conceptual Appoach*", AIAA Education Series, 1992

[6] Roskam J., "*Airplane Design: Part I, Preliminary Sizing of Airplanes*", DAR Corporation, 1997

[7] Roskam J., "*Airplane Design: Part II, Preliminary Configuration Design and Integration of the Propulsion System*", DAR Corporation, 1997

[8] Roskam J., "*Airplane Design Short Course AA31010*", the University of Kansas Continuing Education, August 5-9 2002

[9] Stinton D., "*Flying qualities and Flight Testing of the Airplane*", AIAA Education Series, 1995

[10] Torenbeek E., "*Synthesis of Subsonic Airplane Design*", Delft University Press, 1982

WORLD WIDE WEB

[11] http://www.boeing.com/assocproducts/aircompat/777.htm

[12] http://www.bh.com/companions/aerodata/

[13] http://www1.airweb.faa.gov/Regulatory_and_Guidance_Library/rgFAR.nsf/MainFrame?OpenFrameSet

CHAPTER II

PRELIMINARY SIZING OF THE HYDROGEN-FUELLED BOEING 777

In this chapter, the preliminary sizing of a hydrogen-fuelled Boeing 777 is described. Since both the kerosene-fuelled and the hydrogen-fuelled version of the 777 would have to fly the same missions, the mission specification of Chapter I is reused here.

In addition, this chapter also uses the same construction as Chapter I. Only the order of the paragraphs has changed. The estimation of the drag polars is done this time before the estimation of wing area and take-off thrust. This is done because of the uncertainty on the drag data due to the "new" shape of the fuselage. In order to have an idea of the influence of the additional drag on the aircraft performance a sensitivity analysis is executed on the drag polars.

Finally, it is assumed that the engine ratings are the same for both hydrogen and kerosene as a fuel. Therefore, the factors F_{cr}, $F_{MaxCont}$ and F_{8sec} have the same value for both fuels.

II.1 ESTIMATION OF TAKE-OFF GROSS WEIGHT, EMPTY WEIGHT AND MISSION FUEL WEIGHT OF THE H_2-FUELLED BOEING 777

II.1.1 DETERMINATION OF THE MISSION PAYLOAD AND CREW WEIGHT

Since the global idea behind this simulation is to compare both designs with different fuels, the mission payload weight is the same as for the kerosene fuelled Boeing 777. Thus, a mission payload weight of 79.500 lbs (36.061 kg) is taken. As for the mission in Chapter I this would mean 360 passengers and 10 crewmembers.

Figure 2.1 The location of the hydrogen tanks (ref. [8])

However, in this case the weight of the fuel tanks and system is also added to the payload. Due to its cryogenic properties, hydrogen fuel namely requires cylindrical fuel tanks to limit the boil-off. These tanks will be placed on top of the existing fuselage (cf. Figure 2.1). Furthermore, a substantial amount of insulation and several extra pumps will also be needed. Thus, the weight of this tank system has to be included in the simulation. Since the weight of the structure is determined through statistical data and since there are no hydrogen-fuelled aircraft to derive this data from, this weight can not be added to the weight of the structure in the Class I analysis in AAA. A Class II analysis would allow more modifications to the architecture of the plane and would thus yield better results. The amount of work needed in this analysis is much bigger though. Therefore, only a Class I sizing will be done here.

The weight of the fuel system is derived from reference [1]. In this reference, Brewer compares several possible configurations for the fuel containment and supply system and selects the two “best” alternatives[20]. For these two alternatives, an estimation of the fuel system weight is given too. Here, an average is made between the two values proposed by Brewer. This average is:

$$\frac{W_{SYS}}{W_{FUEL}} = 0{,}387$$

Since the weight of the fuel system is given as a fraction of the fuel weight, this weight has to be known to be able to calculate the total payload weight. An iteration is thus in order. This iteration leads to:

$$W_{PL} = 95{,}159 \text{ lb}$$

II.1.2 GUESSING A LIKELY VALUE OF TAKE-OFF WEIGHT, $W_{TO,\,GUESS}$

Since there is no actual data available concerning the weight of a hydrogen-fuelled airplane, it is difficult to make a proper estimate of the take-off weight. The fuel mass will not only be much smaller, the structural weight of several components will also be altered. However, this estimate only serves to trigger off the iteration. Any value will cause the iteration to converge, the accuracy of the initial estimate only determines the number of iterations that will have to be executed and thus the computer time needed. Since no logical evolution of the take-off weight due to the fuel change can be given, the original take-off weight of the kerosene-fuelled Boeing 777 is taken here as the initial estimate.

$$W_{TO,\,guess} = 535.000 \text{ lbs } (242.630 \text{ kg})$$

[20] Considering weight, safety, reliability and economic factors.

II.1.3 DETERMINATION OF MISSION FUEL WEIGHT, W_F

The mission fuel weight is determined from the mission specification of the airplane under investigation. The mission for this design is given in paragraph I.1. Below, this mission specification is used to determine the values for the fuel fractions of each phase. The distinct phases used here (and their numeration) can again be found in this mission specification or in paragraph I.2.

II.1.3.1 PHASE 1: ENGINE START AND WARM-UP

The begin weight of this phase is the gross take-off weight W_{TO}. The end weight is W_1. The fuel fraction for this phase is by previous definition given by: W_1/W_{TO} .

As indicated in Chapter I, Roskam (see ref. [4]) gives a value of 0.990 for the fuel fraction of the engine start and warm-up segment for the jet transport category of aircraft. Raymer on the other hand (ref. [3]) only gives values for the warm-up, taxi and take-off segments together. He suggests values between 0.97 and 0.99 for the fraction of all three phases together. Multiplying the values given by Roskam (see also II.1.3.2 and II.1.3.3) would lead to a total fraction of 0.9752 (0.9900*0.9900*0.9950) for those three phases.

However, the engines of the airplane under consideration are now running on hydrogen. Since this reduces the fuel flow by a factor of approximately 3, the values mentioned above seem too low. Therefore, the 3 separate weight fractions of Roskam are multiplied by the same factor[21] to obtain a value of 0,99 for the total fraction of the 3 phases together (as given by Raymer). This namely was the high end value given in reference [3]. This method leads to:

$$\frac{W_1}{W_{TO}} = \sqrt[3]{\frac{0.9900}{0.9752}} * 0.9900 = 0.9950 .$$

II.1.3.2 PHASE 2: TAXI

The begin weight of this phase is the end weight of the previous phase, W_1. The end weight is W_2. The fuel fraction for this phase is by previous definition given by: W_2/W_1 .

Again, the value given by Roskam (0.99) is adapted via the method given above. This gives:

$$\frac{W_2}{W_1} = 0.9950 .$$

II.1.3.3 PHASE 3: TAKE-OFF

The begin weight of this phase is the end weight of the previous phase, W_2. The end weight is W_3. The fuel fraction for this phase is thus given by: W_3/W_2 .

Again, Roskam 's value (0,995) is adapted to hydrogen-fuelled engines by means of the method described in subsection II.1.3.1. This leads to:

$$\frac{W_3}{W_2} = 0.9999 .$$

II.1.3.4 PHASE 4: CLIMB

The begin weight of this phase is the end weight of the previous phase, W_3. The end weight is W_4. The fuel fraction for this phase is thus given by: W_4/W_3 .

As in subsection I.2.3.4, the climb phase is again considered as a fuel-intensive phase. Therefore, the Breguet equation for endurance is used to determine the fuel fraction for this flight phase. To

[21] The factor by which the separate fractions of Roskam are multiplied is: $\sqrt[3]{\frac{0.9900}{0.9752}}$

determine the fuel fraction used during climb, it is thus necessary to estimate or calculate average values for c_j and for (L/D) during climb. Since AAA calculates the endurance based on the average rate of climb and the altitude to climb to, these values must also be given. In this simulation, the values from the simulation of the Boeing 777-200 running on kerosene (cf. Chapter I) are used where possible. The fuel consumption is changed though for obvious reasons. Again, a reduction in fuel flow by a factor 3 is assumed. Finally, the lift-to-drag ratio of the hydrogen-fuelled Boeing 777 is changed too. The fuel tank on top of the fuselage will namely increase the fuselage drag and thus decrease the lift-to-drag ratio. As shown in [1], the proportion of the lift-to-drag ratio of the kerosene-fuelled aircraft to the lift-to-drag ratio of the hydrogen-fuelled aircraft is close to 1.12 for all the configurations examined by Brewer. Since no extra data is available, this proportion is used here too. This leads to the following input for the climb phase in the mission profile module of AAA:

$$c_j = 0.233 \frac{\text{lb/hr}}{\text{lb}} = 0.0238 \frac{\text{kg/hr}}{\text{N}}$$

$$\left(\frac{L}{D}\right)_{cl} = 8{,}93$$

$$\text{RC} = 1{,}794.87 \ \frac{\text{ft}}{\text{min}} = 9.1179 \frac{\text{m}}{\text{s}}$$

h = 35,000 ft = 10,668 m

Based on the values of the altitude and the average rate of climb, the endurance can be calculated (E=h / RC). Using (1.7), this leads to:

$$\frac{W_4}{W_3} = 0.9915 \ .$$

II.1.3.5 PHASE 5: CRUISE

The begin weight of this phase is the end weight of the previous phase, W_4. The end weight is W_5. The fuel fraction for this phase is thus given by: W_5 / W_4 .

Again, as for the climb phase, this flight phase is considered as a fuel-intensive phase. As in Chapter I, the Breguet equation for range is used to determine the fuel fraction for this flight phase. As for the climb phase, the values have to be adapted to hydrogen fuel. To do this, the thrust specific fuel consumption is, once more reduced by a factor of 3 compared to the simulation of Chapter I and the lift-to-drag ratio is adapted as explained in subsection II.1.3.4. This leads to the following values:

$$V = 478.56 \text{ kts} = 886.29 \frac{\text{km}}{\text{hr}}$$

$$c_j = 0.167 \frac{\text{lb/hr}}{\text{lb}} = 0.0170 \frac{\text{kg/hr}}{\text{N}}$$

$$\left(\frac{L}{D}\right)_{cr} = 13.39$$

R = 4,240 nm = 7,852.48 km

The value for the cruise fuel fraction is now determined with (1.8) as:

$$\frac{W_5}{W_4} = 0.8956 \ .$$

II.1.3.6 PHASE 6: DESCENT

The begin weight of this phase is the end weight of the previous phase, W_5. The end weight is W_6. The fuel fraction for this phase is thus given by: W_6 / W_5 .

The descent phase will be considered as a fuel un-intensive flight phase in this simulation so the statistically estimated fractions suggested by Roskam and Raymer will be used again after adaptation to hydrogen as a fuel. To do this, the factor from subsection II.1.3.1 is used again. With this factor, Roskam 's and Raymer 's value (0.99) leads to the following fuel fraction:

$$\frac{W_6}{W_5} = 0.9950 .$$

II.1.3.7 PHASE 7: LANDING, TAXI & SHUTDOWN

The begin weight of this phase is the end weight of the previous phase, W_6. The end weight is W_7. The fuel fraction for this phase is thus given by: W_7/W_6 .

As in Chapter I, this phase is considered as a fuel un-intensive phase since only a relatively small amount of fuel is used in this flight phase. Therefore, the statistical estimations are used again. Roskam suggests a value of 0.992 for this phase for jet transports while Raymer indicates a range between 0.992 and 0.997. Again, since the plane will fly on hydrogen, the high end value given by Raymer will be used:

$$\frac{W_7}{W_6} = 0.9970 .$$

II.1.4 THE RESULTS FOR W_{TO}, W_E AND W_F

Again, as in Chapter I, an iteration is now executed by AAA with the take-off weight option from the weight sizing module. In order to perform the calculation, the following input is given:

A = 0.0833	$W_{TO, est}$ = 535,000 lbs	M_{tfo} = 0.5%
B = 1.0383	W_{PL} = 95,159 lbs	$M_{F, res}$ = 10%

The trapped fuel and oil fraction, M_{tfo}, is kept constant for both hydrogen and kerosene as a fuel. In reality this will not be the case due to the different specific densities of the fuels, the different pressures in the tanks and the difference in boil-off rate of the fuels. However, since no actual data on the trapped fuel and oil fraction can be found, this fraction is kept constant here independent of the fuel type.

With these values and the fuel fractions from the previous paragraphs, the program gives as output:

M_{ff} = 0.8720	W_F = 40,424.1 lb	$W_{F, res}$ = 3,674.9 lb	W_E = 150,184.6 lb
$W_{F, used}$ = 36,749.2 lb	$W_{F, max}$ = 40,424.1 lb	W_{tfo} = 1,436.0 lb	W_{TO} = 287,203.7 lb

Furthermore, a mission profile table is also given. In this simulation the table is as follows:

	Mission Profile	W_{begin} (lb)	?$W_{F, used}$ (lb)	$W_{F, begin}$ (lb)
1	Warm-up	287,203.7	1,436.0	40,424.1
2	Taxi	285,767.6	1,428.8	38,988.1
3	Take-off	284,338.8	28.4	37,559.2
4	Climb	284,310.4	2,404.1	37,530.8
5	Cruise	281,906.2	29,435.8	35,126.7
6	Descent	252,470.5	1,262.4	5,690.9
7	Land/Taxi	251,208.1	753.6	4,428.5

II.1.5 COMPARISON WITH THE RESULTS FOR THE KEROSENE-FUELLED B777-200

Even though not very much detail was put into the simulation, it is useful to compare the results for the hydrogen-fuelled Boeing with these for the kerosene-fuelled 777 from Chapter I. Some remarks have to be made beforehand since the current simulation in AAA is not totally adapted to hydrogen as a fuel. Statistical data is namely used and there are no airplanes flying on hydrogen yet. Therefore, the wing weight used will be different from the “real” one. The hydrogen fuel is namely stored in the fuselage instead of in the wing and can thus no longer alleviate the wing root bending moment due to lift. This calls for a bigger wing box.

II.1.5.1 THE EMPTY WEIGHT

The empty weight of the hydrogen-fuelled airplane is much smaller than the empty weight of its kerosene counterpart. The AAA calculations indicate an empty weight of only 150,224.4 lb (68,140.6 kg) for the plane with hydrogen fuel while the empty weight for the kerosene-fuelled aircraft is given as 270,600.6 lb (122,742.4 kg). This means a reduction of 44.5 % in empty weight.

In reality, this weight reduction will be less explicit due to several reasons. As mentioned before, the wing box weight (and thus also the wing weight fraction) will have to increase compared to a conventional wing with kerosene tanks. Additionally, the fuselage weight will also increase due to the higher internal volume needed (the hydrogen tanks also need to be placed inside the fuselage). The higher internal volume will namely bring about a bigger total surface area and thus a bigger fuselage (shell) weight. Additionally, the fuselage structure will have to be strengthened to be able to carry the hydrogen tank on top of the passenger cabin. The engines and the landing gear weight on the other hand will be reduced due to the lower take-off weight so it is hard to make an accurate estimation of the actual weight change. Therefore, no adaptations are made in this Class I analysis to the results of AAA.

II.1.5.2 MISSION FUEL WEIGHT

Since the thrust specific fuel consumption of the hydrogen engines is only approximately one third of that of the engines running on kerosene, the mass of fuel needed to perform the same mission will be much lower using hydrogen as a fuel. Furthermore, the gross weight of the plane will also be much lower for hydrogen fuel (cf. subsection II.1.5.2), which diminishes the mission fuel weight even further even if the drag of the hydrogen-fuelled aircraft will be higher than with kero. AAA calculations lead to a reduction in mission fuel weight from 160,486.1 lb (72,795.3 kg) for kerosene to 36,784.6 lb (16,685.2 kg) for hydrogen. A reduction of 77.1 % is thus achieved.

II.1.5.3 THE TAKE-OFF GROSS WEIGHT

As can be seen from sections II.1.4 and I.2.6, the take-off gross weight is decreased from 529,281.8 lb (240,078.2 kg) to 287,282.9 lb (130,309.3 kg) due to the fuel switch. The take-off gross weight for the hydrogen-fuelled plane is only 54.3% of that for the kerosene-fuelled plane with the same mission. Again, as for the empty weight, the real reduction will be lower.

II.1.6 SENSITIVITY CALCULATIONS

Again, as for the kerosene-fuelled Boeing 777, the sensitivities are now calculated. Here, the value of some sensitivities will be of major importance since some variables have quite a big margin of uncertainty. Especially the take-off weight to empty weight sensitivity will need some attention. Below, the different sensitivities are simply given. Only the take-off weight to empty weight sensitivity will be shortly discussed. For the meaning and determination method of the different sensitivities, the reader is referred to Chapter I (part I.2.8) or reference [4].

$$\frac{\partial W_{TO}}{\partial W_{PL}} = 2.85$$

$$\frac{\partial W_{TO}}{\partial W_{E}} = 1.99$$

Table II.1 The results for the sensitivities

	$\P W_{TO}/\P c_j$ (lb-hr)	$\P W_{TO}/\P R$ (lb/nm)	$\P W_{TO}/\P(L/D)$ (lb)	$\P W_{TO}/\P E$ (lb/hr)
Climb	28,609.4	- - -	-747.5	20,540.1
Cruise	520,149.5	20.4	-6,474.4	- - -

The take-off weight to empty weight sensitivity is calculated by AAA as 1.99. For every pound of weight added to the empty weight the take-off weight is thus increased by almost 2 pounds. Seen the remarks given in the previous subsections, the reduction in take-off gross weight due to the fuel switch will be reasonably less than indicated by AAA.

As can be seen from the data of subsection I.2.8 in Chapter I, these values are lower than the values given for the kerosene-fuelled Boeing 777-200. The take-off weight to payload weight sensitivity is lowered from 5.91 to 2.85 while the take-off weight to empty weight ratio is slightly reduced from 2.03 to 1.99. The formulae for these sensitivities, given in I.2.8, explain significantly the evolution of the values. Both sensitivities are namely proportional to the take-off weight. The lower take-off weight of the hydrogen version of the Boeing 777 reduces its sensitivities. Furthermore, the sensitivity of take-off weight to payload weight also depends on the value of that payload weight. The artificial introduction of fuel system weight in the payload weight has thus altered the results.

II.2 ESTIMATION OF THE DRAG POLARS OF THE H_2-FUELLED BOEING 777

As can be seen from Figure 2.1, the fuel tanks for hydrogen are placed inside the fuselage on top of the passenger cabin. This will change the form of the cross-section and thus also the fuselage drag of the airplane. Not only the form drag will rise due to the less aerodynamically efficient shape of the fuselage, the skin friction drag will rise too due to the larger wetted area of the fuselage.

Since this drag rise is not exactly known, a sort of sensitivity analysis is used to determine the influence of the additional fuselage drag. An artificial rise in $C_{D,0}$ is introduced and the Oswald efficiency factor e is slightly reduced too. The new fuselage will namely not only result in a drag rise, the distribution of the lift along the wing span will change too. A $C_{D,0}$ increment of +10 and +20% and a change in Oswald efficiency factor of –2% and –4% are used. This leads to the following 9 "alternatives".

Table 2.1 The different alternatives

	$C_{D,0}$		
e	+0%	+10%	+20%
-0%	Alternative 0	Alternative 1	Alternative 2
-2%	Alternative 3	Alternative 4	Alternative 5
-4%	Alternative 6	Alternative 7	Alternative 8

For each different aircraft, the drag polars will be given below. Only for the drag polar for the clean airplane (subsection II.2.1), all figures will be included here. For the other configurations the drag polar will only be given in analytical form.

II.2.1 THE DRAG POLAR FOR THE CLEAN AIRPLANE

Below, the drag polars for the clean aiplanes of the different alternatives are given. The first alternative is used to comment on the values used as input for AAA. From the second alternative on, only the values that differ between the different alternatives are dealt with. The change in $?C_{D0,\ clean}$ and e_{clean} is explained each time.

II.2.1.1 ALTERNATIVE 0

As can be seen from Table 2.1, alternative zero uses the standard values for both $C_{D,0}$ and e. The input for the Class I drag calculations can thus be derived from the values given as input in paragraph I.4.3 and can be found in Table 2.2. As can be seen from that table, the only value that has changed compared to the data from I.4.3 is the take-off gross weight. Since the standard values are used for both $C_{D,0}$ and e for this "alternative", the values for $?C_{D0,\ clean}$ and e_{clean} from subsection I.4.3 are namely reused. Furthermore, since the same wing would be used as for the kerosene-fuelled Boeing 777, the values from the real 777 are used again for both wing area and aspect ratio. Finally, the values for regression coefficients a,b,c and d are also retained from the kerosene-fuelled Boeing 777 simulation. Even though changing c and d would lead to another wetted area for the same take-off weight and thus also to another value for $C_{D,0}$, it has been chosen not to adjust the drag this way. It will namely be easier to directly change $C_{D,0}$ instead of searching for new values for c and d to obtain the desired zero-lift drag coefficient. The latter would only be worth investigating if reasonable data can be used concerning the increase in wetted area.

Table 2.2 The input for alternative 0

W_{TO} = 287,203.7 lbs	d = 0.7531	S_W = 4,833.31 ft²	$C_{Lplot,\ min}$ = 0
AR_W = 8.27	a = -2.5229	e_{clean} = 0.8500	$C_{Lplot,\ max}$ = 2
c = 0.0199	b = 1.000	$?C_{D0,\ clean}$ = 0.0005	

With the input from Table 2.2, the following output is calculated in AAA:

S_{wet} =13,504.01 ft²	$C_{D0,\ clean}$ = 0.0084	$B_{DP,\ clean}$ = 0.0453

$f = 40.51$ ft² $C_{D0,\ clean,\ M} = 0.0089$

Comparing these values with the values calculated for the kerosene-fuelled Boeing 777 (cf. subsection I.4.3) shows us that both the wetted and the equivalent parasite area are reduced by approximately 37%[22] due to the reduction in take-off gross weight. The drag polar is: $C_D = 0.0089 + 0.0453 * C_L^2$. The plot of this drag polar of the clean "alternative 0" plane at Mach 0.83 can be found in Figure 2.2.

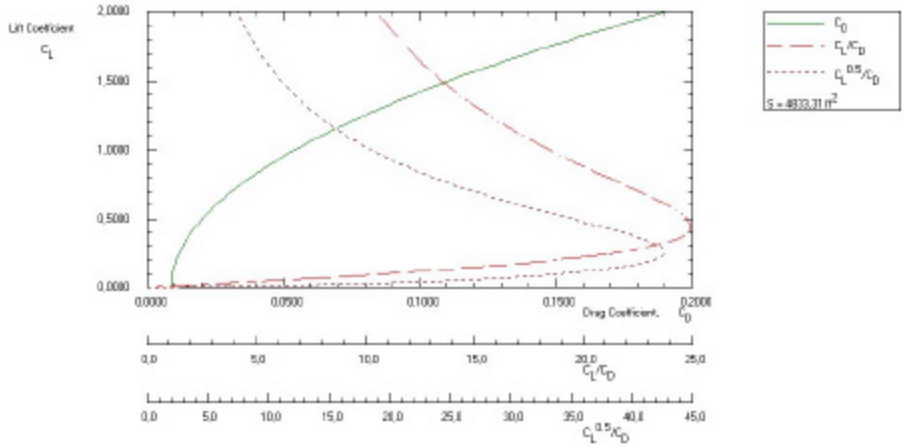

Figure 2.2 The drag polar for the clean airplane of 'alternative 0'

II.2.1.2 ALTERNATIVE 1

As can be seen from Table 2.1, only the value of $C_{D,0}$ is changed to go from alternative 0 to alternative 1. The Oswald efficiency factor e is kept as 0,85. The table shows us that $C_{D,0}$ has to be increased with 10%. This is done as follows. The value for $C_{D0,\ clean,\ M}$ of the previous subsection is multiplied by 0.1 to give us the desired change in $C_{D,0}$ and this value is then added to the $?C_{D0,\ clean}$ from the previous simulation. Doing this results in the input of Table 2.3 and in the drag polar of Figure 2.3. This drag polar is $C_D = 0.0098 + 0.0453 * C_L^2$

Table 2.3 The input for alternative 1

W_{TO} = 287,203.7 lbs	d = 0.7531	S_W = 4,833.31 ft²	$C_{Lplot,\ min}$ = 0
AR_W = 8.27	a = -2.5229	e_{clean} = 0.8500	$C_{Lplot,\ max}$ = 2
c = 0.0199	b = 1.000	$?C_{D0,\ clean}$ = 0.0014	

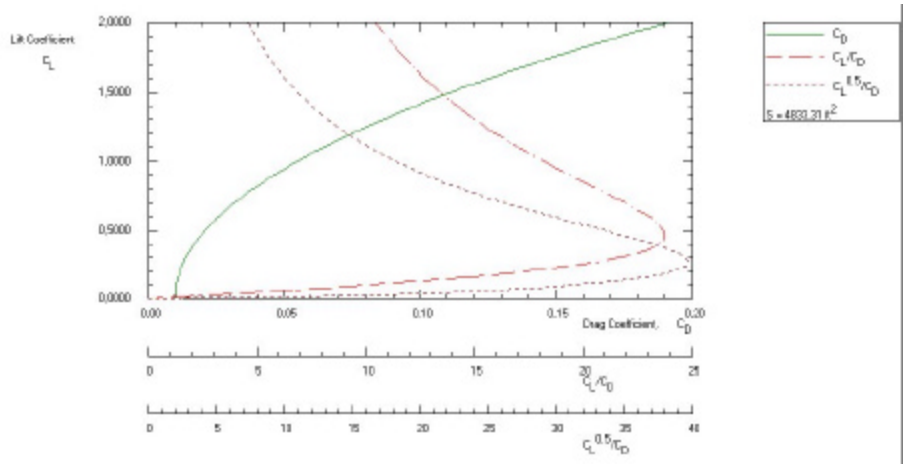

Figure 2.3 The drag polar for the clean airplane of 'alternative 1'

II.2.1.3 ALTERNATIVE 2

Again, only the value for $C_{D,0}$ has to change. An increase in zero-lift drag coefficient of 20% is postulated. The calculations are done using the method explained in subsection II.2.1.2. This leads to the values from Table 2.4.

Table 2.4 The input for alternative 2

W_{TO} = 287,203.7 lbs	d = 0.7531	S_W = 4,833.31 ft²	$C_{Lplot,\,min}$ = 0
AR_W = 8.27	a = -2.5229	e_{clean} = 0.8500	$C_{Lplot,\,max}$ = 2
c = 0.0199	b = 1.000	?$C_{D0,\,clean}$ = 0.0023	

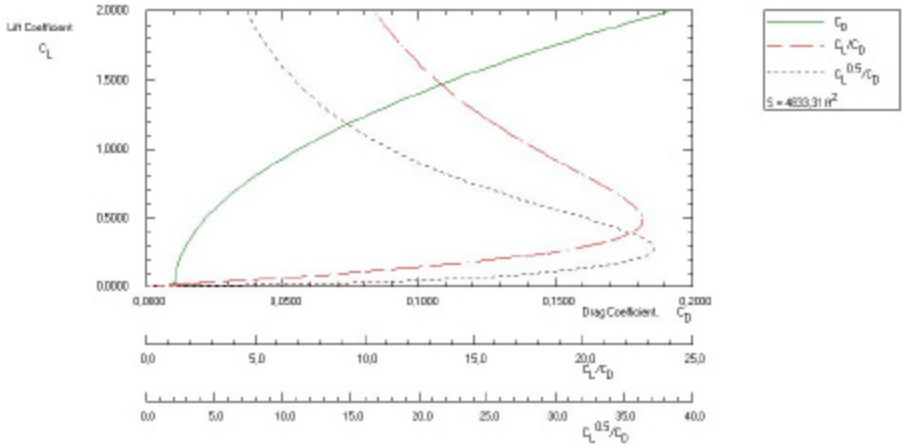

Figure 2.4 The drag polar for the clean airplane of 'alternative 2'

With this input, the drag polar is calculated as $C_D = 0.0107 + 0.0453 * C_L^2$. This drag polar can be found in Figure 2.4.

II.2.1.4 ALTERNATIVE 3

Table 2.1 shows us that for alternative 3 the Oswald efficiency factor has to change. Using a change of –2% and a base value of 0,85 this leads to an Oswald efficiency factor of 0,833. The input then is:

W_{TO} = 287,203.7 lbs	D = 0.7531	S_W = 4,833.31 ft²	$C_{Lplot,\,min}$ = 0
AR_W = 8.27	A = -2.5229	e_{clean} = 0.833	$C_{Lplot,\,max}$ = 2
c = 0.0199	b = 1.000	?$C_{D0,\,clean}$ = 0.0005	

With this input the drag polar is calculated as $C_D = 0.0089 + 0.0462 * C_L^2$. This drag polar can be found in Figure 2.5.

[22] This reduction can directly be found from equation (1.36). For the other alternatives, the increase in $C_{D,0}$ though diminishes this effect as can be seen from equation (1.35) and from C_{D0}=f / S.

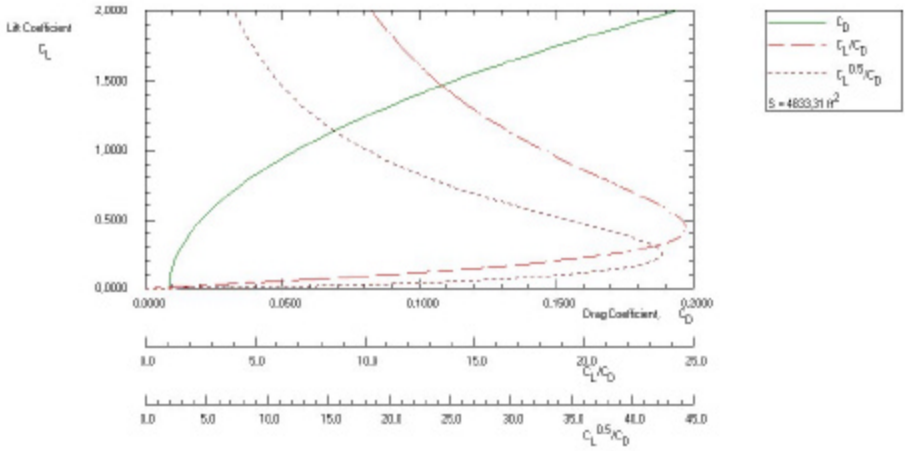

Figure 2.5 The drag polar for the clean airplane of 'alternative 3'

II.2.1.5 ALTERNATIVE 4

For alternative 4 an increase in $C_{D,0}$ of 10% and a decrease of e of 2% is used. This leads to the following input for AAA:

W_{TO} = 287,203.7 lbs	d = 0.7531	S_W = 4,833.31 ft²	$C_{Lplot,\,min}$ = 0
AR_W = 8.27	a = -2.5229	e_{clean} = 0.833	$C_{Lplot,\,max}$ = 2
c = 0.0199	b = 1.000	? $C_{D0,\,clean}$ = 0.0014	

With this input the drag polar is calculated as $C_D = 0.0098 + 0.0462 * C_L^2$. This drag polar can be found in Figure 2.6.

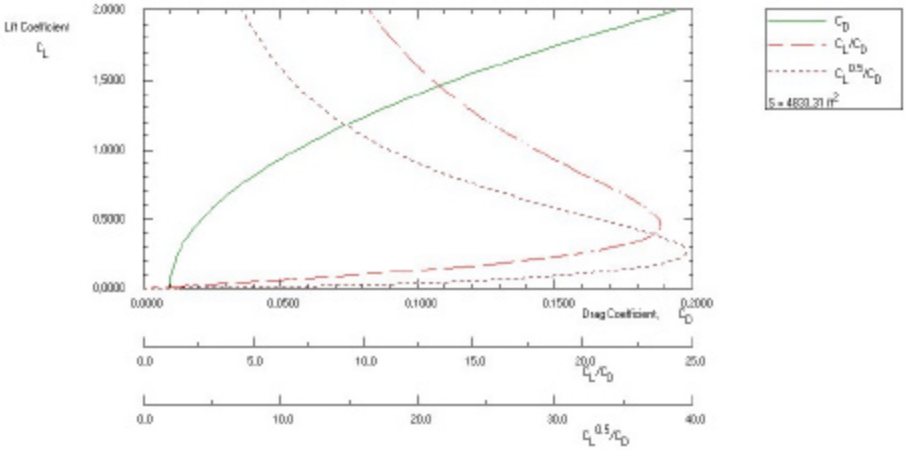

Figure 2.6 The drag polar for the clean airplane of 'alternative 4'

II.2.1.6 ALTERNATIVE 5

For alternative 5 an increase in $C_{D,0}$ of 20% and a decrease of e of 2% is used. This leads to the following input :

W_{TO} = 287,203.7 lbs	d = 0.7531	S_W = 4,833.31 ft²	$C_{Lplot,\,min}$ = 0
AR_W = 8.27	a = -2.5229	e_{clean} = 0.833	$C_{Lplot,\,max}$ = 2
c = 0.0199	b = 1.000	? $C_{D0,\,clean}$ = 0.0023	

With this input the drag polar is calculated as $C_D = 0.0107 + 0.0462 * C_L^2$. This drag polar can be found in Figure 2.7.

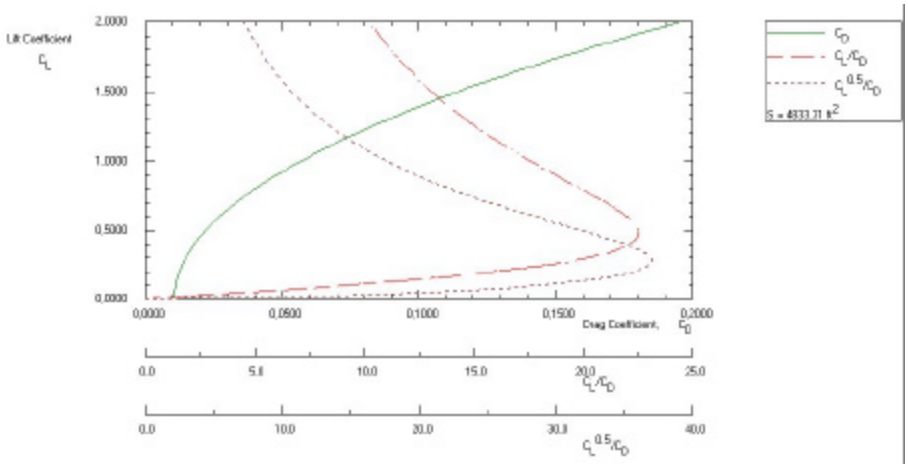

Figure 2.7 The drag polar for the clean airplane of 'alternative 5'

II.2.1.7 ALTERNATIVE 6

For the following alternatives, a decrease in Oswald efficiency factor of 4% is used. The value entered as input for AAA then becomes 0.816. With a $C_{D,0}$ increase of 0% this then leads to:

W_{TO} = 287,203.7 lbs	d = 0.7531	S_W = 4,833.31 ft²	$C_{Lplot,\,min}$ = 0
AR_W = 8.27	a = -2.5229	e_{clean} = 0.816	$C_{Lplot,\,max}$ = 2
c = 0.0199	b = 1.000	?$C_{D0,\,clean}$ = 0.0005	

With this input the drag polar is calculated as $C_D = 0.0089 + 0.0472 * C_L^2$. This drag polar can be found in Figure 2.8.

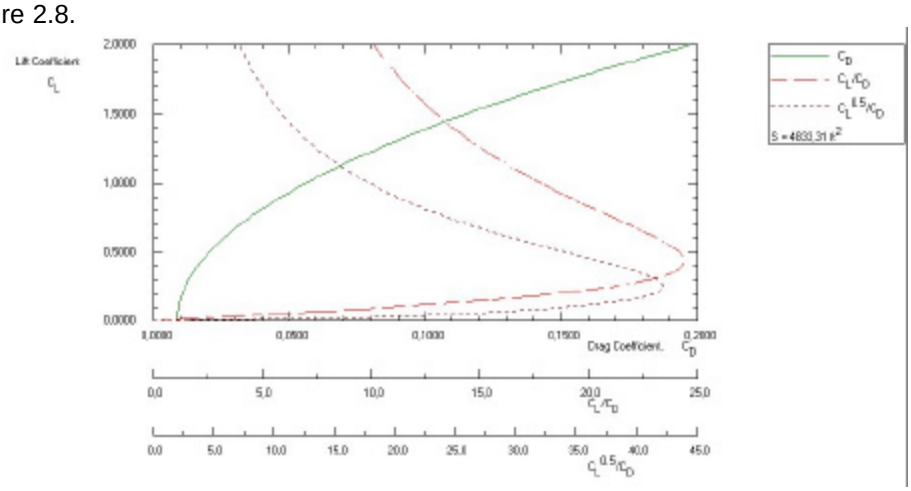

Figure 2.8 The drag polar for the clean airplane of 'alternative 6'

II.2.1.8 ALTERNATIVE 7

This time, the values used for e and ?$C_{D0,\,clean}$ are respectively 0,816 and 0.0014. With this input the drag polar is calculated as $C_D = 0.0098 + 0.0472 * C_L^2$. This drag polar can be found in Figure 2.9.

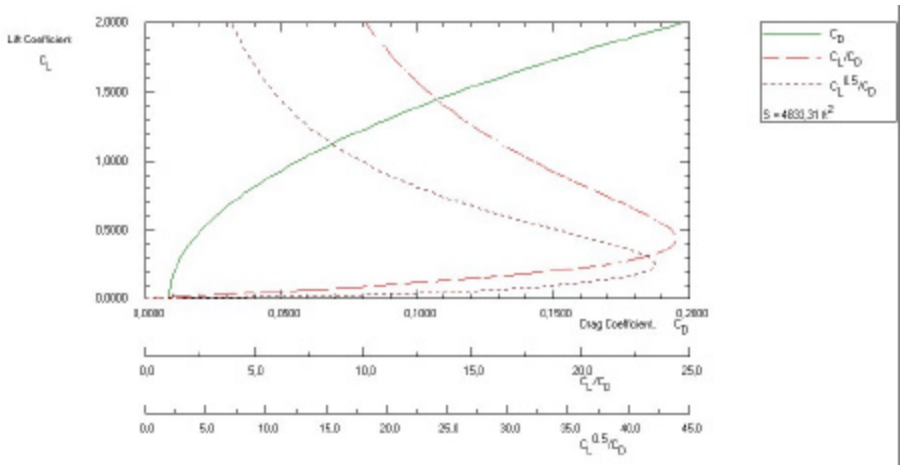

Figure 2.9 The drag polar for the clean airplane of 'alternative 7'

II.2.1.9 ALTERNATIVE 8

Finally, an increase in the zero-lift drag coefficient of 20% and a decrease in Oswald efficiency factor of 4% are assumed. The values used for e and $?C_{D0,\,clean}$ then become respectively 0,816 and 0.0023. With this input the drag polar is calculated as $C_D = 0.0107 + 0.0472 * C_L^2$. This drag polar can be found in Figure 2.10.

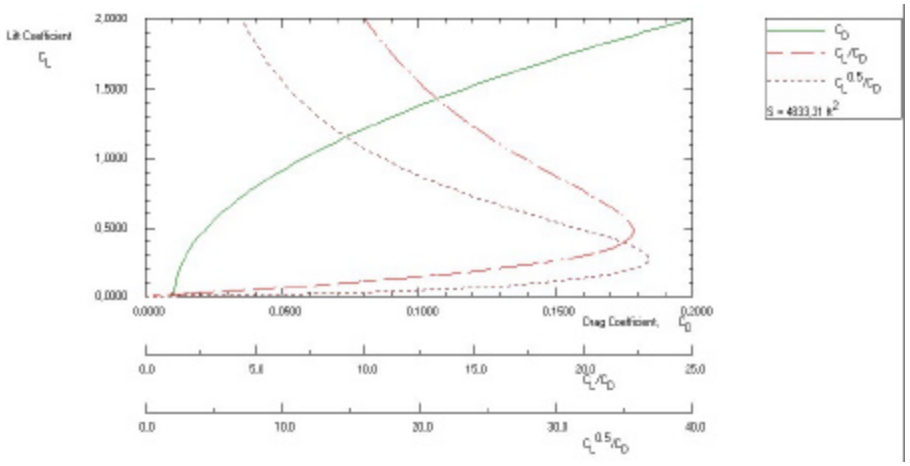

Figure 2.10 The drag polar for the clean airplane of 'alternative 8'

II.2.1.10 COMPARISON BETWEEN ALTERNATIVES ZERO AND EIGHT

Since alternatives zero and eight represent the two extremities investigated, those two cases will be compared here. Alternative zero represents the design with no additional drag or thus the fuselage from the kerosene-fuelled 777 while alternative eight can be seen as the "worst case scenario" under investigation. Comparing alternatives eight and zero thus gives us an idea of the increase in drag due to the fuel tank on top of the passenger cabin.

First of all, the maximum lift-to-drag ratio for alternative zero is approximately 24.9 at a lift coefficient of 0.45. For alternative eight the maximum lift-to-drag ratio is lowered to 22.3 at a lift coefficient of 0.47. This means a reduction by a factor of 1.12 for the maximum lift-to-drag ratio, which is remarkably consistent with the values given by Brewer and mentioned in paragraph II.1.3.4.

It is also interesting to compare the drag coefficients at a certain lift coefficient. Doing this for both alternatives results in the following table:

C_L	C_D for alternative Zero	C_D for alternative Eight
0	0.0089	0.0107
0.5	0.0202	0.0225
1.5	0.1108	0.1169

At a lift coefficient of zero, the drag is increased by 20% (as imposed). At higher lift coefficients, the relative increase in drag is reduced though due to the difference in the Oswald efficiency factor. At a lift coefficient of 1.5, for instance, the increase in drag only amounts to 5.5%. The absolute difference in drag on the other hand rises from 0.0018 at a lift coefficient of zero to 0.0061 at a lift coefficient of 1.5.

II.2.2 THE DRAG POLARS FOR THE AIRPLANE IN THE OTHER CONFIGURATIONS

Compared to the clean airplane, an increment in the zero-lift drag coefficient has to be added now. The magnitude of this increment depends on the configuration used and on flap type and landing gear size. Since the flaps and the landing gear are considered to be reused from the kerosene-fuelled Boeing, the same increments are used for each alternative. Table 2.5 gives the values used in our simulation for these increments.

Table 2.5 The increment in $C_{D,0}$ for the different configurations

Configuration	**Increment**
Take-off gear up	0.0145
Take-off gear down	0.0345
Landing gear up	0.0550
Landing gear down	0.0750
OEI	0.0800

For the take-off and landing configurations the Oswald efficiency factor e must also change. For the original Boeing 777 simulation of Chapter I, a ?e of -0.5 is used for the take-off configuration[23] and a ?e of –1.0 is used for the landing configuration. For the different alternatives simulated here, these increments are also used. For instance, for alternative 3 the following values are used:

Configuration	**Oswald efficiency factor**
Clean	0.833
Take-off	0.783
Landing	0.733

Once these increments are known it is easy to calculate the remaining drag polars for all the different alternatives. This is done below. For each drag polar, only the analytical form will be presented here. Based on this equation, the figures can namely be easily composed.

[23] The Oswald efficiency factor e is changed from 0.85 for the clean airplane to 0.80 for the airplane in the take-off configuration.

II.2.2.1 THE DRAG POLAR FOR THE AIRPLANE IN THE TAKE-OFF CONFIGURATION WITH THE GEARS UP

As can be seen from Table 2.5, the increment in zero-lift drag coefficient due to the flaps in the landing configuration is taken as 0.0145. With the clean airplane drag polars of subsection II.2.1 this leads to the following drag polars for the different alternatives in the take-off configuration with the flaps up:

Alternative	Drag Polar
0	$C_D = 0.0234 + 0.0481 * C_L^2$
1	$C_D = 0.0243 + 0.0481 * C_L^2$
2	$C_D = 0.0252 + 0.0481 * C_L^2$
3	$C_D = 0.0234 + 0.0492 * C_L^2$
4	$C_D = 0.0243 + 0.0492 * C_L^2$
5	$C_D = 0.0252 + 0.0492 * C_L^2$
6	$C_D = 0.0234 + 0.0502 * C_L^2$
7	$C_D = 0.0243 + 0.0502 * C_L^2$
8	$C_D = 0.0252 + 0.0502 * C_L^2$

II.2.2.2 THE DRAG POLAR FOR THE AIRPLANE IN THE TAKE-OFF CONFIGURATION WITH THE GEARS DOWN

As can be seen from Table 2.5, the increment in zero-lift drag coefficient due to the landing gear is taken as 0.02 (0.0345-0.0145). The total increment in zero-lift drag coefficient for the aircraft in the take-off configuration is thus (as given in Table 2.5) 0.0345. With the clean airplane drag polars of subsection II.2.1 this leads to the following drag polars for the different alternatives in the take-off configuration with the flaps up:

Alternative	Drag Polar
0	$C_D = 0.0434 + 0.0481 * C_L^2$
1	$C_D = 0.0443 + 0.0481 * C_L^2$
2	$C_D = 0.0452 + 0.0481 * C_L^2$
3	$C_D = 0.0434 + 0.0492 * C_L^2$
4	$C_D = 0.0443 + 0.0492 * C_L^2$
5	$C_D = 0.0452 + 0.0492 * C_L^2$
6	$C_D = 0.0434 + 0.0502 * C_L^2$
7	$C_D = 0.0443 + 0.0502 * C_L^2$
8	$C_D = 0.0452 + 0.0502 * C_L^2$

II.2.2.3 THE DRAG POLAR FOR THE AIRPLANE IN THE LANDING CONFIGURATION WITH THE GEARS UP

Again, the increment in zero-lift drag coefficient used can be found in Table 2.5. Using the increment given there leads to the following drag polars.

Alternative	Drag Polar
0	$C_D = 0.0639 + 0.0513 * C_L^2$
1	$C_D = 0.0648 + 0.0513 * C_L^2$
2	$C_D = 0.0657 + 0.0513 * C_L^2$
3	$C_D = 0.0639 + 0.0525 * C_L^2$
4	$C_D = 0.0648 + 0.0525 * C_L^2$
5	$C_D = 0.0657 + 0.0525 * C_L^2$
6	$C_D = 0.0639 + 0.0538 * C_L^2$
7	$C_D = 0.0648 + 0.0538 * C_L^2$
8	$C_D = 0.0657 + 0.0538 * C_L^2$

II.2.2.4 THE DRAG POLAR FOR THE AIRPLANE IN THE LANDING CONFIGURATION WITH THE GEARS DOWN

As for the aircraft in the take-off configuration, an increment of 0.02 for the zero-lift drag coefficient is used to include the effect of the deployment of the landing gear. This leads to the increment value given in Table 2.5. Using this value leads to the following drag polars.

Alternative	Drag Polar
0	$C_D = 0.0839 + 0.0513 * C_L^2$
1	$C_D = 0.0848 + 0.0513 * C_L^2$
2	$C_D = 0.0857 + 0.0513 * C_L^2$
3	$C_D = 0.0839 + 0.0525 * C_L^2$
4	$C_D = 0.0848 + 0.0525 * C_L^2$
5	$C_D = 0.0857 + 0.0525 * C_L^2$
6	$C_D = 0.0839 + 0.0538 * C_L^2$
7	$C_D = 0.0848 + 0.0538 * C_L^2$
8	$C_D = 0.0857 + 0.0538 * C_L^2$

II.2.2.5 THE DRAG POLAR FOR THE AIRPLANE WITH ONE ENGINE INOPERATIVE

Finally, the drag polar for the airplane with one engine inoperative is determined. Again, as in Chapter I, an additional increment in zero-lift drag coefficient due to the windmilling engine of 50 counts is used. Adding this increment to the value from the landing configuration with the gears down[24] gives us the value that must be entered (cf. Table 2.5). This value then leads to the following drag polars.

Alternative	Drag Polar
0	$C_D = 0.0889 + 0.0513 * C_L^2$
1	$C_D = 0.0898 + 0.0513 * C_L^2$
2	$C_D = 0.0907 + 0.0513 * C_L^2$
3	$C_D = 0.0889 + 0.0525 * C_L^2$
4	$C_D = 0.0898 + 0.0525 * C_L^2$
5	$C_D = 0.0907 + 0.0525 * C_L^2$
6	$C_D = 0.0889 + 0.0538 * C_L^2$
7	$C_D = 0.0898 + 0.0538 * C_L^2$
8	$C_D = 0.0907 + 0.0538 * C_L^2$

[24] This configuration is chosen to evaluate the OEI drag since this is the worst configuration compared to drag.

II.3 ESTIMATION OF WING AREA, TAKE-OFF THRUST AND MAXIMUM LIFT COEFFICIENT FOR ALTERNATIVE ZERO

In this section, all the sizing requirements will be calculated for alternative zero and the method used will be briefly introduced. Since the hydrogen-fuelled plane would have to fly the same mission as its kerosene-fuelled counterpart, the same performance criteria will be met. Finally, the matching plot is made and the design point is given.

II.3.1 SIZING TO STALL SPEED REQUIREMENTS

For the method used to determine the stall speed requirements, the reader is referred to subsection I.3.1. Here only the input and output of the AAA module for stall speed sizing is given. Since the hydrogen-fuelled Boeing 777 would have to be able to fly the exact same mission as its kerosene counterpart, the inputs for the altitude, stall speed and maximum lift coefficient are the same for both planes.

In order to perform the stall speed sizing, the weight at which stall is evaluated normally has to be selected now. Nevertheless, here, the sizing calculations are done in the opposite direction. The wing loading at take-off is kept constant to be able to determine the stall speed weight. The following input is needed to provide a wing loading at take-off of approximately 114 lb/ft²:

h_S = 39,000 ft	W_S = 257,749.0 lb	$C_{L,\,max,\,S}$ = 1.2
V_S = 311.34 kts[25]	W_{TO} = 287,203,7 lb	

The weight at which the stall speed requirement needs to be evaluated to give the take-off wing loading of the kerosene-fuelled counterpart is thus:

$$W_S = 257{,}749.0 \text{ lb}$$

This means that the ratio of W_S to W_{TO} is 0.897 for both the hydrogen- and the kerosene-fuelled Boeing 777.

II.3.2 SIZING TO TAKE-OFF DISTANCE REQUIREMENTS

Again, the hydrogen-fuelled counterpart of the 777 must be able to meet the same requirements as its kerosene-fuelled sister. Therefore, the same input is given for both planes. The following values are thus entered:

h_{TO} = 0 ft	?T = 0.0°R	$C_{L,\,max,\,TO}$ = 2.0
F_{TO} = 1.000	S_{TO} = 7,600 ft	Plot ?$C_{L\,max}$ = 0.4

With these values, AAA calculates the required thrust-to-weight ratio at take-off for a range of wing loadings. Equation (1.24) is used for this purpose:

$$\left(T/W\right)_{TO} = \frac{\left(W/S\right)_{TO}}{0.0267 * \sigma * C_{L,max\,TO} * S_{TO} * F_{TO}} \qquad (1.24)$$

As can be seen from this equation, the relationship between wing loading and thrust-to-weight ratio to meet a given take-off distance requirement (S_{TO}) only depends on both the atmospheric conditions (altitude, temperature and humidity) during take-off (through s and F_{TO}) as well as on the value of the lift coefficient at take-off. For both aircraft, the same values were used, so the results of the sizing for take-off distance requirements will be the same. Thus, these results can be found on Figure 1.4 in subsection I.3.2.

[25] This speed is taken from the example file included with AAA. Later, it will be checked whether this speed is actually also equal to 1.3 times the lift-off speed.

II.3.3 SIZING TO LANDING DISTANCE REQUIREMENTS

As in the previous sections, the aircraft running on hydrogen must also meet the landing distance requirement for the kerosene-fuelled Boeing 777. Therefore, the values entered as input for the hydrogen are mostly the same as the values for the kerosene-fuelled plane. Only the landing and take-off weights are set to the values obtained by AAA and given in subsection II.1.4. The following input is used:

h_L = 0 ft W_L = 252,000 lbs $C_{L, max, L}$ = 2.4 S_L = 3,710 ft
?T = 0.0°R W_{TO} = 287,203.7 lbs Plot ?$C_{L\,max}$ = 0.4

With these values, the result from Figure 2.11 is obtained.

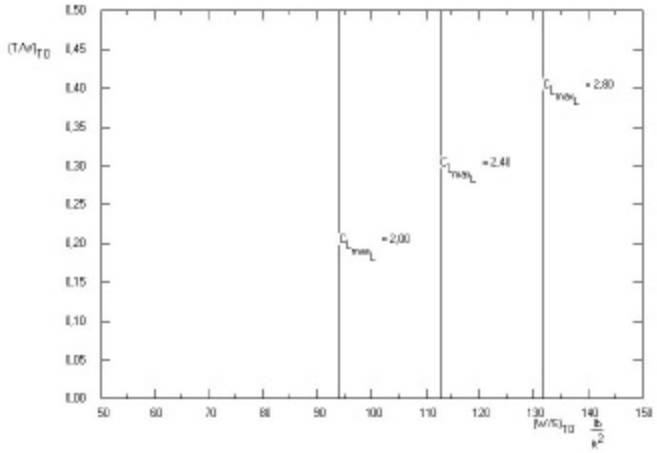

Figure 2.11 The results for the landing distance sizing submodule

Comparing the results from this figure with Figure 1.7 shows us that the landing distance requirement for the hydrogen-fuelled aircraft is far more severe than for its kerosene-fuelled opponent with the same lift coefficient at landing. This is logical since the landing weight to take-off weight ratio is much higher for hydrogen fuel than for kerosene. Less weight of fuel is namely burnt during flight. With the same landing requirements, the maximum allowable wing loading at take-off will thus be lower. Therefore, the landing configuration will need special attention for an airplane flying on hydrogen fuel. A high value of $C_{L, max, L}$ will namely be necessary to be able to guarantee that the hydrogen-fuelled Boeing 777 will be able to land on the runways that the Boeing 777 uses today.

II.3.4 SIZING TO CLIMB REQUIREMENTS

Since the drag polars are already determined, the climb requirements can now easily determined through AAA. Again, as in Chapter I, the airplane is a FAR 25 certified airplane thus the same climb requirements must be met. The AAA input for the climb requirement can be found in Figure 2.12. Again, several parameters have to be determined. Most of them were already determined in Chapter I since the plane under consideration has to meet the same requirements as the kerosene-fuelled Boeing. Therefore, both the climb gradients as well as the wing parameters and the engine ratings ($F_{MaxCont}$ and F_{8sec}) specified in the figure are taken the same as in Chapter I. The values for the Oswald efficiency factor and the $C_{D,0}$'s shown in the figure on the other hand are derived from the drag polars of paragraph II.2 while the weights are taken from the weight sizing module.

Input Parameters

$F_{MaxCont}$	0,800	W_{TO}	287203,7	lb	$C_{D_{TO\_up}}$	0,0234	$CGR_{25.121_T}$ 0,000
F_{8sec}	0,900	W_L	252000,0	lb	$C_{D_{TO\_down}}$	0,0434	$CGR_{25.121_{SS}}$ 0,024
$C_{L_{max_{clean}}}$	1,200	AR_w	8,27		e_L	0,7500	$CGR_{25.121_{ER}}$ 0,012
$C_{L_{max_{TO}}}$	2,000	e_{clean}	0,8500		$C_{D_{L\_down}}$	0,0839	$CGR_{25.121_L}$ 0,021
$C_{L_{max_A}}$	2,200	$C_{D_{D_{clean,M}}}$	0,0089		$\Delta C_{D_{0_A}}$	0,0000	$CGR_{25.119}$ 0,032
$C_{L_{max_L}}$	2,400	e_{TO}	0,8000		$CGR_{25.111}$	0,012	

Output Parameters

$B_{pP_{clean}}$	0,0453	$B_{pP_{TO\_up}}$	0,0481		$B_{pP_{TO\_down}}$	0,0481	$B_{pP_{L\_down}}$ 0,0513

Figure 2.12 The input for the calculation of the climb requirements

As for all previous sizing requirements, the output is again given in a graphical way. The result can be found in Figure 2.13.

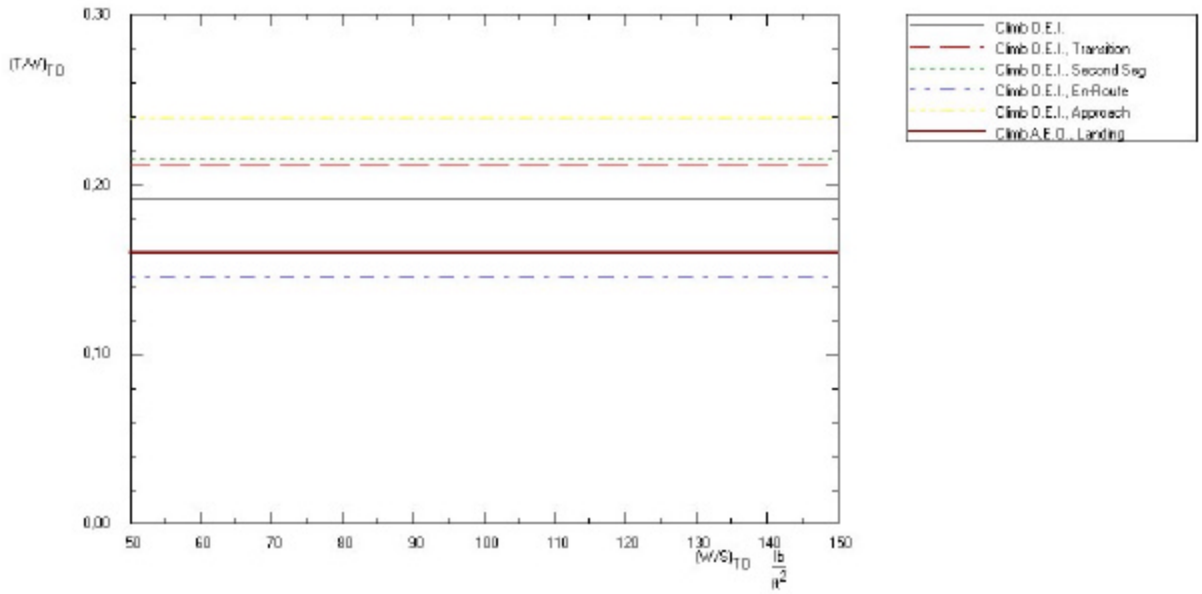

Figure 2.13 The results for the climb requirements submodule

II.3.5 SIZING TO MANOEUVRING REQUIREMENTS

As mentioned in Chapter I, this sizing requirement normally does not apply to FAR 25 certified airplanes. Nevertheless, this requirement is imposed to our design here since it could be of importance for the design of the mothership.

As in the previous subsections, the hydrogen-fuelled 777 must again meet the same performance requirements as its kerosene-fuelled counterpart. Therefore, most of the data given in subsection I.3.5 of Chapter I is used here too. Only the weight at which the manoeuvre is executed and the zero-lift drag coefficient for the clean airplane are altered. The weight at which the manoeuvring sizing is evaluated is determined as follows:

$$\left(\frac{W_b - W_M}{W_b - W_e}\right)_{H_2} = \left(\frac{W_b - W_M}{W_b - W_e}\right)_{kerosene}$$

where:

W_b is the weight of the plane at the beginning of the cruise phase
W_e is the weight of the plane at the end of the cruise phase
W_M is the weight of the plane at the manoeuvring point

This leads to the following data:

h_M = 35,000 ft	W_{TO} = 287,203.7 lbs	AR_W = 8.27
V_M = 478.56 kts	W_M = 274,220 lbs	$C_{D0,\ clean,\ M}$ = 0.0089
n = 0.93 g	F_M = 0.18	e_{clean} = 0.85

With these input values, the sizing plot can be made with AAA. The result is given in Figure 2.14.

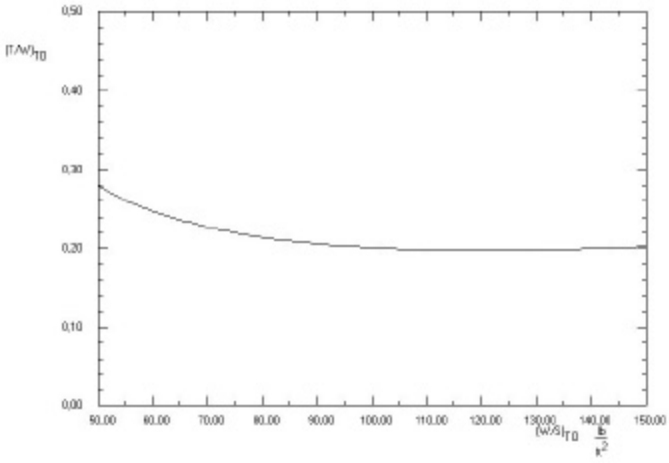

Figure 2.14 The results for the manoeuvring sizing

II.3.6 SIZING TO CRUISE SPEED REQUIREMENTS

As for the kerosene-fuelled Boeing 777, the maximum cruise speed is taken as Mach 0.87 at 35,000 ft and the weight at which the cruise speed requirement is evaluated is taken equal to the weight at which the manoeuvring requirement is checked. This leads to the following input:

h = 35,000 ft	W_{TO} = 287,203.7 lbs	$V_{Cr,\,max}$ = 501.62 kts	$C_{D0,\,clean,M}$ = 0.0089
F_{Cr} = 0.18	W_{Cr} = 274,220 lbs	AR_W = 8.27	e_{clean} = 0.85

With this input the results of Figure 2.15 are obtained.

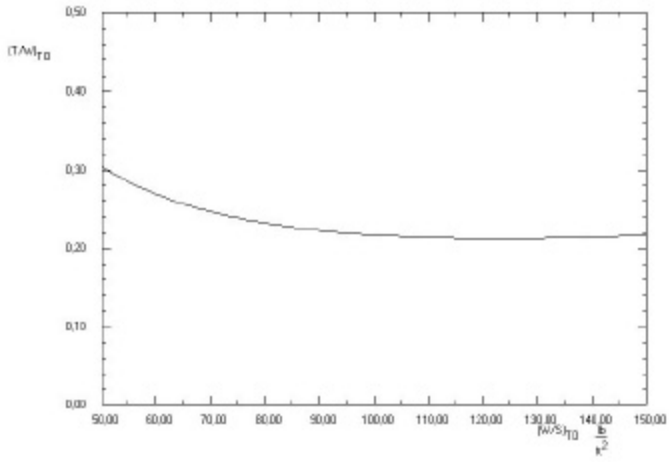

Figure 2.15 The results for the cruise speed sizing

II.3.7 MATCHING OF ALL SIZING REQUIREMENTS

As for the kerosene-fuelled Boeing 777 of Chapter I, it is now time to overlay all sizing requirements in one figure in order to be able to determine the highest possible wing loading and the lowest possible thrust-to-weight ratio which are consistent with all the requirements. This can easily be done in AAA and results in Figure 2.16.

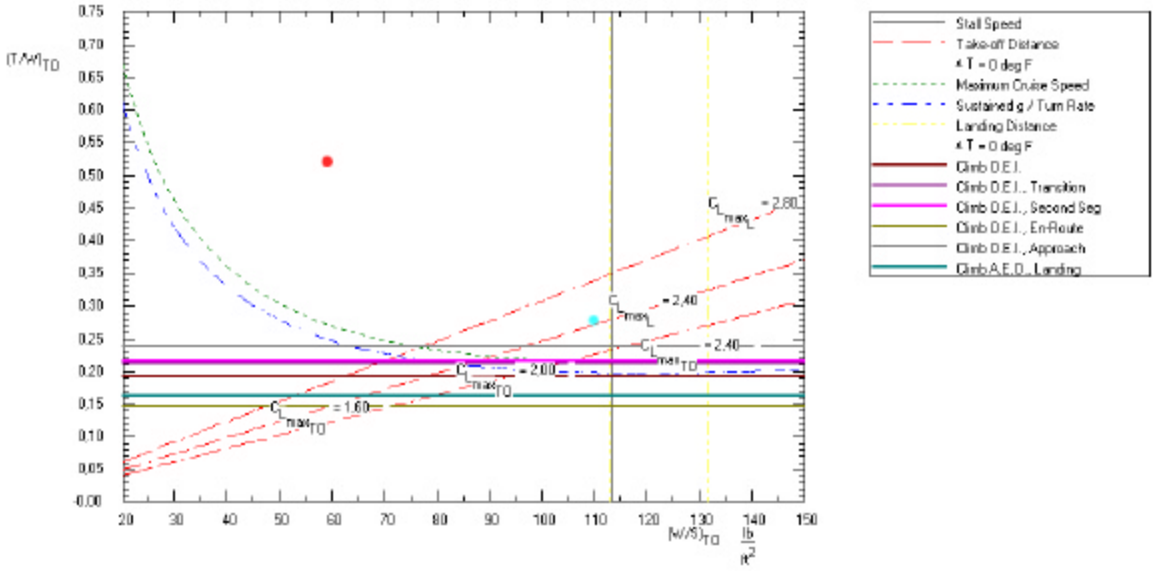

Figure 2.16 The matching plot for the hydrogen-fuelled Boeing 777

On Figure 2.16, the design point for this simulation is indicated with a red dot. It is namely assumed that both the wing area and the engine thrust are retained from the original Boeing 777. With the take-off gross weight of paragraph II.1.4, this leads to:

$$\frac{W}{S} = 59 \frac{lb}{ft^2}$$

$$\frac{T}{W} = 0.522$$

As mentioned before, the real take-off gross weight of the plane will be reasonably higher than the calculated one due to several reasons. This would increase the wing loading and decrease the thrust-to-weight ratio. As can be seen from the figure, the take-off gross weight of the airplane could approximately be doubled without giving problems with regard to sizing requirements. The hydrogen-fuelled airplane with these characteristics would thus be able to perform at least the same mission as its kerosene-fuelled counterpart.

Furthermore, Figure 2.16 also shows the original design point of the kerosene-fuelled 777 as a light blue/aquamarine dot. As can be seen from the figure even this point would be feasible with this H_2-fuelled design.

II.4 THE MATCHING PLOTS FOR THE OTHER ALTERNATIVES

In this paragraph, the matching plot for the other eight alternatives considered is given. The separate sizing requirements will not be repeated here since they can be found in paragraph II.3. Each requirement used here to create the matching plot for the different alternatives is exactly the same as the respective one given in the previous paragraph. Only the values for the zero-lift coefficient and the Oswald efficiency factor are adapted to the values given for different alternatives in paragraph II.2

II.4.1 ALTERNATIVE 1

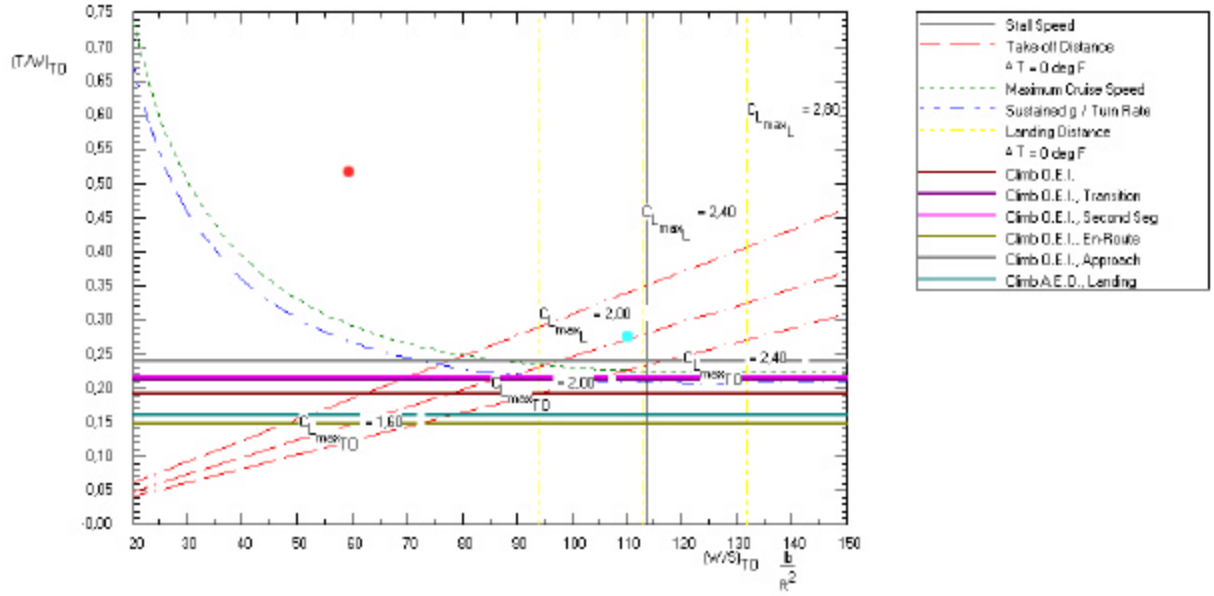

Figure 2.17 The matching plot for alternative 1

II.4.2 ALTERNATIVE 2

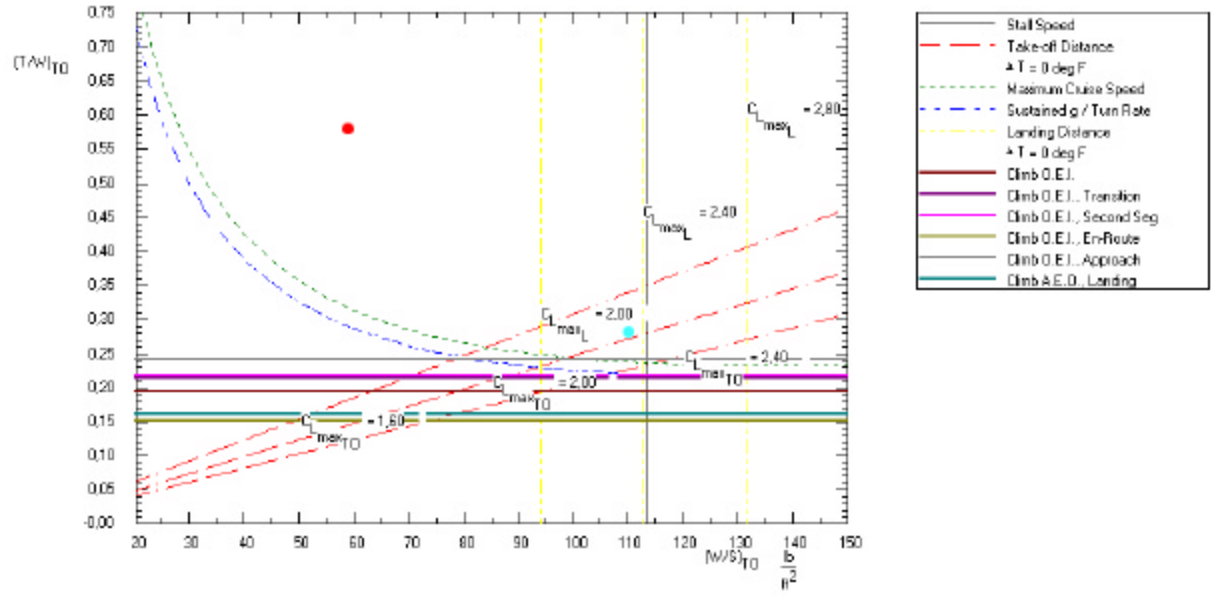

Figure 2.18 The matching plot for alternative 2

II.4.3 ALTERNATIVE 3

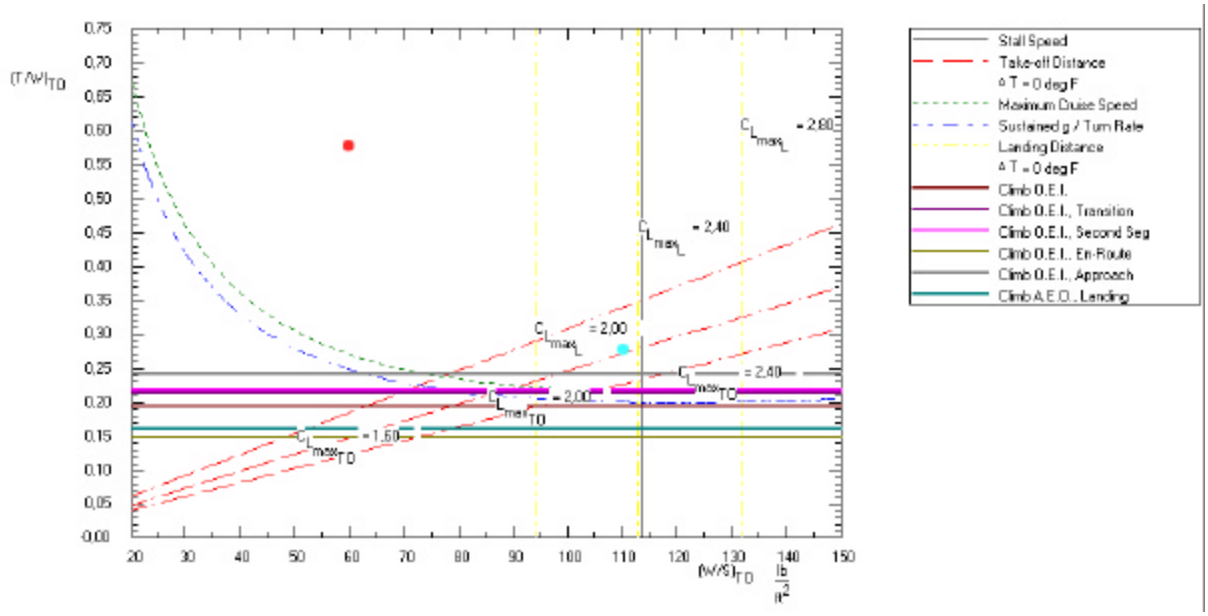

Figure 2.19 The matching plot for alternative 3

II.4.4 ALTERNATIVE 4

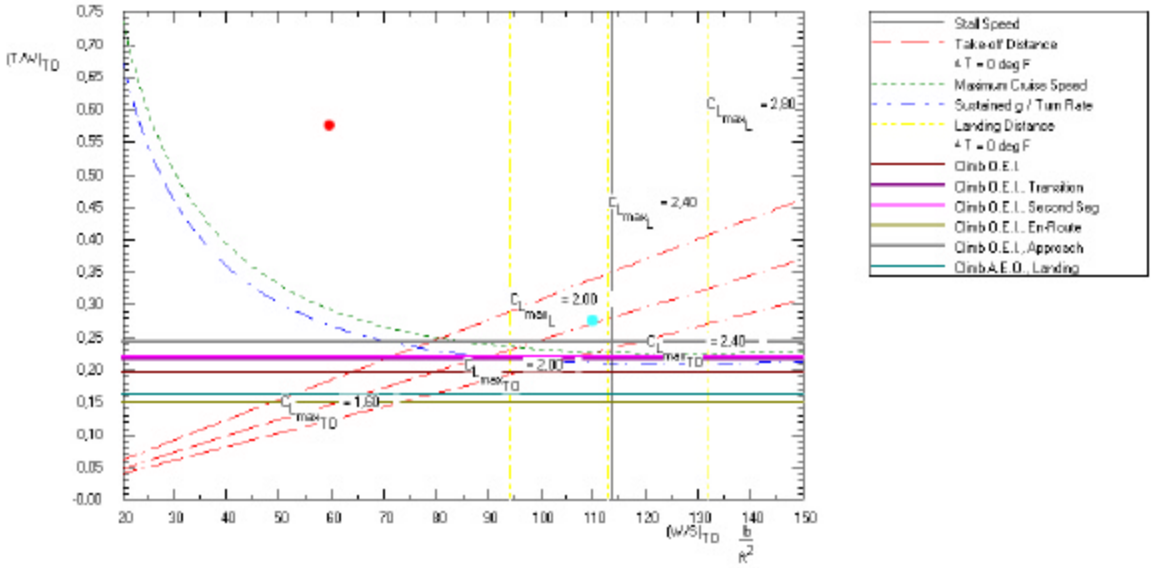

Figure 2.20 The matching plot for alternative 4

II.4.5 ALTERNATIVE 5

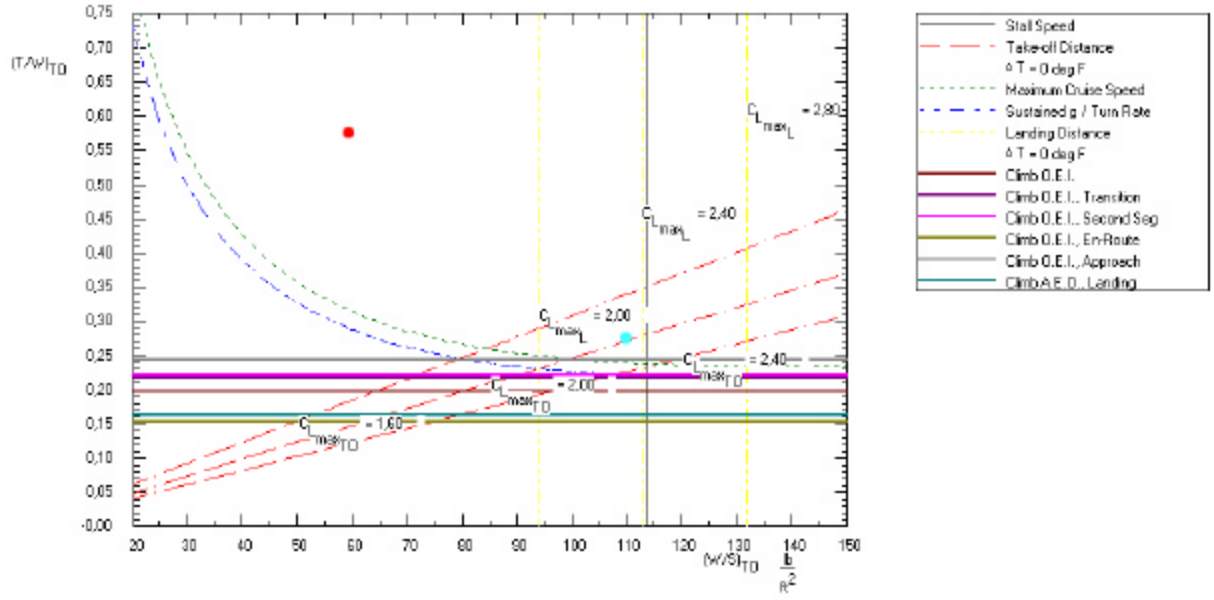

Figure 2.21 The matching plot for alternative 5

II.4.6 ALTERNATIVE 6

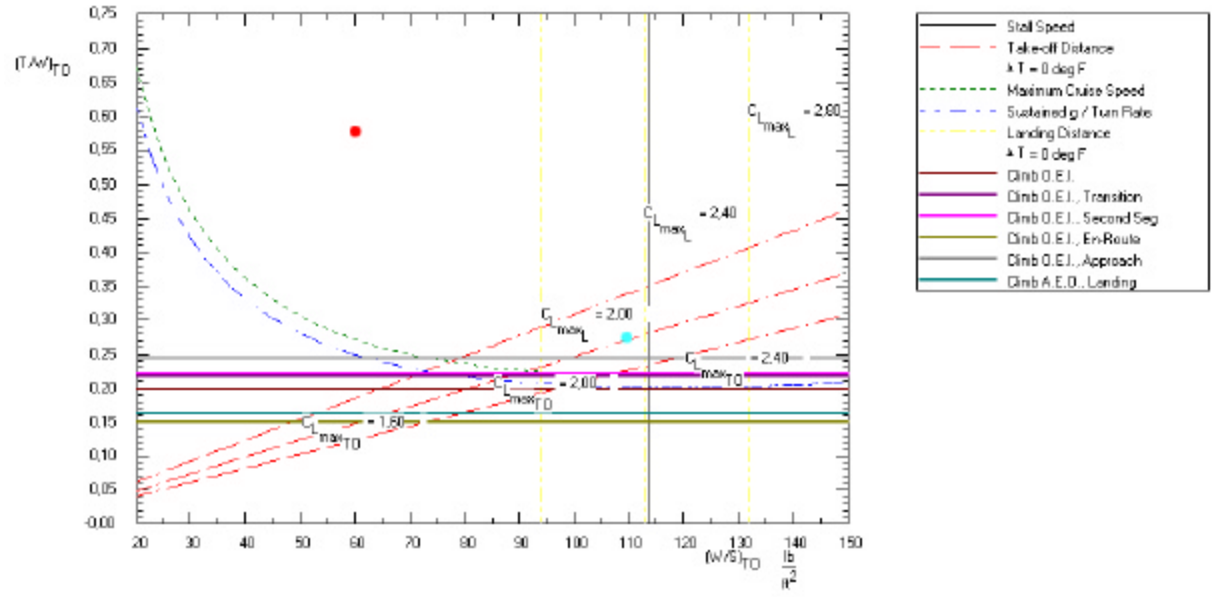

Figure 2.22 The matching plot for alternative 6

II.4.7 ALTERNATIVE 7

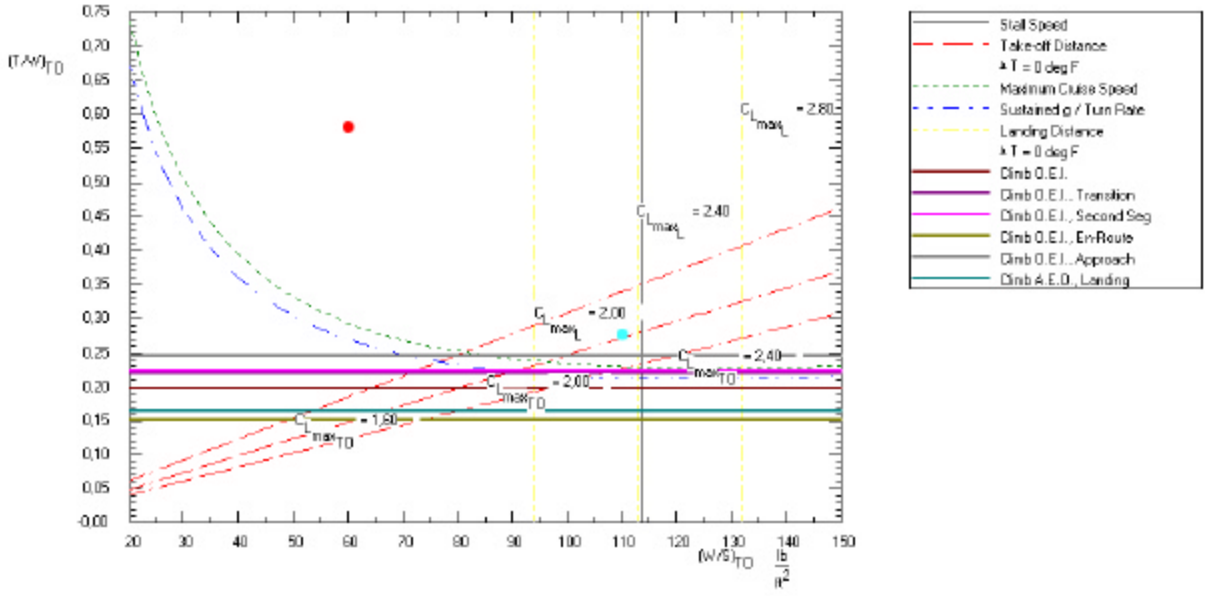

Figure 2.23 The matching plot for alternative 7

II.4.8 ALTERNATIVE 8

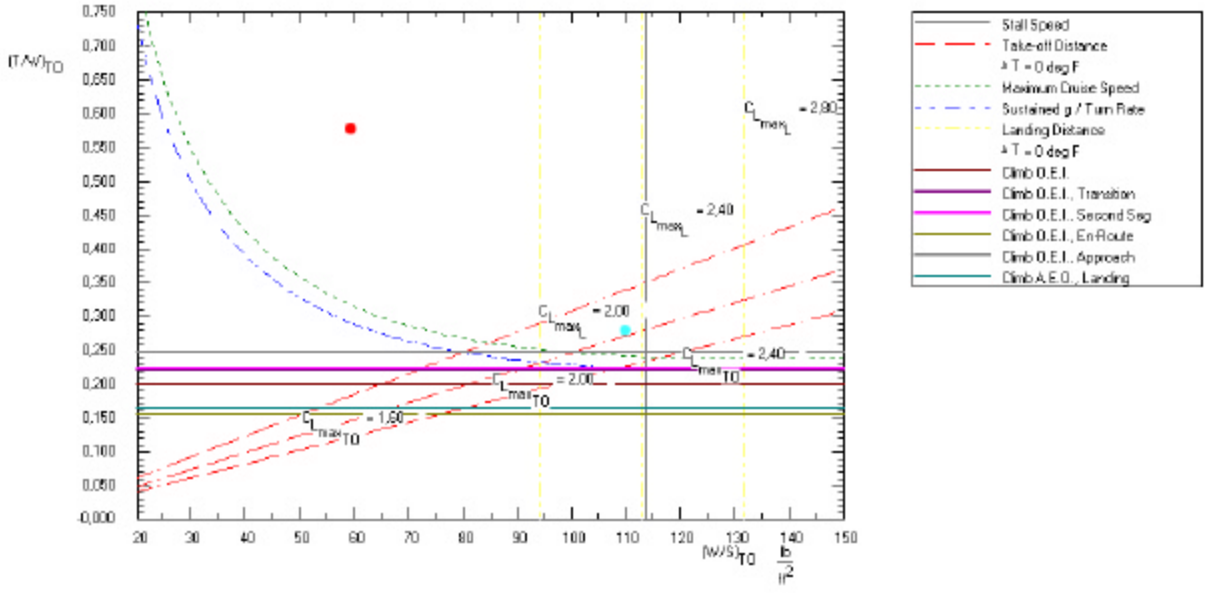

Figure 2.24 The matching plot for alternative 8

II.4.9 COMPARISON OF THE DIFFERENT MATCHING PLOTS

Here, a comparison will be made of the matching plots of alternatives zero and eight. These two alternatives are chosen since they represent the extremes of the considered range for both the zero-lift coefficient and the Oswald efficiency factor. Figure 2.16 and 2.24 will thus be compared.

This comparison shows us the relatively small influence of the drag polar on the sizing requirements. As can be seen from the figures, both the take-off and landing as well as the stall speed requirements even remain unchanged since they depend on the maximum lift coefficient but not on the drag of the airplane. The climb requirements on the other hand will be influenced by the drag polar. The minimum required thrust-to-weight ratio therefore slightly increases from 0.24 for alternative zero to 0.25 for alternative 8. Finally, both the manoeuvring and maximum cruise speed sizing requirements will change slightly too. Comparing the thrust-to-weight ratio at a wing loading of 20 lb/ft² shows us that the required thrust-to-weight ratio for the cruise speed sizing requirement increases from 0.67 for alternative 0 to 0.80 for alternative 8. The same comparison made at a wing loading of 150 lb/ft² shows us an increase from 0.22 to 0.24.

II.5 CONCLUSIONS

Since there is no actual data available for the hydrogen-fuelled Boeing 777, it is hard to make conclusions concerning the accuracy of AAA calculations. It is nevertheless possible to make some general remarks concerning the results. First of all, it can be seen that even a reasonable increase in drag (20% at zero-lift) has a relatively small influence on the sizing requirements for the airplane. Comparing the matching plots of alternatives zero and eight shows us that there hardly is a difference between them even though the drag polars show a reasonable variance.

Furthermore, the matching plot shows us that reusing the engines and the wing of a large transport jet after "refuelling" the plane with hydrogen would most certainly be possible. This would though give a rather large surplus in take-off thrust and a very low wing loading. It would thus be better to redesign the plane (that's what will be done for the mothership!). As the preliminary sizing results show, it would be possible to use the exact same wing loading and thrust-to-weight ratio for the hydrogen fuelled counterpart as for the original kerosene-fuelled Boeing. This would not only lower the weight of the engines, but the fuel consumption will diminish too due to the lower maximum thrust required. Finally wing area and thus weight will be a lot smaller too.

II.6 REFERENCES

BOOKS

[1] Brewer G.D., "*Hydrogen Aircraft Technology*", CRC Press, 1991

[2] Darcorporation, "*Advanced Aircraft Analysis Version 2.3 help files*", Darcorporation, 2001

[3] Raymer D.P., "*Aircraft Design: a Conceptual Appoach*", AIAA Education Series, 1992

[4] Roskam J., "*Airplane Design: Part I, Preliminary Sizing of Airplanes*", DAR Corporation, 1997

[5] Roskam J., "*Airplane Design: Part II, Preliminary Configuration Design and Integration of the Propulsion System*", DAR Corporation, 1997

[6] Roskam J., "*Airplane Design Short Course AA31010*", the University of Kansas Continuing Education, August 5-9 2002

[7] Torenbeek E., "*Synthesis of Subsonic Airplane Design*", Delft University Press, 1982

WORLD WIDE WEB

[8] http://www.eads.net/eads/en/index.htm?/xml/en/businet/airbus/cryoplane/cryoplane.xml&airbus

CHAPTER III
DESIGN CONSIDERATIONS CONCERNING THE TWIN-FUSELAGE MOTHERSHIP

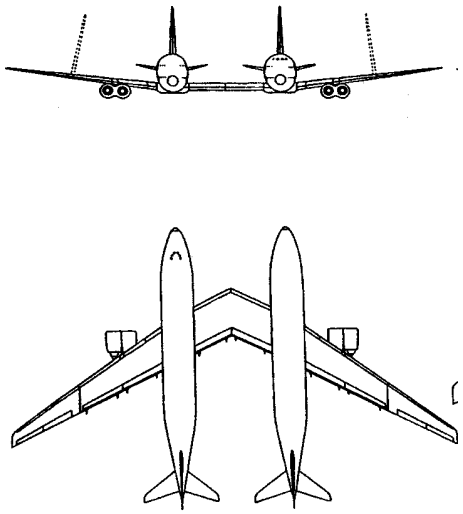

Figure 1 A twin-fuselage design

The main reason for the choice of the twin-fuselage design (cf. Figure 1) is, in our case, the space needed for the storage of the hydrogen fuel[1]. Even though the hydrogen fuel weight will be decreased by at least 65%[2] compared to a conventional kerosene-fuelled plane, the volume needed to store the fuel will be increased by a factor of approximately 4. With an upper average fuel flow of approximately 36 m³/hr/engine, as calculated in Part II Chapter V, with a maximum flight-time of 16 hours and 4 engines, almost 2175 m³ is needed to store the hydrogen. Assuming an integral internal tank that fills practically the whole Boeing 777 cabin, a tank diameter of 5.5 m and a tank length of 46 m seem realistic[3]. With these assumptions, approximately 1100 m³ of hydrogen could be stored in a single Boeing 777 fuselage. Therefore, two Boeing 777-like fuselages will certainly be sufficient for our mission and a twin-fuselage design was the appropriate choice. Besides that, a twin-fuselage design also incorporates some other advantages compared to a conventional aircraft design, briefly described in the first paragraph. Subsequently, some of the possible disadvantages or problems with the twin-fuselage layout are also given. Again, only a short description is provided here. A more detailed discussion of both the advantages and disadvantages of the twin-fuselage design can be found in the references. However, some of the points mentioned there are not applicable to this design since all the references mainly focus on passenger aircraft.

III.1 ADVANTAGES OF THE TWIN-FUSELAGE LAYOUT

III.1.1 WING BENDING LOAD ALLEVIATION

One of the main advantages of the twin fuselage layout is a substantial alleviation of the wing bending loads due to the separation of a large central mass into two outboard-positioned masses (cf. Figure 2). This allows the use of higher-aspect-ratio wings without weight penalty[4] (or with an even lighter wing structure) and the better aerodynamic performance of higher aspect ratio wings may thus thereby be realised (L/D is proportional to $\sqrt{AR}$). In our case, this advantage is somehow less pronounced due to the absence of the fuel in the wing. But the presence of two GE90-90B engines[5] on one pylon per wing (instead of one as for the genuine Boeing 777) on the other hand reduces the influence of the absence of the fuel.

[1] Which is needed to chill down the air for the ACES system and then liquefy the oxygen for storage in the second stage.
[2] The TSFC of the HBPR turbofans is alleviated by approximately 65% (for a constant thrust) due to the switch to hydrogen as a fuel and the thrust required will be less due to the lower gross take-off weight. But this thrust increases during the cruise phase due to the collection of liquid enriched air.
[3] With a cabin length for the Boeing 777of 49.1 m and a internal cabin diameter of 5.87 m.
[4] cf. subsection III.1.2
[5] The installed GE90-90B on the Boeing 777 weight approximately 18,700 lb (8,500 kg).

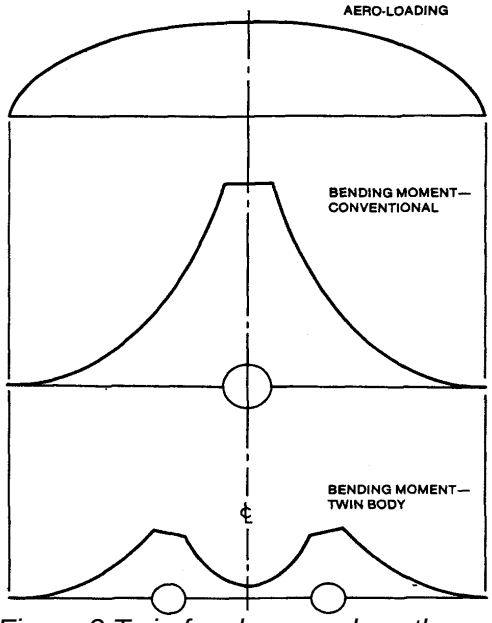

Figure 2 Twin fuselages reduce the peak bending moment (ref. [1])

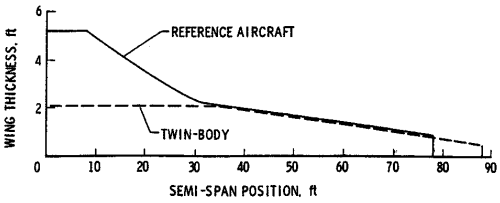

Figure 3 Wing thickness variation for a 280 passenger design (ref.[1])

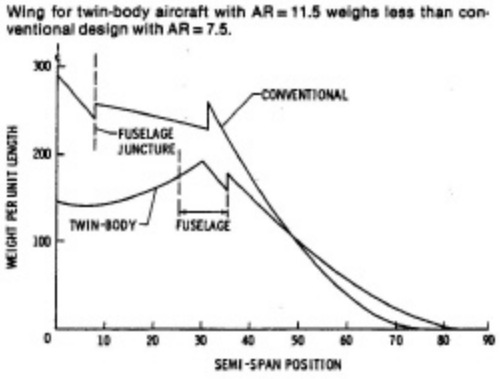

Figure 4 Wing load-carrying weight (ref.[1])

The weight per unit length of wing structural bending material can be shown to be proportional to *m/h,* where *m* is the bending moment and *h* is the wing thickness. To keep weight low, *m* should be low and *h* large. The large thickness desired for structural reasons, however, conflicts with the thinness desired to reduce drag, and so thinness choice becomes a compromise. In conventional aircraft design, control of the bending moment *m* is limited, so emphasis is placed on thickness control in the region of very large bending moment through the clever use of chord and thickness flaring. By contrast, the twin-fuselage arrangement allows for focussing on bending moment control. Thickness can thus be dictated more by aerodynamic concerns. In our case, the choice of the wing thickness is even more unrestrained since fuel volume does not play a role[6]. Results from reference [1] found in considering a 280-passenger design illustrate the thickness and wing weights involved. Figure 3 shows the wing thickness results for the conventional reference design and for a comparable twin-fuselage configuration. Note the greatly increased thickness near the root for the conventional design due to root flaring[7]. Wing weight distributions for the load carrying structure are shown in Figure 4. The aspect ratio[8] for the conventional design was taken as 7.5, and for the twin-body designs, 11.5. In spite of this large difference in aspect ratio, and even though root flaring was used in the conventional design and not in the twin-body version, the structural weight for the wing for the twin-fuselage design is less. Separate fuselages thus powerfully reduce bending moments.

Of course, this reduction in wing bending moment also depends on the distance between the two fuselages. The greater this distance, the more the bending moment is relieved. On the other hand, the main disadvantage of the two outboard-positioned fuselages is the increase in the rolling moment of inertia. Furthermore, landing gear spacing and the adverse yaw effect due to an engine-out situation are also increased with a bigger fuselage-separation distance. Investigations (ref. [1]) have

[6] As mentioned before wing weights will be slightly higher in our design due to the absence of the wing bending load alleviation due to the fuel weight, but, again as mentioned before, the presence of the two engines reduces this weight disadvantage.

[7] According to the author of reference [1], wing layout practices normally used, namely, to use flaring in the wing of both the thickness and chordwise directions as the root is approached, are incorporated carefully in designing the reference conventional single fuselage aircraft.

[8] The aspect ratio of a wing is defined as: $AR = \frac{b^2}{S}$ where b is the wing span and S is the gross wing area

shown that an optimum fuselage spacing (centerline to centerline) of about 0,35 times the wing span is a good practical choice. For our design, this leads to a fuselage spacing of approximately 32.81 m (107 ft 8 inch).

III.1.2 HIGHER ASPECT RATIO WING WITHOUT PENALTY

As mentioned before, the separation of a large central mass into two outboard-positioned masses substantially alleviates wing bending loads. As shown in the previous paragraph, this allows the use of higher-aspect-ratio wings without weight penalty (or with an even lighter wing structure) and the better aerodynamic performance of higher aspect ratio wings may thus thereby be realised (L/D is proportional to $\sqrt{AR}$).

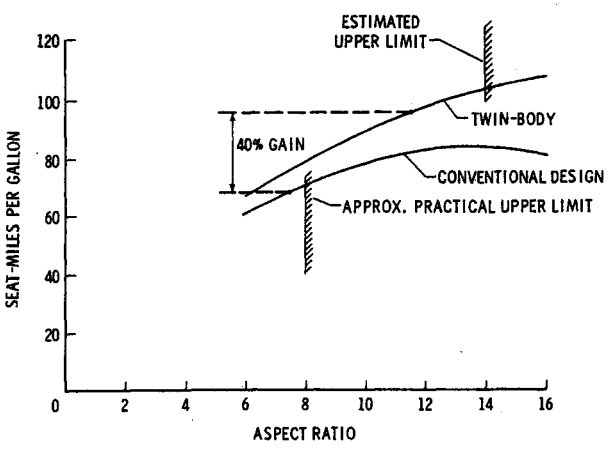

Figure 5 Twin-fuselage gain through aspect ratio (ref.[1])

For conventional subsonic aircraft, problems of growing wing weight (wing bending material varies as $AR^{1.5}$), fuel volume, gear storage and aeroelasticity preclude the use of aspect-ratio values higher than about 10. For years the upper practical limit has even been around 8. A twin-fuselage concept on the other hand removes these limitations. The practical upper limit for these aircraft is of course not known yet, but according to Houbolt (ref [1]), the limit is judged to be on the order of 14 to 16. Given the aerodynamic benefits of a higher aspect ratio, this leads to a substantial decrease in fuel consumption. Figure 5 shows that a decrease of approximately 40% in seat-miles per gallon could be gained with a twin-fuselage design compared to the conventional 280-passengers reference aircraft. Even though the figure also uses a reduction in wetted area due to the better allocation of the passengers (cf. reference [1] for more details) these results will globally also be applicable to our design.

III.1.3 NORMAL LANDING GEAR SIZE

In our particular design, an additional advantage of the twin-fuselage aircraft can be found in the landing gear size. The design under consideration namely carries the orbiter in a ventral position to facilitate the launch of the orbiter. Using this configuration in a conventional single fuselage layout would lead to a huge increase in landing gear height and thus also landing gear weight. Since this landing gear weight normally already attributes to approximately 4.5 % of the maximum take-off weight (cf. reference [3]), a relatively large weight saving is thus achieved by choosing the twin fuselage design.

III.2 POTENTIAL PROBLEMS WITH THE TWIN-FUSELAGE LAYOUT

Nevertheless, several potential problems arise with the consideration of a twin-fuselage aircraft. Below these problems are only briefly cited. Future research must investigate whether these issues will prove to cut potential advantages significantly or not.

One of the main “unknowns” used in the investigations of a twin-fuselage concept is whether adverse interference drag effects due to the relatively “short” distance between the two large fuselages will occur and whether unfavourable spanwise efficiencies might ensue. This would namely greatly reduce the aerodynamic benefits of the use of a higher aspect-ratio wing. However with the spacing between the fuselages needed in our design to position the orbiter, interference effects seem very unlikely.

Furthermore, the aerodynamic efficiency of the wing might be greatly reduced due to aeroelasticity effects. However, if the aspect ratio of the cantilever portion of the wing is kept near those used in today’s conventional aircraft, aeroelastic problems should generally not be critical.

Besides these mainly aerodynamic issues several dynamic loads and structural problems must be investigated. Particularly the gust-encounter problem and the dynamic behaviour of the configuration during an asymmetric landing impact might be critical. Moreover, if the two fuselages would also be joined together by the horizontal tail unit, this layout could cause different stress distributions in the fuselages. Incidentally, the measures taken to avoid these potential issues, eliminating fuselage union by the horizontal tail, could have the more undesirable effect of torsion of the central wing section owing to possible pitch oscillations, with opposite phase, of the two fuselages. The structural stress situation of the central wing should thus also be investigated in detail.

Finally, lateral behaviour and stability of the twin-fuselage aircraft is expected to be different. Specifically, because of the increased roll inertia due to the separated fuselages, roll control is a question. However, according to reference [1], simulations have shown that adequate roll can be achieved. The considerable distance of the centre of each fuselage from the centre of roll rotation at the same time also produces great inertial and centrifugal forces which will impact pilot comfort and thus perhaps also performance. The position of the pilot could finally also cause problems due to the unnatural “feel” for the aircraft that is coupled with the off-centre position of the flight deck.

III.3 CONCLUSION

Despite several potential problems with a twin-fuselage design, this configuration seems to be the appropriate choice for our design. Not only will the landing gear height (and thus also weight) be limited due to this choice, an aerodynamically more efficient wing could also be used due to the possibility of a higher aspect ratio wing. Furthermore, a substantial wing bending load alleviation results from the separation of a large central mass into two outboard-positioned masses. This wing bending load alleviation is even more important in our design since the “classic” alleviation of this bending moment due to the presence of the fuel in the wing is absent here due to the choice of hydrogen as a fuel.

Since our initial design calculations (cf. previous Parts and Chapters) assumed the reuse of the Boeing 777 wing for the outer wings, a double central wing design also seems an appropriate configuration. Not only will this increase the wing area, so that “conventional” wing loadings can be used, it also ensures the availability of a reasonable stiff structure to

attach the orbiter while liquid enriched air is collected. However, since a high interfuselage wing will be used, the Antonov 225 wing (a high wing) is also a viable option (fig. 6).

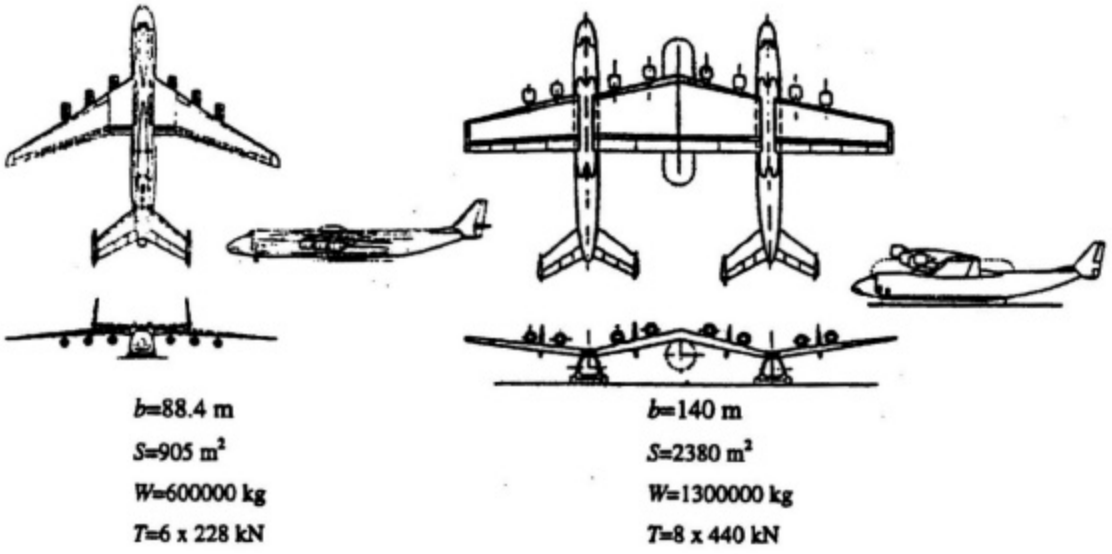

Figure 6 An Antonov 225 twin-fuselage design (ref. [2])

III.4 REFERENCES

[1] John C. Houbolt, *"Why Twin-Fuselage Aircraft?"* Astronautics and Aeronautics, April 1982, pp. 26-35.

[2] S. Chiesa, M. Di Siuva and P. Maggiore, *"The double-fuselage layout: a preliminary case study of a possible way of reducing the development costs for new high capacity aircraft?"* Proc. Instn Mech Engrs, Vol 214, Pt. G, pp. 85-95, 2000

[3] L.R. Jenkinson, P. Simpkin and D. Rhodes, *"Civil Jet Aircraft Design"* AIAA Education Series, 1999

[4] J. Roskam, "*Airplane Design: Part II, Preliminary Configuration Design and Integration of the Propulsion System*", DAR Corporation, 1997

General Conclusion

In this study, the Air Collection and Enrichment System (ACES) propulsion scheme studied in the 1960's and the early 1990's by the US Air Force at the Wright Laboratory (J. Leingang's USAF team) has been applied to a TSTO where the collection phase is realized in subsonic cruise and the stage separation is also subsonic at an altitude between 30 and 40.000 feet. The turbofan propulsion of the carrier plane (or mothership) is with hydrogen fuel. The orbiter (upper stage) can use cryogenic (H_2-O_2) rocket engines or LOX-kerosene rocket engines.

This subsonic concept constitutes an alternative, or more correctly a first step (but which is already a launcher with good performance) in the ACES approach. That is a system where margins are present and which could prove the concept and permits the testing of the collection plant elements in not too difficult flight conditions.

In this short study, the different aspects of this subsonic ACES TSTO launcher have been presented with the calculation of the launcher performance (Part 1), the carrier plane hydrogen-fueled propulsion (Part 2) and the carrier plane pre-design from a performance and sizing point of view (Part 3).

It has been shown that the performance of such a reusable or semi-reusable air-launch space vehicle are acceptable even with not too optimistic performance of the airborne collection plant, that the propulsion system should not give any problem in the near future and that the concept of a large motherplane using a twin-fuselage configuration seems interesting and acceptable.

A more detailed study of the motherplane performance and mainly its structure is necessary as well as an experimental study of the two critical technologies for this air-launch vehicle concept, i.e. first the air separation unit and, secondly, the heat exchangers. The first technology is currently evaluated at the Royal Military Academy of Belgium through an ESA contract studying a Rotary Distillation Separator (RDS) with the development and testing of two different breadboards in 2003 and 2004.